Lecture Notes in Mechanical Engineering

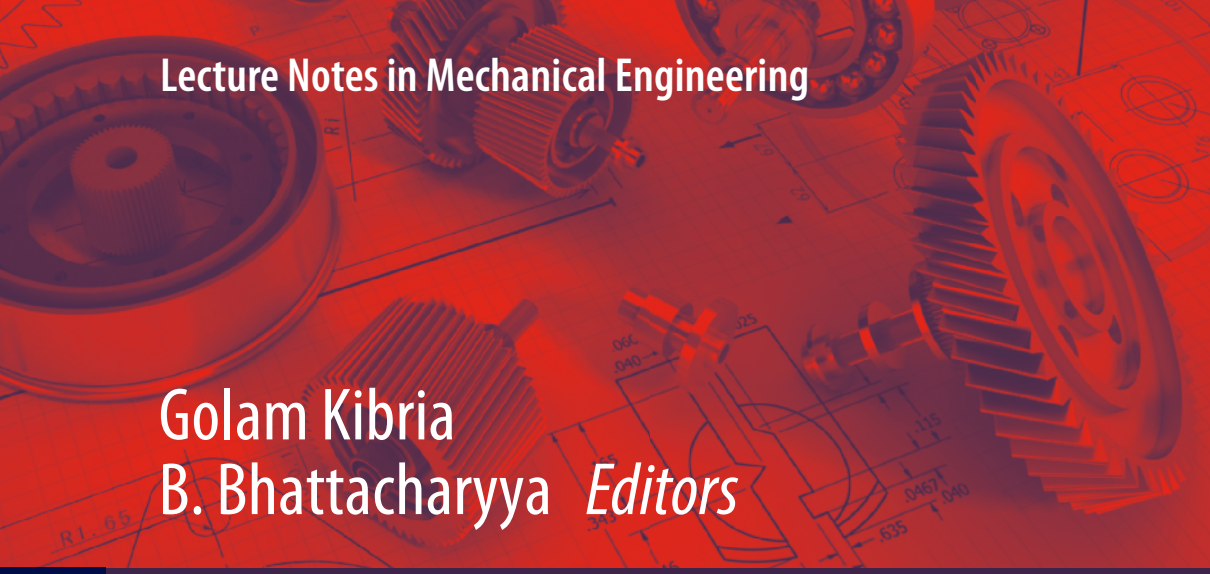

Golam Kibria
B. Bhattacharyya *Editors*

Accuracy Enhancement Technologies for Micromachining Processes

Springer

Lecture Notes in Mechanical Engineering

Lecture Notes in Mechanical Engineering (LNME) publishes the latest developments in Mechanical Engineering - quickly, informally and with high quality. Original research reported in proceedings and post-proceedings represents the core of LNME. Volumes published in LNME embrace all aspects, subfields and new challenges of mechanical engineering. Topics in the series include:

- Engineering Design
- Machinery and Machine Elements
- Mechanical Structures and Stress Analysis
- Automotive Engineering
- Engine Technology
- Aerospace Technology and Astronautics
- Nanotechnology and Microengineering
- Control, Robotics, Mechatronics
- MEMS
- Theoretical and Applied Mechanics
- Dynamical Systems, Control
- Fluid Mechanics
- Engineering Thermodynamics, Heat and Mass Transfer
- Manufacturing
- Precision Engineering, Instrumentation, Measurement
- Materials Engineering
- Tribology and Surface Technology

To submit a proposal or request further information, please contact the Springer Editor in your country:

China: Li Shen at li.shen@springer.com
India: Dr. Akash Chakraborty at akash.chakraborty@springernature.com
Rest of Asia, Australia, New Zealand: Swati Meherishi at swati.meherishi@springer.com
All other countries: Dr. Leontina Di Cecco at Leontina.dicecco@springer.com

To submit a proposal for a monograph, please check our Springer Tracts in Mechanical Engineering at http://www.springer.com/series/11693 or contact Leontina.dicecco@springer.com

Indexed by SCOPUS. The books of the series are submitted for indexing to Web of Science.

More information about this series at http://www.springer.com/series/11236

Golam Kibria · B. Bhattacharyya
Editors

Accuracy Enhancement Technologies for Micromachining Processes

Springer

Editors
Golam Kibria
Department of Mechanical Engineering
Aliah University
Kolkata, India

B. Bhattacharyya
Department of Production Engineering
Jadavpur University
Kolkata, India

ISSN 2195-4356 ISSN 2195-4364 (electronic)
Lecture Notes in Mechanical Engineering
ISBN 978-981-15-2116-4 ISBN 978-981-15-2117-1 (eBook)
https://doi.org/10.1007/978-981-15-2117-1

This Springer imprint is published by the registered company Springer Nature Singapore Pte Ltd.
The registered company address is: 152 Beach Road, #21-01/04 Gateway East, Singapore 189721, Singapore

Preface

Research challenges and developments in the direction of micromanufacturing of macro- and micro-components for successful applications in the fields of biomedical, microelectronics, optical, automotive, and aerospace are increasing day by day due to the demand of fulfillment of such components with specific surface features, dimensional accuracy, tolerance, and complex shapes. For this, a lot of research activities in micromachining, as well as the development of micromachines, are needed across the globe. Achieving desired surface finish, intricate profiles with accuracy and tolerance, and geometrical dimensions is always a challenging task for the manufacturing technocrats and research scientists. Since inception, a lot of micromachining processes have been developed for achieving the mentioned requirements for the products. However, due to the lack of complete understanding of the physical phenomenon behind the processes, such degree of precision, geometrical features, and surface characteristics have not been attained even today. The development of materials with enormous material properties is also playing the influencing factor of these deficiencies. A few research activities have been performed by research scientists to implement novel strategies in micromachining for augmenting these features related to quality, dimensional accuracy, and productivity. Some of the strategies have also been successfully employed in several micromachining techniques.

The present book entitled *Accuracy Enhancement Technologies for Micromachining Processes* attempts to collect research activities in different conventional as well as non-conventional micromachining processes implementing various novel machining strategies for improving the accuracy and features of components. Chapter "Accuracy Improvement in Tool-Based Micromachining" describes the methodologies of accuracy improvement in tool-based micromachining processes such as micro-turning, micro-drilling, and micro-milling for achieving defect-free components and desired surface finish and accuracy. In chapter "Strategies for Improving Performance of Ultrasonic Micromachining Process," the details of technologies of accuracy improvements in ultrasonic micromachining are described with several developments in the process mechanism itself such as rotary USM, workpiece vibration for the intention to achieve a high degree of accuracy and

surface profile. In chapter "Accuracy Improvement and Precision Measurement on Micro-EDM," the details of micro-electrical discharge machining with its performance and operating parameters are described upon which the accuracy of machining depends on. Further, this chapter also deals with discussions on several factors that cause inaccuracies in micro-EDM. Chapter "Improvement of Profile Accuracy in WEDM—A Novel Technique" deals with accuracy improvement techniques in wire electrical discharge machining process for cutting different complex profiles. Authors developed a new method of detection of wire lag phenomenon and proposed mathematical models to compensate for the inaccuracy in profile cutting. Chapter "Laser-based Fabrication of Micro-channels" deals with the description of possibilities of inaccuracies during the generation of micro-channels utilizing high-power laser beam. Authors have also discussed the underwater laser micro-channeling process and techniques to improve the profile accuracy. Chapter "Pulsed Nd:YAG Laser Cutting: Accuracy Improvement and Parametric Influences" describes the possibilities of accuracy improvement during Nd:YAG laser cutting of a variety of materials ranging from metals, non-metals, ceramics, composites, etc, for establishing the reliability of Nd:YAG laser cutting process. Chapter "Improvement in Surface Finish and Geometrical Accuracy by Laser Micro-turning" describes the novel technique to improve the dimensional accuracy and surface finish during micro-turning process utilizing pulsed Nd:YAG laser. Authors have carried out detailed experimental investigation and analysis to improve surface features of laser micro-turning components made of alumina ceramics. "Accuracy Improvement Techniques in Electrochemical Micromachining (EMM)" describes the details of accuracy improvement techniques for micromachining using electrochemical phenomena. Authors have proposed several novel strategies to augment the geometrical accuracy and surface features. Microtool insulation, IEG control, design, and development of microtool have been proposed by the authors. In chapter "Surface Micromachining—Advances and Advanced Characterization Techniques," the accuracy issues in various surface micromachining methods such as photolithography, reactive ion etching, deep reactive ion etching, as well as some advanced methods of micromachining such as focused ion beam fabrication, electron beam lithography, are discussed. Chapter "Generation of Nano-level Surface Finish by Advanced Nanofinishing Processes" presents details of several advanced nanofinishing techniques such as abrasive flow finishing, magnetic abrasive finishing, and magnetorheological abrasive flow finishing for the in-depth understanding of the processes as well as for improving surface characteristics in nano-finishing techniques.

Therefore, the present book offers a comprehensive overview of various micromachining techniques and accuracy improvement techniques/strategies for increasing the value addition of micro- and macro-products. This book will definitely draw innovative and valuable reference to engineers and R&D researchers attached to micromachining processes. Moreover, the book can be used as a reference book for final-year undergraduate engineering courses and a course of micromachining processes at the postgraduate level. Furthermore, this book can

serve as a useful reference for academics, researchers, mechanical, manufacturing, industrial and materials engineers, professionals in micromachining processes, and related industries.

The editors acknowledge Springer for providing this opportunity and for their enthusiastic and professional support. Finally, the editors would like to thank all the chapters' contributors for their availability to complete this work.

Kolkata, India

Golam Kibria
B. Bhattacharyya

Acknowledgements

This book has become a reality due to the constant inspirations and encouragement received from the senior professors and colleagues such as Dr. B. Doloi, Dr. D. Banerjee, Dr. S. Chakraborty, and Dr. B. R. Sarkar of Production Engineering Department, Jadavpur University, Kolkata. The editors would like to convey warm regards to Dr. V. U. Rathod, Dr. Mukandar Sekh, Dr. Shamim Haider for constant support and active participation in preparing the manuscripts of this book.

Financial support from the University Grants Commission (UGC), All India Council for Technical Education (AICTE), Department of Science and Technology (DST), and Council of Scientific and Industrial Research (CSIR) for carrying out research in this area has proved to be useful for utilizing research outcomes to enrich this book.

The editors acknowledge Springer for this opportunity and for their enthusiastic and professional support. The team members of Springer like Anil Chandy, Managing Director, Springer Nature Singapore Pte Ltd., William Achauer, Editorial Director, Business, Economics, Political Sciences and Law—Books, Springer Singapore, Divya Meiyazhagan (Ms.), Project Coordinator, Book Production of Springer Nature, Aninda Bose (Mr.), Senior Editor—Hard Sciences Publishing have put their constant effort in transforming this book into its final shape. Finally, we would like to thank all the chapters' contributors for their availability for this work.

Kolkata, India
September 2019

Golam Kibria
B. Bhattacharyya

Contents

Editors and Contributors

About the Editors

Dr. Golam Kibria is an Assistant Professor in Department of Mechanical Engineering in Aliah University, Kolkata, India. He graduated in Mechanical Engineering from Kalyani Government Engineering College, West Bengal, India. He completed his M.Tech in Production Engineering from Jadavpur University, Kolkata in 2008. He completed Ph.D. Degree from Jadavpur University, Kolkata in 2014. He has worked as Senior Research Fellow (SRF) in Council of Scientific & Industrial Research (CSIR) sponsored Extra Mural Research (EMR) scheme from 2008 to 2011. After one year service in Sikkim Manipal University, Sikkim, India, he joined Aliah University, Kolkata. His research interests include non-conventional machining processes, micromachining and advanced manufacturing and forming technology. He is a life member of The Institution of Engineers (IEI), India. He has several International and National Journal research papers and research papers in reputed national and international conferences proceedings. He has also published several books chapters in different research oriented books (Springer, Elsevier, Nova etc). He has attended various repute Workshops, International and National Conferences and Seminars at various cities of India. He is editorial board member as well as reviewer of a number of reputed international journals.

Dr. B. Bhattacharyya is fellow of Indian National Academy of Engineering (INAE) and Professor and Ex-Head of the Production Engineering Department and Ex-Coordinator of Center of Advance Study (CAS) Programme under University Grants Commission and Quality Improvement Programme under AICTE of Jadavpur University. His research areas include non-traditional machining, micro machining, advanced manufacturing systems, etc. He has published 140 research papers in National and International Journals and 271 research papers in National and International Conferences. He has published several book chapters and conference proceedings. Recently, he has published one book titled “Electrochemical

Micromachining for Nanofabrication, MEMS and Nanotechnology", William Andrew Applied Science Publishers, Micro & Nano Technologies Series, Elsevier Inc, USA. Recently, he published a book "Modern Machining Technology", published from Academic Press. Several PhD theses have been completed under his guidance. He has completed several research projects. He is recipient of various awards, e.g. Gold Medal and Certificate of Achievements for research papers and thesis as well as the Career Award of the UGC, New Delhi.

Contributors

Bappa Acherjee Production Engineering Department, Birla Institute of Technology: Mesra, Ranchi, India

A. Barman Department of Mechanical Engineering, IIT Guwahati, Guwahati, Assam, India

B. Bhattacharyya Production Engineering Department, Jadavpur University, Kolkata, India

M. Das Department of Mechanical Engineering, IIT Guwahati, Guwahati, Assam, India

S. Das Mechanical Engineering Department, Swami Vivekananda Institute of Science & Technology, Kolkata, India

B. Doloi Production Engineering Department, Jadavpur University, Kolkata, India

Girish Dutt Gautam Department of Mechanical Engineering, Jaypee University of Engineering and Technology, Guna, Madhya Pradesh, India

Arjyajyoti Goswami Department of Mechanical Engineering, National Institute of Technology Durgapur, Durgapur, West Bengal, India

Siddhartha Kar Department of Mechanical Engineering, National Institute of Technology Silchar, Silchar, Assam, India

Golam Kibria Mechanical Engineering Department, Aliah University, Kolkata, India

S. Kumar Production Engineering Department, Jadavpur University, Kolkata, India

S. P. Leo Kumar Department of Production Engineering, PSG College of Technology, Coimbatore, India

Dhananjay R. Mishra Department of Mechanical Engineering, Jaypee University of Engineering and Technology, Guna, Madhya Pradesh, India

Promod Kumar Patowari Department of Mechanical Engineering, National Institute of Technology Silchar, Silchar, Assam, India

V. Rathod Mechanical Engineering Department, Government Polytechnic Mumbai, Mumbai, Maharashtra, India

Mukandar Sekh Department of Mechanical Engineering, Aliah University, Kolkata, India

Amit Kumar Singh Department of Mechanical Engineering, National Institute of Technology Nagaland, Dimapur, Nagaland, India

Accuracy Improvement in Tool-Based Micromachining

S. P. Leo Kumar

Abstract The need for micro part is growing drastically because of technology advancement in biomedical, semiconductor, and aerospace industries, etc. Tool-based micromachining is the advanced approach for the production of parts for enhanced functionality with significant size reduction. Part accuracy is dealt with the degree at which the part approximates the true geometrical shape and size. In this chapter, factors that influence the part geometrical and dimensional accuracy in tool-based micromachining are presented. It is divided into six major elements: (a) cutting tool, (b) work material, (c) environment, (d) cutting phenomenon, (e) process parameters, and (f) machine tool. In this study, tool-oriented conventional micromachining processes are considered. The individual sub factors are represented by a fishbone diagram. The influence of parameters and their cause are described with the published literature, and the possible ways for part accuracy improvement in tool-based micromachining are presented.

Keywords Micro drilling · Micro turning · Micro milling · Part accuracy

1 Introduction

The need for microscale (1–500 μm) and meso (500 μm–10 mm) parts with desired functionality is rapidly increasing in various fields include automobile, aerospace, optical, biomedical industries, etc. The products are available in assortment of materials. Micro manufacturing is the advanced approach for recognition of micro product. Earlier time, watch parts are considered as micro part. Current changes because of technology expansion necessitate micro product for various applications such as medical, biomedical equipments, surgery tool, etc. [1].

S. P. Leo Kumar (✉)
Department of Production Engineering, PSG College of Technology,
Coimbatore 641004, India
e-mail: leo.prod@psgtech.ac.in

G. Kibria and B. Bhattacharyya (eds.), *Accuracy Enhancement Technologies for Micromachining Processes*, Lecture Notes in Mechanical Engineering,
https://doi.org/10.1007/978-981-15-2117-1_1

Any part consists of two or more micro features can be termed as micro part according to the definition of micro/meso mechanical manufacturing (4M) association. It clearly defines that the term micro deals with feature but not part size. There are two kinds of micro manufacturing: lithography and non-lithography techniques. Photolithography approach assists micro manufacturing, but has certain disadvantages in developing elevated aspect ratio (AR) structures, more capital investment, and work material limitation [2]. Later approach overcomes the drawback with lithography techniques for the past two decades. It is grouped into mechanical and advanced micromachining, finishing, and forming processes [3]. Achieving the required accuracy and surface finish is the prime requirements in micromachining. Accordingly, it is classified as precision and ultra-precision machining. In precision machining, the accuracy level is of up to 10 μm and surface finish up to 10 nm. In ultra-precision machining, the achievable accuracy is in the order of 1 μm and surface finish value is of <10 nm [4].

Mechanical micromachining deals with machining using micro tools, and it possesses key features over lithography approach such as handling complex product, processing range of materials, cost, and geometrical accuracy. It is grouped into conventional, advanced, and nano finishing techniques [5]. Conventional process includes micro turning, drilling, and milling. Advanced processes are grouped into mechanical, thermal, and chemical energy-related operation [6].

1.1 Accuracy Improvement

Accuracy of a part or machine is dealt with the degree with which it approximates the geometrical shape and size. In general, it is impossible to manufacture a part or machine tool in accordance with geometrical representation. Hence, deviation from the ideal or theoretical values is taken as the measure of accuracy. These deviations will be compared against the permitted value for the actual function of the part or machine [7]. Accordingly, tolerances will be established for all the quality features of a typical micro part or machine tool.

A typical part accuracy consists of various elements include (a) geometrical accuracy, (b) dimensional accuracy, (c) positional accuracy of surfaces, and (d) surface texture. All the elements have significant influence of functionality of micro part or machine tool. The necessity for miniature and micro parts is growing nature, accuracy improvement toward the theoretical or ideal requirements are inevitable in nature. There are three major area that needs development in the field of micro fabrication: (a) process characteristics study, (b) micromachining tool development, and (c) online metrology. Accuracy improvement in micromachining covers broad spectrum and having huge research scope for the development in the field of micromachining.

In this chapter, some fundamental aspects of tool-based micromachining process are introduced. Geometrical and dimensional part accuracy produced by tool-based micromachining greatly affected by workpiece, cutting tool, cutting phenomenon, machining parameters, and plant and machine tool parameters. Effects of major

parameters on accuracy are described with the help of literature. Possible way for enhancement of part accuracy is presented based on published results. Quantum of chapter is based on investigations done by the author's research group.

2 Tool-Based Micromachining

The necessity for concentrated weight, size, and desired surface quality with enhanced accuracy, at reduced component costs from electromechanical equipments to medical tools is the forces driving miniaturization [8]. Tool-based micromachining includes micro turning, drilling, milling, grinding, etc., have many merits include user friendly, less investment cost, precision surface finish with geometrical accuracy, etc. However, challenges associated with processes are yet to be solved as the machining unit is reduced [2]. Accuracy of micromachine tools lacks with ultra-precision machine tools due to deficiency in construction, positioning error, etc. [9]. In this chapter, conventional micromachining processes are considered for part accuracy-related characteristics study. Basic principles behind the process are discussed first, and then overall criteria that affect part accuracy and the possible way for the improvement are presented.

2.1 Micro Turning

Micro turning technique received authoritative research concentration for the development of micro system on diverse engineering materials and alloys. The working principle is similar to conventional turning process. The material removal process possesses certain behavior due to size diminution [5]. Micro turning of tungsten carbide (WC) with polycrystalline diamond tool depicted in Fig. 1.

2.2 Micro Drilling

Mechanical micro drilling is the cost proficient approach for the generation of μm size hole. Work material physical property will not influence the micro drilling operation. Wide group of engineering metals, alloys, and polymers can be processed effectively. Micro drilling investigational setup is depicted in Fig. 2. Processing time can be preserved if appropriate machining parameters are set for micro drilling.

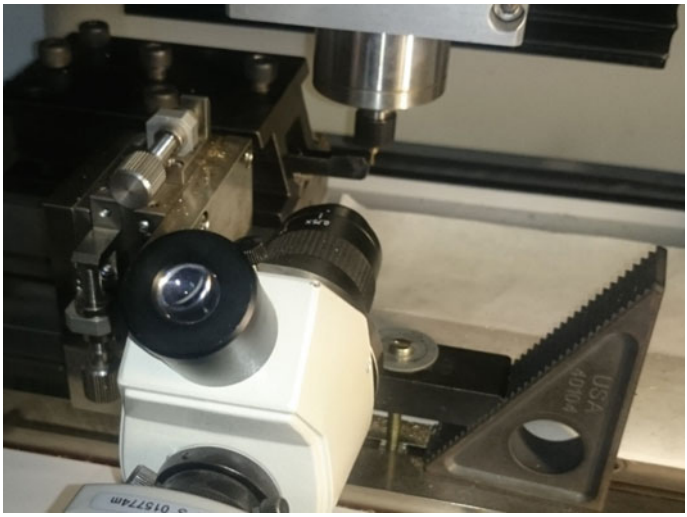

Fig. 1 Micro turning setup with WC insert

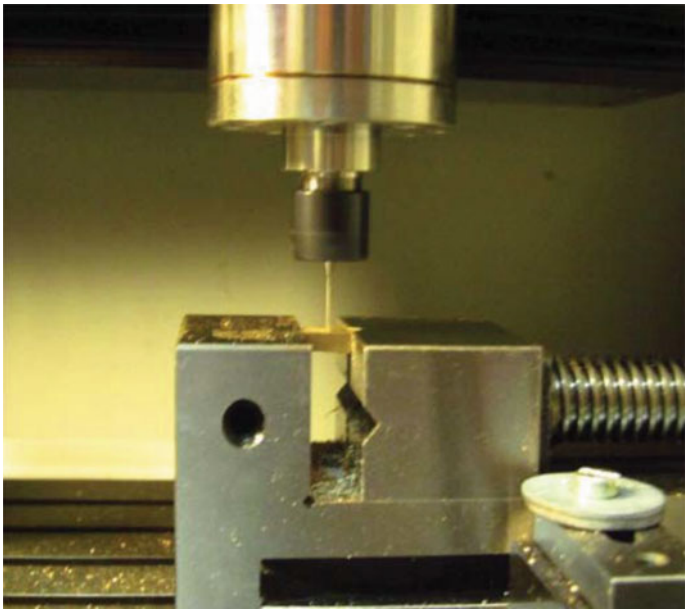

Fig. 2 Micro drilling on brass material [5]

2.3 Micro Milling

Multifaceted 2.5 and 3D micro parts can be produced by micro milling process, and the working principle is analogous to conventional milling operation [10]. Micro milling application includes the production of micro parts in the field of mold making, die, channels, gears, fluidic devices, propellers, etc. It overcomes the difficulties associated with electric discharge machining (EDM) process and grinding processes [11].

End mill and ball nose-type tool made up of WC is commonly employed for milling. Diamond tool is used for machining non-ferrous-type work material. Size up to 100 μm is normally available and up to 25 μm shaped by ion beam machining. Micro milling setup for machining polymethyl methaacrylic (PMMA) material is depicted in Fig. 3. Micro milling has more highlight between all micromachining processes. Since it can achieve desired accuracy, surface finish with high material removal rate (MRR), it is widely used for the production of miniature mold and dies [13].

3 Process Criteria

Part accuracy in tool-based micromachining affected by various factors, since it has direct and indirect influence on geometry and functionality of the micro part. Ishikawa diagram for factors that determines part accuracy is shown in Fig. 4. The inaccuracy in micromachining can arise from serious factors such as elastic deformation in machine, tool, and workpiece deflection due to cutting forces, thermal deformation, wear and tear of cutting tool, work material composition, workpiece distortion due

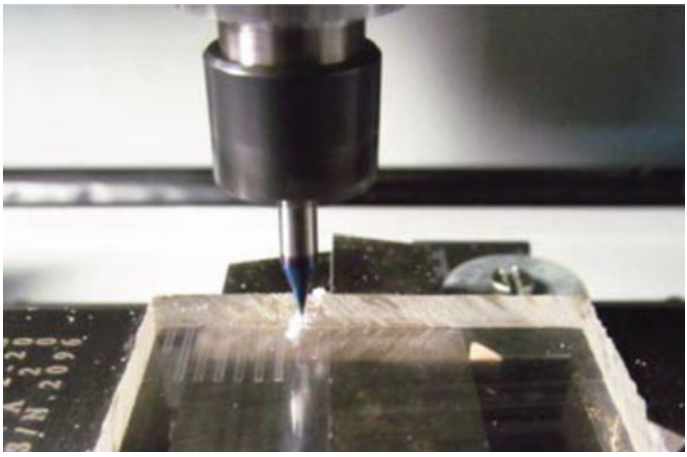

Fig. 3 Micro milling of PMMA material [12]

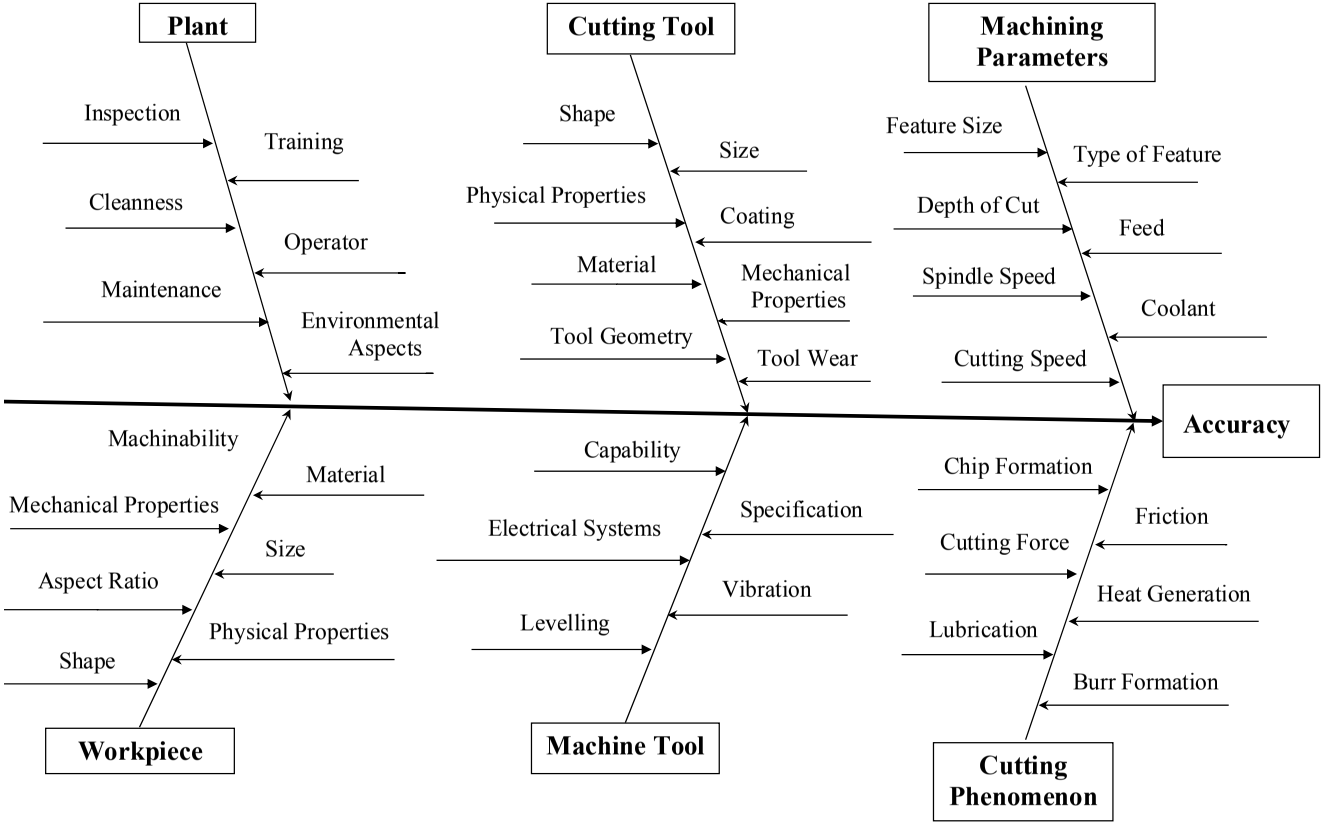

Fig. 4 Ishikawa diagram for accuracy in tool-based micromachining

to clamping force, geometry irregularities in the cutting tool, residual stress in the work material, fluctuations in input parameters, material non-homogeneity, etc. The selection of suitable manufacturing process from micro cutting, milling, micro-EDM, micro-electrochemical machining (ECM), etc. is a challenging task. Geometrical accuracy, aspect ratio, and surface integrity are the characteristics that should be considered while selecting a particular micromachining process [14].

In this chapter, the factors that influence both geometrical and dimensional accuracy are classified into six major categories: (i) plant, (ii) machine tool, (iii) workpiece, (iv) cutting phenomenon, (v) cutting tool, and (vi) machining parameters. Sub elements of each factor have significant impact on part accuracy. Significant number of research work addressed the effect of such factors in tool-based micromachining processes. The generalized Ishikawa diagram for part accuracy covers the major factors of conventional tool-based micromachining processes. Significant functions of independent variables and their influence on part accuracy are discussed in the subsequent section.

4 Cutting Tool

In conventional tool-based micromachining, cutting tool performs machining action on the workpiece to produce desired part geometry. Range of tool material varies from high-speed steel to diamond which depends on the work material characteristics. Size of cutting tool varies from 50 μm to 10 mm, and insert shape and size will vary accordingly. A good cutting tool should permit chip formation and removal from the machining zone, possess sharp cutting edge for minimum cutting force and undeformed chip thickness, proper geometry for minimum friction, and be able to manufacture by robust manufacturing process for economic feasibility. Various factors include tool geometry, shape, size, physical and mechanical properties, geometry, manufacturing methods, tool wear, etc., a have significant influence on accuracy in tool-based micromachining.

4.1 Tool Fabrication

Micro tools include end mill and drill are normally made from WC that has hardness and strength at elevated temperatures. Micro milling tool of size 50 μm is available, and their helix angle is formed by precision grinding [15]. Micro mills are made by grinding method, and their cutting teeth possess considerable effect on performance in terms of tool life and surface quality.

Aurich [16] manufactured end mills with the diameters between 10 and 50 μm with variable helix angle and inferred that grinding is an appropriate method for the production of precision micro milling tool, which combines geometrical accuracy with shorter processing time. Also inferred that it can be possible to machine a

titanium alloy with 20 μm tool size and PMMA with 10 μm tool diameters. Gao et al. investigated failure of cutting edge in grinding of cemented carbide cutter. Width edge damage and surface roughness of teeth flank are measured. Result shows the formation of micro fracture, cracks at the cutting edge, and also micro pit in the grinding surface. Grain size and composition possess an impact on cutting edge failure. Edge damage width increases with addition of cobalt and WC grains [17].

4.2 Tool Geometry

The cutting geometry extensively affects the surface integrity and burr formation. Rounded and chamfered geometries are established as the favorable one for fine surface finish. The recent study reveals that it is indispensable to examine the cutting geometry. The demand for precision micro dies and molds made of tool steel experienced a phenomenal growth due to the demand for micro systems. Tool geometry plays significant job in the assortment of cutting conditions for micromachining of difficult to machine materials. It is a confront task due to shorter tool life in comparison with macroscale machining. Aramacharoen and Mativenga analyzed size effect in H13 steel. It is inferred that optimum surface finish is obtained at the condition at which the depth of cut (a_p) is equal in magnitude with the tool edge radius (ER). The lowest burr size was found when 'a_p' is larger than tool edge radius [18].

Baburaj et al. studied ball end mill ER at normal and transverse planes with the help of kinematic associations in computer-aided design background. Confocal and stereo microscopes were used for ER measurement. Ball end mill geometry was analyzed by virtual sectioning approach in order to study the association between ER in both planes. Real-time cutting ER becomes suitable for transverse plane. The cutting ER in normal plane is computed by applying helix angle correction value at the selected point [19].

4.3 Tool Wear

The tool wear is a key for accuracy and surface quality of micro milled part. Zhu and Yu proposed a tool wear monitoring technique in accordance with tool wear image. In contrast to traditional tool wear width criteria, an algorithm based on Morphological Component Analysis (MCA) was developed to detect and dig out the wear region. It decomposes creative tool image into target and noise image. Experiment result shows that MCA algorithm can effectively extract wear image and indication of wear condition [20]. Filiz et al. demonstrated the capability of the micro milling by generating micro barbs in PMMA with size (width between 68 and 174 μm), edge sharpness (60° and 90°), and height (between 84 and 460 μm) [21].

The low chip thickness to the cutting ER ratio, workpiece hardness, low stiffness of tool and wear leads to increase of tool deflection. It implies that reduction of

accuracy as the tool size is abridged. Bissacco proposed a solution that consists of increased feed per tooth and their effect on cutting force components was appraised in terms of tool deflection and part accuracy [22].

4.4 Coating of Tool

Geometrical accuracy of a workpiece is affected by precision of coating tools. The protection of coated tools is influenced by factors such as interface temperature, force, and strain rates. Uniform coating of micro tool is a complicated task. Aramcharoen reported wear mechanism in coated micro milling tool on machining of tool steel. Physical vapor deposition coating was examined based on numerous tool wear criteria and inferred that TiN coating ensures best performance with minimum tool wear and better surface quality [23].

Coating plays significant role in part accuracy even though the tool substrate is in high-dimensional accuracy. Sui et al. performed TiAlTaN/Ta coating on cemented carbide tool by sputtering technique. Scanning electron microscope analysis exposed that growth of Ti–Al–Ta–N crystals is broken up by layered design. There is an increase in coating hardness with decreased bilayer thickness [24].

4.5 Tool Deflection and Failure

Erratic tool life and early tool breakdown are a major problem that affects the part accuracy significantly. The rigidity of D-type mill is superior than two flute end mill when the diameter is below 100 μm. Machining quality is better than triangular-type end mills that has large negative rake angle [25]. Tool deflection seriously affects chip formation and part accuracy in micromachining [26]. Chae et al. observed that cutting marks because of run out contribute surface finish and newer tool holder design may resolve the problems [27]. Rivin also reported that passive or active control of tool holder is necessary to pay off for vibration and run out [28].

Drill nomenclature in relation to feature size will affect the accuracy considerably [29]. Positional accuracy of micro tool influences hole positioning, while repeatability influences the shape and size of hole. High strength work materials demand for drill bit with exceptional positional accuracy and tool life for printed circuit board application. Factor that concerns the drilling accuracy is the forces that acting on the drills that cause drill breakage. Since the strength is lower than cutting force, the tool failure occurs. Condition monitoring during its pre-failure phase will help to predict the failure in advance to eliminate inaccuracy in micro drilling operation.

5 Machining Parameters

Process parameters have significant influence on part accuracy fashioned by tool-based micromachining. Process variable includes cutting speed, spindle speed, number of pass, feed rate, depth of cut, feature size, coolant, etc. Unique process parameters should be incorporated for specific micromachining processes in order to achieve specific geometrical and surface finish requirements. Micromachine tools are capable enough to produce precision micro part but not intelligent enough to choose appropriate process parameters. Significant amount of research work exemplified to develop optimum parameters and their influence on part accuracy and performance. Higher peripheral speed is commonly used for micromachining, and computer numerical control (CNC) programming is used for the control of tool path accurately.

End milling has significant effect on surface integrity due to heat generation at the cutting zone. Masmiati et al. performed end milling on S50C steel and inferred that combination of high cutting speed, low 'a_p,' and intermediate feed condition yields less cutting force. Feature depth has significant influence on part accuracy. Appropriate feed rate controls the hole quality and tool breakage [30]. Micro drill characteristics influence the machining accuracy, and process variables affect the process quality. Other factors include drill size, endurance limit of tool, alignment, pecking order, and lubrication effect to be optimized for better quality holes.

Periyanan et al. incorporated Taguchi technique for the maximization of MRR. Spindle speed ranges between 60,000 and 80,000 rpm. It is inferred that medium cutting speed, high feed, and 'a_p' conditions are the optimum parameters for aluminum (Al) [31]. Lekkala et al. presented the authority of process variables include peripheral speed, tool diameter, flute number, feed rate, and 'a_p' on burr formation in milling of Al2124 and SS-304 material with WC tool of size 300 μm and 400 μm, respectively. It is inferred that 'a_p' and the tool diameter influence burr size. However, feed rate and speed have negligible effect [32]. Leo Kumar et al. exemplified micro drilling on brass material and micro milling on PMMA and resulted that amalgamation of medium 'v_c' and feed rate leads to fine surface finish [33].

5.1 Built-Up Edge Effects

Built-up edge (BUE) formation significantly affects surface quality. Free particles due to BUE formation affect surface finish. Stable BUE can guard the tool from wear that obstruct micromachining operation. Oliaei and Karpat investigated the association between BUE in micro milling of Ti–6Al–4V alloy. The relationship between tool geometry, surface finish, and cutting force was studied. It is inferred that optimum selection of feed and 'a_p' condition is an important reflection for stable BUE formation [34].

5.2 Cutting Temperature

As machining temperature increases, tools become softer and wear more, ultimately it shortens tool life and part accuracy. Relatively, larger feed rate and small 'a_p' should be incorporated to ensure minimum cutting temperature. Cui and Guo inferred that feed rate and 'a_p' possess special effects on heat flux during chip formation [35].

5.3 Cutting Fluids

Cutting fluid is used to reduce the efforts of friction. Cutting fluids are also used to remove heat from the cutting zone that causes damage to the microstructure [36]. The result of high cutting temperature is a premature failure of the tools in the cutting zone and causes poor dimensional accuracy. Proper use of coolants helps to improve the part quality and dimensional accuracy.

6 Workpiece Characteristics

Work material characteristics have significant effect on part dimensional accuracy. It includes parameters such as material type, physical and mechanical characteristics, size, and shape. Due to size reduction, the part functionality is influenced by the material property. Robinson and Jackson carried out review of micromachining in materials perspective [37]. High-quality requirements concerning dimensional accuracy, shape, and surface finish must be fulfilled, when cutting high performance materials [38]. Sekulic et al. performed face milling on EN42CrMo4 steel, EN-GJS-500-7 nodular cast iron and inferred that work material hardness and tensile significantly influence the cutting force. Other material properties include microstructure, crystal grain size and shape, and type and amount of impurities also exert influence on the main cutting force [39]. Machining of wear-resistant materials necessitated the use of drill with positioning accuracy and long tool life [29]. Work material property determines cutting conditions suitable for desired surface quality. Investigation on miniature milling C360 copper alloy under dry cutting condition resulted that amalgamation of low spindle speed and feed rate conditions yields fine surface finish, Leo Kumar [40].

6.1 Material Structure

Material grain size plays an imperative task on edge radius effect for achieving high-quality surface finish in micromachining. Surface integrity is mainly affected by ER

of the tool. Material microstructure influences the edge radius effect, and surface finish varies for same cutting conditions with different work materials according to its physical and mechanical properties [41]. Attanasio et al. analyzed the influence of Ti–6Al–4V alloy in terms of microstructure which includes bimodal, lamellar, fully equiaxed, and annealed type that are analyzed. The mechanical sample properties were assessed by micro hardness test. It is inferred that minimum cutting force and tool wear are observed with fully lamellar microstructures [14].

Brittle materials micro fabrication is one of the thrust areas for micro cutting. Ductile mode machining at low 'a_p' is normally preferred for machining brittle materials, and it can be machined in ductile fashion, while machining below the critical 'a_p' with desired accuracy [42].

7 Cutting Phenomenon

Cutting phenomenon is generally unpredictable and complex in nature in actual machining conditions. The factors include chip formation, cutting force, burr formation, friction, heat generation, lubrication, size effect, energy consumption, etc. Significant amount of work is presented in the recent scenario.

Rigidity of the machine tool parts is important since that affects surface accuracy. However, it is not ensured by conventional quick stop devices. Hence, the cutting stability and DOC would be affected. Consideration of proper quick stop devices will enhance the part accuracy [43].

7.1 Size Effect

Size effect plays a significant role for accuracy improvement in micromachining. Tool geometry, grain size, and orientation become dominant factors as the unit material removal rate decreases and it strongly influences accuracy and surface integrity [8]. There is a connection between chip thickness and cutting ER on machining accuracy, and it will vary with work material. There is a critical 'a_p' below which surface finish gets reduced. When the unit MRR size decreases, tool geometry and machining variables become foremost factors that strongly persuade resulting accuracy [44]. Shimada et al. carried out molecular dynamic simulation to decide attainable accuracy. It is observed that chip thickness is to be 5% of cutting ER for Cu and Al alloy [45]. Yuan et al. performed diamond turning on Al alloys and inferred that chip thickness fluctuates with ER, work material and type of machining process [46].

7.2 Cutting Force

Cutting force has significant influence on geometrical and dimensional accuracy. High machining force limits the part accuracy due to workpiece and tool deflection. Tool wear also influences the cutting forces [47]. Zhang et al. investigated the consequence of ER, size effect, tool deflection, run out and flute profile that cause uneven cutting force. The cutting force is considerably predisposed by run-out. However, tool deflection shows the way for the reduction of run out on cutting forces, particularly in 'x' and 'y' axis [48].

The control of reacting force is a predominant factor for accuracy improvement. The cutting force should be lower than reaction force in order to prevent the workpiece deflection and it is the major bottleneck in micromachining that affects the precision [49]. Step cutting is normally incorporated to prevent work deflection in micro turning [50].

7.3 Heat Generation

Heat generation due to tool and workpiece interaction in micro cutting has considerable effects on machining accuracy. Hence, special consideration should be given in order to minimize heat generation. Moriwaki et al. observed that the pattern of temperature raise and machining error is based on tool feed direction. When the feed direction is from workpiece circumference to the center, there is a sudden temperature raise and drop. If the tool is fed in the opposite direction, there is a gradual increase in temperature. Frequent tool replacement will reduce the heat generation [51].

7.4 Burr Formation

Burrs are undesirable since that cause tool breakage, jamming, misalignment and reduce work and tool life. In drilling operation, burr is normally generated at entrance and exit of feature surface. Entrance burr is formed due to plastic flow and exit burr due to protrusion of work material at exit surface [29]. Deburring is the process of removal of burr that becomes highly challenging one in micro drilling. The burr leads to drill run out that affect the hole superiority. The factors such as cutting speed, feed per revolution, drill wear, and material affect the burr size.

8 Plant Factors

There are some miscellaneous parameters that affect part dimensional and geometrical accuracy in direct as well as indirect manner. It includes factors such as environmental effect, inspection, maintenance, measurement uncertainty, cleanliness, type of operator, and quality of training. The demand for measurement accuracy increases for applications ranging from simple geometry to highly complicated free form surfaces. Measurement system and their resolution play a major in determining part feature accuracy as the feature size decreases. Appropriate measurement system is inevitable for decision making and to take corrective action against part quality.

Machining environment significantly affects the machining accuracy. Environment-friendly techniques can enhance the part accuracy. Warmness environment will try to expand the work material and machine elements, Fratila [52]. Environmental impact not only includes machining process but also includes associated process such as material preparation and cutting fluid preparation. [53]. Expertise of the operator will significantly influence the machining operation and the related product quality. Since process capability of the machine tools varies due to dynamic changes in the environment, period inspection is major requirements in order to maintain part accuracy. Measurement uncertainty can be mitigated by implementing automated inspection.

9 Machine Tool Characteristics

Characteristics of the machine tool have significant influence on part geometrical and dimensional accuracy over other factors, since the machine tool is the one producing the part with required precision [54]. Precision of a machine tool is characterized by the capability to fabricate part with required geometry by keeping the tolerances within the acceptable limits. The shape, position, and movement of individual parts of the machine tool should be within the precision level to ensure part geometrical accuracy. Micro part quality depends on machine tool characteristic including its accuracy and lively performance. Various factors include rigidity, process capability, specification, etc. The machine tool capability is essential in order to achieve product requirements include accuracy, finish, and repeatability [27].

Hybrid machining can effectively increase machining accuracy. Asad et al. performed turning-EDM in which EDM was performed in micro shaft fabricated by micro turning process. It reduces clamping error, electrode deflection and consequently improved the machining accuracy [2]. Micromachine tool has the capability to produce different shapes and to process different part, and machine tool dimension has significant influence on part accuracy. It includes straightness and flatness of guide surface, clamping forces, parallelism of axes and guides, etc. [54]. The size of micromachine tool determines the accuracy of micro features. Miniature machine

tool possesses minimum static stiffness due to short structure and normal dynamic stability [15].

Precision machine tools lack in self decision-making capability and purely depend on expertise working with the machine tool. Implementation of artificial intelligence (AI) approach can assist autonomous judgment in manufacturing planning for precision micro part production. Leo Kumar et al. fashioned an intelligent system for manufacturing planning for micro parts. DT110 micromachine tool specification is taken into the consideration, and the manufacturing logic behind micro part development is formulated in terms of knowledge base. Visual studio based application development environment used for system development, integrated with machine tool and validated with a case study implementation [55].

CNC code generation is the final activity of a typical CAD/CAM system. In actual practice, CNC code generation is carried out as a discrete activity in shop floor environment in most of the industries. Tool path generation based on process plan information can ensure the production of precision micro part, thereby it ensures true CAD/CAM integration. Leo Kumar et al. developed a system tool path generation for micro and miniature feature production based on 2.5 dimensional micromachining. Decision-making system was developed for automatic tool path generation based on part feature generation, process parameters, and material information [56].

9.1 Position Measurement and Process Monitoring

Positional accuracy has significant consequence on finished parts accuracy. Mijuskovic et al. incorporated pitch error compensation method for accuracy improvement on precision micro milling center. Laser interferometer was used for positional accuracy measurement, repeatability was calculated as per ISO 230-2 standard, and the measurement uncertainty was estimated for all the axes [57].

Sensor-based process monitoring and control can be incorporated for micromachining. However, manufacturing process characterization is necessary for implementation of sensor for monitoring. Laser encoders are appropriate for position measurement due to high resolution. Process monitoring can be applied to vibration, temperature, and cutting force to enhance micromachining process. The parameters such as tool breakage, wear, and surface damage cannot be measured directly. Hence, monitoring based on acoustic emission, force, and vibration signals can be employed. Advanced control systems are used in ultra-precision machine tool [44].

9.2 Vibration

Ultra-precision machine tools fabricate precision product with nanometer-level tolerances/surface finish. Hence, machine tool vibration and residual vibration stemming should be minimized with the help of proper isolation system. Lee and Okwudire

analyzed the influence of mode coupling on vibration minimization. A rule of thumb was used to locate the isolators such that vibration modes are decoupled [58].

Zhang et al. analyzed vibration characteristics such that active vibration can suppress passive vibration to enhance the surface finish. Air bearings used in ultra-precision machine tool require high accuracy. The fluctuations in compressed air being send to the bearing cause air turbulence that leads to micro vibration [59]. Kawai incorporated laminarization concept for optimal piping design and air bearing surface in order to suppress micro vibration [60]. Numerical control equipment setup, on the degree of contouring errors and smoothness of the movement has influence on the part accuracy [61].

Chucking is a bottleneck during turning in the form of workpiece accuracy. Hence, there is a strong need for hard turning for the production of precision components. Byun and Liu identified the factors include alignment error, kinematic redundancy, locating surface selection and demonstrated the methods to minimize the factors influencing accuracy and repeatability. It is inferred that 20 and 30 times enhancement in accuracy and repeatability was achieved [62].

10 Current and Future Challenges

Technology growth enforces part production with enhanced functionality and significant reduction in size. Many challenges are associated with the production of micro and miniature parts, in which accuracy improvement is having a major scope for improvement. In this chapter, tool-based micromachining processes and their influence on part accuracy are presented. The factors associated with accuracy are divided into six major elements: It includes machine tool, cutting phenomenon, process parameters, workpiece, cutting tool and plant effects. The factors specific effect on part dimensional and geometrical accuracy are analyzed and their outcomes are presented.

10.1 Future Challenge

Machine tool improvement, on machine micro/nano metrology, and process development are required to achieve desired accuracy and surface finish [2]. High-dimensional accuracy while fabricating microstructures can be achieved by hybridizing conventional material removal processes with advanced machining processes like EDM, ECM, etc. Provision for closed loop control and error reparation will ensure high accuracy in micromachine tool.

Part accuracy and surface finish are directly related to machine tool in which problems include tool wear, deflection, chatter, etc., leads to surface weakening [44]. To

minimize tool wear and thermal loads, proper cutting fluid needs to be applied effectively. Machine tool should have characteristics that include high stiffness, thermal stability, accurate drive system, and short response time.

10.1.1 Cutting Tool and Process Parameters

Size effect should be controlled such that (a_p) should be equal to tool radius in order to ensure good surface finish. Cutting geometry significantly influences surface finish and burr formation. Tool material in relation to work material and tool wear affects the geometrical and surface integrity. Type of coating and their thickness should be controlled critically. Cutting force needs be minimum to minimize workpiece and tool deflection.

Process parameters should be controlled critically. In general, the amalgamation of high (v_c), medium feed rate, and low (a_p) yields minimum cutting force to ensure geometrical accuracy. Appropriate feed rate and pecking order control the hole quality and tool breakage in micro drilling. Higher spindle speed should be maintained irrespective of other parameters to ensure geometrical and dimensional accuracy. Since burr formation is inevitable in micro milling, incorporation of optimum process parameters is necessary. Stable BUE formation can protect the tool against wear and ensure good surface finish when appropriate parameters were set. Incorporation of proper coolants can help improve part quality and dimensional accuracy. Hence, higher productivity and machinability can be considered for increased tool life, surface finish, and size accuracy. Machining parameters optimization in relation to work material properties can reduce the cutting force significantly. Thereby, it improves part accuracy [63].

10.1.2 Workpiece Characteristics and Cutting Phenomenon

Work material hardness and tensile strength have a considerable effect on cutting force. Material grain size plays an imperative role on the edge radius effect for achieving high-quality surface finish in micromachining. Ductile mode machining is best suitable for machining brittle material with desired accuracy and surface finish.

Size effect should be controlled critically. Cutting force has direct influence on heat generation, tool wear, geometry, and quality of the finished surface. Reaction force should be controlled critically. Tool and workpiece temperature rise need to be controlled with the help of coolant. Burr formation is to be controlled by using appropriate cutting parameters. Incorporation of step cutting process will minimize the deflection considerably, thereby it will enhance the part accuracy [64].

10.1.3 Machine Tool and Environment

Fundamental dimension of a micromachine tool includes flatness and straightness of guide surface, clamping forces, parallelism of axes and guides, etc., need to be controlled effectively for part accuracy improvement. Micro vibration of air bearing used in precision machine tool is to be suppressed effectively. Positional accuracy of micromachine tool is to be controlled to ensure part dimensional accuracy. Incorporation of advanced control system including adaptive control can achieve nm level control resolution. The machine tool should have accuracy at nm level to perform ultra-precision machining. It can be achieved by ensuring necessary features to machine tool such as vibration stability, air bearing spindles, and closed loop controller with precision feedback system. Fusion of CAD/CAM system and intelligent system into tool-based micromachining will enhance the capability to produce precision micro parts.

Part quality depends on machine tool properties including accuracy and dynamic performance. Thermal compensation of machine tool and workpiece needs to be investigated. Sophisticated systems are required to look at accuracy and part quality. For higher-speed requirement, air bearing spindles with air turbines are generally used. Air bearing spindle that exceeds 200,000 rpm is commercially available. High accuracy in table movement is necessary in precision micromachining. Vibration isolation provided by granite base will enhance the hole quality. Micromachining high-speed spindle with hydrostatic bearing enhances the dynamic characteristics of the spindle, thereby enhances hole quality. Linear motor direct drives will provide better stiffness, smoothness, and accuracy. Piezoelectric actuators can be employed for fine tool positioning. Miscellaneous parameters include environment, maintenance of the machine tool, type of operator, and training and noise factors to be monitored and controlled to ensure desired geometrical and dimensional accuracy.

Since the requirements for micro parts are growing in personality, always there is a scope for accuracy improvement in tool-based micromachining. Incorporation of all the factors will be helpful to meet the requirements of micro part in terms of enhanced functionality and production with desirable quality.

References

1. Masuzawa T (2000) State of the art of micromachining. CIRP Ann Manuf Technol 49:473–488
2. Asad ABMA, Masaki T, Rahman M, Lim HS, Wong YS (2007) Tool-based micro-machining. J Mater Process Technol 192–193:204–211
3. Piljek P, Keran Z, Math M (2014) Micromachining—review of literature from 1980 to 2010. Interdisc Description Complex Syst 12:1–27
4. Taniguchi N (1983) Current status in and future trends of ultra precision machining and ultra fine material processing. CIRP Ann 2:573–582
5. Leo Kumar SP, Jerald J, Kumanan S, Prabakaran R (2014) A review on current research aspects in tool-based micromachining processes. Mater Manuf Processes 29:1291–1337
6. Jain VK (2011) Introduction to micromachining. Narosa Publishing House, New Delhi
7. Murty RL (2005) Precision engineering in manufacturing. New Age International, New Delhi

8. Dornfeld D, Min S, Takeuchi Y (2006) Recent advances in mechanical micromachining. CIRP Ann Manuf Technol 55:745–768
9. Okazaki Y, Mishima N, Ashida K (2004) Micro factory—concepts, history and developments. J Manuf Sci Eng 126:837–844
10. Filiz S, Conley CM, Wasserman MB, Ozdoganlar OB (2007) An experimental investigation of micro-machinability of copper 101 using tungsten carbide micro-endmills. Int J Mach Tools Manuf 47:1088–1100
11. Malekian M, Park SS, Jun MB (2009) Modeling of dynamic micro-milling cutting forces. Int J Mach Tools Manuf 49:586–598
12. Leo Kumar SP, Jerald J, Kumanan S, Aniket N (2015) Process parameters optimization for micro end-milling operation for CAPP applications. Neural Comput Appl 25:1941–1950
13. Lauro CH, Brandão LC, Panzera TH, Davim JP (2015) Surface integrity in the micromachining: a review. Rev Adv Mater Sci 40:227–234
14. Attanasio A, Gelfi M, Pola A, Ceretti E, Giardini C (2013) Influence of material microstructures in micromilling of Ti6AL4V alloy. Materials 6:4268–4283
15. Cox D, Newby G, Park HW, Liang SY (2004) Performance evaluation of a miniaturized machining center for precision manufacturing. ASME International Mechanical Engineering Congress and Exposition, Anaheim, CA
16. Aurich JC, Reichenbach IG, Schüler GM (2012) Manufacture and application of ultra-small micro end mills. CIRP Ann Manuf Technol 61:83–86
17. Gao P, Liang Z, Wang X, Zhou T, Li S, Zhang S, Liu Z (2017) Cutting edge damage in grinding of cemented carbides micro end mills. Ceram Int 43:11331–11338
18. Aramcharoen A, Mativenga PT (2009) Size effect and tool geometry in micromilling of tool steel. Precis Eng 33:402–407
19. Baburaj M, Ghosh A, Shunmugam MS (2017) Study of micro ball end mill geometry and measurement of cutting edge radius. Precis Eng 48:9–17
20. Zhu K, Yu X (2017) The monitoring of micro milling tool wear conditions by wear area estimation. Mech Syst Signal Process 93:80–91
21. Filiz S, Xie L, Weiss LE, Ozdoganlar OB (2008) Micromilling of microbarbs for medical implants. Int J Mach Tools Manuf 48:459–472
22. Bissacco G, Hansen HN, De Chiffre L (2005) Micromilling of hardened tool steel for mould making applications. J Mater Process Technol 167:201–207
23. Aramcharoen A, Mativenga PT, Yang S, Cooke KE, Teer DG (2008) Evaluation and selection of hard coatings for micro milling of hardened tool steel. Int J Mach Tools Manuf 48:1578–1584
24. Sui X, Li G, Jiang C, Gao Y, Wang K, Wang Q (2017) Improved surface quality of layered architecture TiAlTaN/Ta coatings for high precision micromachining. Surf Coat Technol 320:298–303
25. Fang FZ, Wu H, Liu XD, Liu YC, Ng ST (2003) Tool geometry study in micromachining. J Micromech Microeng 13:726
26. Ilan A, Mehmet A (2016) Micromachining. Int J Mech Prod Eng 4:23–25
27. Chae J, Park SS, Freiheit T (2006) Investigation of micro-cutting operations. Int J Mach Tools Manuf 46:313–332
28. Rivin EI (2000) Tool structure-interface between cutting edge and machine tool. Ann CIRP 49:591–600
29. Hyacinth Suganthi X, Natarajan U, Ramasubbu N (2015) A review of accuracy enhancement in microdrilling operations. Int J Adv Manuf Technol 81:199–217
30. Masmiati N, Sarhan AAD, Hassan MAN, Hamdi M (2016) Optimization of cutting conditions for minimum residual stress, cutting force and surface roughness in end milling of S50C medium carbon steel. Measurement 86:253–265
31. Periyanan P, Natarajan U, Yang S (2012) A study on the machining parameters optimization of micro-end milling process. Int J Eng Sci Technol 3:237–246
32. Lekkala R, Bajpai V, Singh RK, Joshi SS (2011) Characterization and modeling of burr formation in micro-end milling. Precis Eng 35:625–637

33. Leo Kumar S, Jerald J, Kumanan S (2015) Feature-based modelling and process parameters selection in a CAPP system for prismatic micro parts. Int J Comput Integr Manuf 28:1046–1062
34. Oliaei SNB, Karpat Y (2017) Built-up edge effects on process outputs of titanium alloy micro milling. Precis Eng 49:305–315
35. Cui X, Guo J (2017) Effects of cutting parameters on tool temperatures in intermittent turning with the formation of serrated chip considered. Appl Therm Eng 110:1220–1229
36. Sharma H, Sharma M (2014) Influence of cutting fluids on quality and productivity of products in manufacturing industries. Int J Eng Manage Sci 1:8–11
37. Robinson G, Jackson M (2005) A review of micro and nanomachining from a materials perspective. J Mater Process Technol 167:316–337
38. Denkena B, Hasselberg E (2015) Influence of the cutting tool compliance on the workpiece surface shape in face milling of workpiece compounds. Procedia CIRP 31:7–12
39. Sekulić M, Jurković Z, Hadžistević M, Gostimirović M (2010) The influence of mechanical properties of workpiece material on the main cutting force in face milling. Metalurgija 49:339–342
40. Leo Kumar SP (2018) Experimental Investigation and empirical modeling for optimization of surface roughness and machining time parameters in micro end milling using Genetic Algorithm. Measurement 124:386–394
41. Rahman MA, Amrun MR, Rahman M, Kumar AS (2016) Influence of material grain size on tool edge radius effect and observations on 'burnishing-like' mechanism in micro turning
42. Takeuchi Y, Sawada K, Sata T (1996) Ultraprecision 3d micromachining of glass. CIRP Ann Manuf Technol 45:401–404
43. Woon KS, Rahman M, Neo KS, Liu K (2008) The effect of tool edge radius on the contact phenomenon of tool-based micromachining. Int J Mach Tools Manuf 48:1395–1407
44. Piljek P, Keran Z, Math M (2014) Micromachining. Interdisc Description Complex Syst 12:1–27
45. Shimada S, Ikawa N, Tanaka H, Ohmori G, Uchikoshi J, Yoshinaga H (1993) Feasibility study on ultimate accuracy in microcutting using molecular dynamics simulation. CIRP Ann Manuf Technol 42:91–94
46. Yuan Z, Zhou M, Dong S (1996) Effect of diamond tool sharpness on minimum cutting thickness and cutting surface integrity in ultraprecision machining. J Mater Process Technol 62:327–330
47. Alting L, Kimura F, Hansen HN, Bissacco G (2003) Micro engineering. CIRP Ann Manuf Technol 52:635–657
48. Zhang X, Ehmann KF, Yu T, Wang W (2016) Cutting forces in micro-end-milling processes. Int J Mach Tools Manuf 107:21–40
49. Lu Z, Yoneyama T (1999) Micro cutting in the micro lathe turning system. Int J Mach Tools Manuf 39:1171–1183
50. Rahman MA, Rahman M, Kumar AS, Lim HS, Asad ABMA (2006) Development of micropin fabrication process using tool based micromachining. Int J Adv Manuf Technol 27:939–944
51. Moriwaki T, Horiuchi A, Okuda K (1990) Effect of cutting heat on machining accuracy in ultra-precision diamond turning. CIRP Ann Manuf Technol 39:81–84
52. Fratila D-F (2013) Research of environment-friendly techniques influence on gear accuracy in context of sustainable manufacturing
53. Dahmus JB, Gutowski TG (2004) An environmental analysis of machining
54. Kuric I, Jozwik J, Tofil A (2013) Quality of CNC machine tools and monitoring of their accuracy. In: Expert conference with international participations "QUALITY 2013", Neum, pp 609–614
55. Leo Kumar S, Jerald J, Kumanan S (2014) An intelligent process planning system for micro turn-mill parts. Int J Prod Res 52:6052–6075
56. Leo Kumar SP (2017) Automation of tool path generation in multi-process micromachine tool for micromachining of prismatic and rotational parts. Int J Comput Integr Manuf 1–22
57. Mijušković G, Krajnik P, Kopač J (2013) Improvement of positional accuracy of precision micro milling center using pitch error compensation. Tech Gaz 20:629–634

58. Lee J, Okwudire CE (2016) Reduction of vibrations of passively-isolated ultra-precision manufacturing machines using mode coupling. Precis Eng 43:164–177
59. Zhang SJ, To S, Zhang GQ, Zhu ZW (2015) A review of machine-tool vibration and its influence upon surface generation in ultra-precision machining. Int J Mach Tools Manuf 91:34–42
60. Kawai T, Ebihara K, Takeuchi Y (2005) Improvement of machining accuracy of 5-axis control ultraprecision machining by means of laminarization and mirror surface finishing. CIRP Ann Manuf Technol 54:329–332
61. Biris C, Bologa O, Girjob C (2015) Researches on improving the manufacturing accuracy of CNC cutting machines. Buletinul AGIR 2:52–56
62. Byun J, Liu CR (2004) Methods for improving the accuracy and repeatability in the position of a workpiece in chucking, pp 122–127
63. Senthilkumar V, Muruganandam S (2012) State of the art of micro turning process. Int J Emerg Technol Adv Eng. ISSN 2250–2459
64. Rahman M, Lim HS, Neo KS, Senthil Kumar A, Wong YS, Li XP (2007) Tool-based nanofinishing and micromachining. J Mater Process Technol 185:2–16

Strategies for Improving Performance of Ultrasonic Micromachining Process

B. Doloi, S. Kumar, S. Das and B. Bhattacharyya

Abstract Advanced materials are not easy to machine due to technological and industrial development and which discover extensive applications in nuclear engineering, aviation industries, etc. The manufacture of complex shape with high-quality surface finish and superior accurateness can be easily obtained by nonconventional machining processes. This manuscript covers the significant issues about the performance improvement of ultrasonic micromachining process. This book chapter also focuses on accuracy of ultrasonic micromachining process with process development. The two types of ultrasonic micromachining processes, i.e., stationary USM and rotary USM, are also discussed. Novel development for accuracy on ultrasonic micromachining (USMM) process has been emphasized and discussed. Strategies for development of ultrasonic micromachining system for performance enhancement are discussed for both stationary and rotary ultrasonic micromachining in this chapter. Micro-type tools developments for ultrasonic micromachining process with various strategies have been presented. In this section, influences of process parameters of USMM on different responses have been studied.

Keywords Ultrasonic micromachining · Transducer · Horn · Micro-tool · Taper angle · Micro-channel

B. Doloi · S. Kumar (✉) · B. Bhattacharyya
Production Engineering Department, Jadavpur University, Kolkata 700032, India
e-mail: santosh14fiem@gmail.com

B. Doloi
e-mail: bdoloionline@rediffmail.com

B. Bhattacharyya
e-mail: bb13@rediffmail.com

S. Das
Mechanical Engineering Department, Swami Vivekananda Institute of Science & Technology, Kolkata 700145, India
e-mail: somnath96@gmail.com

G. Kibria and B. Bhattacharyya (eds.), *Accuracy Enhancement Technologies for Micromachining Processes*, Lecture Notes in Mechanical Engineering,
https://doi.org/10.1007/978-981-15-2117-1_2

1 Introduction

Recent concept of manufacturing is utilizing sources of energy like light, sound, chemical, electrical, electrons, mechanical and ion beams. Rapid advancement in the material science area has lead to innovative brittle and hard materials like glass, composite, high tech ceramics materials, etc. These materials have high-quality mechanical properties and thermal characteristics. With the technological and industrial development, these materials are not easy to machine, and it also finds an ample range of extensive applications in nuclear engineering, aviation industries, etc. Nonconventional machining has developed to machine these advanced materials. The complex shape with high accurateness and good quality surface finish can be fabricated by utilizing nonconventional machining.

Efficient micromachining methods with higher accuracy are demanded for producing parts in micro-electro-mechanical system (MEMS), biomedical, chemical and optical systems [1–3]. In present scenario, producing miniaturized components and microstructures is the main target but at the same time, accuracy improvement must be focused [1]. Micro-engineering methods originate from conventional manufacturing procedures by reducing the machining part to the microscale. Nonconventional machining process approximating micro-EDM and micro-ECM, etc. cannot make the correct profile and dimension on hard and brittle materials. Irregular, square, complex type holes and surface impressions on those materials are also not possible using other nontraditional machining methods. Ultrasonic micromachining process can be employed for this reason. Acceptable finish of surface with exact dimensions and close tolerances on hard and fragile materials can be attained through USMM procedure [4]. Every brittle and hard material is able to machined using USMM process [5].

Various investigations have been explained in m USMM process. Novel developments for accuracy on ultrasonic micromachining (USMM) process with various strategies have also been discussed. Detail description of various types of ultrasonic micromachining setup and removal of work material technique has discussed here. Micro-tools developments with various strategies for USMM process have also been presented. This chapter also describes the influences of USMM process parameters for various responses. Improvements in machining rate and exact geometrical features generation in USMM have also been explored. USMM mainly comes from macro-type USM, which has been previously explored experimentally and described broadly. Ultrasonic micromachining is the most excellent nonconventional machining method for creating micro-features on nonconductive, fragile and hard materials without thermal damage. Ultrasonic micromachining process utilizes a micro-tool which vibrates at ultrasonic frequency (generally, 20 kHz and sometimes more than 35 kHz) to force abrasive particle to hit workpiece material and erode it. Stationary and rotary ultrasonic micromachining processes are applied for generation of different machining procedures such as micro-cutting, micro-drilling, micro-groove, micro-slot, micro-channel, etc. Various strategies have been adopted to increase the performance of ultrasonic micromachining process.

2 Basic Principle of Ultrasonic Micromachining (USMM) Process

The basic principle of ultrasonic micromachining (USMM) is similar to USM but the micro-tool is used in USMM for micromachining applications. The micro-tool of USMM process is vibrated with ultrasonic frequency about 20–40 kHz, and some times more than 40 kHz. The mixture of irregularly shaped abrasive grain particles among water is supplied into the gap between workpiece and tool. When the end tool tip strikes the free moving abrasives particles in the slurry, then they get energized and apply force on the machining area of workpiece. Material is taking away from the machining zone owing to continue hammering with micro-chipping by the regular abrasion of the solid microparticles of abrasive. Further, collapsing of the gas bubbles, also called cavitations, can take part in a material removal at micro-level. The chemical contaminants present in the abrasive slurry medium can cause immediate loss of the workpiece material, resulting in material loss. The debris from the machining region is removing by continuous supply of abrasive slurry between workpiece and tool and refills this gap with new abrasive slurry.

Therefore, based on the consideration of USMM investigation, the material removal technique in the case can be stated as:

(i) Micro-chipping phenomenon is happened due to apply force of the abrasive particles which are freely moving with slurry,
(ii) Mechanical abrasion against the workpiece surface by abrasive grain particles,
(iii) Cavitations effect by ultrasonic vibration,
(iv) Chemical procedures with the liquid are used.

3 Types of Ultrasonic Micromachining (USMM) Process

Basically, two types of ultrasonic micromachining are available. The first process is stationary ultrasonic micromachining and the second process is rotary ultrasonic micromachining. Another hybrid machining process is found, which is ultrasonic-assisted micromachining. Various classes of ultrasonic micromachining processes are represented in Fig. 1.

3.1 Stationary Ultrasonic Micromachining (USMM)

Figure 2 illustrates the experimental setup of stationary ultrasonic micromachining setup where a simple cylindrical micro-tool is employed. The tool tip vibrates with ultrasonic frequency. A major drawback of USMM process is tool wear. Continuous shortening of tool length is a major problem and consequently, enforce obstacles

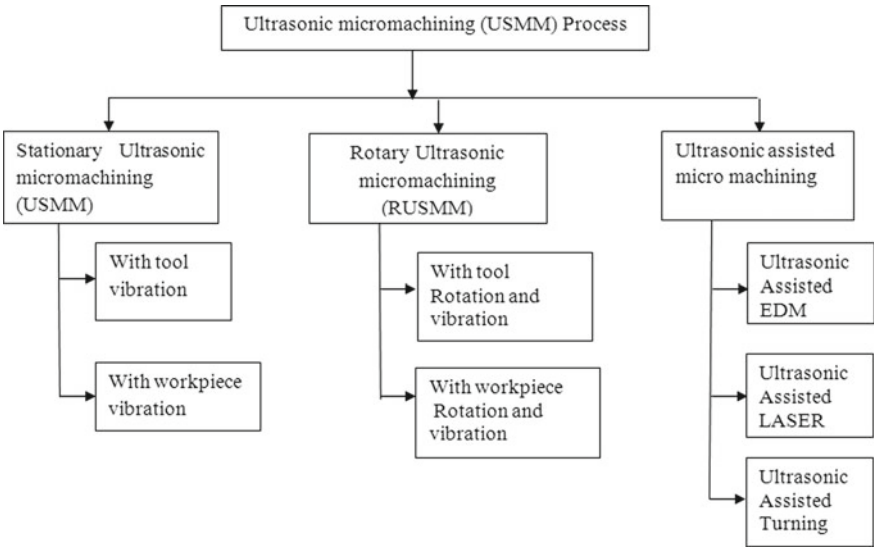

Fig. 1 Classification of ultrasonic micromachining (USMM) process

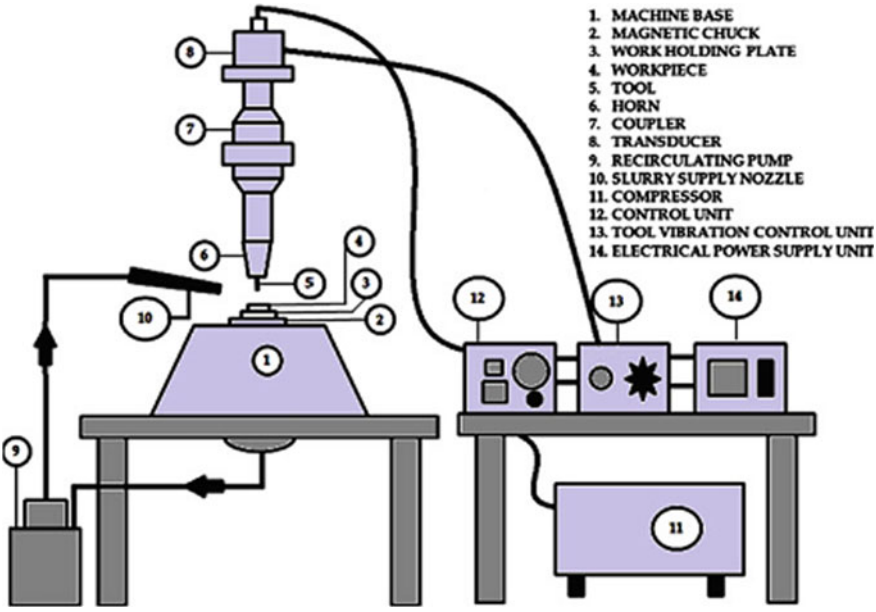

Fig. 2 Experimental setup of USMM [7]

with keeping consistent vibration at the end of tool tip is very difficult. Ultrasonically vibration is given to the workpiece has been established and it is a preferable process for reducing tool wear. Furthermore, the workpiece vibration helps in the moving of abrasive particles during machining to develop the impacting of abrasive grains in the region of machining and take away debris [6].

3.2 Rotary Ultrasonic Micromachining (RUSMM)

Past investigations stated that the stationary USM was upgraded in the form of rotary ultrasonic machine (RUM) [8, 9] for improving the performance of ultrasonic micromachining process. Characteristically, RUM was utilized for making drill holes in brittle and hard materials and milling and surface finishing purposes also. In 1964, the rotary ultrasonic machine process was first introduced by Mr. Percy Legge at the UK Atomic Energy Authority (UKAEA) [8, 10]. Legge's patented device was highlighted a beneficial enhancement. The rotating ultrasonic transducer was fixed to this stationary ultrasonic machine. So that ultrasonic vibration and rotation were provided simultaneously to the end of the tool. This development of rotating transducer head is more advantageous for producing excellent dimensional accuracies on the workpiece. Various process variations have been attaining by different categories of tools. Surface texturing, face milling in side, screw threading, internal/external grinding and slot machining are the little of the process variation which is effectively done with the help of rotary ultrasonic machine (RUM). RUM had been observed as advancement to overcome the drawbacks of USM, i.e., tool wear and slow rate of machining. A number of additional ways of describing the RUM process were explored in this text. Conventional diamond grinding and USM process are combined together and develop rotary ultrasonic machine (RUM) [8, 11]. Sometimes, it is used for drilling [10], twist drilling, grinding with ultrasonic vibration [8]. Komaraiah and Reddy [12] proposed different techniques about RUM which involved workpiece rotation also.

4 Strategies for Development of Ultrasonic Micromachining (USMM) System for Performance Improvement

The strategies for developments of ultrasonic micromachining (USMM) system for improvement of machining performance are discussed hereinafter.

4.1 Strategies for Stationary Ultrasonic Micromachining (USMM)

In simple stationary ultrasonic micromachining, there are some problems faced by researchers like preparation of micro-tool, boost of ultrasonic vibration, control of vibration amplitude, etc. To solve these problems, some strategies are adopted in the development of ultrasonic micromachining setup.

Some difficulties faced in fabrication of micro-tools and mounting them on the USMM setup. Hence, to solve these difficulties, Egashira, K. et al. developed a machining process to produce micro-tool in same setup which is shown in Fig. 3. In this setup, electro-discharge grinding with wire (WEDG) technique used to fabricate micro-tool and workpiece vibrates in which ultrasonic transducer is directly attached to workpiece. Self-aligned multilayer machining and assembly (SAMMA) was another manufacturing system, which was a combination of machining as well as assembly of micro-parts be performed on a similar machine instead of other machining and assembly.

An innovative production process merges electroplating, lithography, μ-EDM and micro-USM. It has been elaborated to fabricate unusual patterns on various ceramics efficiently with the help of lithographic mask [14]. For generation of 3D structure of hard and fragile materials, a new approach has been useful in micro-USM with the help of ultrasonic vibration spindle with high precision [15]. A new monitoring technique with measurement was developed in micro-USM system, which is used to measure static force as well as workpiece clamping and tooling for better machining conditions in micro-USM [16]. One another method was proposed, called electrophoretically assisted micro-ultrasonic machining (EPAMUSM). Within this method, an electric field is utilized to maintain a sufficient amount of abrasive particle

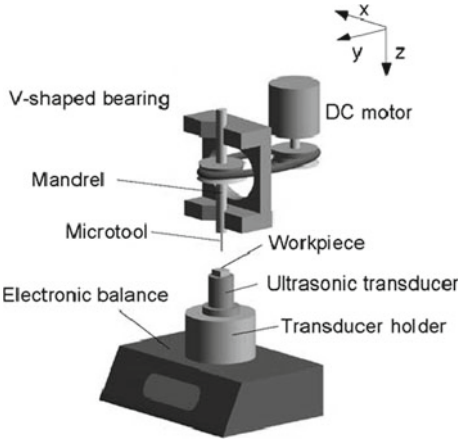

Fig. 3 USMM setup with online tool preparation and workpiece vibration [13]

in machining area to make sure high precision [17]. Figure 6 shows the effect of electrophoretic in EPAMUSM setup where absorption layer of abrasives in micro-tool surface improves MRR and also edge chipping of the surface.

4.2 Strategies for Rotary Ultrasonic Micromachining (RUSMM)

Rotary ultrasonic micromachining (RUSMM) is a mixture nontraditional machining method that merges the conventional grinding with diamonded tool and static USM. High MRR is achieved by this machining process [18–21]. In this machining procedure, a rotary type core drill tool with diamond added abrasives is vibrated ultrasonically and constantly feeds toward the workpiece. Coolant is continuously supplied in the machining area, which prevents jamming and overheating of the drill hole inside wall area [22–24]. As compared to the micro-USM, more material removal rate has been found in micro-RUSM. Figure 4 illustrates the various types of tools used in RUSMM process. The RUSMM process is also considered a nonelectrical, nonchemical and nonthermal machining technique [25–27]. Various operations such as drilling, surface texturing, face grinding and side face milling, etc. have been done with the help of rotary ultrasonic machining [18, 28–30].

5 Mode of Operation of Ultrasonic Micromachining (USMM)

Generally, ultrasonic micromachining operation has been done in two ways, namely

(a) Ultrasonic micromachining (USMM) with tool vibration.
(b) Ultrasonic micromachining (USMM) with workpiece vibration.

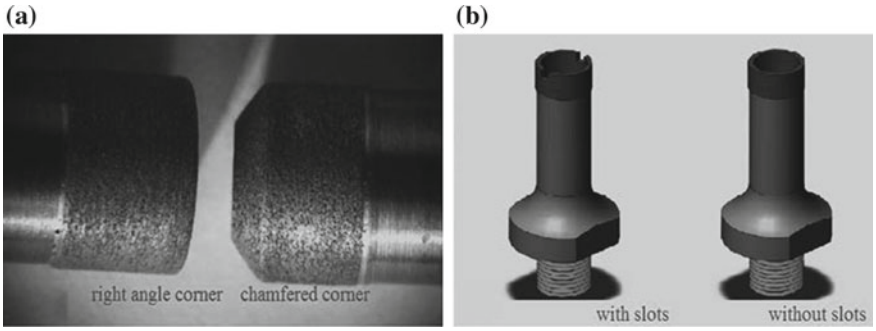

Fig. 4 Various tool used in RUSMM process [30]

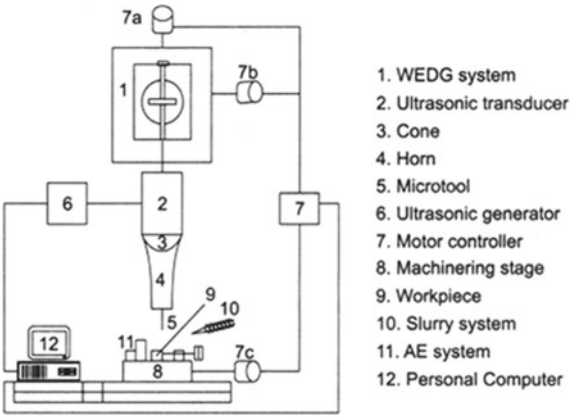

Fig. 5 Schematic diagram of USMM system with tool vibration [33]

The mode of operation of both machining processes is discussed under subsequent subsections.

5.1 USMM with Tool Vibration

Ultrasonic micromachining begins from the idea of "micromachining using micro-tool" [31, 32] wherein no rotary motion is supplied to the tool or workpiece. Cylindrical type micro-tool was employed for micromachining purpose. Figure 5 presents the ultrasonic micromachining (USMM) system with vibration of tool.

5.2 USMM with Workpiece Vibration

To solve the problem associated with USMM with tool vibration, a new technique has been developed in USMM with workpiece vibration. In this technique, workpiece is directly fixed with transducer. The workpiece oscillates with ultrasonic frequency instead of tool. Figure 6 illustrates the schematic diagram of USMM setup with workpiece vibration.

6 Elements of USMM System

The ultrasonic micromachining setup consists of six basic elements namely power supply, transducer, horn, abrasive slurry, micro-tool and workpiece. These elements are illustrated in the following section.

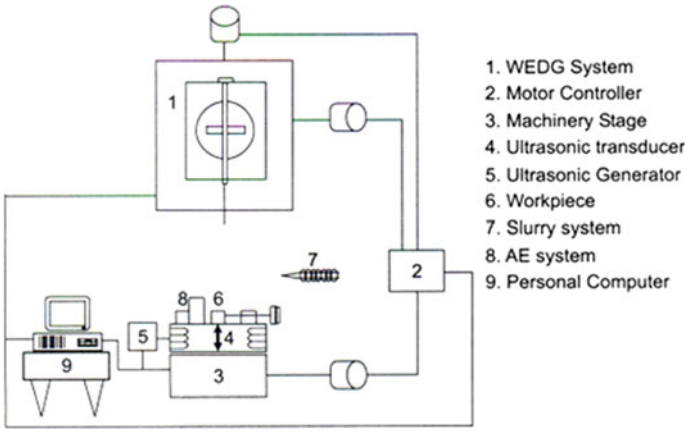

Fig. 6 Schematic diagram of USMM system with workpiece vibration [33]

6.1 Power Supply

In this text, power supply unit for USMM is explained. A sine-wave generator with high power is utilized for controlling the generated signal and frequency [34]. With the help of this low power, 50 Hz electric frequency is converted to high frequency, generally more than 20 kHz. This high-frequency electrical signal is provided to the transducer and mechanical vibration motion is generated by this transducer [34, 35].

6.2 Transducer

In ultrasonic micromachining, transducer is converted electrical energy into mechanical energy to produce ultrasonic vibration [34, 35]. In this generator scheme, the horn and tool are attached together. It is tuned by regulating their dimensions to get resonance. In recent times, generators with resonance following developed into accessible which regulate automatically the high-frequency output to competition the accurate resonance of the horn/tool assembly. It can also prove any type of small error in setup and showing least amount of acoustic energy loss in small heat generation due to tool wear. The power supply is depended on the capacity of the transducer. Two types of transducers are utilized for USMM based on two special principles [34].

A. **Piezoelectric Transducer**: In this transducer, mechanical vibration is generated through the piezoelectric effect. To get this vibration, specific materials, lead zirconate titanate or quartz are used to produce a little electric current at what time they are compressed. Alternatively, when the electric current is applied, size of these materials is increased. After the current is detached, the material intently

returns to its original shape. In piezoelectric transducer, the electro-mechanical conversion efficiency is extremely high (up to 96%), which is very advantageous and does not need water cooling [34].

B. **Magnetostrictive Transducer**: Laminated stock of nickel or sheets of nickel alloy is used for making this transducer. Strong magnetic field is created and its length is changed. Magnetostrictive transducers are strong but electro-mechanical conversion efficiencies range is 20–30% [34]. The low efficiency means that the water cooling of transducer device is required. Power capabilities of magnetostrictive transducers are up to 2400 W. The magnitude of the length change that can be achieved by both piezoelectric and magnetostrictive transducer is limited by the power of transducer material. In both types of transducer, the limit is approximately 0.025 mm (0.01 in.).

6.3 Horn

When the mechanical vibration motion is produced by the transducer and imparts this to workpiece, horn amplifies. It is a velocity transformer and it is made quietly shorter than the half wavelength. The amplitude of the transducer is very small and it is generally not enough for material removal purpose. The horn is connected to the transducer for producing the desired amplitude on the tool end. The amplitude of the vibrations at the tool end is gradually increased by reducing the cross-section of the horn at the tool end. The horns are particularly fabricated to supply a reduction in cross-section at the tool end. Seeing that the horn should be fabricated special sizes and shape, it is mechanically resonant or tuned to the frequency of the transducer vibrations.

6.4 Abrasive Slurry

In ultrasonic micromachining, abrasive particles are the actual cutting tool. The abrasive particles are mixed with any liquid medium which has low density. The abrasives concentration 1–60% by weight is generally used. The liquid medium is used generally water or sometimes oil. Abrasive particles, for example, silicon carbide, boron carbide, aluminum oxide and diamond dust, are commonly used. The slurry with abrasives in the USMM should be harder than the workpiece; otherwise, abrasive life will then be reduced. Average dimension and profile of abrasive particles are parameters for abrasive particles. Once abrasive has been chosen for particular application of work materials, after that it is mixed through water and accumulated in a slurry tank of the USMM machine. This water mixed abrasive slurry is supplied through a recirculation pump to the tool–workpiece interface.

6.5 Micro-Tool

The micro-tool fabrication for ultrasonic micromachining is very difficult task and it is also not easy to maintain the accuracy. To solve this problem, some method is introduced. By applying electroless, Ni–P composite plating around 20 μm micro-tool was fabricated [36]. The multi-tool made by cemented carbide of 4 × 4 array was fabricated and the diameter of every single tool is 25 μm [37]. One micro-tool was developed for stepped circular hole with good surface finish [38]. This micro-tool is not properly cylinder with tapered, which has been fabricated by ultrasonic vibrated grinding wheel [15]. Park et al. [39] were fabricated micro-diamond tools for micro-USM using electroless Ni–P composite plating. The diameter of tool was achieved of 115–120 μm after production for every diamond size [39]. Tool life was investigated through the generation of micro-grooving on silicon and found that when larger diamond grit was used, life becomes longer. Figure 7a, b shows the microscopic image and SEM image of electroplated diamond tool, respectively. The outer diameter of tool is 300 μm with 30 μm grain size and 100 μm wall thickness [40]. Figure 7a, b show the micro-tool before and after machining, respectively. This figure confirms the tool wear during machining in ultrasonic micromachining.

Either solid or hollow cylindrical tool is fabricated and extensively used in applications of ultrasonic micromachining. Tools must be made from comparatively ductile but hard materials such as brass, mild steel and stainless steel due to decrease tool wear. Curodeau et al. were proposed another option for tool material. Visco-elastic thermoplastic composite material was used as tool making to perform USMM operations [41]. This estimated tool material was effectively considered for micro-polishing and micromachining for tool steel surface.

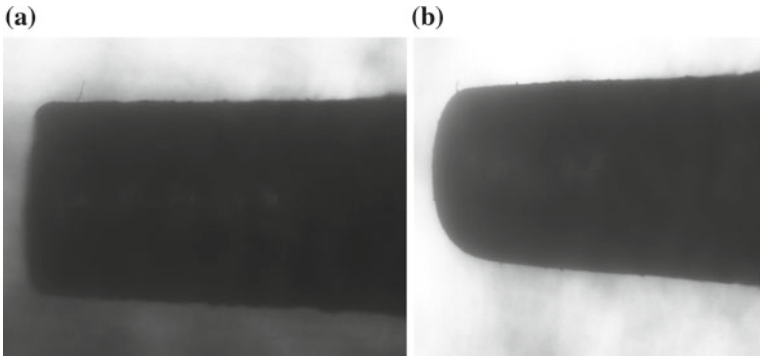

Fig. 7 Tool tip **a** before machining **b** after machining

6.6 *Workpiece*

Ultrasonic micromachining (USMM) process is used in several manufacturing including fabrication of any shapes on fragile and hard materials such as ceramics, titanium carbide, tungsten carbide and diamond. But there is no constraint for range of materials that can be machined except for the material that could not be reacting or dissolved with slurry media. The materials that can also be machined with the help of USMM are germanium, ferrite, glass and quartz, silicon, which exhibit high hardness and impact brittleness. In micromachining area, some of the hard and brittle materials and applications of these are listed in Table 1.

7 Improvement in Machining Rate of Ultrasonic Micromachining (USMM)

Research activity on USMM has been broadly carried out concerning all the output performance. However, some limited publications have focused on the strategies for improvement of performances. The major task of performance enhancement for USMM is to efficiently machine a micro-feature with no outside surface damage, super surface finish, high-dimensional accurateness and complex 3D microfeatures. The parametric correlation for USMM is very complex owing to the contribution of several reasons and associated parameters that might affect the performances outputs. Figure 8 shows the input–output model of USMM.

Table 1 Some hard and brittle materials and its applications

Workpiece material	The area of application
Glass	Monolithic grid structure, accelerometers, micro-fluidic systems, lab-on-a-chip, membrane in fuel cell, micro-device for blood analysis
Quartz crystal	Accelerometers, pressure sensor, filter and sensor, optical chopper
Lead zirconate titanate (PZT)	Medical imaging transducers, actuators
Alumina	Micro-gimbal, vacuum windows
Silicon carbide	Micro-gas turbine engine, vibration sensor, high temperature pressure sensor
Silicon nitride	Solid immersion lens, biaxial pointing mirrors

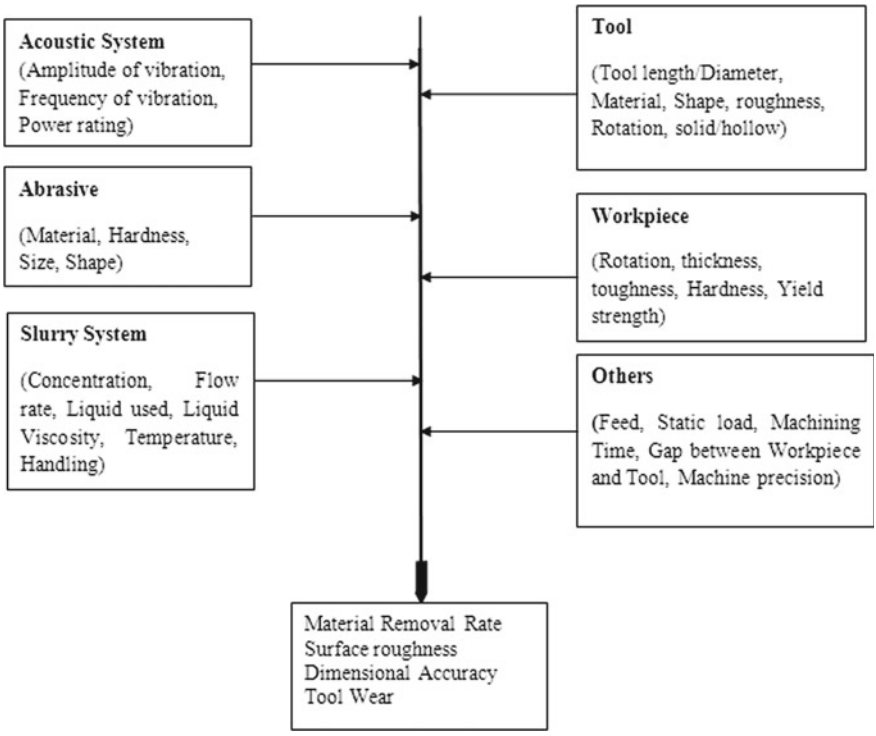

Fig. 8 Associated parameters in input–output model of USMM

7.1 Stationary Ultrasonic Micromachining (USMM)

In USMM, machining rate is most affected by abrasive size, shape and types. The machining rate is improved by increasing the size of abrasives. The machining rate is also increased by expanding the average stationary load. Machining rate in USMM greatly increased by using multi-tool of cemented carbide. The diameter of a single hole of 20 μm has been generated by micro-USM. The chemical-assisted ultrasonic machining (CUSM) technique is initiated for improving performance output. To achieve better MRR, low concentration hydro-fluoric solution with acid is added to the alumina slurry and reported that the MRR was improved up to 40% for micro-drilling [42]. Kumar et al. [43] reported that for achieving higher MRR (0.6436 mm^3/min) during micro-hole into quartz by USMM, all the process parameters setting, i.e., power rating (400 W), tool feed rate (1.2 mm/min) and slurry concentration of abrasive (40%), should be at higher value.

Concentration of abrasive slurry is most important parameter which influences the machining characteristics. The response surface graph shown in Fig. 9 illustrates the influence of concentration of abrasive slurry and power rating on MRR at the same preset values of feed rate of the tool. Higher MRR can be achieved using higher

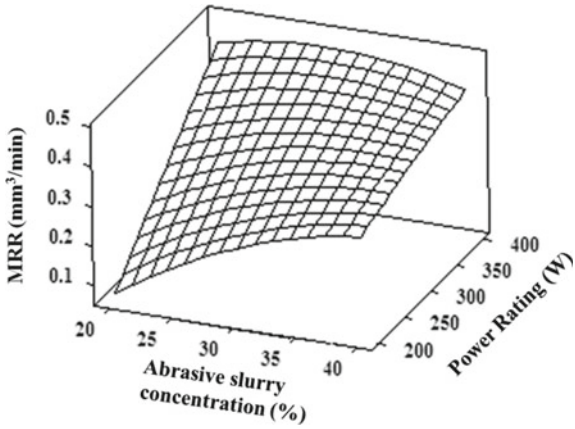

Fig. 9 Influences of slurry concentration of abrasive and power rating on MRR

value of power rating and abrasive slurry concentration. Extra material is removed from machining zone of the workpiece, when higher abrasive slurry concentration is used. When the high power rating is used, abrasive particles strike on the machining zone of the workpiece with high force; as a result, MRR becomes high at high value of concentration of abrasive slurry and power rating [44].

7.2 Rotary Ultrasonic Micromachining (RUSMM)

Various researchers have investigated the MRR through rotary ultrasonic machining (RUM) of highly developed advanced materials and confirmed that this machining technique is one of the most appropriate techniques for achieving higher MRR. Ya et al. [45] proposed that the influences of machining parameters on MRR of glass and stated that high MRR can be achieved using RUM compare to stationary USM process. Cong et al. [19] investigated the influences of RUSMM process parameters on the quality aspect in RUM on CFRP/Ti stacks. Tool rotary motion and power of ultrasonic were very significant process parameters. The MRR value of 3.56 mm^3/s was obtained and which was superior compared to any traditional drilling methods. This enhancement of MRR was possible due to the collective effect of mixed up mechanisms, i.e., USM and normal grinding in the RUM process. At high feed rates, MRR was high because depth of indentation of diamond abrasives was more with high feed rate. The speed of spindle and power of ultrasonic have no such effect on MRR [24].

8 Improvement in Geometrical Features of Ultrasonic Micromachining (USMM)

The improvement in geometrical features of ultrasonic micromachining (USMM) is discussed in this chapter.

8.1 Stationary Ultrasonic Micromachining (USMM)

Stationary-type ultrasonic micromachining (USMM) is employed for generating different geometrical micro-features, for example, through holes, blind holes, slots, micro-channel, 3D cavities, etc. USMM has a drawback in mounting micro-tools to its tool head with precision. Hence, a system was introduced for utilizing on-the-machine micro-tool fabrication by wire electro-discharge grinding (WEDG). With the help of this method, the fabricated micro-tool is used for generating micro-holes of 20 μm in diameter and 50 μm depth on a quartz and silicon plate. Egashira et al. (1997) reported that triangular and square holes created on silicon using the micro-tool, which was generated by using WEDG method [32]. Ultrasonic micromachining was also produced micro-holes of 5 μm diameter in silicon and soda–lime glass [32]. Figure 10 shows arrays of micro-pillars in lead zirconate titanate (PZT). The every pillar diameter is 280 μm and depth is 6000 μm which were fabricated using a steel disk with an array of 300 μm diameter of holes. It was shown like a honeycomb structure [46]. Such production is evidently more complicated than fabricating straightforward cylindrical tool. The recent development of micro-ultrasonic-assisted lapping method shows the capability for producing microstructures of different geometrical forms [47]. From a single tool tip, the various drilling operation is time-consuming in USMM. So, for remedies, the multiple tool of cemented carbide fabricated using

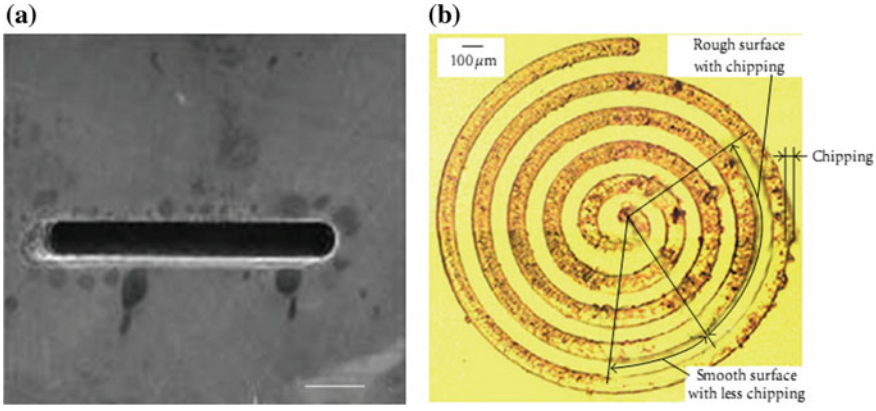

Fig. 10 **a** Straight micro-slot, **b** spiral groove [47]

reverse micro-EDM can be utilized [37]. The multi-tool is further used in USMM and generated array of micro-holes.

Figure 10a illustrates a straight slot (length 500 μm, width 47 μm and depth 60 μm) with vertical sidewall and fabricated by a contouring mode layer by layer using USMM system. Moreover, contouring mode USMM exhibits by producing a spiral groove on low-melting glass, which is shown in Fig. 10b [48]. Using a cylindrical shaped micro-tungsten tool, 3D micro-cavity was fruitfully made up of silicon [49]. With the help of CAD/CAM method, the micro-tool was determined in every three axes and go after an intended tool path shaped during machining. In micro-ultrasonic machining, dies of micro-tungsten were utilized as tools to get pattern shape in alumina [50].

Micro-channel has been machined on silicon by using micro-tool which is developed during electroless Ni–P composite plating [39]. It contains deep reservoir channel at entrance with depth 400 μm and width 300 μm and at exit regular channel by way of a depth of 100 μm and a width of 115 μm. A high-resolution micro-ultrasonic machining (HR μUSM) has been done using a different type of slurry and surface roughness has been analyzed.

Microstructure with smooth sidewalls and large aspect ratio (>6) has been attained using fine. Figure 11 illustrates the entry profile of the machined holes on glass. It shows that surface roughness was improved using the chemical-assisted ultrasonic

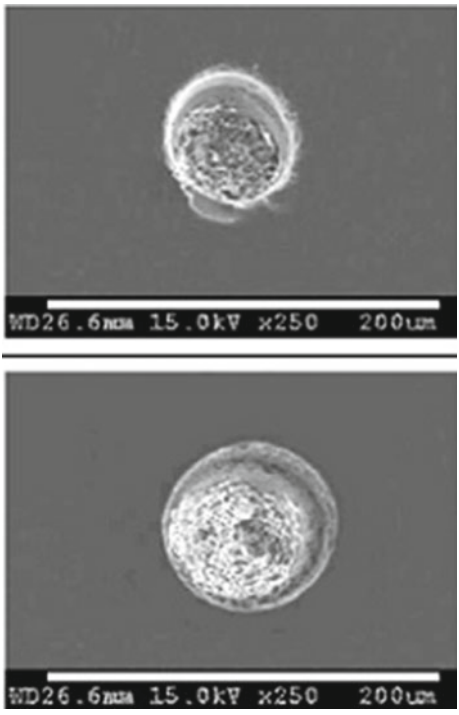

Fig. 11 Profile of hole entrance [42]

machining (CUSM) and also a smoother entrance profile was achieved compared to the USM. Figure 12 shows micro-holes drilled consecutively using a single tool (tool diameter 9 μm and drilling depth 20 μm) at a penetration of 0.125 μm/s. Every hole is drilled with no fractures or cracks in the region of edge. A micro-channel with aspect ratio more than 5 has been produced and a throughout micro-channel of 2 cm length, less than 350 μm width, was fabricated on the 2.0-mm thick glass slide by using ultrasonic micromachining. Figure 13 shows the SEM image of the micro-holes, produced by micro-USM on metallic glass ($Zr_{60}Cu_{30}Ti_{10}$) and better accuracy

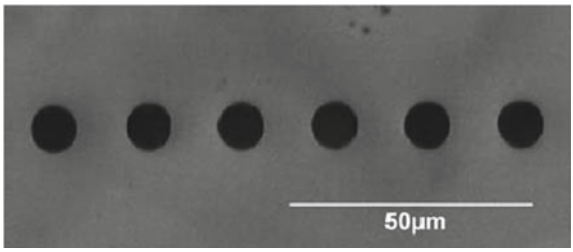

Fig. 12 Micro-holes drilled consecutively using a single tool [13]

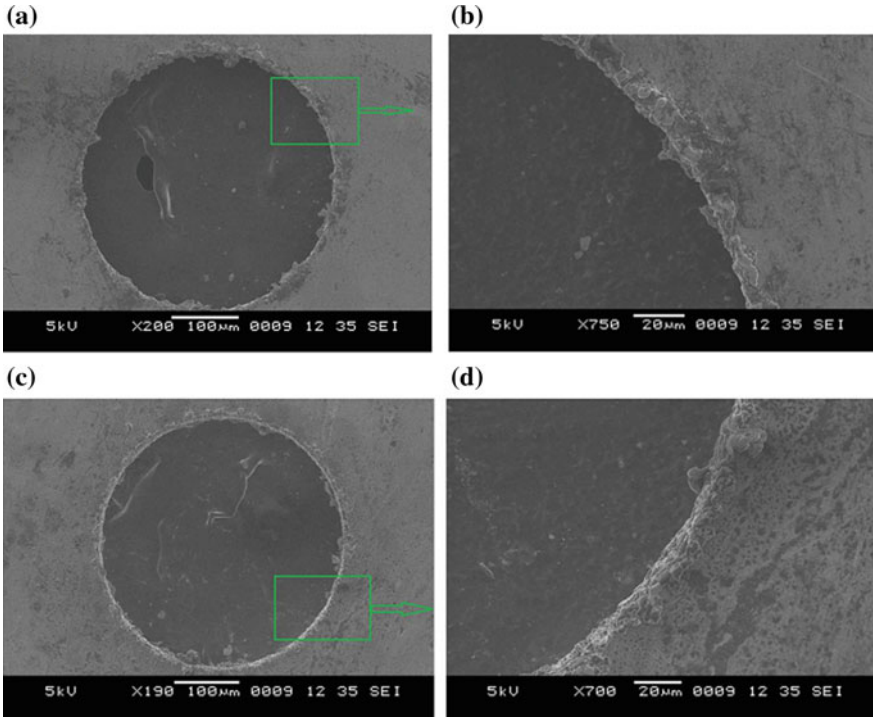

Fig. 13 SEM images of micro-hole **a** entrance **b** edge of entrance, **c** exit **d** edge of exit [51]

has been found when finer abrasive is used. Figures 14 and 15 show pictorial view of the machined workpiece at multi-objective parametric setting.

Figure 16 illustrates the influence of concentration of abrasive slurry and power rating on overcut of hole at the same preset values of tool feed rate. From the graph, it is clear that lowest value of overcut of micro hole has been observed at the low value of concentration of abrasive slurry and power rating. Material removed from the workpiece is very less, when low value of concentration of abrasive slurry and power rating is used. With small power rating and abrasive grain, particles strike on the workpiece with minimum force; as a result, material removal rate becomes low at low value of power rating. So that the minimum overcut is achieved.

Figure 17 illustrates the influence of power rating and concentration of abrasive slurry on taper angle at the same preset values of feed rate of tool. The less material is removed at what time abrasive slurry concentration is low. With low rating of power,

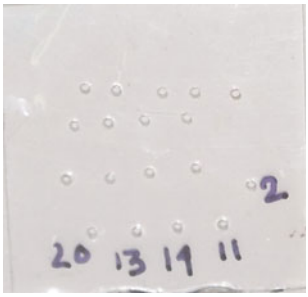

Fig. 14 Photographable view of the machined workpiece after machining

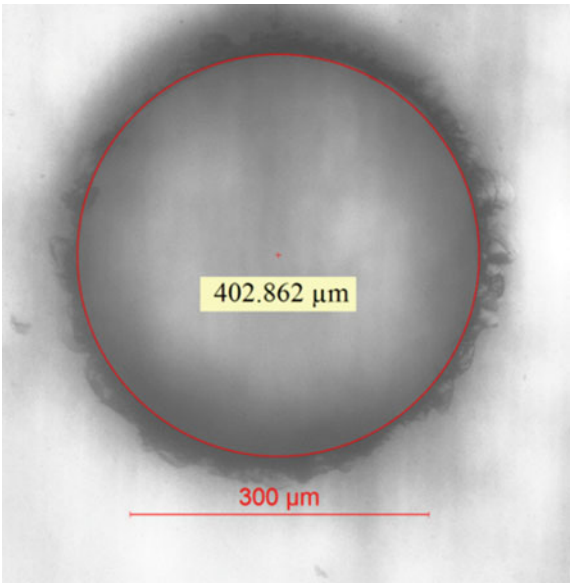

Fig. 15 Pictorial view of the machined workpiece at multi-objective parametric setting

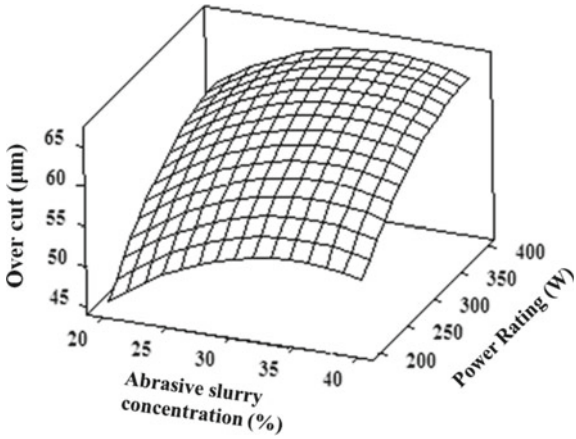

Fig. 16 Influences of power rating and concentration of abrasive slurry on overcut

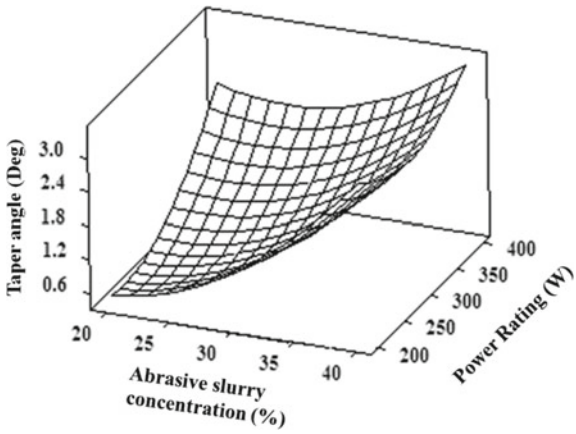

Fig. 17 Influences of slurry concentration of abrasive and power rating on taper angle

abrasive grain particles strike on the workpiece with minimum force. For this reason, the accuracy is good at the corner area of the hole. Hence, minimum taper angle has been obtained with low value of slurry concentration of abrasive and power rating.

8.2 Rotary Ultrasonic Micromachining (RUSMM)

A variety of investigational and theoretical studies on rotary ultrasonic micromachining (RUSMM) has been conducted for machining different ceramic materials. Sapphire is usually used in the electronics industries, mostly for the production of chips and circuits can also be fabricated with RUSMM. The slot produced by RUSMM on dental ceramics. RUSMM was produced surface on PZT material by different slurry mediums (water, milk and PCD) during the experimentation. It has

been experientially proved that the maximum force of cutting of RUM is around 34.5% lower than conventional diamond side grinding.

9 Future Scope of Research

The most important issue is enhancing the performance of ultrasonic micromachining process. Few discussions are available about material removal mechanism till at this time but more investigation of the material removal during micromachining is required for USMM process. Micro-tools preparation with proper mechanism handling and micro-tools fixing with the tool holder are also difficult parts of the research. The accurateness of USMM processes depends on this circumstance of the micro-tools. In micromachining, there is lessening in dimension of tool, abrasive grain measurement, amplitude of vibration, etc. Environmental aspects are most important issues of modern manufacturing process which have hardly been addressed. The fabrication of micro-fluidic components using ultrasonic micromachining process is the most exploring parts. There is a possibility of investigation in the region of production of micro-channels on glass and silicon for micro-heat exchanger and microsensors purposes by USMM process.

10 Summary

This chapter includes the significant issues about performance improvement of ultrasonic micromachining process. It also focuses on the setup improvement of ultrasonic micromachining process and basic principle of ultrasonic micromachining process. The types of ultrasonic micromachining processes, i.e., stationary ultrasonic micromachining and rotary ultrasonic micromachining, are also discussed in detail. Strategies for development of ultrasonic micromachining system for performance improvement are discussed for both stationary and rotary ultrasonic micromachining. Micro-channels have been produced with good dimensional accuracy, i.e., depth of 400 μm and width of 300 μm on silicon by using developed micro-tool. Applying the machine micro-tool production method by wire electro-discharge grinding (WEDG), micro-tool is fabricated for generating micro-holes of 20 μm in diameter and 50 μm depth on a silicon and quartz. Better surface quality has been achieved on the brittle and hard materials using rotary ultrasonic micromachining process. The smaller surface roughness values are obtained by RUSMM compared to stationary ultrasonic micromachining. Various strategies for improvements in machining rate, geometrical and dimensional features of stationary ultrasonic micromachining and rotary ultrasonic micromachining have also been discussed in this book chapter.

References

1. Brinksmeier E, Riemer O, Stern R (2001) Machining of precision parts and microstructures. In: Proceedings of the 10th International conference on precision engineering (ICPE) initiatives of precision engineering at the beginning of a millennium, Yokohama, Japan, 18–20 July, pp 3–11
2. Masuzawa T (2000) State of the art of micromachining. CIRP Ann 49(2):473–488
3. Masuzawa T, Tonshoff HK (1997) Three-dimensional micromachining by machine tools. Ann CIRP 46(2):621–628
4. Amin SG, Ahmed MHM, Youssef HA (1995) Computer aided design of acoustic horns for ultrasonic machining using finite element analysis. J Mater Process Technol 55:254–260
5. Thoe T, Aspinwall D, Wise M (1998) Review on ultrasonic machining. Int J Mach Tools Manuf 38(4):239–255
6. Egashira K, Masuzawa T (1999) Microultrasonic machining by the application of workpiece vibration. CIRP Ann Manuf Technol 48(1):131–134
7. Kibria G, Bhattacharyya, B, Davim JP (2017) Non-traditional micromachining processes. Fundamentals and applications. Materials forming, machining and tribology. ISBN 978-3-319-52009-4:61-91
8. Churi N (2010) Rotary ultrasonic machining of hard-to-machine materials. Doctoral dissertation, Kansas State University, USA
9. Neugebauer R, Stoll A (2004) Ultrasonic application in drilling. J Mater Process Technol 149(1):633–639
10. Legge P (1964) Ultrasonic drilling of ceramics. Ind Diamond Rev 24(278):20–24
11. Legge P (1966) Machining without abrasive slurry. Ultrasonics 4(3):157–162
12. Komaraiah M, Reddy PN (1991) Rotary ultrasonic machining—a new cutting process and its performance. Int J Prod Res 29(11):2177–2187
13. Egashira K, Mizutani K, Nagao T (2002) Ultrasonic Vibration Drilling of Microholes in Glass. CIRP Ann Manuf Technol 51(1):339–342
14. Li T, Gianchandani YB (2006) A micromachining process for die-scale pattern transfer in ceramics and its application to bulk piezoelectric actuators. J Microelectromech Syst 15(3):605–612
15. Kuriyagawa T, Shirosawa T, Saitohand O, Syoji K (2001) Micro ultrasonic abrasive machining for three-dimensional milli-structures of hard-brittle materials. In: Proceedings of 16th annual meeting of the ASPE, Crystal City, Virginia, USA, pp 525–528
16. Zarepour H, Yeo SH, Tan PC, Aligiri E (2011) A new approach for force measurement and workpiece clamping in micro ultrasonic machining. Int J Adv Manuf Technol 53:517–522
17. Lian HS, Guo ZN, Liu JW, Huang ZG, He JF (2016) Experimental study of electrophoretically assisted micro-ultrasonic machining. Int J Adv Manuf Technol 85:2115–2124
18. Pei ZJ, Ferreira PM (1999) An experimental investigation of rotary ultrasonic face milling. Int J Mach Tools Manuf 39(8):1327–1344
19. Cong WL, Pei ZJ, Treadwell C (2014) Preliminary study on rotary ultrasonic machining of CFRP Ti stacks. Ultrasonic 54(6):1594–1602
20. Jiao Y, Liu WJ, Pei ZJ, Xin XJ, Treadwell C (2005) Study on edge chipping in rotary ultrasonic machining of ceramics: an integration of designed experiments and finite element method analysis. J Manuf Sci Eng 127(4):752–758
21. Zvoncan M, Beno M, Kovac M, Peterka J (2012) Cross section of machined layer for rotary ultrasonic machining with a hollow drill. Manuf Ind Eng 11(3):11–13
22. Churi NJ, Pei ZJ, Shorter DC, Treadwell C (2009) Rotary ultrasonic machining of dental ceramics. Int J Mach Mach Mater 6(3):270–284
23. Zhang C, Cong W, Feng P, Pei Z (2014) Rotary ultrasonic machining of optical K9 glass using compressed air as coolant: a feasibility study. Proc Inst Mech Eng Part B J Eng Manuf 228(4):504–514
24. Churi NJ, Pei ZJ, Treadwell C (2006) Rotary ultrasonic machining of titanium alloy: effects of machining variables. Mach Sci Technol 10(3):301–321

25. Zhang C, Feng P, Zheng S, Wu Z, Yu D (2011) Experimental investigation of rotary ultrasonic face milling of K9 glass. Adv Mater Res 230–232:644–648
26. Gong H, Fang FZ, Hu XT (2010) Kinematic view of tool life in rotary ultrasonic side milling of hard and brittle materials. Int J Mach Tools Manuf 50:303–307
27. Pei ZJ, Ferreira PM, Kapoor SG, Haselkorn M (1995) Rotary ultrasonic machining for face milling of ceramics. Int J Mach Tools Manuf 35(7):1033–1046
28. Zhang C, Feng P, Zhang J, Wu Z, Yu D (2012) Theoretical and experimental research on the features of cutting force in rotary ultrasonic face milling of K9 glass. Appl Mech Mater 157–158:1674–1679
29. Zhou M, Wang M, Dong G (2015) Experimental investigation on rotary ultrasonic face grinding of SiCp/Al composites. Mater Manuf Process 31(5):673–678
30. Wang Q, Cong W, Pei ZJ, Gao H, Kang R (2009) Rotary ultrasonic machining of potassium dihydrogen phosphate (KDP) crystal: an experimental investigation on surface roughness. J Manuf Process 11(2):66–73
31. Masuzawa T, Tonshoff HK (1997) Three-dimensional micro machining by machine tools. CIRP Ann Manuf Technol 46(2):621–628
32. Egashira K, Masuzawa T, Fujino M, Sun XQ (1997) Application of USM to micromachining by on-the-machine tool fabrication. Int J Electr Mach 2:31–36
33. Jain VK. Introduction to micromachining, 2nd edn. ISBN: 978-81-8487-361-0
34. Gary FB (1987) Non traditional manufacturing processes, vol 6. Marcel Dekker Inc., New York, pp 67–86
35. Thoe TB, Aspinwall DK, Wise MLH (1998) Review on ultrasonic machining. Int J Adv Manuf Technol 38(4):239–255
36. Jain V, Sharma AK, Kumar P (2011) Recent developments and research issues in micro ultrasonic machining. Int Sch Res Netw ISRN Mech Eng. https://doi.org/10.5402/2011/413231
37. Egashira K, Taniguchi T, Tsuchiya H, Miyazaki M (2004) Micro-ultrasonic machining using multitools. In: Proceedings of the 7th international conference on progress machining technology (ICPMT 04)
38. Wang AC, Hwa YB, Li XT, Huang F (2002) Use of micro ultrasonic vibration lapping to enhance the precision of micro holes drilled by micro electro discharge machining. Int J Mach Tools Manuf 42:915–923
39. Park H, Onikura H, Ohnishi O, Sharifuddin A (2010) Development of micro diamond tools through electroless composite plating and investigation into micromachining characteristics. Precis Eng 34:376–386
40. Jain AK, Pandey PM (2016) Experimental studies on tool wear in μ-RUM process. Int J Adv Manuf Technol 85(9–12):2125–2138
41. Curodeau A, Guay J, Rodrigue D, Brault L, Gagne D, Beaudoin LP (2008) Ultrasonic abrasive μ-machining with thermoplastic tooling. Int J Mach Tools Manuf 48(14):1553–1561
42. Choi JP, Jeon BH, Kim BH (2007) Chemical-assisted ultrasonic machining of glass. J Mater Process Technol 191:153–156
43. Kumar S, Hansda B, Das S, Doloi B, Bhattacharyya B (2016) Experimental investigation into ultrasonic micromachining on quartz. In: Proceedings of 6th international & 27 All India manufacturing technology, design and research conference (AIMTDR-2016)
44. Hansda B (2016) ME thesis, Production Engineering, Jadavpur University
45. Ya G, Qin HW, Xu YW, Zhang YS (2001) An experimental investigation on rotary ultrasonic machining. Key Eng Mater 202:277–280
46. Boy JJ, Andrey E, Boulouize A, Malek CK (2010) Developments in micro ultrasonic machining (MUSM) at FEMTO-ST. Int J Adv Manuf Technol 47(1–4):37–45
47. Zhang C, Rentsch R, Brinksmeier E (2005) Advances in micro ultrasonic assisted lapping of microstructures in hard-brittle materials: a brief review and outlook. Int J Mach Tools Manuf 45(7–8):881–890
48. Sun XQ, Masuzawa T, Fujino M (1996) Micro ultrasonic machining and self-aligned multilayer machining/assembly technologies for 3D micromachines. In: Proceedings of the IEEE micro electro mechanical systems (MEMS '96), pp 312–317

49. Yu ZY, Rajurkar KP, Tandon A (2004) Study of 3D micro-ultrasonic machining. J Manuf Sci Eng 126(4):727–732
50. Yang Y, Li X (2003) Micro ultrasonic machining of ceramic MEMS with micro metallic dies. In: ASME international mechanical engineering congress and exposition micro electromechanical systems, Washington, DC, USA, 15–21 Nov
51. Kuriakose S, Patowari PK, Bhatt J (2017) Machinability study of Zr-Cu-Ti metallic glass by micro hole drilling using micro-USM. J Mater Process Technol 240:42–51

Accuracy Improvement and Precision Measurement on Micro-EDM

Amit Kumar Singh, Siddhartha Kar and Promod Kumar Patowari

Abstract Micro electrical discharge machining (μEDM) is used for fabricating microstructures and micro components such as arrays of micro tools, micropillars, and complex three-dimensional shapes. These micro features are extensively used in the field of micro-electro-mechanical systems (MEMS), bio-MEMS, environmental and information technology, and so on. μEDM variants such as micro electrical discharge drilling (μED-drilling), reverse micro electrical discharge machining (R-μEDM), drilling with in situ fabricated tool, block micro electrical discharge grinding (B-μEDG), micro wire electrical discharge grinding (μWEDG), and micro electrical discharge milling (μED-milling) are equally contributing toward the fabrication of microscale parts and components. For the last few decades, researchers have mainly concentrated on the dimensional accuracy and precision measurement while fabricating microstructures for quantifying the response measures to determine the quality machining in micro level. Several factors such as machining parameters (electrical and non-electrical), tool and workpiece fixation, resolution, and repositioning capacity of the machine control dimensional accuracy and precision altogether. In addition, for machining the micro features, micro tools have been used. So, it is very important to study the tool wear because it directly affects the accuracy of micro features during machining. Tool wear cannot be completely avoided, but it can be minimized up to a significant level. Moreover, it can also be done using tool wear compensation. These errors are highly responsible for getting the inaccurate dimension of the microstructure. It is important to analyze the effect of each factor meticulously to achieve a precise and accurate dimension of micro components.

A. K. Singh
Department of Mechanical Engineering, National Institute of Technology Nagaland, Dimapur 797103, Nagaland, India
e-mail: amit.kumar965@yahoo.com

S. Kar · P. K. Patowari (✉)
Department of Mechanical Engineering, National Institute of Technology Silchar, Silchar 788010, Assam, India
e-mail: ppatowari@yahoo.com

S. Kar
e-mail: siddkar.nita@gmail.com

G. Kibria and B. Bhattacharyya (eds.), *Accuracy Enhancement Technologies for Micromachining Processes*, Lecture Notes in Mechanical Engineering,
https://doi.org/10.1007/978-981-15-2117-1_3

Keywords Micro-EDM · Micromachining · Precision measurement · Accuracy · Tool wear

List of Abbreviations

μEDM	Micro electrical discharge machining
MEMS	Micro-electro-mechanical systems
μED-drilling	Micro electrical discharge drilling
R-μEDM	Reverse micro electrical discharge machining
B-μEDG	Block micro electrical discharge grinding
μWEDG	Micro wire electrical discharge grinding
μED-milling	Micro electrical discharge milling
LBM	Laser beam machining
LIGA	Lithography, Electroplating, and Molding
μUSM	Micro ultrasonic machining
IBM	Ion beam machining
μECM	Micro electrochemical machining
μWEDM	Wire electrical discharge machining
RC	Resistance–capacitance
E_{RC}	Discharge energy per pulse in RC circuit
C	Capacitance
V_g	Gap voltage
E_T	Discharge energy per pulse in transistor circuit
I_p	Current of a single pulse
V_p	Voltage of a single pulse
T_{on}	Pulse duration
T_{off}	Pulse interval
W_i	Initial weight of workpiece
W_f	Final weight of workpiece
h	Depth of hole
IEG	Interelectrode gap
TF	Tangential feed
CCD	Charge–coupled device
UWM	Uniform wear method
MRR	Material removal rate
TWR	Tool wear rate
BSA	Based on scanned area
HTF	Horizontal tool feed rate
LT	Layer thickness
TRS	Tool rotational speed
LDCA	Layer depth constrained algorithm
SCAA	*S*-curve accelerating algorithm

1 Introduction

Micromachining has plenty of applications in electronics industries, aerospace engineering, biomedical, etc. [1, 2]. Micro parts and components are one of the inevitable parts of the human life because of their distinguishing advantages such as they utilize less energy and material, require low power consumption, and have high sensitivity. Considering these distinctive advantages of micro features, researchers have got attracted toward it and contributed a lot toward the development of micro features. Based on different fabrication method, micro features with various shapes and sizes have been fabricated till today. The challenging task while fabricating micro features is ensuring the dimensional accuracy of the final product so that the product is solely based on the desired measurement.

To meet the increasing demand of micromachining, number of manufacturing processes such as laser beam machining (LBM), lithography, electroplating, and molding (LIGA), micro ultrasonic machining (μUSM), micro electrical discharge machining (μEDM), ion beam machining (IBM), and micro electrochemical machining (μECM) have been identified [1]. The last two decades saw a tremendous growth in the application of μEDM in microdomain due to its inherent capability of using a variety of machining techniques (drilling, milling, grinding, etc.) with ease of use and lower processing cost. μEDM is one of the assuring micromachining technology used for fabricating high aspect ratio profiles in electrically conductive materials regardless of their hardness [3] as shown in Fig. 1. μEDM, being a contact-free process, is free from chatter and vibration problems of the tool and workpiece and their actuated inaccuracies [4, 5]. Several machining techniques such as drilling, grooving, grinding, milling, and deburring can be performed in microdomain in a single setup of μEDM. However, the process suffers a setback in the form of tool wear which is an intrinsic feature of any EDM process [6]. The tool wear affects the shape and size of the desired microcavity resulting inadequacy in dimensional accuracy and precision [7]. Tool wear cannot be diminished entirely in μEDM, but measures

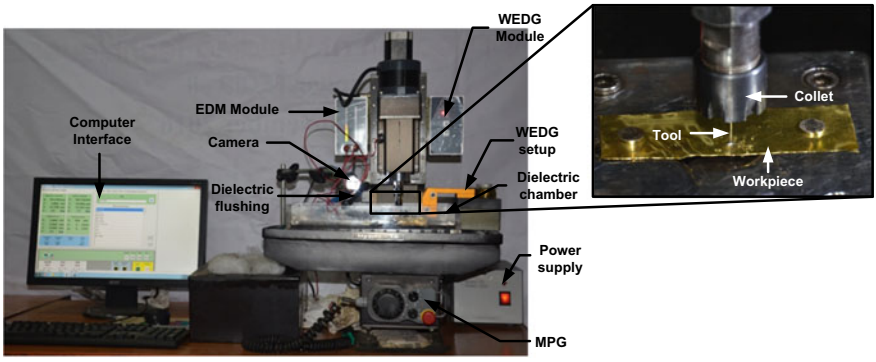

Fig. 1 Photographic view of micro electrical discharge machining (μEDM) (Model: Hyper-15, Make: Sinergy nano systems, Mumbai, India)

can be taken to minimize it. The first and foremost necessity is the selection of processing parameters of μEDM such that tool wear is minimum without impacting machining efficiency and surface quality. A trade-off is often required between surface quality and machining efficiency to attain dimensional accuracy and precision. To remunerate the effect of tool wear, application of tool wear compensation strategy is necessary. The framing of a compensation technique for μEDM requires plenty of pre-examined data on tool wear and its trend on the variation of the process parameters of μEDM. The accuracy of a certain applied compensation technique depends on the correctness of the pre-examined or real-time data. Accordingly, faulty data will lead to overcompensation or undercompensation of tool wear thus hindering dimensional accuracy. Estimation of the relative tool wear ratio, i.e., the ratio of tool wear rate to workpiece wear rate plays the most important role in formulating any compensation strategy. Compensation techniques can be categorized as off-line and on-line types. Off-line techniques rely on the extensive pre-examined data to incorporate relative tool wear ratio, whereas real-time techniques depend on some sorts of in situ measurement methods to predict or estimate the wear ratio.

μEDM and their variants are applicable in micromachining, so it is essential to be aware of the effect of individual processing factors in each of the variants to apply the proper tool wear compensation techniques. Besides the machining conditions, for instance, discharge energy, feed rate, tool rotation, etc., the inherent machine setup parameters such as resolution and repositioning capacity of the machine along with human partake in tool and workpiece fixation also plays a huge role in accuracy and precision of micromachined components. Thus, it is essential to consider all the factors involved with μEDM to achieve dimensional accuracy and precision in the micro features.

This chapter comprises process mechanism of μEDM, a detailed overview of the different variants of μEDM, dimensional accuracy and precision measurement of various features obtained by different variants of μEDM, and the state of art of different variants of μEDM in detail.

2 Process Mechanism of Micro Electrical Discharge Machining (μEDM)

The material removal mechanism in μEDM is based on electrothermal energy, which is utilized in between the tool and the workpiece during the sparking process as shown in Fig. 2. The electrical energy results in a series of discharges in between the tool electrode and the workpiece to erode materials from tool and workpiece simultaneously [8]. The discharged energy is employed in the form of thermal energy causing melting and vaporization of the materials. The process takes place in the dielectric medium, which is ionized due to the collision of electrons emitted from the tool electrode. This phenomenon leads to dissociation of ions from the molecules of the dielectric fluid, and as a result of this, the concentration of electrons and ions

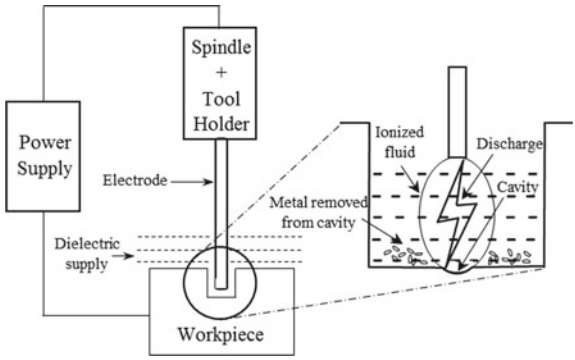

Fig. 2 Mechanism of μEDM

becomes high and such high concentration of electrons and ions is characterized as plasma. The plasma channel provides the path for flowing sparks to remove materials from the electrodes. The working principle of μEDM is similar to macro *EDM*, but the former differs from the latter in certain aspects which can be listed as [9]:

a. *Plasma channel diameter*: The width of the plasma channel determines the size of the unit removal of material that will expel out due to discharge. Unlike macro *EDM*, where the size of the tool is several times larger than the plasma channel diameter; in μEDM, due to the smaller diameter of tool electrodes used, the plasma channel diameter may equal or even exceed the tool diameter. The pulse duration controls the expansion phenomenon of the plasma channel. It is very important to limit the pulse duration until the plasma channel exceeds tool diameter as the wear phenomenon of material in such cases are unpredictable.
b. *Electrode heating*: Electrode of diameter less than 1 mm is used for μEDM. Since the smaller electrode is used, it does not possess sufficient mass to transport the heat from the discharge site. This property acts as a limiting source to the amount of energy that can be supplied in the μEDM process and affects the erosion rate of materials accordingly.
c. *Viscous force of dielectric on electrode*: The tool electrode is more susceptible to deflection by the viscous force of dielectric due to its smaller size. This phenomenon limits the volume and velocity of dielectric that can be supplied where fluid friction possesses the capability to distort the tool electrode. Due to this reason, in most of the μEDM process, jet flushing is used, which can be adjusted to exert a minimum force on the tool electrode.

To achieve a micromachined profile with desired accuracy and precision, it is very important to understand the factors that are acting and their effects in the material removal mechanism of tool and workpiece. Besides the machining factors that directly contribute to the μEDM process, some equipment setup parameters also play a pivotal role in the quest for accuracy and precision. The factors affecting the accuracy and precision in μEDM are listed in Fig. 3.

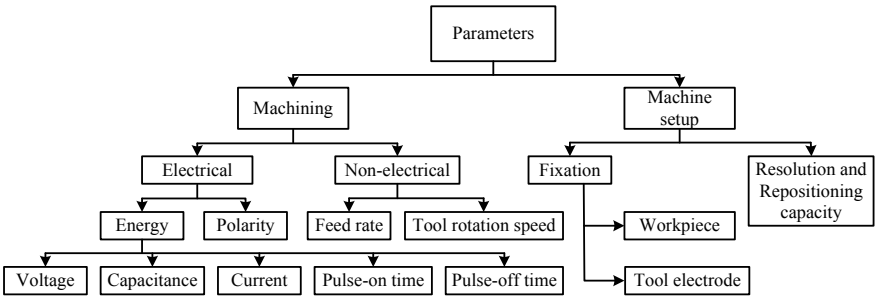

Fig. 3 Classification of the factors affecting accuracy and precision in μEDM

2.1 Machining Parameters

The machining parameters play the most vital role in achieving dimensional accuracy and precision as they directly affect the erosion mechanism of tool and workpiece. Thus, it is essential to correctly select the machining parameters to obtain accurate and precise micro features. The machining parameters affecting the wear of tool electrode and the workpiece in μEDM can be grouped into electrical and non-electrical factors. The electrical and non-electrical factors can be further subdivided into more discrete elements which are discussed below.

a. *Discharge energy*: To produce micro features by μEDM, the supply of energy in the inter-electrode gap has to be so minimal that it is just sufficient for the required unit removal of material for micromachining. Resistance–capacitance (RC) type pulse generator has been widely used to supply lower energy in μEDM where maximum discharge energy per pulse (E_{RC}) can be written as depicted in Eq. (1) [10]:

$$E_{RC} = \frac{1}{2} C V_g^2 \tag{1}$$

where, capacitance and gap voltage are denoted by C and V_g, respectively. The capacitor stores the energy until discharge occurs whereas voltage determines the breakdown limit for current flow through the dielectric fluid. Imperative parameters such as current and pulse duration are taken care by capacitance in RC-type pulse generator [11]. Capacitor mainly controls the melting and vaporization of materials during μEDM process whereas voltage controls the pulse initialization factor. Transistor-type circuit has also been used in many μEDM applications where discharge energy per pulse is expressed as shown in Eq. (2) [12]:

$$E_T = V_p I_p \frac{T_{on}}{T_{on} + T_{off}} \tag{2}$$

where V_p, I_p, T_{on}, and T_{off} represent the voltage of a single pulse, current of a single pulse, pulse duration, and pulse interval, respectively. The discharge energy per pulse in transistor type is significantly higher and can be compared to that of conventional macro EDM [13]. Current and voltage directly influence the discharge energy in proportionality. Higher energy results in a powerful spark and produces deeper craters on the workpiece surface, deteriorating the surface quality and dimension [14]. The term "$\frac{T_{on}}{T_{on}+T_{off}}$" is also known as the duty cycle which can be defined as the ratio between pulse duration and the total cycle time (pulse duration + pulse interval). This parameter plays an important role in the transistor-pulse-type generator of μEDM [15]. Although minimum T_{off} increases efficiency, a suitable combination of T_{on} and T_{off} is required for stable machining and in most of the cases, the value of T_{off} is selected based on T_{on} value. Transistor-type generator increases efficiency but leads to poor surface quality and imprecise dimension. Elsewhere, *RC*-type generator renders higher dimensional accuracy and precision by commanding the voltage and capacitance, which in turn controls the discharge energy.

b. *Polarity*: Polarity determines the direction of current flow throughout the circuit. When tool electrode (linked to spindle) is joined to the cathode (negative polarity), the polarity is termed as straight, whereas when it is joined to the anode (positive polarity), the polarity is termed as the reverse. In either of the cases, the workpiece is joined to the opposite terminal to that of the tool electrode. For the purpose of micromachining, straight polarity is used, whereas when the desire is to remove the maximum amount of material from the electrode linked with the spindle, the reverse polarity is beneficial.

c. *Feed rate*: Feed rate in μEDM should not be correlated with the feed rate of conventional machining where it determines the machining rate. The parameter 'feed rate' in all the variants of μEDM signifies the speed at which the tool adjusts itself to maintain sufficient gap for discharge between tool and workpiece. Feed rate principally performs two functions [16]. Firstly, when the process runs into short-circuiting, the tool flinches back and accelerates with the action of a servo control for maintaining stable sparking gap. Secondly, when the gap between tool and workpiece is more than the spark gap, the tool positions itself with the closest point of the workpiece surface for sparking to occur. An increase in feed rate decreases the non-machining or idle time, thus increasing the processing efficiency. But higher feed rate causes unwanted surface damage due to secondary sparking caused by the trapped debris particles as they do not get sufficient time to flush away from the discharge site.

d. *Tool rotation speed*: Tool rotation imparts a centrifugal force that supports in order to throw away debris particles from the discharge region [17]. It also produces an agitation effect and allows proper functioning of dielectric fluid by enabling it to flow through the inter-electrode gap [18]. Tool rotation becomes imperative in higher depth micromachining as the jet flushing would constrain up to a certain limit, and the debris would adhere to the tool and workpiece surface. Vibration-assisted tool holder or workpiece holder can produce agitation and remove the trapped debris, but it requires an additional auxiliary setup. Thus, tool rotation at

certain revolutions per minute (rpm) provides a subtle alternative for enhancing the molten metal flow and debris flushing from the working zone [19]. The surface quality also improves as rotation splits the spark and changes the spark position ensuing in smaller craters on the workpiece surface.

2.2 Machine Setup Parameters

Some miscellaneous factors such as equipment motion capacity and human share in the handling of tool and workpiece also affect the dimension of the micro features. These parameters act as a vital source of errors in micromachining, although in maximum study effect of these sources are neglected. The effects of the machine setup parameters are discussed below.

a. *Tool electrode and workpiece fixation*: Tool and workpiece fixation plays a significant role in inhibiting positioning errors. Wang et al. [18] analyzed different errors of a μEDM system associated with the end surface, shaft, and hole positioning. The end-surface positioning type is applicable for positioning of mutually perpendicular surfaces such as rectangular workpiece where an angle exists between the ideal and actual position of the workpiece. The hole-positioning type is applicable for micro wire electrical discharge machining (μWEDM) where the wire electrode has to be inserted into the pre-drilled hole. The challenge lies in positioning the wire electrode exactly at the center of the pre-drilled hole where positioning error can be reduced by minimizing the hole and wire diameter. The positioning of a rod, wheel, and other cylindrical structures can be executed by a shaft-positioning technique which is similar to the hole-positioning method except for possessing an electrode. The diameter of the electrode and roundness of the cylindrical body affects the positioning error. Apart from positioning shift, improper tool–workpiece fixation may also lead to tapering and breakage of tool electrode, thus hindering any form of accuracy and precision [19]. A high-resolution vision system will allow a platform to visualize the errors inhibited in clamping and rectification can be carried out by analyzing the images accordingly. To machine complex microstructures, integrated technique (combination of μWEDM, μED-milling, etc.) is preferable to increase processing efficiency and achieving higher accuracy. Reclamping of tool and workpiece should be avoided as it would inadvertently produce an error in clamping that would transmit to the machined product, so the processing route should be focussed on minimum numbers of reclamping of tool and workpiece, preferably in single setting [20].
b. *Resolution and repositioning capacity*: Resolution refers to the smallest measurable decrement or increment in the position of the machine tool, whereas repositioning refers to the repeatability with which the machine can revert to a particular position within the maximum travel of all the axes of the machine tool. Multiple to and fro movements are often required to machine a complex microcavity. In such scenario, the precise positioning of work coordinates is required, which depends

on the repositioning capacity of the machine tool. Pham et al. [21] reported nonattainment of positioning accuracy and repeatability as one of the important roots of error. In their research, they used laser interferometer for measuring the positioning repeatability and accuracy. Technically, lower the resolution and position accuracy value, higher would be the chances of acquiring accurate work coordinates, thereby increasing the probability of precise dimension of machined micro features.

3 Different Variants of Micro Electrical Discharge Machining

μEDM can be divided into several variants depending upon the micro features desired, and thus, the movement of the electrode and workpiece needs to be maneuvered accordingly. The several variants of μEDM which are in practice for micromachining can be listed as follows:

3.1 Micro Wire Electrical Discharge Grinding (μWEDG)

μWEDG is used for fabrication of micro-rods whose processing mechanism is similar to the μWEDM. In this process, a larger diameter rod is rotated and fed vertically against the wire electrode to reduce the diameter of the rod. Compared to other μEDM variants, μWEDG produces micro-rods with higher dimensional accuracy and precision as the effect of tool wear is negligible or minimum in this case. This is due to the continuous passing of fresh wire during machining. A sketch diagram and photographic image of the μWEDG process are depicted in Fig. 4.

3.2 Block Micro Electrical Discharge Grinding (B-μEDG)

B-μEDG is used for fabricating micro-rods, where a larger diameter rod is rotated and fed horizontally into a solid block. The solid block acts as a sacrificial electrode in this process. A sketch diagram and photographic view of the B-μEDG process are shown in Fig. 5. The machining efficiency of the B-μEDG process is higher than μWEDG process as the rotating tool remains in the vicinity of a larger surface of block compared to the wire in the μWEDG process. But, some tapering prevails in the micro-rods fabricated due to the trapped debris between the tool and the block along the axes of the tool. This leads to secondary discharges and a non-uniform gap between the tool and block electrode.

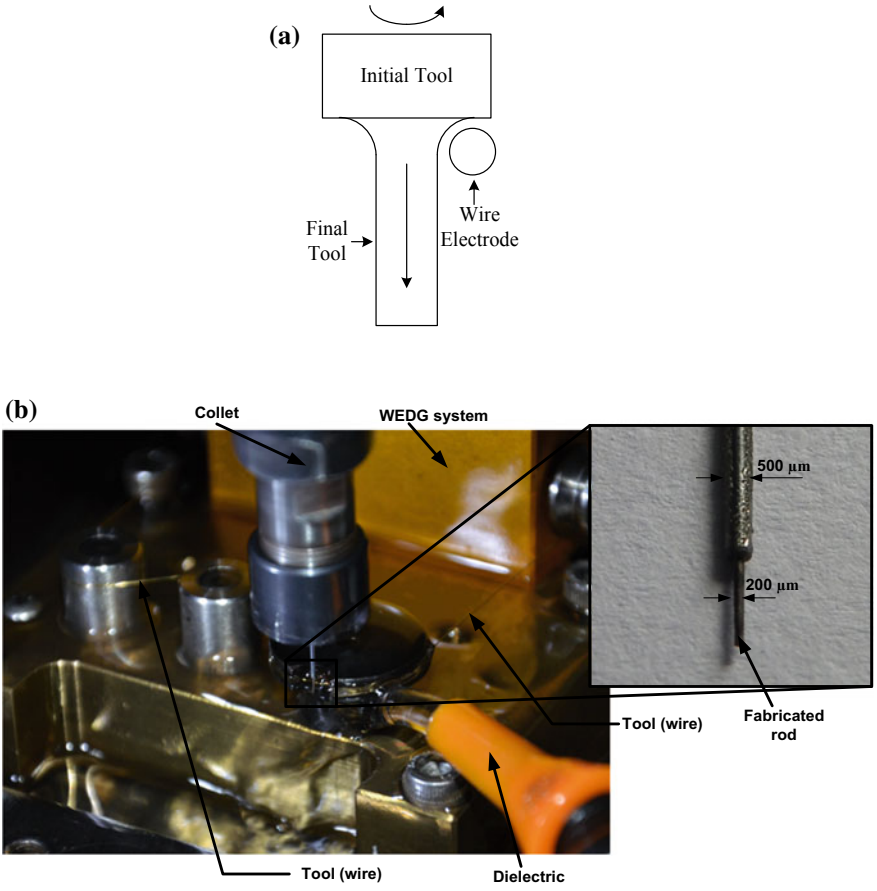

Fig. 4 **a** Schematic diagram of µWEDG. **b** Pictorial image of the process of µWEDG

3.3 Micro Electrical Discharge Drilling (µED-Drilling)

In µED-drilling, a tool electrode is vertically fed against the workpiece until a desired depth of the drilled hole is achieved. Figure 6 represents the schematic diagram and pictorial image of µED-drilling where the tool electrode is rotated and fed vertically against the workpiece. Drilling may be attained simply by vertical feeding, but rotation increases machining efficiency and improves circularity in shape. This process may be used for drilling blind holes as well as through holes according to desired applicability. Precise machining of the blind hole is an exhausting task compared with through holes due to the difficulty in estimation of the hole depth in a blind hole.

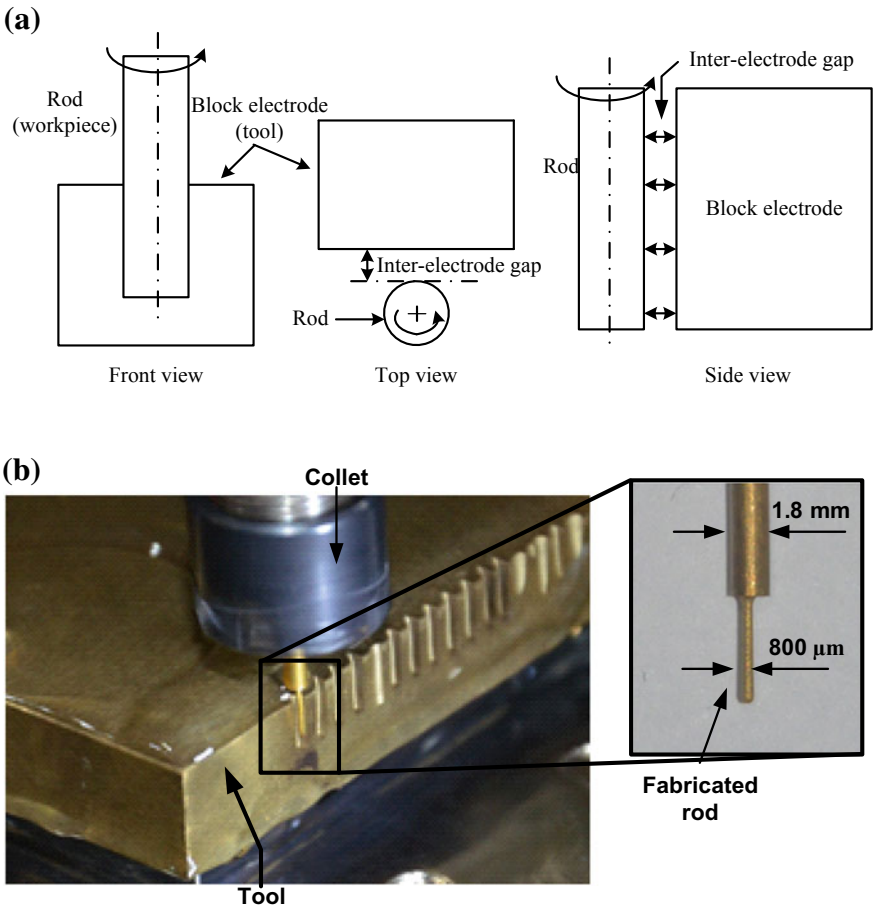

Fig. 5 **a** Schematic diagram of B-µEDG. **b** Pictorial image of the process of B-µEDG

3.4 Reverse Micro Electrical Discharge Machining (R-µEDM)

Generally, in µEDM operation, the tool electrode is joined to the negative terminal whereas the workpiece is joined to the positive terminal to impart high material removal from the workpiece. But R-µEDM works on opposite polarity to that of conventional µEDM with the motive of imparting more material removal in the form of debris from the tool electrode connected to the spindle. This phenomenon is used for fabrication of micro-rods, where larger diameter rods are fed against pre-drilled holes on a plate with the intention of reducing the diameter of the rod to that of pre-drilled holes. A schematic diagram of the R-µEDM process along with its pictorial image is shown in Fig. 7. This process also allows fabrication of an

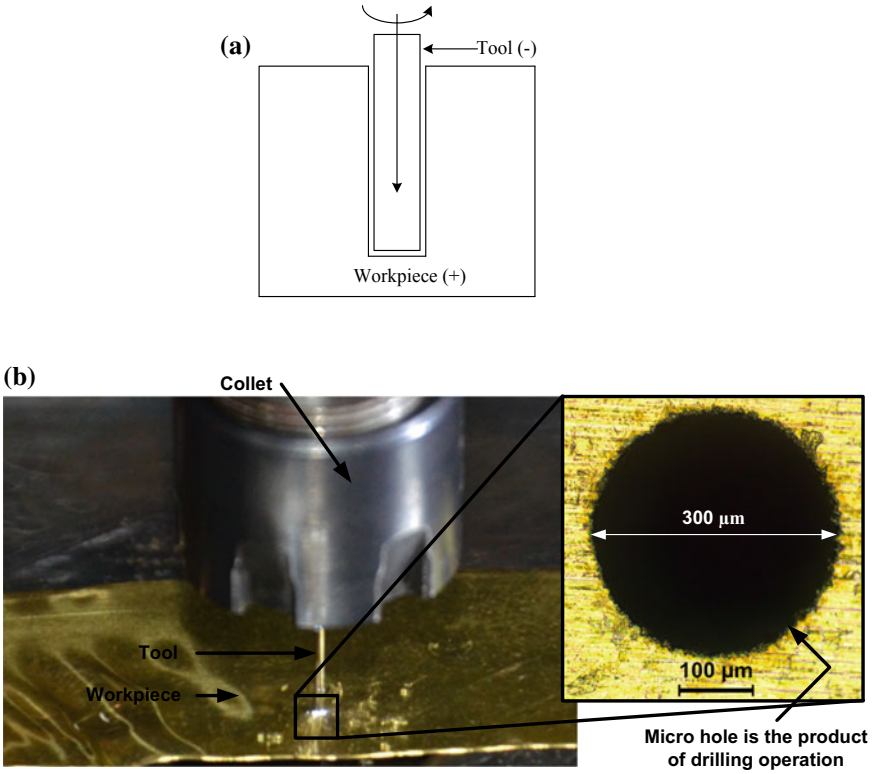

Fig. 6 **a** Schematic diagram of µED-drilling. **b** Pictorial representation of µED-drilling process

array of micro-rods when the rod is fed against an array of pre-drilled holes. The spindle cannot be rotated in such cases as rotation would vanish any microstructure fabricated on the rod on its periphery other than its center.

3.5 Drilling with in Situ Fabricated Tool

This technique is accomplished in two steps. In the first step, −ve polarity is assigned to the tool electrode to drill micro hole in the plate electrode (Fig. 8a, b). In the second step, +ve polarity is assigned to the same tool electrode (rod), which is now treated as a workpiece for the reduction of its diameter. The same electrode is then withdrawn and moved slightly in the lateral direction (*x*-axis or *y*-axis) to make an eccentricity with the drilled hole (Fig. 8c). Thereafter, the rotating workpiece (rod) is moved downward to interact with the side of the drilled hole as shown in Fig. 8d. While being fed downwards, the workpiece loses material from the surface resulting in a decrease in its diameter. Thus, a micro rod is fabricated, which can be used as a

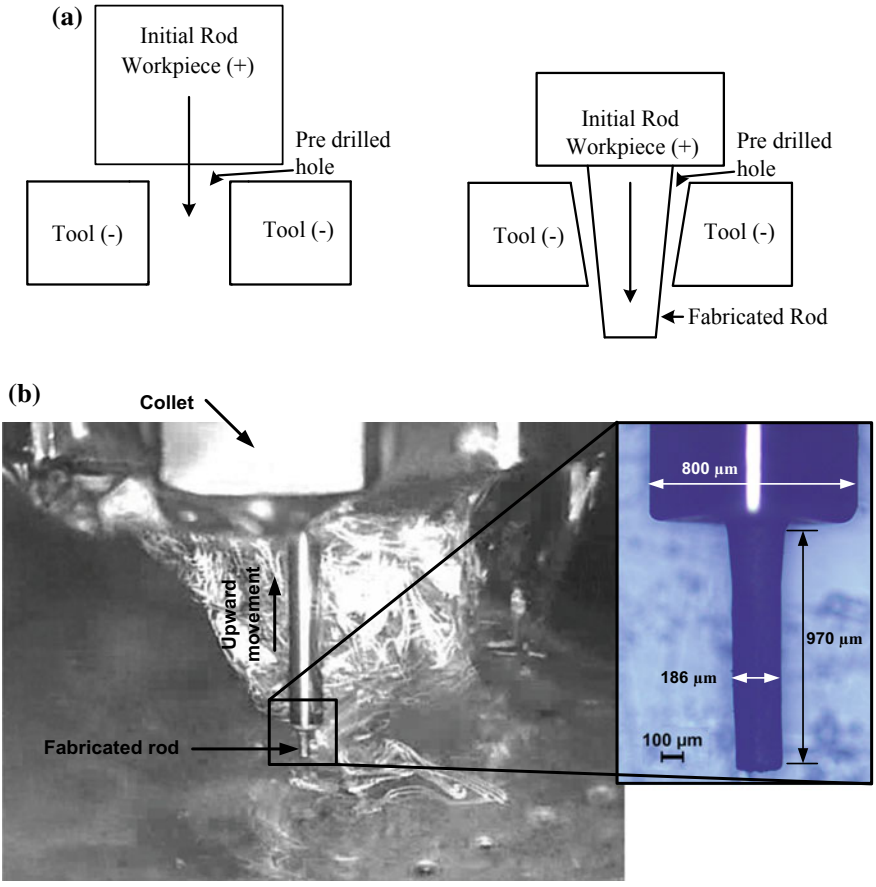

Fig. 7 **a** Schematic diagram of R-µEDM. **b** Pictorial representation of R-µEDM

micro tool. This process is known as drilling with an in situ fabricated tool because the fabricated micro rod is further used as a tool electrode. The fabricated micro rod used later as a tool to drill micro holes on the metallic plates is depicted in Fig. 8e, f.

3.6 Micro Electrical Discharge Milling (µED-Milling)

µED-milling is the technique through which tool electrode is continuously fed in horizontal (x–y) direction with a predetermined depth of cut which is set at the beginning of machining. It is generally performed as a layer by layer machining process, where each layer contributes a certain depth of cut. Figure 9a represents the sketch diagram of a µED-milling process used for fabricating microchannels. Micro slots fabricated on copper by µED-milling process are shown in Fig. 9b. The

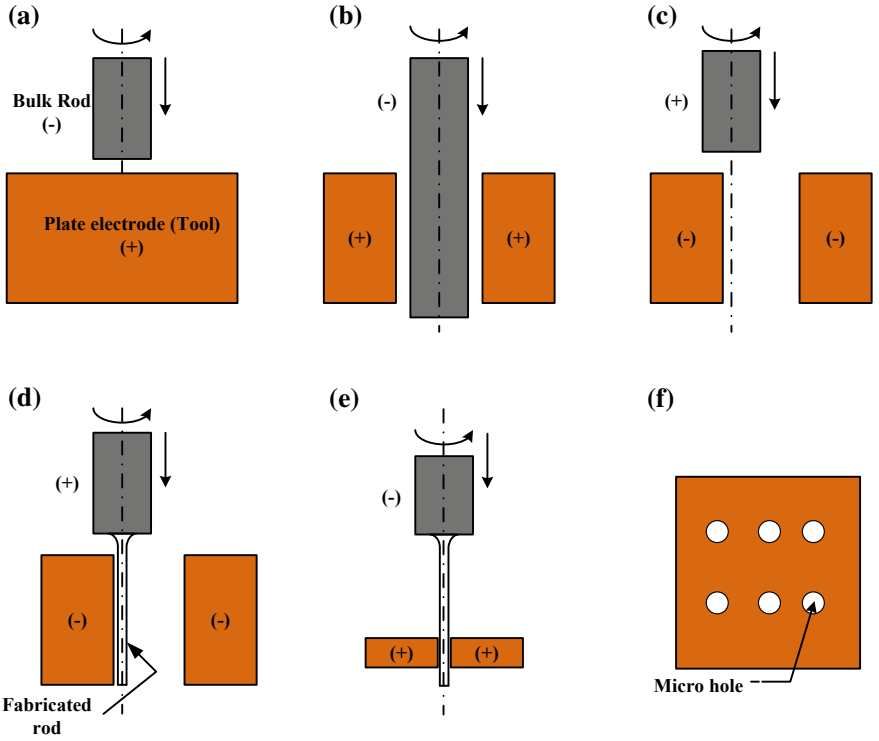

Fig. 8 Schematic diagram of drilling with in situ fabricated tool

movement mechanism of μED-milling allows machining of complex microcavities with the use of simple cylindrical micro tools. Thus, the process eliminates the use of complex-shaped tools for machining 3D cavities as in the case of die-sinking μEDM process. But tool wear is a concern to maintain the dimensional accuracy of the features to be machined on the workpiece. In this case, to get accurate dimension and precise measurement of the machined cavity, tool wear needs to be compensated by some form or other.

4 Dimensional Accuracy and Precision Measurement

μEDM is broadly used for fabricating micro features, for example, micro-rods, micro slots, and micro holes due to their broad applicability in industries. Quantitative evaluation of these micro features is essential to achieve accuracy and precise dimension. The performance measures by which the micro features can be analyzed are described in this section.

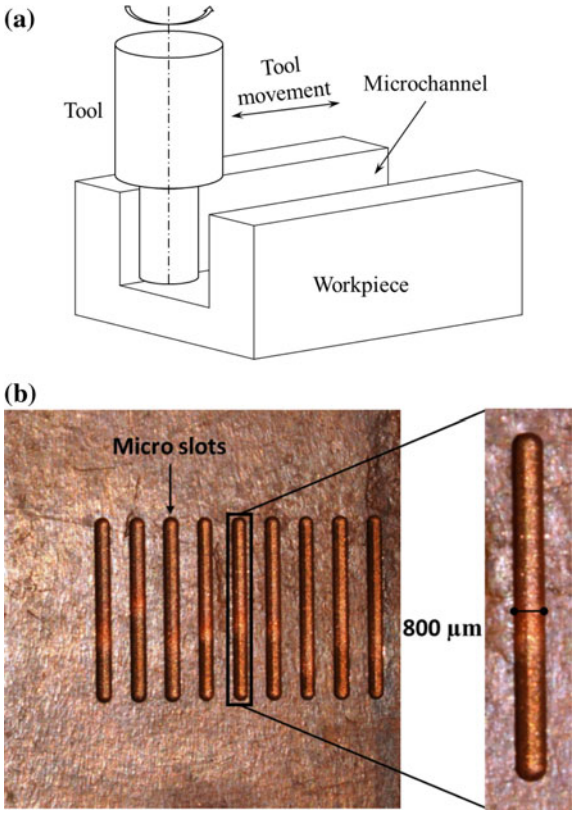

Fig. 9 **a** Sketch diagram of microchannel fabricated by μED-milling. **b** Micro slots fabricated by μED-milling process

4.1 Micro-rods

Machining time, surface roughness, standard deviation in diameter, and average diameter are the response measures needed to be quantified in order to obtain the micro features with target diameter and length along the surface of the micro rod.

Average diameter: The secondary sparking between the tool and workpiece causes non-uniform tool wear leading to a tapered micro feature. In case of micro-rods, taperness can be assessed by calculating the average diameter of the rod along its entire length, i.e., from tip to root. Figure 10a shows a schematic diagram depicting the target diameter and obtained diameter of a micro rod. A micro rod fabricated by μEDM is represented in Fig. 10b. The diameter of the rod is evaluated at different position along the length of the rod. The tip and middle part of the rod show desired diameter. However, a signification variation of diameter is observed in the root of the rod. To clarify the difference in diameter of the micro rod, the deviation of the micro rod diameter is plotted along its entire length as represented in Fig. 10c. The straightness of the fabricated micro rod holds good till it reaches 700 μm length.

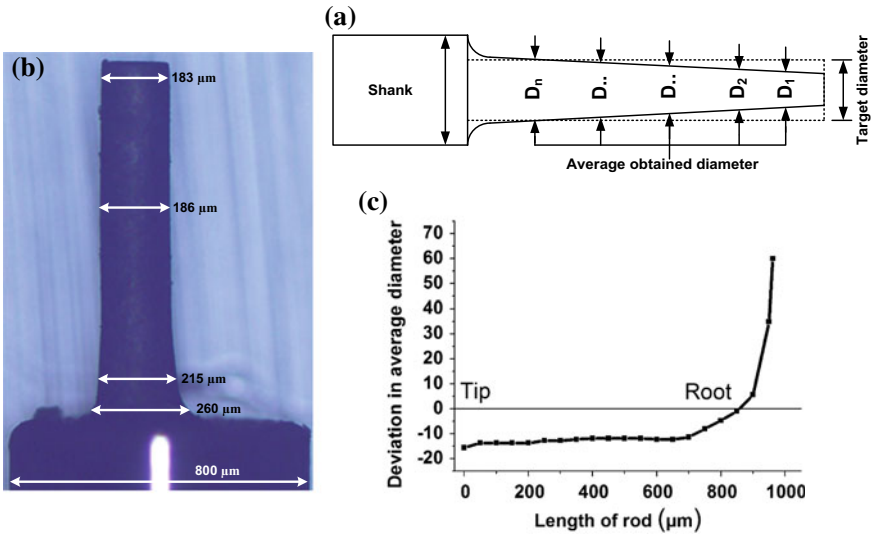

Fig. 10 Representation of average diameter

Beyond 700 µm, i.e., in the root of the micro rod, a high amount of deviation is observed.

Standard deviation in diameter: It can be used to study the deviation in straightness along the top surface of the micro rod. Straightness should be constantly maintained on the entire length of the micro rod. Deviation of straightness along the length of the micro rod can be assessed by calculating the standard deviation in diameter. Minimum standard deviation of diameter is desired to achieve accurate and precise micro rod.

4.2 Micro Holes

Tool wear rate (TWR), material removal rate (MRR), overcut, circularity, taper angle, edge sharpness, and recast layer are the response parameters which are directly involved in the evaluation of micro holes in order to characterize them.

Tool wear rate: It is the amount of tool material which erodes slowly from the tool per unit time during the machining process. *TWR* is to be controlled to obtain the error-free micro features with higher dimensional accuracy. The schematic diagram depicted in Fig. 11 shows the ideal condition and the real condition of the tool after the machining process.

Material removal rate: Material removal rate (MRR) is the quantity of undesirable material which comes out from the metal surface per unit time for getting the desired features. It can be evaluated by measuring the weight before and after the machining

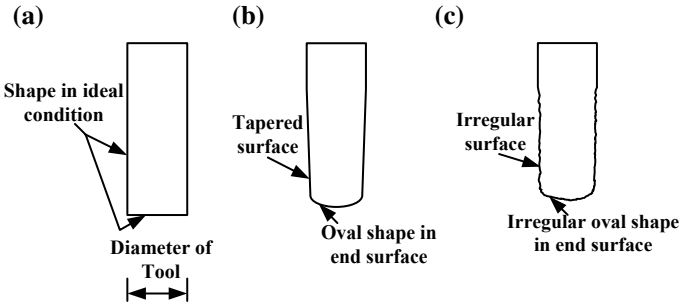

Fig. 11 Shape of the tool after machining in ideal and in real condition. **a** In ideal condition. **b** Tapered and oval shape along the length and end surface, respectively, in real condition. **c** Irregular surface and irregular oval shape along the length and end surface, respectively, in real condition

process as depicted by Eq. (3). Further, MRR can be also determined by calculating the volume of material removed after an operation or measuring the irregular geometrical features as depicted by Eqs. (4)–(6) and the corresponding schematic diagrams as shown in Fig. 12a–c, respectively.

$$\text{MRR} = \frac{W_\text{i} - W_\text{f}}{\text{Machining time}} \tag{3}$$

where, initial weight (before machining) and final weight (after machining) of the workpiece are denoted by W_i and W_f, respectively.

$$\text{MRR in ideal condition} = \frac{\pi r^2 \times h}{\text{Machining Time}} \tag{4}$$

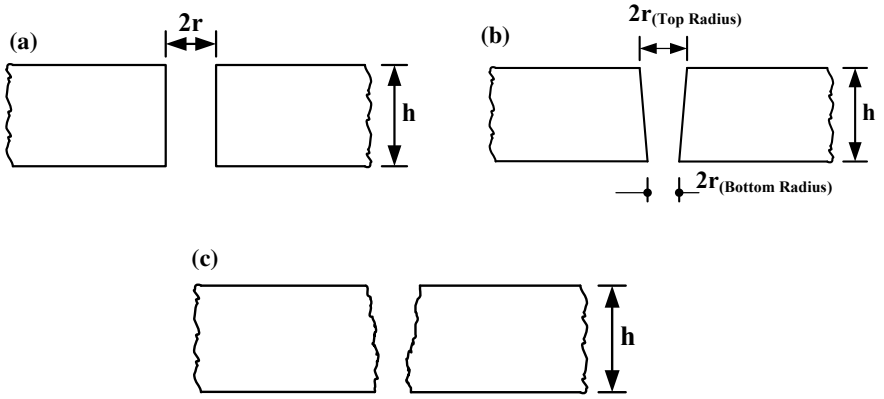

Fig. 12 **a** MRR in ideal condition. **b** MRR in case taper shape feature. **c** MRR of irregular shape feature

$$\text{MRR(in case of frustum shape)} = \frac{\pi / 3\left[r^2_{\text{Top Radius}} + r_{\text{Top Radius}} r_{\text{Bottom Radius}} + r^2_{\text{Bottom Radius}}\right] \times h}{\text{Machining Time}} \quad (5)$$

$$\text{MRR(in case of irregular shape)} = \frac{\text{Volume of irregular shape features}}{\text{Machining time}} \quad (6)$$

where h denotes depth of the hole and r indicates different radii.

Overcut: It occurs due to the spark gap or inter-electrode gap (IEG) existing between the tool and the workpiece. Overcut can be calculated by Eq. (7) and its corresponding sketch diagram is represented in Fig. 13. As the IEG is an inevitable situation in EDM; hence, overcut is an unavoidable phenomenon. Although it brings some deviation in the size of the drilled hole than the size of the tool concerning diameter, in turn, it is an advantageous situation for EDM. Overcut helps in maintaining the IEG between the electrodes. Hence, a healthy machining without short circuit takes place. Moreover, the overcut provides the clearance between tool and workpiece which provides the free passage of the debris particles to come out of the machining zone. It varies with the increase in voltage and capacitance and can be minimized by proper adjustment of the process parameters.

$$\text{Overcut} = \frac{\text{Hole diameter} - \text{Tool diameter}}{2} \quad (7)$$

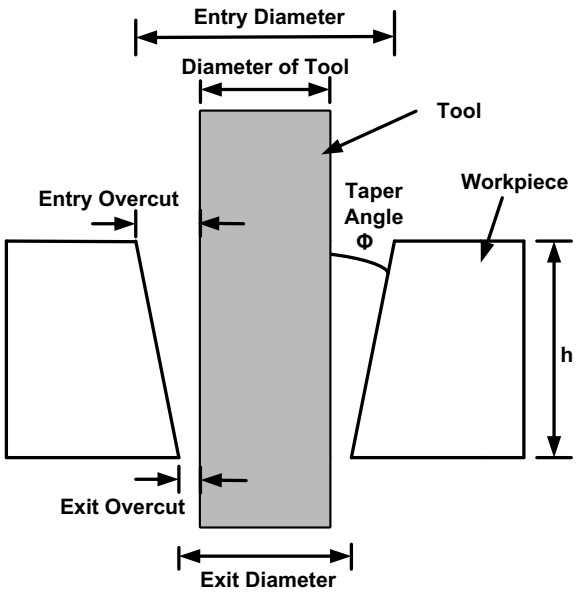

Fig. 13 Representation of overcut and taper angle

Taper angle: The tapered surface starts from the entry edge of the hole and ends with exit edge of the hole of the workpiece as shown in Fig. 13. The taper angle subtended by this surface is mathematically expressed in Eq. (8). Taper angle occurs due to secondary sparking, which removes more material gradually from the entry side when the sidewall of the tool interacts with the wall of the already machined hole while moving downward. Moreover, the inevitable phenomenon of tool wear in EDM is also responsible for causing taperness in drilled hole.

$$\text{Taper angle}(\theta) = \tan^{-1}\left(\frac{\text{Entry diameter} - \text{Exit diameter}}{2h}\right) \tag{8}$$

where h represents depth of the hole.

Circularity: It defines the roundness of the circular features of machined parts. Practically, circularity demands the edge of the features to be round. The deviation in the circular features, i.e., out of roundness of a micro hole is known as circularity error. Circularity error of a hole can be measured by a technique using circumscribed and inscribed circle of the hole as shown in Fig. 14. The difference between the radius of the circumscribed and inscribed circle is used to measure the circularity error of the hole as depicted in Eq. (9). Circularity error mainly occurs due to non-uniform sparking at the edges of the hole.

$$\text{Circularity error} = \frac{\text{Circumscribed diameter} - \text{Inscribed diameter}}{2} \tag{9}$$

Edge sharpness: It is defined as the uniformity on the edge of the micro hole throughout the circumference. The irregularity in edges of a hole known as edge deviation, occurs due to non-uniform sparking in the form of arc pulses, short circuit pulses, open-circuit pulses, etc. [22], during the machining process. Edge deviation is the average gap between the circles circumscribing and inscribing at the edge of a certain segment in the hole. It is calculated by measuring the diameter of the curves inscribing and circumscribing the edge as shown in Eq. (10) corresponding to Fig. 15.

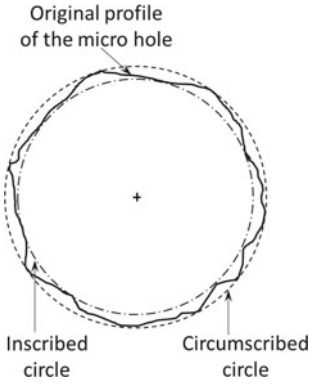

Fig. 14 Circularity error

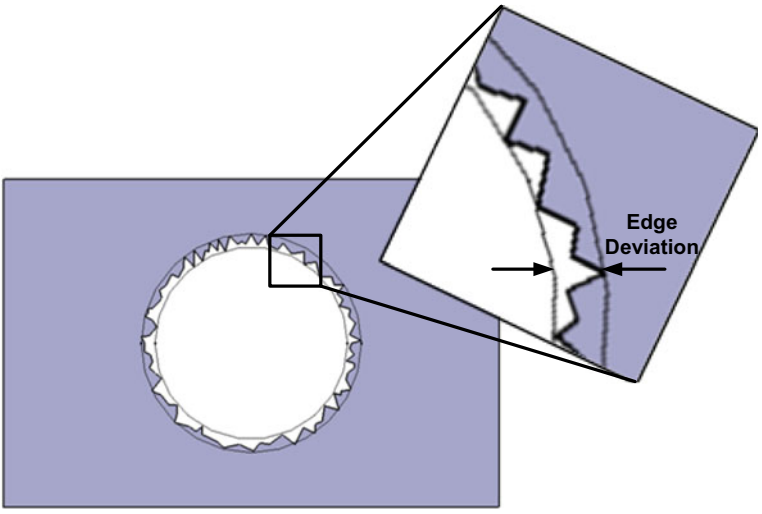

Fig. 15 Edge deviation

$$\text{Edge deviation} = \frac{\text{Maximum diameter} - \text{Minimum diameter}}{2} \tag{10}$$

Recast layer: During the sparking process, a high temperature is generated in the working zone which causes the metals to melt and vaporize and flushes away from the sparking region in the form of debris. But a small portion which does not get flushed away from sparking region remains deposited on the finished work surface. The deposited amount on the finished work surface in the form of molten metal, after solidification, is known as recast layer as shown in Fig. 16. This also has an effect on the quality of the drilled holes. Hence, it is important to assess the thickness of the recast layer.

Fig. 16 Recast layer

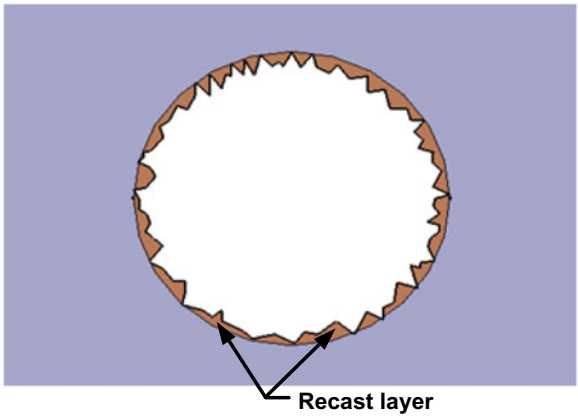

4.3 Micro Slots

The effect of tool wear in μED-milling of one layer is represented in Fig. 17. It is detected that, as the milling progresses along the length, the width and depth of the slot decrease leading to inaccuracy and imprecision. The dimensional inaccuracies in μED-milling of one layer are further classified in Fig. 17a, where d_1 and d_2 represent the depth of the slots at start and end; w_1 and w_2 represent the width of the slots at start and end of the top surface; w_{b1} and w_{b2} represent the width of the slots at start and end of the bottom surface, respectively. Deviation of the slot along the width and depth is clearly visible. Figure 17b represents the effect of tool wear on the micro slots due to single-layer machining by μED-milling process. The width and the depth of the slot gradually diminish as the length of the milling proceeds. To overcome the problem of deviation, tool wear compensation techniques need to be used. Many tool wear compensation techniques have been proposed by several researchers which are mentioned in details in Sect. 5.6. Traditionally, to and fro scanning method is used to get similar dimensional features over the two ends of a milling slot as depicted in Fig. 17c. But for achieving precise and accurate dimensional features, tool wear compensation techniques need to be employed.

5 State of the Art of μEDM

The dimensional accuracy and precision measurement are few of the important aspects by which one can judge the progress, improvement, and advancement of process capabilities and dimensional errors of the micro features fabricated by μEDM process. There are different variants of μEDM such as μED-drilling, R-μEDM, drilling with in situ fabricated tool, μWEDM, μWEDG, B-μEDG, and μED-milling, and their progress by many researchers are mentioned in the following subsections.

5.1 Micro Wire Electrical Discharge Grinding (μWEDG)

μWEDG utilizes traveling wire as a tool electrode. This process is applicable for grinding micro-rods to reduce their diameter further. In the year *1985*, Masuzawa et al. [23] introduced a method called μWEDG for the machining of small diameter rods. The process provided little accuracy and excellent repeatability with an error $< 1\,\mu m$. Moreover, they also fabricated many thin shape parts and components such as needle-shaped parts, electron emitters, punches, and electrode for EDM. Sheu [24] introduced a new hybrid technique combining one pulse discharge (OPD) with μWEDG to machine multi-micro-spherical probes. Using this method, he found a better result in the form of instantaneous fabrication of micro-spherical probes of

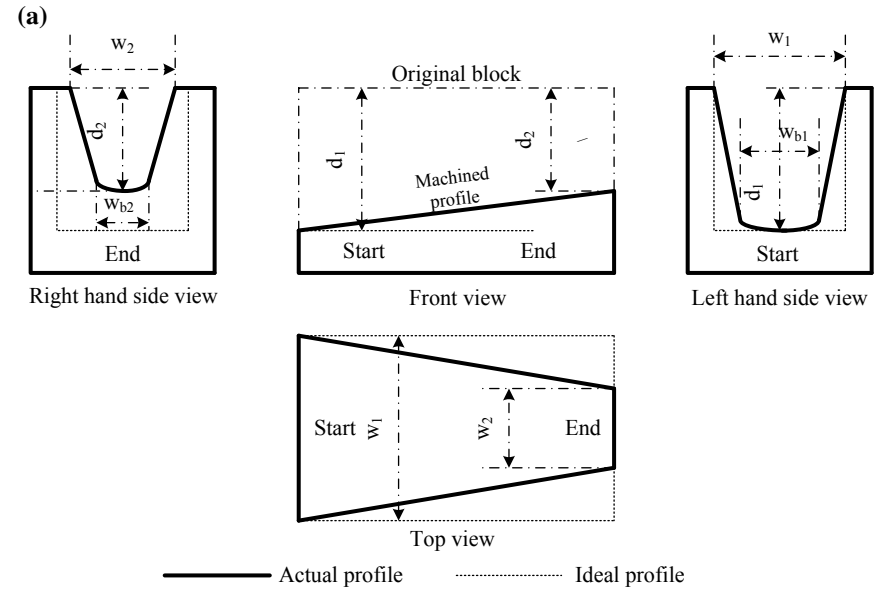

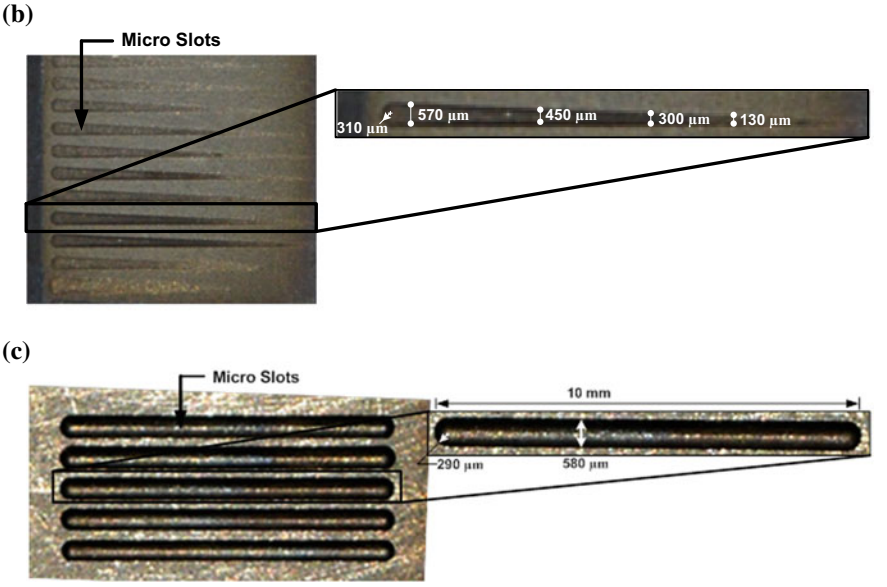

Fig. 17 **a** Sketch diagram of micro milling with different views shows the actual profile and the ideal profile of the micro slot. **b** Represents the effect of tool wear after fabricating micro slots in µED-milling process. **c** Shows the micro slots after applying compensation method

approximately 40 μm diameter. Rees et al. [25] combined the μWEDG with a rotating submergible spindle for carrying out the machining operation. They conducted an experimental study to find out the statistically significant parametric condition using optimization technique which influences the surface quality more during the main cut. μWEDG and B-μEDG processes were combined by Oliaei et al. [26] to machine milling tools in micro size of variant geometries on tungsten carbide (WC) and polycrystalline diamond (PCD). In their study, they maintained the quality while fabricating the microfluidics chips, which was actually a prototype, using micro end mill tool. For improving the processing efficiency and the consistency accuracy of the μWEDG operation, Tangential feed WEDG (TF-WEDG) technique was taken by Zhang et al. [27]. They combined TF-WEDG to real-time measurement system through the charge-coupled device (CCD). Moreover, they joined the self-drilling holes method with TF-WEDG for further enhancement of the machining efficiency while fabricating micro-rods. Using the fabricated micro-rods, micro hole drilling was performed. The results of their study demonstrated repeated machining accuracy of micro-rods to be around or lower than 2 μm and consistency accuracy of arrayed micro holes to be around ±1.1 μm [27].

5.2 Block Micro Electrical Discharge Machining (B-μEDG)

B-μEDG involves a multi-pass process in which certain amount of material erodes from each side of the workpiece to minimize the dimensions of the micro features. Ravi and Huang [28] have developed the B-μEDG method for fabricating symmetrical sections such as rectangular, tapered, circularly, stepped, and triangular. They found the process to be feasible for fabricating micro features with various shapes. Zhao et al. [29] proposed a tangential feeding method of B-μEDG to overcome the difficulties encountered while fabricating micro-rods of desired dimensions. Experimental results of their research highlighted the present method to be effective in terms of producing accurate dimensions of the micro-rods. Formation of the taper angle is one of the major problems in the B-μEDG method, and for solving this problem, Jahan et al. [30] introduced electrode in the form of a moving block while fabricating micro-rods.

5.3 Micro Electrical Discharge Drilling (μED-Drilling)

The μED-drilling process is frequently used for drilling micro holes in a vast scope of demands, for instance, biomedical, automotive, aerospace, MEMS, and nuclear sector. In the recent past, a significant contribution has been made by many researchers toward the enhancement of the accuracy of the edges of the micro features. The improvement made by different researchers regarding the machining of micro hole is stated here.

Pham et al. [31] introduced a simple technique based on geometrical information for evaluating the volumetric wear ratios of the tool electrode, i.e., tube and rod types. They briefly discussed the electrode shape variation during the machining process consisting of various machining parameters and suggested possibilities of some wear compensation techniques. Pradhan and Bhattacharyya [32] proposed a novel technique for improving the accuracy of micro holes concerning straightness. They introduced a method of changing the polarity in a particular interval of time, which removes debris particles efficiently from the inter-electrode gap to improve the accuracy of micro holes. Puranik and Joshi [33] explored the connection among the achieved depth of the micro hole and their accuracy in μEDM. They observed that the micro hole with depth 5.0 mm could be easily achieved using 200 μm tool electrode by controlling the input conditions. Further increase of depth was not possible due to the occurrence of debris accumulation and secondary sparking. Transistor and RC-type generators in μEDM have been studied and explored by Jahan et al. [14] for obtaining quality micro holes. They found that RC-type was more appropriate for obtaining better micro holes in terms of accuracy and surface finish. Aligiri et al. [34] introduced a technique for improvement of tool wear in μED-drilling, wherein compensated length was calculated and adjusted until the target volume of removed material was reached. Result confirmed that the developed technique was more reliable than the uniform wear method (UWM). Jahan et al. [35] proposed vibration-assisted μEDM, in which workpiece was vibrated with low frequency for improving the performance of μEDM deep hole drilling. It was observed that the current approach improves the internal surface of the deep micro holes in terms of surface quality and accuracy. Heinz et al. [36] utilized non-magnetic materials in magnetic-field-assisted μEDM in their novel work. The result showed improvement in terms of increased volume removal and decreased tool wear, i.e., 28% and 50% between 0.33T and 0.66T, respectively, during the machining process. Maity and Singh [37] optimized the controlling parameters of the μEDM operation like capacitance, voltage, speed of rotation, and feed of tool, which influenced the response measures such as machining time, recast layer, and circularity error for drilling micro holes. Jahan et al. [38] utilized workpiece vibration-assisted μEDM machine for calculating the effectiveness of the low-frequency vibration for deep hole drilling. The result showed that 75 Hz vibration frequency and their corresponding amplitude of 1.5 μm to be appropriate for improving the performance of both machining characteristics and the accuracy of the micro holes. Ferraris et al. [39] applied an innovative method for drilling micro holes having an aspect ratio greater than 30. For doing so, they insulated the sidewall of the tools employing a coating to prevent the secondary sparks during the drilling process. They successfully drilled a 0.2 mm diameter micro holes with an aspect ratio of around 120 within a time duration of 1 h. Natarajan and Suresh [40] performed the machinability study of stainless steel grade 304 during μED-drilling operation. They observed that lower range of current and pulse on time enhanced the quality of the micro holes in terms of surface, while the higher range of current and pulse on time deteriorated the quality of the surface. D'Urso and Ravasio [41] investigated the effect of variant process parameters and the properties of the workpiece, for example, stainless steel, tungsten carbide,

and aluminium, and electrode materials such as tungsten carbide and brass, respectively, while drilling micro holes. They applied appropriate fitting equation with an acceptable coefficient of determination to analyze the summarized behaviours.

5.4 *Reverse Micro Electrical Discharging Machining (R-μEDM)*

In general, reverse machining in EDM means polarity conversion from negative to positive and vice versa. But the term used R-μEDM by many researchers in μEDM is different from the above. R-μEDM is a normal machining method where instead of keeping the workpiece on the work table, it is attached to the spindle through collet, and on the other hand, the tool is held on the work table.

From the last decades, work on reverse μEDM has been in constant progress. In the year *2006*, Kim et al. [42] successfully machined micro rod using different values of voltages and capacitances. For enhancing the accuracy of the micro features, they calculated the wear ratio at various values of input conditions and obtained the optimum input condition. They also fabricated different shapes of micro features on stainless steel such as channels (slots), grooves, micro hole, and rod arrays. To characterize the R-μEDM process while fabricating micro-rods, Taguchi methodology was applied by Mujumdar et al. [43], Mastud et al. [22], and Singh et al. [44]. Mujumdar et al. [43] used a bulk brass rod as a workpiece having diameter 2 mm and a thick copper plate of 200 μm with pre-drilled 200 μm circular hole and 400 μm square hole as a tool. They observed the gap voltage and capacitance to have more influence on response parameters such as dimensional accuracy, zero error length, and surface roughness. Moreover, they noticed that gap voltage was the utmost important factor accountable for the accuracy of the micro-rods along their length. Mastud et al. [22] used tungsten carbide 0.8 mm diameter as a workpiece and tungsten copper as a tool electrode having thickness 300 μm with a pre-drilled micro hole of 100 μm. They observed the erosion rate to advance with the passage of time during machining. Moreover, they found that lower thickness of tool electrode was more responsible for the enhancement of surface roughness of the fabricated micro-rods. Singh et al. [44] used a copper plate and tungsten rod as tool electrode and workpiece, respectively. The thickness of the tool was 293 μm with a drilled hole of 212 μm, on the contrary, the diameter of the workpiece was 0.8 mm. They focused on the accuracy of micro-rods to detect the deviation in length and the diameter from the target length and diameter in the form of input feed length and pre-drilled hole, respectively. They also detected the capacitance and feed rate to have more influence on the deviation in length of the micro rod. On the contrary, gap voltage, capacitance, and feed rate were uniformly responsible for the deviation in average diameter. Moreover, voltage contributed more toward the straightness of micro-rods throughout the length.

Jahan et al. [45] machined microstructures with lower machining time and showed improvement in the machining accuracy at optimum condition of machining parameters. Nirala and Saha [46] introduced a new method for tool wear compensation in R-μEDM. They compared the method with uniform wear method [47] and normal machining (without compensation) and found reduction in errors (i.e., existing method by 2%, normal machining by 18.2–22.4%, and uniform wear method by 4.0–8.3%). In the year *2016*, a simple analytical model for evaluating the tool wear and material removal from workpiece was developed by Singh et al. [48]. They achieved lower tool wear, lower material removal, and less taper along the length of a long micro rod of 2 mm at lower parametric conditions (100 V, 100 pF) compared with higher parametric conditions (150 V, 10^4 pF).

5.5 *Drilling with In Situ Fabricated Tool*

In this method, a micro hole is first drilled using a negatively charged rod electrode, and then the rod electrode is retracted to its original position. After that, the rod electrode is moved at a certain distance horizontally from its original position (i.e., offset), and subsequently, the reverse polarity is applied. Finally, either of the condition such as with or without rotation is used to feed the tool into the plate electrode during the machining process and thus a micro rod with lower diameter is obtained. The benefits of this technique are that no adjustment is required while machining micro rod. Yamazaki et al. [49] used different values of off-centered, i.e., 60, 75, 78, 80, 85, and 90 μm based on off-centering concept chart. Their research highlighted an improvement in the accuracy of the micro rod in the form of machining straight micro rod without taper. Using this method, Yamazaki et al. also machined straight, stepped, multi micro-rods, and other complicated shape features.

In the subsequent papers of Yamazaki et al. [50–52], they worked on a process where they tried to reduce the plate electrode wear while fabricating straight and long micro-rods. For enhancing the precision of the machining process, they adopted two-step method, run out measuring method, and dummy hole diameter measuring method. Utilizing the adopted method, they obtained high accuracy micro rod without even coinciding the rod with the axis of rotation.

5.6 *Micro Electrical Discharge Milling (μED-Milling)*

μED-milling is the technique in which the tool electrode advances in the horizontal *x–y* direction at a particular depth of cut initiated at the beginning of machining. It is generally performed as a layer by layer machining process, where each layer contributes a certain depth of cut. To get an accurate dimension and precise measurement of machined cavity tool wear needs to be compensated by some form or

other. Compensation can be applied based on the extracted dimensional features in real-time or can be predetermined based on wear ratios of tool and workpiece.

In the year 1989, Sato et al. [53] fabricated a wide groove of 50 μm on metal block using μED-milling. Later, Masuzawa and Tönshoff [54] have verified the result obtained by Sato et al. Electrode deformation is one of the major problems in μED-milling due to tool wear. For the rectification of tool wear problem, Yu et al. [6, 47] presented a technique which combined uniform wear method (UWM) with longitudinal wear compensation. The outcome confirmed the applicability of this approach for 3D microstructures. Moreover, mathematical relations were derived for tool wear compensation and applied in machining square cavities with sharp corners and inclined planes. Bissacco et al. [55] investigated tool wear and material removal (workpiece) using μED-milling process, in which they selected typical process parametric combinations for roughing and finishing operation. Volume measurement and discharge counting have been made for several energy levels and their effect in terms of errors on material removal per discharge and electrode wear per discharge was found to be relatively high. Karthikeyan et al. [15] used design software in order to evaluate the eroded amount of material from the tool and the workpiece. They detected that the rotation speed shows a major role in getting the desired material removal rate (MRR). Moreover, they also observed that the tool rotation affects the final shape of the features due to debris flushing and partially re-deposition of the molten metal [11]. In the consequent work [56], they developed a simple empirical equation with 95 and 99% confidence level for MRR and TWR. The results demonstrated the contribution of more energy and speed in the case of a single performance study, whereas feed was a significant contributor in the case of multi-performance analysis. Material removal from the tool significantly affects the machining efficiency while fabricating microchannel and it is one of the major problems in μED-milling. For solving this problem, a new compensation method was introduced by Li et al. [57], which was based on scanned area (BSA) that removes materials layer by layer. The BSA method improved the machining efficiency compared to that of UWM and the combination of both UWM and linear compensation. Jafferson et al. [58] applied ultrasonic vibration and magnetic field at the same time and at a different time in their work. The experimental results of their study highlighted an improvement in the machining efficiency in case of using ultrasonic vibration and magnetic field separately. On the other hand, they got poor results in case of jointly using ultrasonic vibration and magnetic field. Moreover, they [16] also analyzed the effect of non-electrical parameters, for example, horizontal tool feed rate (HTF), layer thickness (LT), and tool rotational speed (TRS), and found significant results in case of using speed and horizontal feed rate. The roots of the faults in μED-milling were examined by Tong et al. [59] and they proposed a layer depth constrained algorithm (LDCA) and an *S*-curve accelerating algorithm (SCAA) to decrease the errors. They found improvement in the results in terms of getting machined microcavities of less than 800 μm with enhanced machining accuracy and MRR. Zhang et al. [60] used fixed length compensation method, in which geometrical and mathematical models were formulated. Later, several trials were used to confirm the model. The developed model was taken to predict the fabricated work surface and the tool surface

electrode. Wang et al. [61] established an in situ pulse monitoring system for understanding the process dynamic and a combined off-line and in-line adaptive tool wear compensation. Dimensional accuracy and tool wear rate of stainless steel (S304) were investigated by Ali et al. [62]. They also analyzed the TWR and width of the microchannel data and developed a corresponding empirical relation. They obtained minimum microchannel width and TWR at a voltage of 91 V and feed rate of 10 μm/s [62].

6 Summary

μEDM is one of the established processes through which micro features, for example, micro-rods, micro holes, and micro slots can be fabricated easily on electrically conductive metals irrespective of their hardness. From the last few decades, many researchers have contributed a lot of their work on which they show the improvement in the fabrication of microstructures while using μEDM. The progress and improvement in μEDM for the fabrication of micro features are increasing continuously because of their wide application in the area of electronics, nuclear sectors, biomedical, MEMS, etc.

The main concern which affects the accuracy and dimensions of the micro features is the tool wear. It is detected by the researchers that the elimination of tool wear can resolve almost all the problems that lead to the incorrect dimensional variation of the micro features in terms of shape and size. For reducing the tool wear, researchers have developed many compensation methods. Still, researchers are trying to develop improved methods of compensation. Tool wear can also be reduced significantly by the proper selection of parametric conditions such as voltage, capacitance, current, and tool material.

In the current era, researchers are engaged in fabricating error-free micro features by the use of suitable compensation techniques. This chapter has provided a brief explanation about the progress of the machining efficiency of μEDM in terms of accuracy improvement and precision measurement. The recent advances of the different variants of μEDM have also been presented in this chapter.

References

1. Kibria G, Bhattacharyya B (2011) Investigation into micro-hole geometrical accuracy during micro-EDM of Ti-6Al-4V employing different dielectrics. Int J Mach Mach Mater 10:310
2. Kibria G, Shivakoti I, Pradhan BB, Bhattacharyya B (2017) Electrical discharge microhole machining process of Ti–6Al–4V: improvement of accuracy and performance. In: Non-traditional micromachining processes. Springer International Publishing, pp 93–144
3. Kibria G, Sarkar BR, Pradhan BB, Bhattacharyya B (2010) Comparative study of different dielectrics for micro-EDM performance during microhole machining of Ti-6Al-4V alloy. Int J Adv Manuf Technol 48:557–570

4. Ho KH, Newman ST (2003) State of the art electrical discharge machining (EDM). Int J Mach Tools Manuf 43:1287–1300
5. Kadirvel A, Hariharan P, Gowri S (2012) A review on various research trends in micro-EDM. Int J Mechatron Manuf Syst 5:361–384
6. Yu Z, Masuzawa T, Fujino M (2000) 3D micro-EDM with simple shape electrode Part 1: machining of cavities with sharp corners and electrode wear compensation. In: Proceedings KORUS 2000 4th Korea-Russia international symposium on science and technology. IEEE, pp 102–105
7. Jahan MP (2013) Micro-electrical discharge machining. In: Nontraditional machining processes. Springer, London, pp 111–151
8. Kibria G, Bhattacharyya B (2017) Microelectrical discharge machining of Ti-6Al-4V. In: Microfabrication and precision engineering. Elsevier, pp 99–142
9. Katz Z, Tibbles CJ (2004) Analysis of micro-scale EDM process. Int J Adv Manuf Technol 25:923–928
10. Masuzawa T (2001) Micro-EDM. In: Proceedings of the thirteen international symposium on electro machining, pp 3–19
11. Karthikeyan G, Garg AK, Ramkumar J, Dhamodaran S (2012) A microscopic investigation of machining behavior in μeD-milling process. J Manuf Process 14:297–306
12. Son S, Lim H, Kumar AS, Rahman M (2007) Influences of pulsed power condition on the machining properties in micro EDM. J Mater Process Technol 190:73–76
13. Han F, Wachi S, Kunieda M (2004) Improvement of machining characteristics of micro-EDM using transistor type isopulse generator and servo feed control. Precis Eng 28:378–385
14. Jahan MP, Wong YS, Rahman M (2009) A study on the quality micro-hole machining of tungsten carbide by micro-EDM process using transistor and RC-type pulse generator. J Mater Process Technol 209:1706–1716
15. Karthikeyan G, Ramkumar J, Dhamodaran S, Aravindan S (2010) Micro electric discharge milling process performance: an experimental investigation. Int J Mach Tools Manuf 50:718–727
16. Jafferson JM, Hariharan P, Ram Kumar J (2016) Effect of non-electrical parameters in μED milling: an experimental investigation. Int J Adv Manuf Technol 85:2037–2047
17. Vidya S, Barman S, Chebolu A et al (2015) Effects of different cavity geometries on machining performance in micro-electrical discharge milling. J Micro Nano-Manuf 3:11007
18. Wang C, Chu X, Liu G et al (2013) The design of integrated route in micro-EDM. Mater Manuf Process 28:1348–1355
19. Karthikeyan G, Ramkumar J, Dhamodaran S (2014) Block EDG: issues and applicability in multiple pass μED-milling. Mach Sci Technol 18:120–136
20. Rahman M, Lim HS, Neo KS et al (2007) Tool-based nanofinishing and micromachining. J Mater Process Technol 185:2–16
21. Pham DT, Dimov SS, Bigot S et al (2004) Micro-EDM—recent developments and research issues. J Mater Process Technol 149:50–57
22. Mastud S, Singh RK, Joshi SS (2012) Analysis of fabrication of arrayed micro-rods on tungsten carbide using reverse micro-EDM. Int J Manuf Technol Manage 26:176
23. Masuzawa T, Fujino M, Kobayashi K et al (1985) Wire electro-discharge grinding for micro-machining. CIRP Ann Manuf Technol 34:431–434
24. Sheu DY (2004) Multi-spherical probe machining by EDM: combining WEDG technology with one-pulse electro-discharge. J Mater Process Technol 149:597–603
25. Rees A, Brousseau E, Dimov SS et al (2013) Development of surface roughness optimisation and prediction for the process of wire electro-discharge grinding. Int J Adv Manuf Technol 64:1395–1410
26. Oliaei SNB, Özdemir C, Karpat Y (2014) On-machine fabrication of PCD and WC micro end mills using micro electro discharge machining. Int J Mechatron Manuf Syst 7:246
27. Zhang L, Tong H, Li Y (2015) Precision machining of micro tool electrodes in micro EDM for drilling array micro holes. Precis Eng 39:100–106

28. Ravi N, Huang H (2002) Fabrication of symmetrical section microfeatures using the electro-discharge machining block electrode method. J Micromech Microeng 12:905–910
29. Zhao WS, Jia BX, Wang ZL, Hu FQ (2006) Study on block electrode discharge grinding of micro rods. Key Eng Mater 304–305:201–205
30. Jahan MP, Rahman M, Wong YS, Fuhua L (2010) On-machine fabrication of high-aspect-ratio micro-electrodes and application in vibration-assisted micro-electrodischarge drilling of tungsten carbide. Proc Inst Mech Eng Part B J Eng Manuf 224:795–814
31. Pham DT, Ivanov A, Bigot S et al (2007) An investigation of tube and rod electrode wear in micro EDM drilling. Int J Adv Manuf Technol 33:103–109
32. Pradhan BB, Bhattacharyya B (2008) Improvement in microhole machining accuracy by polarity changing technique for microelectrode discharge machining on Ti–6Al–4V. Proc Inst Mech Eng Part B J Eng Manuf 222:163–173
33. Puranik MS, Joshi SS (2008) Analysis of accuracy of high-aspect-ratio holes generated using micro-electric discharge machining drilling. Proc Inst Mech Eng Part B J Eng Manuf 222:1453–1464
34. Aligiri E, Yeo SH, Tan PC (2010) A new tool wear compensation method based on real-time estimation of material removal volume in micro-EDM. J Mater Process Technol 210:2292–2303
35. Jahan MP, Saleh T, Rahman M, Wong YS (2010) Development, modeling, and experimental investigation of low frequency workpiece vibration-assisted micro-EDM of tungsten carbide. J Manuf Sci Eng 132:54503
36. Heinz K, Kapoor SG, DeVor RE, Surla V (2011) An investigation of magnetic-field-assisted material removal in micro-EDM for nonmagnetic materials. J Manuf Sci Eng 133:21002
37. Maity KP, Singh RK (2012) An optimisation of micro-EDM operation for fabrication of micro-hole. Int J Adv Manuf Technol 61:1221–1229
38. Jahan MP, Wong YS, Rahman M (2012) Evaluation of the effectiveness of low frequency workpiece vibration in deep-hole micro-EDM drilling of tungsten carbide. J Manuf Process 14:343–359
39. Ferraris E, Castiglioni V, Ceyssens F et al (2013) EDM drilling of ultra-high aspect ratio micro holes with insulated tools. CIRP Ann Manuf Technol 62:191–194
40. Natarajan N, Suresh P (2015) Experimental investigations on the microhole machining of 304 stainless steel by micro-EDM process using RC-type pulse generator. Int J Adv Manuf Technol 77:1741–1750
41. D'Urso G, Ravasio C (2017) Material-Technology Index to evaluate micro-EDM drilling process. J Manuf Process 26:13–21
42. Kim BH, Park BJ, Chu CN (2006) Fabrication of multiple electrodes by reverse EDM and their application in micro ECM. J Micromech Microeng 16:843–850
43. Mujumdar SS, Mastud SA, Singh RK, Joshi SS (2010) Experimental characterization of the reverse micro-electrodischarge machining process for fabrication of high-aspect-ratio micro-rod arrays. Proc Inst Mech Eng Part B J Eng Manuf 224:777–794
44. Singh AK, Patowari PK, Deshpande NV (2015) Experimental analysis of reverse micro-EDM for machining microtool. Mater Manuf Process 31:530–540
45. Jahan MP, Wong YS, Rahman M, Liang TW (2012) In-situ machining of varied-shaped and arrays of microelectrodes using reverse micro-electrodischarge machining. Int J Mechatron Manuf Syst 5:495–515
46. Nirala CK, Saha P (2016) A new approach of tool wear monitoring and compensation in RμEDM process. Mater Manuf Process 31:483–494
47. Yu ZY, Masuzawa T, Fujino M (1998) Micro-EDM for three-dimensional cavities-development of uniform wear method. CIRP Ann Manuf Technol 47:169–172
48. Singh AK, Patowari PK, Deshpande NV (2016) Effect of tool wear on microrods fabrication using reverse μEDM. Mater Manuf Process 32:1–8
49. Yamazaki M, Suzuki T, Mori N, Kunieda M (2004) EDM of micro-rods by self-drilled holes. J Mater Process Technol 149:134–138
50. Yamazaki M, Suzuki T, Mori N, Kunieda M (2006) Electrical discharge machining of micro-rod using self-drilled holes. J Japan Soc Precis Eng Contrib Pap 72:657–661

51. Yamazaki M, Suzuki T, Mori N et al (2008) Minimum diameter of microrods machined by micro-electrical discharge machining using self-drilled holes method. Denki Kako Gakkaishi 42:51–57
52. Yamazaki M, Suzuki T, Mori N et al (2008) Improvement of accuracy of micro EDM using self-drilled holes method. J Japan Soc Precis Eng 74:264–268
53. Sato T, Masuzawa T, Fujino T, Onishi Y (1989) Application of WEDG for microdrilling and microendmilling. In: Proceedings of annual spring assembly of JSPE, pp 1091–1092
54. Masuzawa T, Tönshoff HK (1997) Three-dimensional micromachining by machine tools. CIRP Ann Manuf Technol 46:621–628
55. Bissacco G, Valentincic J, Hansen HN, Wiwe BD (2010) Towards the effective tool wear control in micro-EDM milling. Int J Adv Manuf Technol 47:3–9
56. Karthikeyan G, Ramkumar J, Shalabh Aravindan S (2012) Performance analysis of μeD-milling process using various statistical techniques. Int J Mach Mach Mater 11:183–203
57. Li JZ, Xiao L, Wang H et al (2013) Tool wear compensation in 3D micro EDM based on the scanned area. Precis Eng 37:753–757
58. Jafferson JM, Hariharan P, Ram Kumar J (2014) Effects of ultrasonic vibration and magnetic field in micro-EDM milling of nonmagnetic material. Mater Manuf Process 29:357–363
59. Tong H, Zhang L, Li Y (2014) Algorithms and machining experiments to reduce depth errors in servo scanning 3D micro EDM. Precis Eng 38:538–547
60. Zhang L, Du J, Zhuang X et al (2015) Geometric prediction of conic tool in micro-EDM milling with fix-length compensation using simulation. Int J Mach Tools Manuf 89:86–94
61. Wang J, Qian J, Ferraris E, Reynaerts D (2017) In-situ process monitoring and adaptive control for precision micro-EDM cavity milling. Precis Eng 47:261–275
62. Ali MY, Rahman MA, ZuhaidaZunairi SN, Banu A (2017) Dimensional accuracy of micro-electro discharge milling. IOP Conf Ser Mater Sci Eng 184:12034

Improvement of Profile Accuracy in WEDM—A Novel Technique

Mukandar Sekh

Abstract A thorough investigation on wirelag phenomena was carried out in this study. Here, the effect of wire deflection or wirelag on geometrical accuracy has been explored. A proper control to improve dimensional accuracy of circular job is achieved here. A novel method is presented to measure the wirelag by geometrical analysis. A mathematical model is developed to measure the gap force. Experimental investigations are performed to verify the proposed model.

Keywords WEDM · Wirelag · Profile accuracy · Gap force

1 Introduction

Electrical sparks can erode metal that fact was first noticed by Sir Joseph Priestley in 1770, but it takes time to convert it into technology of machining. In the year 1943, two Russian scientists, B. R. Lazarenko and N. I. Lazarenko, invented the basic principle of electrical spark machining system called as electrical discharge machining (EDM) and subsequently they developed R–C type EDM machine. In the late 1960s, wire EDM was developed to replace the varying tool for different geometry used in EDM. Later, an optical system by D. H. Dulebohn was developed to auto control the geometry of the part to be machined by the WEDM process in 1974. After this development, the popularity of WEDM enhanced rapidly, as the process. In the end of 1970s, WEDM process has come up with computer numerical control (CNC) system and that was the massive invention in the WEDM process. Day by day, this machining process has become one popular non-traditional machining system in the manufacturing sector as it can produce complicated profile for the product.

Accuracy, surface finish and cutting speed are enhancing from inception of this process. But, product accuracy is hampering due to wire deflection or wire bending, and it makes various applications unacceptable. Thus, wirelag is defined as the wire

M. Sekh (✉)
Department of Mechanical Engineering, Aliah University, Kolkata 700160, India
e-mail: mukandar@gmail.com

G. Kibria and B. Bhattacharyya (eds.), *Accuracy Enhancement Technologies for Micromachining Processes*, Lecture Notes in Mechanical Engineering,
https://doi.org/10.1007/978-981-15-2117-1_4

deflection during wire EDM. The wirelag generates imprecision on the workpiece during cutting a corner or curved profile. This imprecision may be in the range of hundreds of microns, and it is beyond tolerance limit for some specific purposes. For obtaining the required product shape and size with acceptable tolerances, proper understanding of wirelag phenomena is very important. A number of research works have been carried out to improve profile accuracy in WEDM. Different research studies show different strategies to minimize this error. Off-line path modification method [1], using sensor for online wire position monitoring system [2], by reducing the cutting speed at corner [3] then a trim cutting method [4] or magnetic effect [5] were tried to increase the corner accuracy of the parts.

It is observed although some researches have been carried out on the wirelag; however, no direct method has come up to measure the correct value of wirelag. But, the bare fact is that to achieve high precision profile the correct value of wirelag is extremely essential.

2 Wire Deflection and Its Impact on Workpiece Accuracy

Wire electrode deforms due to gap force during machining as the wire is thin and flexible which remains under tension. The wire deflection occurs in the reverse to the machining direction as shown in Fig. 1. It is seen that the wire always moves behind the wire guide due to the wire bending. It is understood [2–6] that the cause of this gap force is due to the explosion force from gas bubbles though there are other contributing factors, i.e., hydraulic forces, electromagnetic force, electrostatic force, etc. The force applied on the wire is not fixed; in its place, it changes with respect to time as the unsteady character of the plasma channel and stochastic sparking behaviour, which actually trigger off non-stop vibration in the wire. Overcut and tolerance limit are hampered due to the wire vibration. A number of research scientists [7–9] have discovered this wire deflection behaviour of the wire to improve the accuracy in WEDM. It is obvious that the instantaneous wire position is varied with time. However, it is evident that for particular setup, the average displacement is seen to be constant. This is known as wire deflection or wirelag [9]. Therefore, the wirelag phenomenon is not dynamic behaviour rather it is a static behaviour of the wire. In addition, wirelag is also controlled by several important factors that include wire tension, gap force, workpiece height, distance between job surface and wire guide.

While cutting straight profile, it is difficult to get the actual length of job as the wire is always behind the wire guide. The position difference in between the wire and guide generates a geometrical imprecision during profile cutting at sharp corners. Figures 2 and 3 represent how the wirelag affect the geometrical imprecision during corner and profile cutting.

It is seen from Fig. 2 that the wirelag has a powerful effect on both edges of the corner. From Fig. 3, it is noticed that definite contour produced by the wire centre (r_a) is not machining by the theoretical layout of the wire (r_p) because of wire deflection (δ_0) at workpiece surface. In Fig. 3, ε_{wl} is the perpendicular span

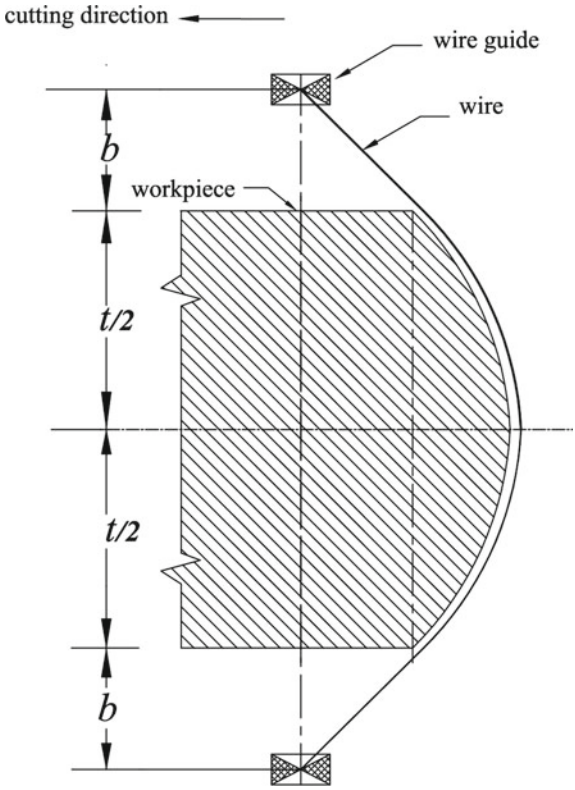

Fig. 1 Wire position during WEDM cutting

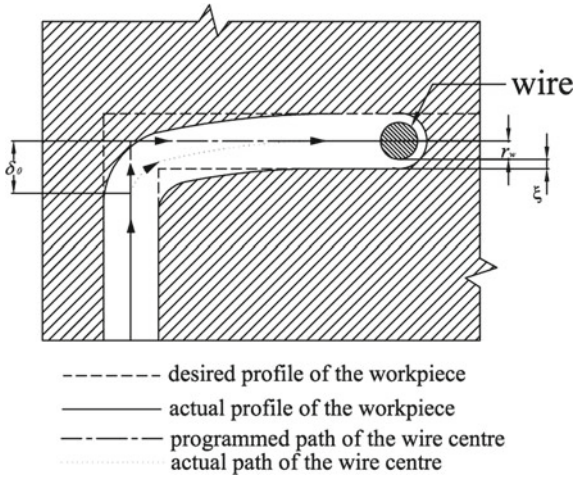

Fig. 2 Influence of wirelag on geometrical imprecision during cutting a sharp corner [11]

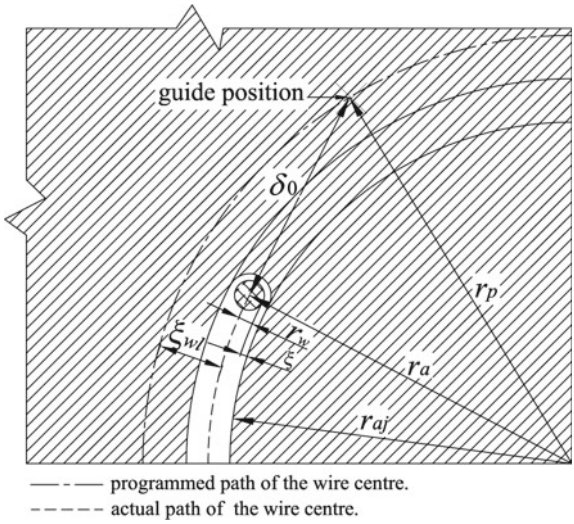

Fig. 3 Effect of wirelag on profile imprecision during circular profile cutting [11]

between theoretical program profile of the wire and actual profile of the wire when a cylindrical workpiece cutting was done, and it is called as wirelag compensation value. Therefore, to attain preferred dimension, the necessary wirelag compensation value $\varepsilon_{\mathrm{wl}}$ is equal to (r_{p}–r_{a}). This ε_{wl} value is needed to include in spark gap (ξ) and wire radius (r_{w}) to calculate compensation value of wire. This value is compulsorily needed to construct CNC program for the cutting. Hence, wire offset value will be as follows to get perfect size job when any circular or curved shape job is being produced;

$$r_{\mathrm{i}} = r_{\mathrm{w}} + \xi + \varepsilon_{\mathrm{wl}} \tag{1}$$

3 Development of a New Method for Determination of WireLag and Gap Force

During rough cutting operation, it has already been mentioned that the wire is subjected to gap force to the reverse direction of the cutting. It is now known that the thin wire vibrates during cutting. The amplitude of vibration influences the amount of overcut, and the mean displacement is basically the wirelag value which has a strong impact on geometrical inaccuracy. This average or mean static displaced position, i.e., wirelag, is governed by average gap force, workpiece height, wire tension and span between the wire guide and workpiece surface. Though, some researchers developed the formula for wirelag as a purpose of gap force only on the straight geometrical

profile cutting. But in this present study, a novel method to estimate the wirelag value for curve profile (circular) cutting is developed.

Measurement of wirelag value for curved profile cutting is very intricate than straight path cutting because gap force is not unidirectional through several curved profile cutting. Depending upon the job height, the value of gap force commonly varies. For this reason, some lateral deflections of the wire are obtained. For the fact, the following assumptions are made for the analytical model to measure the wirelag value

(i) Span between workpiece surface and wire guide are same.
(ii) Gap is constant during cutting with a fixed parameter setting, and the intensity of the gap force also is constant.
(iii) It is assumed that the lateral bending is very negligible, and it is ignored. Figure 4 is showing the position of the wire.
(iv) Wirelag value is only in the range of microns, it is small with respect to the job radius, and for this θ_1 and θ_2 may be considered as a very small value.
(v) Hence, α is very small because θ_1 and θ_2 (Fig. 5a) are small, and so the lateral gap force is also very little.
(vi) It is shown in Fig. 5a, b that gap force q applied on very tiny portion EF is $qRd\beta$. This part of the gap force $qRd\beta\sin\theta$ produces lateral bending on the EDM wire, and component $qRd\beta\cos\theta$ applied in the same plane of wire profile creates bending. When job thickness (t) varies, θ also will vary, so the radius of curvature R will also simultaneously vary. Now, θ has very little value, so the variation of radius of curvature is neglected. It is also known that EDM wire may be treated as flexible wire.

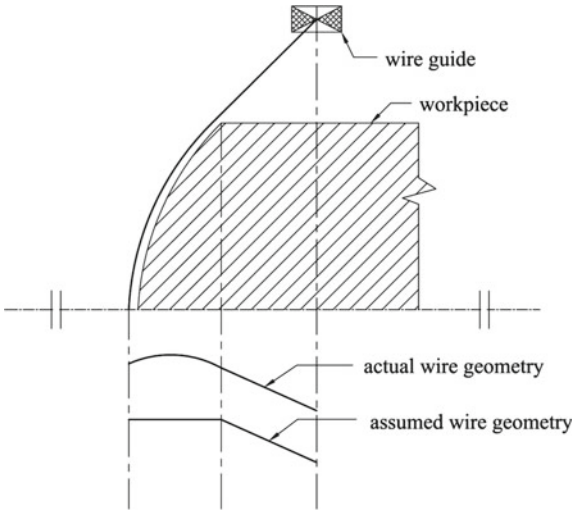

Fig. 4 Wire position (top view) during cutting a circular profile [11]

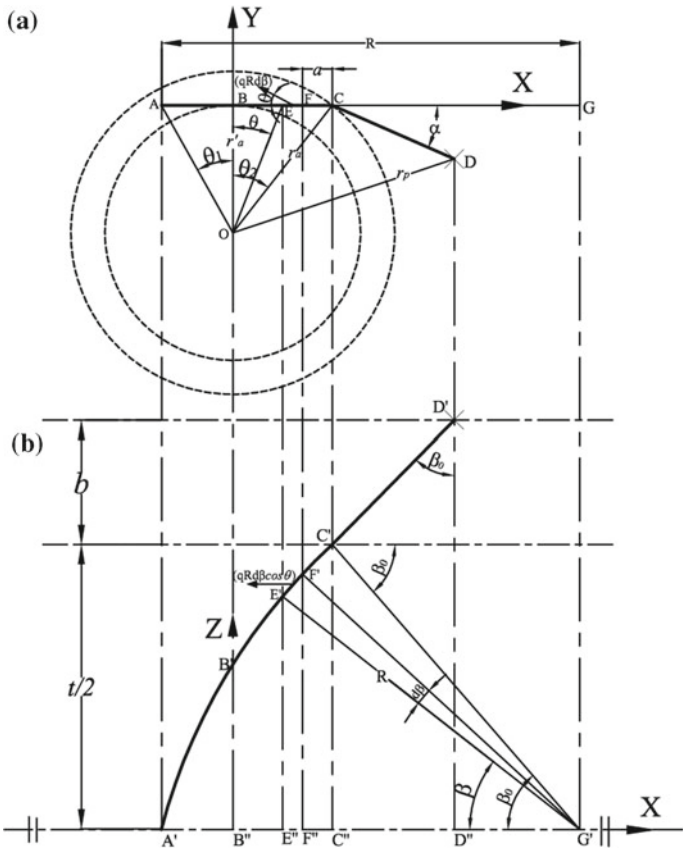

Fig. 5 **a** Line diagram of wire for circular profile cutting (top view). **b** Line diagram of upper half of the wire for circular profile cutting (front view) [11]

(vii) Generally, a small wire deflection occurred between the top and bottom job surfaces (δ_i), and when compared to the job thickness, the wire radius of curvature is typically very big. Therefore, it is assumed that β_0 is small (Fig. 5b).

The *X*-, *Y*- and *Z*-axis are shown in Fig. 5a, b, and it is chosen in a way that origin is met at point B as it is the centre of the wire as shown in Fig. 5a and B'' in Fig. 5b, and the cylindrical job axis is parallel to *Z*-axis. In Fig. 5a, r_a is the gap between cylindrical job centre and wire centre, and r'_a is the shortest length between cylindrical job centre and wire centre. r_w is radius of the wire, and ξ is the of radial overcut or radial spark gap.

The following expression may be written from Fig. 3;

$$r_a = r_{ja} + r_w + \xi \tag{2}$$

where r_{aj} is the largest radius.

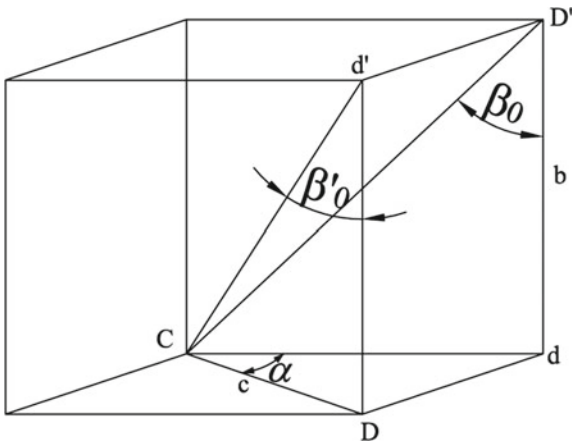

Fig. 6 Location of wire on top of the workpiece surface in 3D spaces [11]

Cd' is the wire position shown in Fig. 6 in the space, and it is above the job surface.

In Figs. 5a and 6, α is angle $\angle DCG$. It is the projected value of wire inclination beyond the job surface on XY plane with regard to XZ plane, with respect to YZ plane β_0' is exact inclination of the straight portion of the wire above the job surface (Fig. 6), this amount is identical to angle between wire guide and wire on XZ plane, and β_0 is the projected value of β_0' (Fig. 6). It is seen that if the value of α is small, $C'D'$ will be tangential to the curve $A'C'$, and so exact inclination of radius of curvature is also β_0 at the point C (Fig. 5b).

CD is the wire position in XY plane, and CD' is wire position in XZ plane top of the workpiece material. The following trigonometric relation is obtained from Fig. 6.

$$\tan \beta_0' = \frac{CD}{Dd'}, \tag{3}$$

$$\tan \beta_0 = \frac{cd}{D'd} \text{ and} \tag{4}$$

$$\cos \alpha = \frac{cd}{CD} \tag{5}$$

Now, dividing Eqs. (3) and (4), one can obtain the following expression

$$\frac{\tan \beta_0'}{\tan \beta_0} = \frac{CD}{Dd'} \times \frac{D'd}{cd} = \frac{CD}{cd}\left[D'd = Dd' = b\right] \tag{6}$$

Putting the value of $\frac{cd}{CD} = \cos \alpha$, the above equation becomes

$$\frac{\tan \beta_0'}{\tan \beta_0} = \frac{1}{\cos \alpha} \tag{7}$$

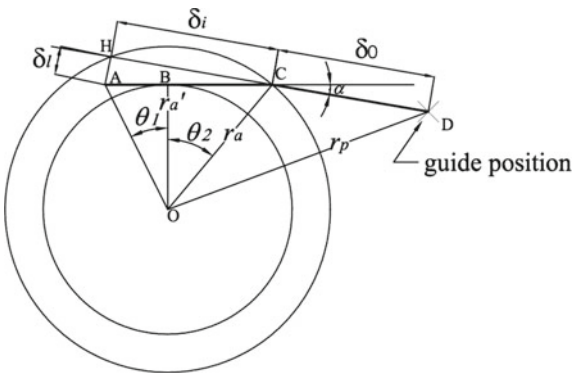

Fig. 7 Wirelag phenomenon during circular profile cutting (top view) [11]

Now, rearranging the above expression, it may be expressed as

$$\tan \beta_0' \cos \alpha = \tan \beta_0 \tag{8}$$

Since α is very small, $\cos \alpha \approx 1$ and β_0' & β_0 are also small. Thus, the above expression becomes

$$\beta_0' = \beta_0 \tag{9}$$

In Fig. 6, $Dd' = b$ is the span between job surface and wire guide support, and the wire bending above the job surface and below the job surface δ_0(=CD) is as shown in Fig. 7 and also can be expressed as follows

$$\frac{CD}{Dd'} = \tan \beta_0' \tag{10}$$

Hence,

$$CD = b \times \tan \beta_0' \tag{11}$$

Now, putting the value of $\tan \beta_0'$ from Eq. (8), it can be expressed as

$$\delta_0 = b \times \frac{\tan \beta_0}{\cos \alpha} \tag{12}$$

Since α and β_0 is small, the above expression becomes

$$\delta_0 = b\beta_0 \tag{13}$$

From Fig. 5b, it is noticed that

$$\sin\beta_0 = \frac{C'C''}{C'G'} = \frac{t/2}{R} \tag{14}$$

As β_0 is small, $\sin\beta_0 \approx \beta_0$. Therefore, the radius of curvature R is expressed as

$$R = \frac{t}{2\beta_0} \tag{15}$$

where t = thickness of the job.

From Fig. 5a, b, it is seen that

$$AE = A'E''$$

Putting the values of above expression in trigonometric form, it becomes

$$\begin{aligned} & r'_a \tan\theta_1 + r'_a \tan\theta = R - R\cos\beta \\ & \Rightarrow r'_a(\tan\theta_1 + \tan\theta) = R(1 - \cos\beta) \end{aligned} \tag{16}$$

For small values of θ_1, θ and β, $\tan\theta_1 \approx \theta_1$, $\tan\theta \approx \theta$ and $\cos\beta \approx 1 - \beta^2/2$, and the above expression becomes

$$\begin{aligned} r'_a(\theta_1 + \theta) &= R\left(1 - 1 + \frac{\beta^2}{2}\right) \\ \Rightarrow r'_a(\theta_1 + \theta) &= \frac{R\beta^2}{2} \end{aligned} \tag{17}$$

Again rearranging, it becomes

$$\theta = \frac{R\beta^2}{2r'_a} - \theta_1 \tag{18}$$

Substituting the value of R from Eq. (15), the above expression may be evaluated as follows

$$\theta = \frac{\beta^2 t}{4r'_a\beta_0} - \theta_1 \tag{19}$$

Again from Fig. 5a, b, it is observed that $a = FC = F''C''$, and a may be expressed as follows

$$\begin{aligned} a &= R\cos(\beta + \mathrm{d}\beta) - R\cos\beta_0 \\ &= R(\cos\beta - \cos\beta_0) \text{ (since } \mathrm{d}\beta \ll \beta) \\ &= R\left(1 - \frac{\beta^2}{2} - 1 + \frac{\beta_0^2}{2}\right) \text{ (since } \beta \text{ and } \beta_0 \text{ are small)} \end{aligned}$$

$$= \frac{R}{2}\left(\beta_0^2 - \beta^2\right) \tag{20}$$

If we consider only upper half of the wire, i.e., AC or $A'C'$, it is in equilibrium under the tensile force and the distributed gap force as shown in Fig. 5a, b. From the figure, it is seen that $E'F'$ is a very small arc and it makes an angle $d\beta$, and the radius of curvature R creates an angle β with negative X-axis. So, $qRd\beta$ is the gap force on this portion of the wire. So, the equilibrium equation may be written as

$$\int_0^{\beta_0} (q\,R d\beta)\cos\theta = T\sin\beta_0'\cos\alpha \tag{21}$$

As radius of curvature R and gap force intensity q are considered as constant, as θ, α and β are small, $\cos\theta \approx 1$, $\cos\alpha \approx 1$ and $\sin\beta_0' \approx \beta_0'$, the above equation can be expressed as

$$qR\int_0^{\beta_0} \mathrm{d}\beta = T\beta_0' \tag{22}$$

Now, solving the above equation, it becomes

$$qR\beta_0 = T\beta_0' \tag{23}$$

As it is obtained that $\beta_0' = \beta_0$, now, the above expression can be rewritten as

$$R = \frac{T}{q} \tag{24}$$

Combining Eqs. (15) and (24), β_0 may be evaluated as follows:

$$\beta_0 = \frac{tq}{2T} \tag{25}$$

Similarly, if equilibrium is considered along Y-axis, then the equation will be as

$$\int_0^{\beta_0} (q\,R d\beta)\sin\theta = T\,\sin\beta_0'\sin\alpha \tag{26}$$

As the R and q are not changing, its value is fixed. For small values of θ, α and β, $\sin\theta \approx \theta$, $\sin\alpha \approx \alpha$ and $\sin\beta_0' \approx \beta_0' \approx \beta_0$ and from Eq. (24), radius of curvature $R = T/q$. So, the above expression becomes

$$\int_0^{\beta_0} T\theta \mathrm{d}\beta = T\beta_0\alpha \tag{27}$$

Putting the value of θ from Eq. (19), it becomes

$$\int_0^{\beta_0} \left(\frac{\beta^2 t}{4r'_a\beta_0} - \theta_1\right)\mathrm{d}\beta = \beta_0\alpha \tag{28}$$

Solving the above equation, it can be evaluated as

$$\frac{t\beta_0^2}{12r'_{\mathrm{a}}} - \theta_1\beta_0 = \alpha\beta_0 \tag{29}$$

Now, rearranging the above equation, α becomes

$$\alpha = \frac{t\beta_0}{12r'_a} - \theta_1 \tag{30}$$

Now, in the XY plane, it is seen from Fig. 5a that moment of the wire about point C will be zero. It may be expressed as

$$\int_0^{\beta_0} a(qR\mathrm{d}\beta)\sin\theta = 0 \tag{31}$$

Now, putting the value of a from Eq. (20) and using $\sin\theta \approx \theta$, the above expression becomes,

$$\frac{qR^2}{2}\int_0^{\beta_0} (\beta_0^2 - \beta^2)\theta \mathrm{d}\beta = 0 \tag{32}$$

Since, $qR^2 \neq 0$,

$$\int_0^{\beta_0} (\beta_0^2 - \beta^2)\theta \mathrm{d}\beta = 0 \tag{33}$$

Now, replacing the θ from Eq. (19) in the above equation, it becomes

$$\int_0^{\beta_0} (\beta_0^2 - \beta^2)\left(\frac{t\beta^2}{4r'_a\beta_0} - \theta_1\right)\mathrm{d}\beta = 0$$

$$\Rightarrow \int_0^{\beta_0} \left(\frac{t\beta^2\beta_0}{4r'_a} - \theta_1\beta_0^2 - \frac{t\beta^4}{4r'_a\beta_0} + \theta_1\beta^2\right)\mathrm{d}\beta = 0 \tag{34}$$

After integrating between the limits, the above expression becomes

$$\frac{t\beta_0^4}{30r'_a} - \frac{2\theta_1\beta_0^3}{3} = 0 \tag{35}$$

Rearranging the above equation, it may be expressed in terms of θ_1 as follows

$$\theta_1 = \frac{t\beta_0}{20r'_a} \tag{36}$$

Now, putting the θ_1 value in Eq. (30), it becomes

$$\begin{aligned}\alpha &= \frac{t\beta_0}{12r'_a} - \frac{t\beta_0}{20r'_a} \\ &= \frac{t\beta_0}{30r'_a}\end{aligned} \tag{37}$$

From Fig. 5a, b, it is noticed that $\theta = \theta_2$ and $\beta = \beta_0$. So, using these limiting values of θ and β in Eq. (19), the expression becomes

$$\theta_2 + \theta_1 = \frac{t\beta_0}{4r'_a} \tag{38}$$

Now, rearranging the above equation by putting θ_1, one can estimate the value of θ_2 as given below:

$$\theta_2 = \frac{t\beta_0}{5r'_a} \tag{39}$$

In Fig. 7, considering ΔOCD, the following relationship is obtained

$$\cos\angle OCD = \frac{OC^2 + CD^2 - OD^2}{2 \times OC \times CD} \tag{40}$$

Putting the value of $OC = r_a, OC = r_a, CD = b\beta_0$, the above expression becomes

$$\cos\left[\pi - \left\{\alpha + \left(\frac{\pi}{2} - \theta_2\right)\right\}\right] = \frac{r_a^2 + b\beta_0 - r_p^2}{2(b\beta_0)r_a}$$
$$\Rightarrow r_p^2 - r_a^2 = b^2\beta_0^2 + 2b\beta_0 r_a \sin(\theta_2 - \alpha)$$
$$\Rightarrow r_p^2 - r_a^2 = b^2\beta_0^2 + 2b\beta_0 r_a(\theta_2 - \alpha) \text{ (Since}(\theta_2 - \alpha) \text{ is very small)} \quad (41)$$

Now, using α and θ_2 and Eqs. (37) and (39), respectively, the above expression becomes:

$$r_p^2 - r_a^2 = b^2\beta_0^2 + \frac{b\beta_0^2 t r_a}{3r_a'} \quad (42)$$

The value of θ_2 is small and as such $r_a' \approx r_a$; hence, the above expression becomes:

$$r_p^2 - r_a^2 = b^2\beta_0^2\left(1 + \frac{t}{3b}\right) \quad (43)$$

Putting the value of $\beta_0 = \frac{tq}{2T}$ using Eq. (25), the above equation may be expressed as

$$r_p^2 - r_a^2 = b^2\left(\frac{tq}{2T}\right)^2\left(1 + \frac{t}{3b}\right) \quad (44)$$

After rearranging the above equation, the gap force q can be calculated as below:

$$q = \left(\frac{2T}{tb}\right)\sqrt{\frac{\left(r_p^2 - r_a^2\right)}{\left(1 + \frac{t}{3b}\right)}} \quad (45)$$

Substituting r_a value as it is in Eq. (2), it becomes:

$$q = \left(\frac{2T}{tb}\right)\sqrt{\frac{\left\{r_p^2 - \left(r_{ja} + r_w + \xi\right)^2\right\}}{\left(1 + \frac{t}{3b}\right)}} \quad (46)$$

Now, ξ can be measured easily from a square or rectangular job and r_{aj}, and also we can get from a circular job which were cut from the job material for a given parameter setting. From the machining condition also we will get job thickness (t), wire tension (T), wire radius (r_w) and the value of b. So, the average gap force intensity can be measured for any specified machining parameter setting using Eq. (46).

Now, using Eq. (43), r_a may be expressed as follows:

$$r_a = r_p\left\{1 - \frac{\beta_0^2 b^2}{r_p^2}\left(1 + \frac{t}{3b}\right)\right\}^{1/2}$$

$$= r_{\mathrm{p}}\left\{1 - \frac{\beta_0^2 b^2}{2r_{\mathrm{p}}^2}\left(1 + \frac{t}{3b}\right) + \frac{\beta_0^4 b^4}{8r_{\mathrm{p}}^4}\left(1 + \frac{t}{3b}\right)^2 - \cdots\right\} \tag{47}$$

Since, β_0 is small, β_0^4 or higher order will be very small and can be neglected. So, the above equation becomes

$$r_{\mathrm{a}} = r_{\mathrm{p}}\left\{1 - \frac{\beta_0^2 b^2}{2r_{\mathrm{p}}^2}\left(1 + \frac{t}{3b}\right)\right\} \tag{48}$$

After rearranging the above expression using the value of Eq. (25), it becomes

$$r_{\mathrm{p}}\left(r_{\mathrm{p}} - r_{\mathrm{a}}\right) = \frac{1}{8}\left(\frac{btq}{T}\right)^2\left(1 + \frac{t}{3b}\right) \tag{49}$$

$$\Rightarrow r_{\mathrm{p}}\varepsilon_{\mathrm{wl}} = K \tag{50}$$

where

$$K = \frac{1}{8}\left(\frac{btq}{T}\right)^2\left(1 + \frac{t}{3b}\right) \tag{51}$$

and

$$\varepsilon_{\mathrm{wl}} = \left(r_{\mathrm{p}} - r_{\mathrm{a}}\right) \tag{52}$$

The right hand side of Eq. (49) will be constant for a specified machining parameter setting. So, the K is constant, and it is called radial wirelag compensation constant.

Now, wirelag compensation value ($\varepsilon_{\mathrm{wl}}$) can be measured for any radius circular or curved job using Eq. (52). This value is used in the CNC part program to get the accurate job dimension.

It is seen from Eq. (50) that smaller radius job will have higher imperfection though usually smaller radius job requires higher precision.

From Fig. 7, it is seen that CD is wire bending at the top surfaces of workpiece. The wire bending above the job surface δ_0 can be evaluated by substituting the value β_0 from Eq. (25) in Eq. (13) as follows:

$$\delta_0 = CD = b\beta_0 = \frac{btq}{2T} \tag{53}$$

Wire deflection or bending between top and below surface of the job in the direction of δ_0 is $HC = \delta_{\mathrm{i}}$ in Fig. 7. Hence, δ_{i} can be estimated as below:

$$\begin{aligned}\delta_{\mathrm{i}} &= HC \\ &= (AC)\cos\alpha\end{aligned}$$

$$= \left(r_a' \tan\theta_1 + r_a' \tan\theta_2\right) \cos\alpha \tag{54}$$

For small values of θ_1, θ_2 and α, the above expression becomes

$$\delta_i = r_a'(\theta_1 + \theta_2) \tag{55}$$

Now, putting the value of $\theta_1 + \theta_2 = t\beta_0/4r_a'$ from Eq. (38) and putting β_0 value as in Eq. (25), it becomes

$$\delta_i = \frac{t^2 q}{8T} \tag{56}$$

So, the total deflection δ_t

$$\begin{aligned} \delta_t &= HD \\ &= HC + CD \\ &= \delta_i + \delta_0 \\ &= \frac{t^2 q}{8T} + \frac{btq}{2T} \end{aligned} \tag{57}$$

It is seen in the earlier research [2, 10] also that the same formula to measure wirelag or wire deflection when straight WEDM cutting was done.

It is already stated that a little amount lateral wire deflection is happening during machining. This deflection will be maximum at the middle length of the wire between upper and lower wire guide. Hence, the total lateral deflection at the middle portion of the wire length as shown in Fig. 7 is expressed as

$$\begin{aligned} \delta_l &= AH \\ &= (AB + BC)\sin\alpha \\ &= \left(r_a' \tan\theta_1 + r_a' \tan\theta_2\right) \sin\alpha \end{aligned} \tag{58}$$

For small values of θ_1, θ_2 and α, the above expression becomes

$$\delta_l = r_a'(\theta_1 + \theta_2)\alpha \tag{59}$$

Now, putting the values of $\theta_1 + \theta_2 = t\beta_0/4r_a'$, α and β_0 as in Eqs. (38), (37) and (25), respectively, and as at top and bottom surface wire deflection is same, then $r_a' \approx r_a$.

Hence, the expression for δ_l becomes

$$\delta_l = \frac{q^2 t^4}{480 r_a T^2} \tag{60}$$

Now substituting r_a value as in Eq. (2), the above expression may be rewritten as

$$\delta_l = \frac{q^2 t^4}{480\left(r_{aj} + r_w + \xi\right)^2} \tag{61}$$

It is seen from the above equation that lateral deflection is proportional with gap force and job thickness where as the wire tension and job radius (r_{aj}) is inversely proportional with lateral deflection. It is obvious that during straight profile cutting job, radius (r_{aj}) will be infinite. So, the lateral deflection will be zero. So, theoretically it proved that during straight profile cutting, no lateral deflection or bending occur.

4 Summary

To estimate gap force and wirelag, a new method is developed based upon the analytical model. Now, the wirelag value can be measured directly for any condition, and it can be used to produce accurate job. To increase the cylindrical or curved profile accuracy, the wirelag compensation value is incorporated in the CNC part program. From the investigation, it is clear that lower radius job is experienced higher wirelag. It is also shown that the lateral deflection is zero for straight profile cutting.

References

1. Dekeyser WL, Snoeys R (1989) Geometrical accuracy of wire-EDM. In: Proceedings of the international symposium for electro-machining, pp 226–232
2. Dauw DF, Beltrami I (1994) High-precision wire-EDM by online wire position control. Ann CIRP 43(1):193–197
3. Lin CT, Chung IF, Huang SY (2001) Improvement of machining accuracy by fuzzy logic at corner parts for wire-EDM. Fuzzy Sets Syst 122(3):499–511
4. Puri AB, Bhattacharyya B (2003) An analysis and optimisation of the geometrical inaccuracy due to wire lag phenomenon in WEDM. Int J Mach Tools Manuf 43(2):151–159
5. Dodun O, Gonçalves-Coelho AM, Slătineanu L, Nagîţ G (2009) Using wire electrical Discharge machining for improved corner cutting accuracy of thin parts. Int J Adv Manuf Technol 41:858–864
6. Sanchez JA, Lacalle LNLD, Lamikiz A (2004) A computer-aided system for the optimization of the accuracy of the wire electro-discharge machining process. Int J Comput Integr Manuf 17(5):413–420
7. Dauw DF, Sthioul H, Delpretti R, Tricarico C (1989) Wire analysis and control for precision EDM cutting. Ann CIRP 38(1):191–194
8. Lee TC, Yue TM, Lau WS (1997) The measurement and analysis of the wire vibration in ultrasonic aided wire cut machining. ICPE Taipei, Taiwan, pp 677–683
9. Mohri N, Yamada H, Furutani K, Narikiyo T, Magara T (1998) System Identification of Wire Electrical Discharge Machining. Annals of the CIRP 47(1):173–176
10. Beltrami I, Bertholds A, Dauw D (1996) A simplified post process for wire cut EDM. J Mater Process Technol 58(4):385–389
11. Sarkar S, Sekh M, Mitra S, Bhattacharyya B (2011) A novel method of determination of wire lag for enhanced profile accuracy in WEDM. Precis Eng 35:339–347

Laser-based Fabrication of Micro-channels

Bappa Acherjee

Abstract Micro-channels are generally used in micro-fluidic devices and heat sinks for biomedical, chemical, microelectronics, and micro-electromechanical applications. A number of processing techniques are used for fabricating micro-channels on different materials. Laser-based micro-channeling techniques are now gaining popularity because of simplicity, flexibility, repeatability, and reliability of the process. Laser is a versatile non-contact machining tool, which can be utilized to machine any profile contour on almost every type of materials. In this chapter, the attempt is made to furnish a comprehensive technical know-how about laser-based fabrication techniques of micro-channels. An overview on fabrication of micro-channels and their applications, including a brief discussion on operation principles of commonly used micro-channeling techniques is presented in the initial sections. The subsequent sections elaborate laser micro-channeling process, including process fundamentals and process requirements. Thereafter, underwater laser processing of micro-channels is also discussed, which is a recent development in this field. The improvements achieved in terms of dimensional accuracy and quality of micro-channels, by using laser-based fabrication techniques, are reported and discussed to justify the effectiveness of these techniques, which are evidenced by several research findings.

Keywords Micro-channel · Micro-fluidic device · Laser micro-channeling · Underwater machining · Quality and accuracy

1 Introduction

Micro-channels are the essential parts of micro-fluidic devices used in biomedical and chemical analytical systems. Micro-channels are also used in microelectronics and micro-electromechanical devices. The chemical and biomedical micro-fluidic devices are used for microbiological testing and analyses such as chromatography, electrophoresis, DNA synthesis, and blood protein analysis. Micro-channels

B. Acherjee (✉)
Production Engineering Department, Birla Institute of Technology: Mesra, Ranchi 835215, India
e-mail: a.bappa@yahoo.com

G. Kibria and B. Bhattacharyya (eds.), *Accuracy Enhancement Technologies for Micromachining Processes*, Lecture Notes in Mechanical Engineering,
https://doi.org/10.1007/978-981-15-2117-1_5

in microelectronics and micro-electromechanical systems are used in telecommunication devices, binary storage devices, inkjet printer nozzles, etc. [1–7]. Several techniques are developed over the years for fabricating micro-channels, from conventional techniques like mechanical micro-machining [8], chemical etching [9], photolithography [10] to the modern ultrafast femtosecond laser micro-machining [2]. The above techniques are widely used for creating micro-channels on different substrates such as glass, polymer, silicon, and metal. Other techniques like injection molding [11], imprinting [12], and hot embossing [13] are often used for creating micro-channels having low aspect ratios. Glass and polymer substrates are generally used for producing biomedical and chemical micro-fluidic devices, whereas silicon and metallic substrates are used for the applications in microelectronics and micro-electromechanical devices. Fabrication techniques play a significant role in the quality of the micro-channel. Though the high aspect ratio micro-channels are used in major applications, the shape, size, and structure of micro-channels differ with the kind of applications. Rectangular, square, circular, semicircular, U-shaped micro-channel cross sections are common in use [1, 14, 15].

Glass and silicon are the mostly used substrate materials for micro-fluidic devices [10, 16–21]. Glass is preferred choice for micro-fluidic devices used in biomedical applications, due to its high degree of transparency and inert behavior. Silicon is widely used as substrate material for producing micro-channels in micro-electromechanical devices, where forced air or liquid circulation through micro-channels is used for cooling the device. Quartz and gallium nitride are also used as semiconductor materials for micro-fluidic applications [22, 23]. Polymers are nowadays replacing the glass and silicon in many applications, due to their lower cost, better machinability, optical transparency, higher strength to weight ratio, etc. [13, 24–26]. Poly(methyl methacrylate) (PMMA) and polydimethylsiloxane (PDMS) are the leading polymers used in varied range of micro-fluidic devices. Due to its higher transparency and biocompatibility, PMMA is used in biomedical applications. Among other polymers, polycarbonate (PC), polypropylene (PP), polyethylene (PE), polystyrene (PS), polyethylene terephthalate (PET) are also used as substrate materials for fabricating micro-channels. Micro-channels in metallic substrates are generally produced in cooling devices for mechanical and electrical applications [27, 28]. Attempts are also made by researchers to produce micro-channels in ceramics and superalloys [29].

2 Fabrication of Micro-channels

A number of micro-channel fabrication techniques are developed over the years, from aged chemical etching to the latest laser-based formation of micro-channels. Chemical etching is the widest used micro-channel fabrication technique, where selective materials removal is carried out through chemical reactions. The patterns are formed by exposing the material to acid or salt solution, and materials are removed by chemical or electrochemical reactions. Protective mask is used to protect the zone which

is not targeted for etching. Chemical etching is mostly used for metallic substrates for biomechanical applications. Etching is sometimes used as secondary process for fabrication of micro-channel. Tapering of walls and overcut are the major problems associated with etching. Exact controlling of micro-channel dimensions is not possible with chemical etching. Lithography is one of the leading techniques for creating micro-channels. This technique is generally used to produce complex profile on substrates. Photolithography is the prominent lithography technique where photochemical reaction is used for selective material removal by exposing the targeted zone to light. X-ray, ion-beam, and electron-beam lithography techniques are used for generating micro-channels having high aspect ratios and complex contour. Lithography techniques are generally employed on polymer and silicon substrates for creating micro-fluidic devices for biomedical and chemical applications. LIGA (German acronym for lithography, electroplating, and molding) is used to produce high aspect ratio micro-channels with depth ranging from 100 to 1000 μm [30]. Lithography techniques require skilled human resource and cleanroom facilities. Mechanical micro-machining techniques are also used for creating micro-channels. Micro-milling and micro-turning are the widely used mechanical micro-machining techniques that used for micro-channeling operations. The application of mechanical micro-channeling has cost advantage and gives reasonable surface finish while achieving tight dimensional tolerances. Mechanical micro-channeling is generally used on metallic substrates for metallic micro-parts and heat sinks. Micro-channels are also formed on metals by using micro-slotting. Wear of cutting tool, generation of cracks, and formation of burrs at ends are the common problems arise during mechanical micro-channeling. Hot embossing technique is used for creating micro-channels on polymer substrate. Silicon or metallic stamps are used for embossing on polymers at elevated temperature, which is the softening temperature of the respective polymers. Sometimes, the hot wires are also used for fabrication of micro-channels on polymers. Imprinting of micro-channels on polymers can be done at room temperature by the application of large pressure. The application of heat can reduce the required pressure for imprinting to a large extent. High lead time and low surface finish are the major concerns for using embossing and imprinting for producing micro-channels. Micro-molding is also used for fabricating micro-channels on polymers. The micro-features can be produced by injection molding of polymers (having low viscosity) by precisely controlling the parameters like temperature, aspect ratio precision micro-channels but the parts possess lower strength. Lasers are now used for fabricating micro-channels and attract much attention from researchers and industry for its several process advantages over other micro-channeling techniques. Laser is a versatile tool which can be used to generate micro-features of almost any shape and on almost every type of materials. It has greater flexibility and does not require cleanroom facility or preparation of masks. This is a clean, non-contact, and non-contaminant process. The point of exposure can be precisely controlled by controlling the beam spot by optical arrangements; thus, the process can produce deep and high aspect ratio micro-channels. The basic mechanism of material removal of laser micro-channeling is heating, melting, and vaporization. As this is a heat ablation process, the formation of heat-affected zone and burrs around micro-channels

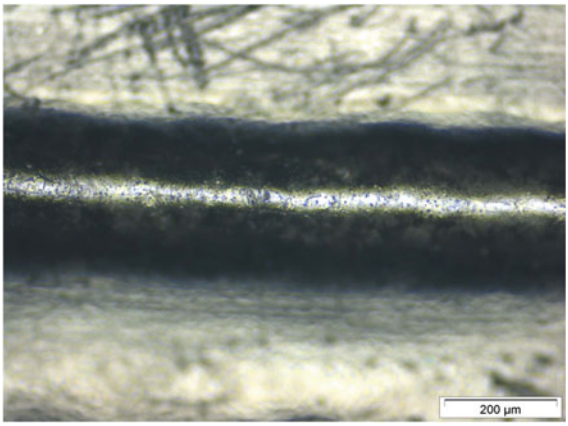

Fig. 1 Photograph of a micro-channel fabricated using laser-based micro-channeling technique on PMMA substrate [15]

cannot be avoided, but can be minimized at optimum machining conditions. High initial capital investment is also a factor of concern. Figure 1 shows a micro-channel fabricated using laser-based micro-channeling technique on PMMA substrate for the application in biomedical micro-fluidic devices.

3 Laser-based Fabrication of Micro-channels

3.1 Overview and Process Fundamentals

Nd:YAG (neodymium-doped yttrium aluminum garnet) and excimer lasers are the most commonly used laser systems for micro-channeling. The lasers having shorter wavelength (shorter ultraviolet wavelength) are preferably used for micro-machining than the lasers having longer wavelength (infrared wavelength), because the higher amount of energy is carried by photons of laser beam having shorter wavelengths. The absorption of laser beam within the material depends on wavelength of the laser, and shorter wavelength lasers have higher degree of absorption within the materials. The use of UV lasers reduces the chances of defects like the formation of wide HAZ, burrs and recast layers, because UV laser ablation of materials takes place by thermal excitation, resulting in ionization through breaking atomic bonds. This phenomenon is known as cold ablation [31]. Thus, these types of lasers are used for machining heat-sensitive materials. However, actual mechanism of ablation during UV laser machining is a combination of thermal and cold ablation, based on the work material used. The infrared lasers like Nd:YAG laser and fiber laser are used for producing micro-channels on metallic substrates. CO_2 laser (mid-infrared) is used for fabricating micro-channels on polymers and organic substrates, due to its higher absorptivity within those materials. Pulsed laser beam is preferred over continuous laser beam for micro-channeling operations. Peak power in the range

of several gigawatts can be obtained by using short laser pulse duration. The use of short laser pulse is resulting in very high-energy density. At very high-energy density, the material ablation is governed by the combination of thermal vaporization and Coulomb explosion, based on the wavelength of the laser beam and pulse frequency and pulse width used [32]. The Coulomb explosion phenomenon is observed during use of pico- and femtosecond pulses [31]. The evacuation of the electrons from the materials due to the application of high-energy ultrashort pulses formed a region where only the positively charged ions exist. Subsequently, a thin layer of the material surface is ejected, caused by electrostatic repulsion. In this way, the layers of materials are gently removed to produce micro-channels of very high surface quality without suffering any evident thermally induced defects. The actual ablation mechanism is a fusion of Coulomb explosion and thermal vaporization, where Coulomb explosion takes place at the initial phase of ablation, followed by thermal vaporization. The use of ultrashort pulse laser exposer does not give enough time to diffuse the heat to the surrounding materials. The micro-channel morphology not only depends on laser wavelength, pulse width, and pulse frequency but also influenced by the temporal and spatial profile of the laser beam [33].

3.2 Improvement of Quality and Accuracy

Laser-based techniques are now widely accepted by researchers and industry for fabrication of high-quality micro-channels and to be used in different micro-fluidic and cooling devices. The application of laser also enhances the repeatability of the process and thus able to produce micro-channels with greater dimensional accuracy at optimized process conditions. Heng et al. [34] employed an excimer laser (of 248 nm wavelength) for creating micro-fluidic channels on PMMA. It is found that the micro-channel depth increases with laser fluence so as the surface roughness, and thus the parameters must be optimized to achieve desired depth and surface quality. By using a third harmonic Nd:YAG laser (of 355 nm wavelength), Fernandez-Pradas et al. [35] successfully produced micro-channels on glass ceramics. Waddell et al. [36] employed a KrF excimer laser with nanosecond pulse for fabricating micro-channels on PMMA substrate. Lim et al. [37] utilized diode-pumped Nd:YAG laser for producing micro-channels with flat walls and herringbone ridges on silicon wafers. Micro-channels of a fixed depth of 125 μm and varying widths of 125, 160, 200, and 250 μm are produced without using any assist gas for cooling and melt ejection. The CO_2 laser is used by Hong et al. [38] for producing polymeric (PMMA) micro-fluidic devices. Kam and Majumder [39] employed a Q-switched Nd:YAG laser for creating micro-channels on silicon which are to be used in biomedical applications. Snakenborg et al. [40] fabricated micro-channels of 100–300 μm deep and 250 μm wide μm on PMMA substrate and able to achieve high-quality wall surface (roughness value around 1–2 μm). Cheng et al. [41] used CO_2 laser to produce micro-channels on PMMA, of varying width, ranging from 100 to 900 μm to maintain the aspect ratio of the channels around 7. The laser system is able to

produce thousands of such micro-channels in a day, and thus the initial investment of laser system can be compensated by utilizing the mass production of the components.

Femtosecond lasers are found to be the most suitable laser sources for micro-channeling operations, as far as dimensional accuracy, repeatability, and surface finish are concerned. Femtosecond lasers are capable of printing complex contours on optically transparent materials. Micro-channels of circular cross sections (8–20 μm diameters) are successfully fabricated on PMMA by Day and Gu [42] using femtosecond laser pulses. The samples are later annealed beyond the glass transition temperature of PMMA, which results in improved surface quality. Farson et al. [2] created clog-free internal micro-channels on PMMA, and those have diameters ranging from 2 to 20 μm and length of 12 mm, for applications in biomedical devices. The irradiation by femtosecond laser can be enhanced by subsequent chemical etching, which is known as FLICE femtosecond laser irradiation followed by chemical etching (FLICE) technology.

4 Underwater Laser Micro-channeling

4.1 Overview and Process Fundamentals

Laser micro-channeling of materials submerged in water produces cleaner structure than in open-air machining condition. Underwater micro-channeling reduces the chances of formation of HAZ, burr, and micro-cracks. The use of water aids in reducing the volume of recast material. During micro-channeling using focused high-intensity laser beam in open-air or gaseous environment, the plasma and the shock wave generated near to the target surface. This causes optical breakdown and ablation of the materials from the top surface in layer by layer [43]. Pressurized air or gas is used for melt ejection. The use of water in underwater laser machining confines the expansion of plasma near the material surface, and thus the plasma-induced pressure increases to a great extent. The bubbles formed during underwater laser micro-channeling affect the material surface. The water layer above the material surface constricts the plasma, and the developed recoil pressure because of this induce shock waves toward material surface which causes compressive failure in addition to the ablation due to the laser heating [44]. The underwater laser micro-channeling increases the cold ablation part as compared to sole thermal ablation during open-air condition, which causes enhanced material removal rate. Bubbles formed in stagnant water may hinder the laser beam from reaching the target surface and also cause light diffraction which results in inaccurate dimension of micro-channels. These problems can be eliminated by the use of flowing water over the material surface. This also helps in the ejection of removed particles.

4.2 Improvement of Quality and Accuracy

Underwater laser machining is an innovative process for producing clean and clog-free micro-channels by exploiting local cooling effect, in addition to decreasing the re-deposition of ablated material on the surface. Ageev [45] first exploited underwater laser processing to investigate the ablation of material during emission spectroscopy. Choo et al. [46] carried out the micro-machining of silicon using excimer lasers, in open-air as well as underwater conditions. The absence of any noticeable thermal damage is observed in the parts machined in underwater condition, while a significant amount of thermal damage is noticed in open-air condition. Muhammad et al. [47] carried out the fiber laser cutting on 200-μm-thick 316L stainless steel tubes. By utilizing underwater laser machining, HAZ and dross are minimized to large extent and zero back wall damage is achieved. Chung and Lin [18] studied the liquid assisted laser micro-drilling and able to produce high aspect ratio holes which are free from cracks and scorches. Wee et al. [21] performed underwater laser micro-machining on silicon wafers in different environmental conditions, in open-air and underwater. As compared to the open-air condition, the underwater laser micro-drilling results in reduced thermal damage and HAZ on both top and bottom surfaces of the material, while producing straight hole. The increase in material removal rate during underwater operation is also reported. The challenge faced during underwater micro-machining is the blocking of laser beam by debris floating in water, and redisposition of material where bubbles are formed, when used stagnant water. The water circulation is advantageous to avoid such problems [19]. By using a Ti:sapphire laser (800 nm wavelength) at 100 fs pulse width for underwater micro-machining of thin nitinol sheet, Muhammad and Li1 [3] could achieve the cutting surfaces free from HAZ, spatters, debris, and burrs. To enhance the material removal rate and quality of the machined surface during laser machining in submerged condition, different acid and salt solutions are also tested instead of using plain water. The use of salt solution during laser micro-channeling on stainless steel by Li and Achara [48] results in the improvement of rate of ablation by 300%, along with drastically reduction in the amount of HAZ and recast layers. Nakashima et al. [23] used hydrochloric acid solution during etching of single-crystal GaN using a femtosecond laser and observed high-quality ablation as compared to open-air condition.

4.3 An Experimental Case Study

A study on underwater laser micro-channeling on PMMA is presented in this section, and the discussion on process and quality is made based on experimental observations. The experimental results are presented previously [15]. Two major objectives are set for the investigation: (i) study of parametric influence on micro-channel dimensions and features to improve quality and accuracy, and (ii) comparison of micro-channels quality achieved by laser micro-channeling in underwater and in open-air

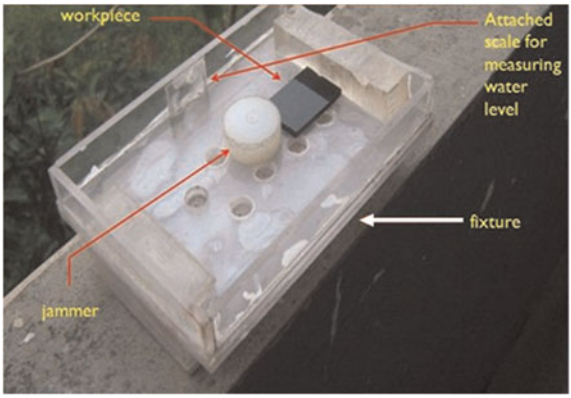

Fig. 2 Fixture used during underwater laser micro-channeling experiments [15]

conditions. A Q-switched Nd:YAG laser is used for fabrication of micro-channels on PMMA substrate. Lamp current (A), pulse frequency (B), pulse width (C), and cutting speed(D) are process parameters opted for carrying out micro-channeling experiments. Lamp current in amperage directly relates to total energy consumed by laser to emit desired pulses. Pulse width is the percentage of "ON" time duration per cycle time (120 ns). A specially designed fixture (Fig. 2) is used for holding the workpiece under a constant level of circulating water. The dimensions of micro-channel are specified in terms of its depth and width. The objective is generally set to increase the depth and decrease the width to achieve high aspect ratio micro-channels. However, low aspect ratio micro-channels are also used in some applications. HAZ and burr formation are major defects associated with laser-based micro-channeling. It is observed that the HAZ is surrounded by tiny burrs and rough protrusions. Therefore, the HAZ is categorized by height and width burrs. The burr width is considered as equal to HAZ width. Thus, micro-channel width, micro-channel depth, burr height, and burr width are measured (in μm) for the evaluation of the micro-channel quality.

Micro-channels of different sizes (width and depth in μm) are successfully produced using selected machining parameters within the range of study. Figure 3 shows the parametric trends, which are useful for finding the parameters and those have a greater influence on micro-channel dimensions and surface quality, and the way they affect the outputs. It is noticed that micro-channel depth and width increase with lamp current. Photon energy and equivalent laser beam energy increase with lamp current, thus transferring more energy to material, which results in increased depth and width of micro-channel. Increasing photon energy produces more amount of plasma which blocks the laser beam and thus the laser beam cannot reach the inner layer of the micro-channel. However, after increasing energy above, a threshold, laser beam can penetrate through the plasma and reaches the inner surface of the micro-channel, thus increases the channel depth. The number of pulses increases with pulse frequency, but energy per pulse decreases. Increasing the pulse frequency increases the channel depth. However, channel width does not change significantly

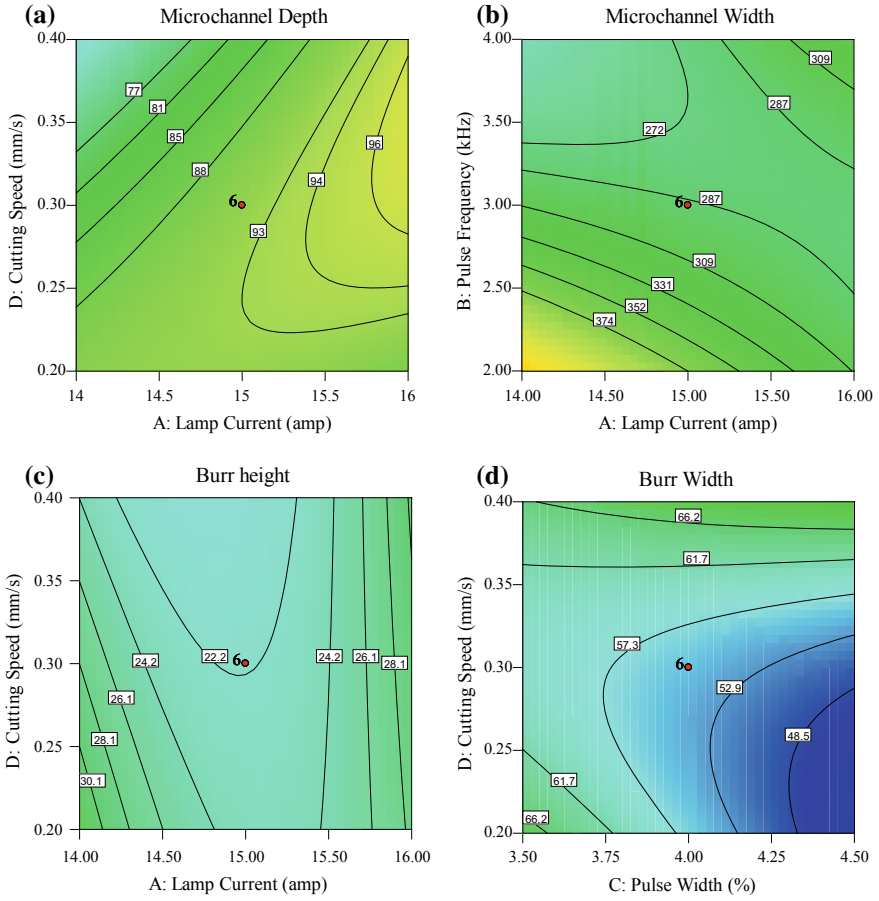

Fig. 3 Contour plots showing the effects of **a** lamp current and cutting speed on micro-channel depth, **b** lamp current and pulse frequency on micro-channel width, **c** lamp current and pulse width on burr height, and **d** pulse width and cutting speed on burr width

with pulse frequency because of the dominant local water cooling effect at material surface, which reduces the impact of low-energy pulses. Increasing pulse width increases laser material interaction time and therefore increases micro-channel depth and width. Micro-channel depth and width decrease with arise in cutting speed, due to less interaction time. Burr height and width increase with lamp current and pulse frequency and decrease with the increase of pulse width and cutting speed.

Figure 4 presents photographs of the micro-channels created on PMMA by using pulsed Nd:YAG laser in (a) underwater and (b) open-air conditions, respectively, for the same parameter combinations. It is observed from this figure that the use of water as the surrounding medium improves the quality of the micro-channels. The use of

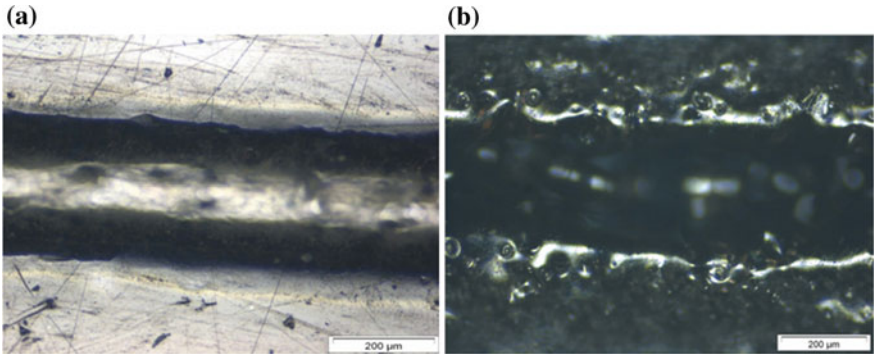

Fig. 4 Photograph of micro-channel created on PMMA using pulsed Nd:YAG laser **a** in underwater, and **b** in open-air conditions, respectively [49]

underwater laser micro-channeling reduced the HAZ and burr formation, significantly, and also improved the quality of micro-channel walls. It is further observed that water level plays an important role during micro-channeling. Increasing the water level above a threshold value decreases the micro-channel depth and increases the formation burrs around the micro-channel, whereas decreasing the water level below the threshold results in greater amount of HAZ. The threshold level of water depends on the composition and size of the workpiece, power and wavelength of laser beam, and the interaction between laser and water during the process. The threshold value of water level for underwater (mineral water having 80–120 ppm total dissolved solids) pulsed Nd:YAG laser (1.064 μm) micro-channeling on PMMA (4 mm thick) is found to be practically 1 mm above the material surface.

5 Summary

Micro-channels are essential parts of any micro-fluidic devices. Different techniques like mechanical micro-machining, chemical etching, photolithography, injection molding, imprinting and hot embossing, laser micro-machining are used for creating micro-channels on different substrates such as glass, polymer, silicon, metal. Laser-based fabrication techniques are gaining popularity due to its ability to generate micro-features of almost any shape and on almost every type of materials. The use of lasers having shorter wavelength (UV lasers) reduces the chances of thermal defects like the formation of wide HAZ, burrs and recast layers, because UV laser ablation of materials takes place by cold ablation. The material ablation during use of ultrashort laser pulses is governed by a combination of thermal vaporization and Coulomb explosion. In Coulomb explosion, the layers of materials are gently removed to produce micro-channels of very high surface quality without suffering any evident thermally induced defects. The micro-channel morphology not only depends

on laser wavelength, pulse width, and pulse frequency but also depends on temporal and spatial profile of the laser beam. Underwater laser micro-channeling produces clean and clog-free micro-channels by exploiting local cooling effect, in addition to decreasing the re-deposition of ablated material on the surface. Underwater micro-channeling produces cleaner structure as compared to open-air machining condition. The underwater laser micro-channeling increases the cold ablation part as compared to sole thermal ablation during open-air condition, which causes enhanced material removal rate and improved micro-channel quality. The application of laser-based micro-channeling techniques enhances the repeatability of the process and thus able to produce micro-channels with greater dimensional accuracy at optimized process conditions.

References

1. Becker H, Locascio LE (2002) Polymer microfluidic devices. Talanta 56:267–287
2. Farson D, Choi HW, Lu C, Lee LJ (2006) Femtosecond laser bulk micromachining of microfluid channels in PMMA. J Laser Appl 18:210
3. Muhammad N, Li L (2012) Underwater femtosecond laser micromachining of thin nitinol tubes for medical coronary stent manufacture. Appl Phys A 107:849–861
4. Atkin M, Hayes JP, Brack N, Poetter K, Cattrall R, Harvey EC (2002) Disposable biochip fabrication for DNA diagnostics. Proc SPIE 4937:125–135
5. Bai X, Roussel C, Jensen H, Girault HH (2004) Polyelectrolyte-modified short micro-channel for cation separation. Electrophoresis 25:931–935
6. Castano-Alvarez M, Fernandez-Abedul MT, Costa-Garcia A (2005) Poly (methyl methacrylate) and Topas capillary electrophoresis microchip performance with electrochemical detection. Electrophoresis 26:3160–3168
7. Phillips RJ (1988) Micro-channel heat sinks. Lincoln Lab J 1(1):31–48
8. Pan M, Zeng D, Tang Y (2009) Feasibility investigations on multi-cutter milling process: a novel fabrication method for microreactors with multiple micro-channels. J Power Sources 192:562–572
9. Kikuchi T, Wachi Y, Sakairi M, Suzuki RO (2013) Aluminum bulk micromachining through an anodic oxide mask by electrochemical etching in an acetic acid/perchloric acid solution. Microelectron Eng 111:14–20
10. Pal P, Sato K (2009) Silicon microfluidic channels and microstructures in single photolithography step. In: Proceedings of the DTIP of MEMS and MOEMS, Rome, New York, pp 419–423
11. Matteucci M, Christiansen TL, Tanzi S, Østergaard PF, Larsen ST, Taboryski R (2013) Fabrication and characterization of injection molded multi level nano and microfluidic systems. Microelectron Eng 111:294–298
12. Martynova L, Locascio LE, Gaitan M, Kramer GW, Christensen RG, MacCrehan WA (1997) Fabrication of plastic microfluid channels by imprinting methods. Anal Chem 69(23):4783–4789
13. Mathur A, Roy SS, Tweedie M, Mukhopadhyay S, Mitra SK, McLaughlin JA (2009) Characterisation of PMMA microfluidic channels and devices fabricated by hot embossing and sealed by direct bonding. Curr Appl Phys 9(6):1199–1202
14. Abdelgawad M, Wu C, Chien WY, Jewett MA, Sun Y (2011) A fast and simple method to fabricate circular micro-channels in polydimethylsiloxane (PDMS). Lab Chip 11:545–551
15. Prakash S, Acherjee B, Kuar AS, Mitra S (2013) An experimental investigation on Nd:YAG laser micro-channeling on polymethyl methacrylate submerged in water. Proc IMech E Part B J Eng Manuf 227:508–519

16. Castano-Alvarez M, Ayuso DFP, Granda MG, Fernandez-Abedul MT, Garcia JR, Costa-Garcia A (2008) Critical points in the fabrication of microfluidic devices on glass substrates. Sens Actuator B Chem 130:436–448
17. Lin C-H, Lee G-B, Lin Y-H, Chang G-L (2008) A fast prototyping process for fabrication of microfluidic systems on soda-lime glass. J Micromech Microeng 11:726–732
18. Chung CK, Lin SL (2010) CO_2 laser micromachined crackles through holes of Pyrex 7740 glass. Int J Mach Tool Manuf 50:961–968
19. An R, Li Y, Dou Y, Gong Q (2005) Simultaneous multi-microhole drilling of soda-lime glass by water-assisted ablation with femtosecond laser pulses. Opt Express 13(6):1855–1859
20. Dwivedi VK, Gopal R, Ahmad S (2000) Fabrication of very smooth walls and bottoms of silicon micro-channels for heat dissipation of semiconductor devices. Microelectr J 31:405–410
21. Wee LM, Ng EYK, Prathama AH, Zheng H (2011) Micro-machining of silicon wafer in air and under water. Opt Laser Technol 43:62–71
22. Qin SJ, Li WJ (2002) Micromachining of complex channel systems in 3D quartz substrates using Q-switched Nd:YAG laser. Appl Phys A Mater 74:773–777
23. Nakashima S, Sugioka K, Midorikawa K (2009) Fabrication of micro-channels in single-crystal GaN by wet-chemical-assisted femtosecond laser ablation. Appl Surf Sci 255:9770–9774
24. Muck A Jr, Wang J, Jacobs M, Chen G, Chatrathi MP, Jurka V, Výborný Z, Spillman SD, Sridharan G, Schöning MJ (2004) Fabrication of poly(methyl methacrylate) microfluidic chips by atmospheric molding. Anal Chem 76:2290–2297
25. Chang TC, Molian PA (1999) Excimerpulsed laser ablation of polymers in air and liquids for micromachining applications. J Manuf Process 18:1–17
26. Jo BH, Lerberghe VLM, Motsegood KM et al (2000) Threedimensional micro-channel fabrication in polydimethylsiloxane (PDMS) elastomer. J Microelectromech Syst 9(1):76–81
27. Kanlayasiri K, Paul BK (2004) A nickel aluminide micro-channel array heat exchanger for high temperature applications. J Manuf Process 6(1):72–80
28. Paulraj P, Paul BK, Peterson B (2012) Development of an adhesive-bonded counterflow micro-channel heat exchanger. Appl Therm Eng 48:194–201
29. Kim M, Yi M, Zhong J, Bau HH, Hu H, Ananthasuresh SGK (1998) The fabrication of flow conduits in ceramic tapes and the measurement of fluid flow through these conduits. In: Proceedings of the ASME dynamic systems and controls division, Anaheim, CA, vol 66, pp 171–177
30. Yi Q (2010) Micro-manufacturing engineering and technology, 1st edn. Elsevier Inc., Oxford
31. Molian P, Pecholt B, Gupta S (2009) Picosecond pulsed laser ablation and micromachining of 4H-SiC wafers. Appl Surf Sci 255:4515–4520
32. Sokolowski-Tinten K, Bialkowski J, Cavalleri A, von der Linde D, Oparin A, Meyer-Ter-Vehn J, Anisimov SI (1998) Transient states of matter during short pulse laser ablation. Phys Rev Lett 81:224–227
33. Prakash S, Kumar S (2015) Fabrication of micro-channels: a review. ProcIMechE Part B J Eng Manuf 229:1273–1288
34. Heng Q, Tao C, Zuo TC (2006) Surface roughness analysis and improvement of micro-fluidic channel with excimer laser. Microfluid Nanofluid 2:357–360
35. Fernandez-Pradas JM, Serrano D, Serra P, Morenza JL (2009) Laser fabricated micro-channels inside photostructurable glass-ceramic. Appl Surf Sci 255:5499–5502
36. Waddell EA, Locascio LE, Kramer GW (2002) UV laser micromachining of polymers for microfluidic applications. J Assoc Lab Autom 7(1):78–82
37. Lim D, Kamotani Y, Cho B et al (2003) Fabrication of microfluidic mixers and artificial vasculatures using a high brightness diode-pumped Nd:YAG laser direct write method. Lab Chip 3:318–323
38. Hong TF, Ju WJ, Wu MC, Tsai CH, Fu LM (2010) Rapid prototyping of PMMA microfluidic chips utilizing a CO_2 laser. Microfluid Nanofluid 9:1125–1133
39. Kam DH, Majumder J (2008) 3-D biomimetic micro-channel network by laser direct writing. J Laser Appl 20:185

40. Snakenborg D, Klank H, Kutter JP (2004) Microstructure fabrication with a CO_2 laser system. J Micromech Microeng 14:182
41. Cheng JY, Wei CW, Hsu KH, Young TH (2004) Direct-write laser micromachining and universal surface modification of PMMA for device development. Sens Actuator B Chem 99:186–196
42. Day D, Gu M (2005) Micro-channel fabrication in PMMA based on localized heating by nanojoule high repetition rate femtosecond pulses. Opt Express 13(16):5939–5946
43. Zheng ZY, Zhang Y, Zhao CC, Hao H, Lu X, Li Y, Zhang J (2007) Ablation pressure of the shock wave generated by laser interaction with solid targets. Optoelectron Lett 3(5):394–396
44. Chen X, Xu RQ, Chen JP, Shen ZH, Jian L, Ni XW (2004) Shock-wave propagation and cavitation bubble oscillation by Nd:YAG laser ablation of a metal in water. Appl Opt 43(16):3251–3257
45. Ageev VA (1975) Investigation of optical erosion of metals in liquids. J Appl Spectrosc 23(1):903–906
46. Choo KL, Ogawa Y, Kanbargi G, Otra V, Raff LM, Komanduri R (2004) Micromachining of silicon by short-pulse laser ablation in air and under water. Mat Sci Eng A Struct 372:145–162
47. Muhammad N, Whitehead D, Boor A, Li L (2010) Comparison of dry and wet fibre laser profile cutting of thin316L stainless steel tubes for medical device applications. J Mater Process Tech 210:2261–2267
48. Li L, Achara C (2004) Chemical assisted laser machining for the minimisation of recast and heat affected zone. CIRP Ann Manuf Techn 53(1):175–178
49. Acherjee B, Prakash S, Kuar AS, Mitra S (2014) Grey relational analysis based optimization of underwater Nd:YAG laser micro-channeling on PMMA. Proc Eng 97:1406–1415

Pulsed Nd:YAG Laser Cutting: Accuracy Improvement and Parametric Influences

Girish Dutt Gautam and Dhananjay R. Mishra

Abstract Laser beam cutting (LBC) demonstrates its superiority over traditional cutting techniques due to its contactless and localized nature between the cutting tool and workpiece surface. Nowadays, pulsed Nd:YAG laser beam cutting is in one of the highly demanded cutting processes for variety of applications in the aircraft, aerospace, marine, defense, etc., sectors. This system is able to cut not only intrinsic and complex shapes for an inclusive variety of materials but also provide higher accuracy and precise cut edge surface. In this chapter, analysis of some key investigations is performed by the previous researchers for pulsed Nd:YAG laser beam cutting of distinct materials like metals, non-metals, and composites have been discussed. The conducted survey has been based on the influence of the variable laser cutting factors on the performance characteristics.

Keywords Nd:YAG laser cutting · Accuracy · Heat-affected zone (HAZ) · Kerf quality · Artificial intelligence

1 Introduction

Townes and Schawlow developed the first functional ruby laser in 1957, based on the Planck's concept of quanta or packets [1]. Higher monochromaticity, coherence, low diffraction (divergence), and high radiance make the laser beam differ from ordinary light beam either natural or manmade [2]. Absorption, population inversion, and emission are the important processes required for the generation of a laser beam.

Generally, lasers are categorized on the basis of their lasing medium such as solid, liquid, and gas lasers. However, all laser systems can be acted in both pulsed and continuous mode, i.e., interrupted and uninterrupted emission of a laser beam. CO_2

G. D. Gautam (✉) · D. R. Mishra
Department of Mechanical Engineering, Jaypee University of Engineering and Technology, Guna 473226, Madhya Pradesh, India
e-mail: girish.gautam1985@gmail.com

D. R. Mishra
e-mail: dhananjay.mishra@juet.ac.in

G. Kibria and B. Bhattacharyya (eds.), *Accuracy Enhancement Technologies for Micromachining Processes*, Lecture Notes in Mechanical Engineering,
https://doi.org/10.1007/978-981-15-2117-1_6

and Nd:YAG laser systems are the most famous type of lasers used for processing of materials in the types of gas and solid-state lasers, respectively [3, 4].

Lasers have a range of numerous uses in the engineering, medical, industrial, defense, marine, aerospace, aircraft and sports sectors, etc., such as laser machining, welding, surgery, imaging, and spectroscopy. These applications require a higher degree of machining due to complex profiles and intrinsic shapes. Laser beam machining (LBM) is a contactless technique which uses the thermal energy of the incident laser beam to remove the material from the surface of workpiece. This is a non-contact type process; therefore, no vibrational forces are generated as compared to conventional machine tools. The removal of material is occurred due to the melting, vaporization, and evaporation. The optical, thermal, and structural properties of the workpiece material ascertain the effectiveness of the LBM process [5]. Thus, low thermal conductive and diffusive materials exhibit a well-suited environment during laser machining. LBM can be categorized on the basis of movement of the laser beam and workpiece. Generally, the relative motion between incident laser beam and workpiece material is expressed in the terms of their dimensional positions [1]. Thereby, laser beam drilling (LBD) is known as one-dimensional laser machining. In the LBD, incident beam remains fixed relative to the workpiece. In this process, the developed erosion front is situated at the bottom side of the produced hole. LBD is used to create holes in turbine blades and combustion chambers. Whereas, in the LBC process workpiece moves and beam remains stationary. Three-dimensional laser machining approaches such as laser turning, laser milling, and laser grooving are used in the applications which needed mass removal of material removal. In these processes, two or more laser beams in either fixed or movable condition are used to cut the materials. LBC is the most popular type of laser machining due to higher dimensional accuracy and precise cutting for an extensive variety of metallic and non-metallic engineering materials. The contactless nature of the process provides absence of the frictional and vibrational forces; therefore, no tool wear takes place. It produces narrow kerf with relatively low heat-affected zone (HAZ) with higher cut edge quality [5, 6]. Assist gas is also used in this process to remove molten material from erosion front and reduce the width of recast layer and spatter formation. Blanking, cutting, and marking are the some important applications of laser cutting. This chapter provides a piece of detailed knowledge about the effects of the vital process parameters on cut edge quality during pulsed Nd:YAG laser cutting of versatile engineering materials like metals, non-metals, and composites.

2 Pulsed Nd:YAG Laser

The wavelength of Nd:YAG laser system is 1.064 μm, however, its operating efficiency is only 4% which is relatively low as compared to CO_2 laser 12%. This is due to that the releasing energy rate through the heat in CO_2 laser is very low compared to the rate of energy release through light. However, the quantum efficiency of both

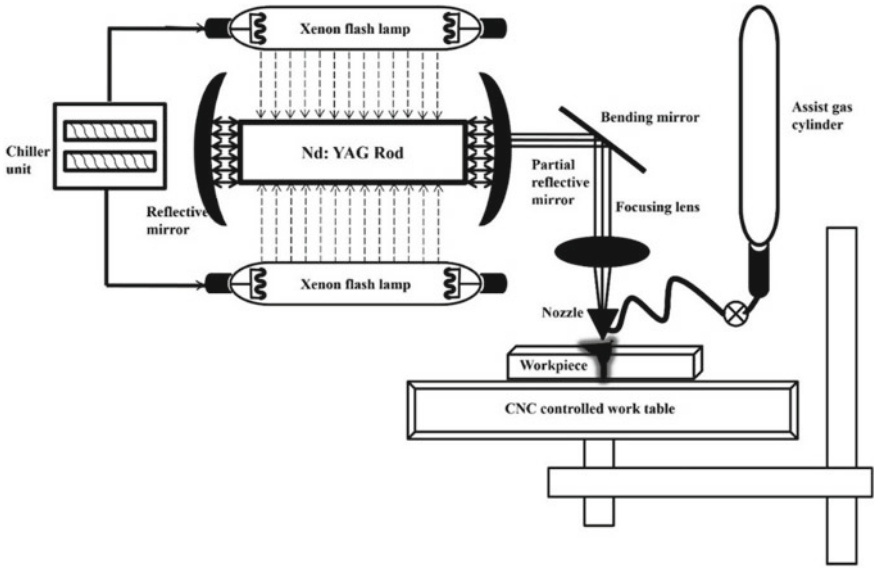

Fig. 1 Schematic diagram of Nd:YAG laser system [7]

lasers is nearly same as 40% for Nd:YAG and 45% for CO_2 laser. The schematic diagram of Nd:YAG laser system with its main components is shown in Fig. 1. To lead the oscillating photons which are generated in the beam generation unit, two optical mirrors are used. In both mirrors, one is 100% reflective, while the other one is 95% reflective or 5% transitive. The delivery of the generated laser beam is performed by optical fibers. These optical resonators are averted by generated fumes and scatter during cutting by the use of different types of assist gases [7, 8]. Nd:YAG laser system can be used evenly both thick and thin sheet of different materials. However, the beam power of Nd:YAG lasers are relatively low but in pulsed mode, it can be used to cut thicker sheets (more than 2 mm) satisfactorily due to higher peak powers. Moreover, for thin sheets, it is also well suited due to shorter pulse duration. This system also proves its appropriateness for highly reflective materials and various super alloys due to its shorter wavelength. These materials are considered as difficult to cut materials.

In this system, a laser beam in the pulsed mode strikes on the outer surface of the workpiece and surge the temperature up to its boiling point (material). As well as the temperature rises, material starts melting and a keyhole is started to form on the work surface. This keyhole acts as a black box and absorbed heat energy of incident laser beam. Thereafter, the temperature in keyhole suddenly surges due to reflections of incident laser beam in various directions. Thereby, vaporization of work material takes place with a higher rate and deepens the keyhole more and results in wider kerf widths. Nd:YAG LBC is hugely used to cut an extensive range of materials for their industrial application. The setup time of this system is very less, therefore, it is

considered as the fastest laser cutting technique. Moreover, it is also more economical for mass production as compared to other advanced machining techniques. Its major area of applications is the automotive, medical, nuclear, marine, civil structural, food processing, consumer goods, chemical sectors, etc. [3, 9, 10].

2.1 Process and Performance Parameters

In the LBC, the performance of process is measured on the basis of three vital characteristics namely quality, geometrical, and metallurgical. Quality characteristics can be classified in mainly two types such as material removal rate (MRR) and surface roughness (SR) of the cut. Whereas, geometrical characteristics are categorized by various attributes of developed kerf like width, deviation, taper, kerf ratio, etc. These features are also known as kerf quality characteristics. In general, the kerf is considered as the loss of material at the starting of the cut. These features provide the profile of the cut surface and ensure the degree of fitness of the as per the requirement. On the other side, metallurgical characteristics such as heat-affected zone (HAZ) and recast layer thickness provide the change or variation into the material microstructure during machining. These performance characteristics depend on the value/range of the various process parameters or cutting parameters. Input factors can be also categorized into three types like beam characteristics, laser characteristics, and cutting characteristics. The classification chart of process and performance characteristics is shown in Fig. 2. Different features of kerf qualities during pulsed Nd:YAG laser cutting are shown in Fig. 3. In the Nd:YAG laser cutting, most of the experimental investigations are focused on the improvement of the geometrical and metallurgical quality of the performed cut. Proper adjustment of the variable cutting parameters is able to ascertain it. Some researchers have used one parameter at a time (OPAT) and some used design of experiments (DOE) techniques to conduct the experiments.

3 Pulsed Nd:YAG Laser Cutting of Metals

A lot of researchers have performed numerous theoretical and experimental investigations during pulsed Nd:YAG laser cutting of distinct ferrous and non-ferrous metals such as steel, aluminim, nickel, and titanium. Ghany and Newishy [12] reported that at higher cutting speed, higher pulse frequency, nitrogen as assist gas is able to reduce the kerf width and improve cut geometry. Moreover, they observed that in pulsed mode, smaller cutting speed provides lower kerf width. Choubey et al. [13] performed laser cutting for dismantling applications of steel sheet having a varying thickness between 4 and 20 mm in dry air and underwater environment. They observed that a rise in pulse width increases the cutting speed due to reduced spot overlapping.

Thermal and electrical properties of aluminum (Al) and its alloys make them challenging to cut by conventional processes. Thus, in these days, laser cutting is widely

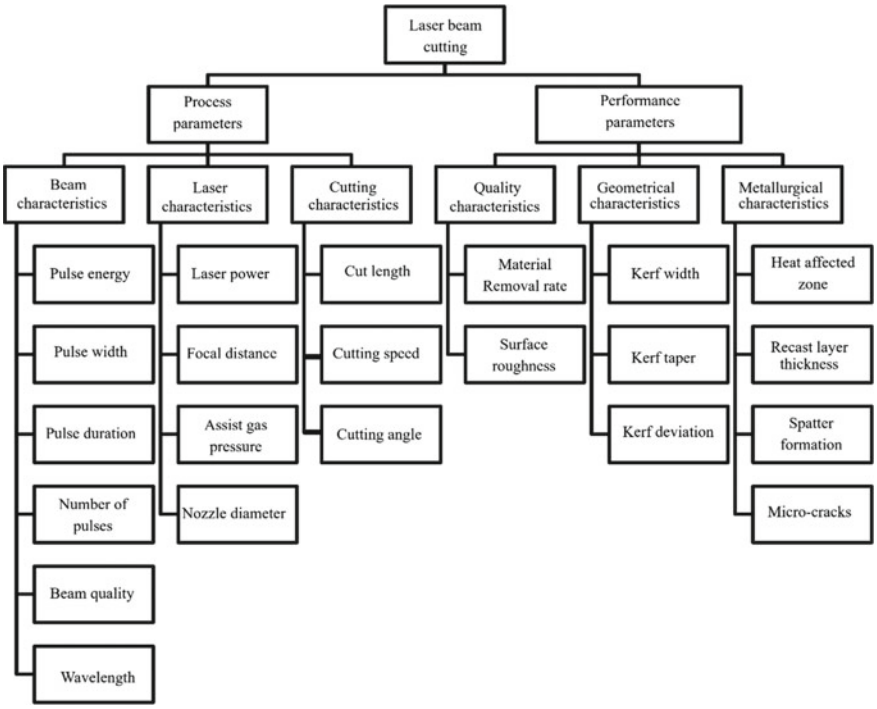

Fig. 2 Classification of various process and performance parameters in LBC

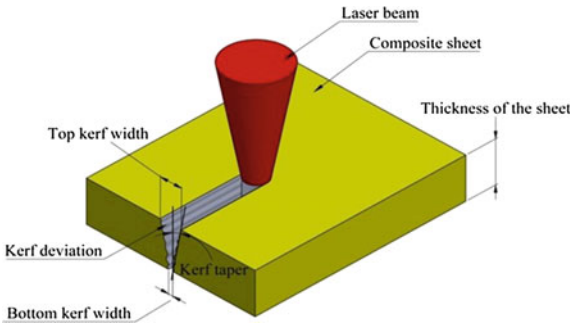

Fig. 3 Kerf quality characteristics during laser cutting [11]

used to cut this type of materials having unique properties like higher reflective, lightweight, etc. Al and its alloys are mostly used in naval, aerospace, and automobile industries. Sharma and Yadava [14] employed a hybrid optimization approach to decide the optimum levels of air pressure, width, and frequency of the pulse and cutting speed to reduce kerf taper and surface roughness during laser cutting of Al-40800 alloy. They found that due to the higher reflectivity of Al alloy, lower cutting speed is able to provide reduced kerf taper. Chaki et al. [15] revealed that higher

settings of cutting speed and pulse energy can increase the material removal rate in laser cutting. The pulse duration also affects the molten material quantity in terms of lower kerf width and surface roughness [16]. Dubey and Yadava [17] have found that pressure of assist air and pulse frequency remarkably influenced the quality of kerf in laser cutting of 8011 Al alloy having thickness of 0.9 mm.

Nickel-based alloys and super alloys are extensively used in aircraft industries for jet engine casting and turbochargers, turbine blades, etc. These specific applications required higher dimensional accurate and precise cutting, which is not possible by conventional cutting techniques. Therefore, laser system is widely used for cutting these types of difficult to cut materials. Thawari et al. [18] revealed that kerf width and surface roughness significantly depend on the overlapping of laser beam spots during laser cutting of Hastalloy X sheet. Dubey and Yadava [19] observed that cutting speed is the most influencing parameter for all output responses during cutting of nickel-based super alloy. In straight and profile cutting of Ni-based super alloy, it is observed that the effect of assist gas pressure is almost the same for kerf width and kerf deviation in both cases [20].

LBC of titanium (Ti) and its alloys is highly used in aerospace and medical component manufacturing industries. These alloys have superior mechanical and structural properties like higher toughness, strength, and stiffness with high corrosive and fatigue resistance. Almeida et al. [21] performed the laser cutting of pure Ti and Ti-6Al-4V sheets to examine consequences of the considered variable input factors to determine the cut edge surface roughness. They found that at the higher overlapping rate and lower cutting speed, surface roughness decreased and dross quantity increased. Shanjin and Yang [22] inspected the influence of various variable input parameters like pulse energy, pulse rate, cutting speed, gas type, and gas pressure on HAZ, surface morphology, and corrosion resistance in laser cutting of TC1 alloy sheet. They found that high values of pressure of assist gas are able to increase the melt material removal rate and provide reduced HAZ due to cooling effect. Nd:YAG laser cutting system in pulsed mode is also employed extensively in the medical sectors to cut nickel- and titanium-based shape memory alloys for surgical instruments, cardio-vascular system devices, dental implants, etc.

4 Pulsed Nd:YAG Laser Cutting of Non-metals

The conventional techniques for cutting of ceramic-like water jet machining, diamond saw are very costly and time taking. Therefore, in the last few decades, the application of Nd:YAG laser system is increased for cutting of non-metallic materials like glass, silicon, ceramics, etc. [8]. Tuersley et al. [23] used a laser system to cut and drill borosilicate glass with SiC fibers to examine the effect of the variable input factors. They observed that MRR significantly influenced by laser peak power. Quintero et al. [24] observed that pulsed Nd:YAG laser cutting system is capable to provide structural cracks free cuts either perpendicular to the cut walls or at the cut end.

5 Pulsed Nd:YAG Laser Cutting of Composites

Besides metals and non-metals, Nd:YAG laser system is also suitable to cut composite materials specially fiber-reinforced polymer (FRP) composites. However, cutting of FRP composites is a tough task due to their integral structural properties. Laser cutting minimizes various issues like a crash in the matrix phase, evacuation of reinforcing fibers, delamination, wear of cutting tool edge, etc. [25, 26], during cutting of FRP composites as compared with conventional cutting systems due to its contact-less nature. It offers higher cut quality and flexibility with a higher production rate [7]. Mathew et al. [27] performed laser cutting of carbon fiber-reinforced polymer (CFRP) composite sheet and observed that the width of kerf decreases with an increase in cutting speed. Moreover, they found that HAZ rises with an increase in repetition rate. Various researchers also successfully performed laser cutting of aramid fiber-reinforced polymer (AFRP) composites and discussed the influence of variable cutting factors on different cut quality characteristics [28–31].

Gautam and Pandey [31] evaluated the consequences of different input parameters on top and bottom deviation of kerf in laser cutting of AFRP composite. They found that due to the difficult to burn properties of Kevlar fiber, lamp current affects mostly the quality of cut. They also observed that higher cutting speed provide un-cut situation due to insufficient burning of Kevlar-29 fibers as shown in Fig. 4a, b.

Gautam and Mishra [32] performed the laser cutting of hybrid FRP composite laminate. They have selected two highly inflammable fibers, Kevlar-29 and Basalt fibers as a reinforcing agent in the epoxy-based matrix. They perceived that the accurateness of the cut edge is not only influenced by the variable laser process parameters but also by the physical, chemical, and mechanical properties of the ingredient fibers. They observed that lower settings of lamp current, pulse frequency, and compressed air pressure, whereas higher settings of cutting speed are favorable to achieve the highly accurate profile of cut for the hybrid composites [11]. In another study, they [33] observed that lamp current is the most prompting parameter for width and taper of the cut during laser cutting of basalt fiber-reinforced polymer (BFRP)

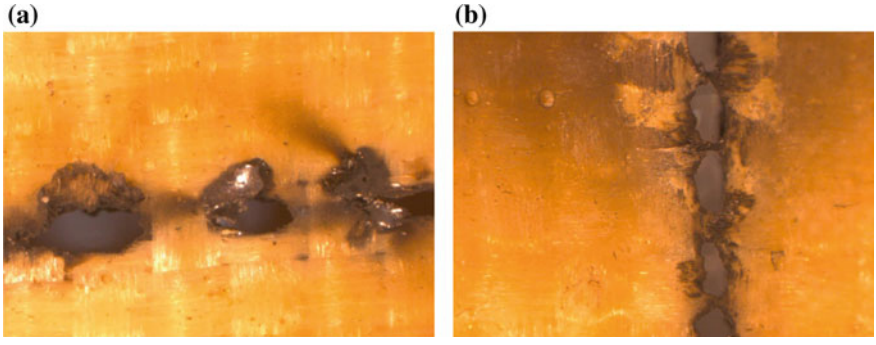

Fig. 4 **a**, **b** No cut situation during laser cutting of AFRP [31]

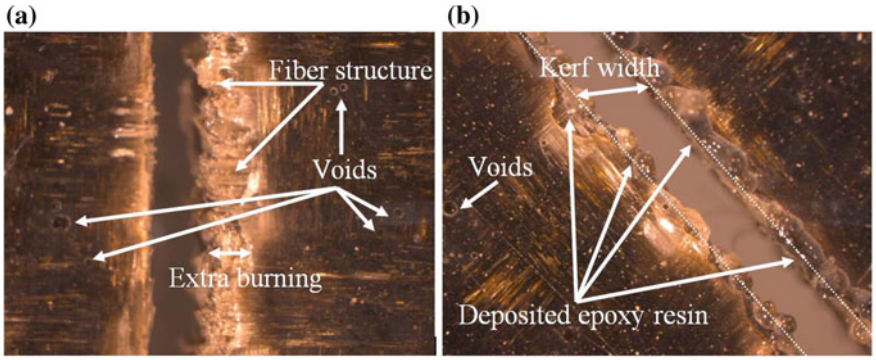

Fig. 5 Issues in laser cutting of BFRP composite [33]

composite. While on the other side kerf deviation was significantly influenced by the cutting speed. Moreover, they observed that pulse frequency was the less influencing parameter for all three output responses. However, they also found that lower values of assist gas pressure and cutting speed reduce the heat dissipation rate and result in deposition of epoxy resin with uneven and extra burning as shown in Fig. 5.

6 Applications of Artificial Intelligence in Pulsed Nd:YAG Laser Cutting

Large range of variable factors makes LBC a highly non-linear and complex process. Therefore, it is a very difficult task to forecast the behavior of input factors. To overcome this problem, various researchers employed different artificial intelligence (AI) techniques such as genetic algorithm (GA), particle swarm optimization (PSO), and firefly algorithm (FA). The robust nature of theses AI techniques makes them favorable to identify interrelationship between input and output process parameters. Various studies show that these techniques are able to provide optimal solutions to improve performance measures.

A 98.48% accurate back-propagation ANN model to estimate the depth and width of the developed cut and HAZ by using three variable process factors was developed by Tsai et al. [34]. An improvement of 19.16 and 17.32% at the optimum combination of variable process parameters for kerf taper and surface roughness were achieved by Pandey and Dubey [35] using GA approach for cutting of titanium alloy sheet. They also proposed a hybrid multiobjective optimization technique gray-fuzzy methodology to simultaneously minimize kerf width, kerf taper, and surface roughness as a single index. They found an overall improvement of 19% in output responses by the proposed approach [36].

Gautam and Pandey [31] employed TLBO algorithm approach for optimization of input parameters in laser cutting of AFRP composite laminates. In this experimental

study, they recorded remarkable improvement in the quality of top and lower kerf deviations by TLBO technique. The same technique further employed by Gautam and Mishra [11] to ascertain the optimal settings of input factors in laser cutting of hybrid composite. They registered a total enhancement of 22.23% in all evaluated kerf qualities at acquired optimum settings of variable process parameters. In another study, Gautam and Mishra [33] employed firefly algorithm (FA) to achieve the optimum setting of variable input factors to minimize different kerf qualities during laser cutting of BFRP composite. They found that used optimization technique is able to provide 26.75% improvement in output quality responses.

7 Summary

The chapter presented here is a critical review of investigations performed by previous researchers in the field of pulsed Nd:YAG laser beam cutting process for distinct materials. The main conclusions enumerated from this chapter are listed below:

1. Nd:YAG laser cutting system in pulsed mode is capable to cut a broad variety of engineering materials.
2. Difficult to machine super alloys can be cut by Nd:YAG laser because of its independence from their mechanical properties.
3. The performance of Nd:YAG laser depends on the various input factors. However, the operating range of these factors is adjusted according to the optical, thermal properties, and composition of workpiece materials.
4. The geometrical, surface quality, and metallurgical quality characteristics are the vital performance measures of the process.
5. FRP composite materials can be cut by Nd:YAG laser system with higher accuracy and minimal processing defects compared to conventional approaches.
6. AI-based optimization techniques can be used to determine favorable settings of variable input parameters to improve process performance.

References

1. Chryssolouris G (1991) Laser machining theory and practice. Springer science+business media, LLC
2. Haken H (1985) Light, vol 2. North Holland
3. Steen WM, Mazumder J (2010) Laser material processing, 4th edn. Springer, Berlin
4. Steen WM (2003) Laser material processing-an overview. J Opt A Pure Appl Opt 5:S3–S7
5. Dubey A, Yadava V (2008) Laser beam machining—a review. Int J Mach Tools Manuf 48:609–628
6. Dubey AK, Yadava V (2008) Experimental study of Nd:YAG laser beam machining—an overview. J Mater Process Technol 195(1–3):15–26
7. Gautam GD, Pandey AK (2018) Pulsed Nd:YAG laser beam drilling: A review. Opt Laser Technol 100:183–215

8. Dahotre NB, Harimkar SP (2008) Laser fabrication and machining of materials. Springer
9. Meijer J (2004) Laser beam machining (LBM), state of the art and new opportunities. J Mater Process Technol 149:2–17
10. Koechner W, Bass M (2003) Solid-state lasers: a graduate text. Springer, New York
11. Gautam GD, Mishra DR (2019) Dimensional accuracy improvement by parametric optimization in pulsed Nd:YAG laser cutting of Kevlar-29/Basalt fiber reinforced hybrid composites. J Braz Soc Mech Sci Eng 41(7):1–22
12. Ghany KA, Newishy M (2005) Cutting of 1. 2 mm thick austenitic stainless steel sheet using pulsed and CW Nd:YAG laser. J Mater Process Technol 168:438–447
13. Choubey A et al (2015) Studies on pulsed Nd:YAG laser cutting of thick stainless steel in dry air and underwater environment for dismantling applications. Opt Laser Technol 71:6–15
14. Sharma A, Yadava V (2012) Modelling and optimization of cut quality during pulsed Nd:YAG laser cutting of thin Al-alloy sheet for straight profile. Opt Laser Technol 44(1):159–168
15. Chaki S, Bathe RN, Ghosal S (2015) Multi-objective optimisation of pulsed Nd:YAG laser cutting process using integrated ANN—NSGAII model. J Intell Manuf 29(1):175–190
16. Leone C, Genna S (2018) Heat affected zone extension in pulsed Nd:YAG laser cutting of CFRP. Compos B 140:174–182
17. Dubey AK, Yadava V (2007) Optimization of kerf quality during pulsed laser cutting of aluminium alloy sheet. J Mater Process Technol 4(2005):412–418
18. Thawari G, Sundar JKS, Sundararajan G, Joshi SV (2005) Influence of process parameters during pulsed Nd:YAG laser cutting of nickel-base superalloys. J Mater Process Technol 170:229–239
19. Dubey AK, Yadava V (2008) Multi-objective optimization of Nd:YAG laser cutting of nickel-based superalloy sheet using orthogonal array with principal component analysis. Opt Lasers Eng 46:124–132
20. Sharma A, Yadava V, Rao R (2010) Optimization of kerf quality characteristics during Nd:YAG laser cutting of nickel based superalloy sheet for straight and curved cut profiles. Opt Lasers Eng 48(9):915–925
21. Almeida IA et al (2006) Optimization of titanium cutting by factorial analysis of the pulsed Nd:YAG laser parameters. Journal of material processing technology 179:105–110
22. Shanjin L, Yang W (2006) An investigation of pulsed laser cutting of titanium alloy sheet. Opt Lasers Eng 44:1067–1077
23. Tuersley IP, Hoult TP, Pashby IR (1998) Nd—YAG laser machining of SiC fibre/borosilicate glass composites. Part I. Optimisation of laser pulse parameters. Compos Part A 29(8):947–954
24. Quintero F et al (2006) Cutting of ceramic plates by optical fiber guided Nd:YAG laser cutting of ceramic plates by optical fiber guided Nd:YAG laser. J Laser Appl 13(84):9–14
25. Komanduri Ranga (1993) Machining fiber-reinforced composites. Mech Eng 115(4):58
26. Komanduri R (1997) Machining of fiber-reinforced composites. Mach Sci Technol Int J 1(1):37–41
27. Mathew J, Goswami GL, Ramakrishnan N, Naik NK (1999) Parametric studies on pulsed Nd:YAG laser cutting of carbon fibre reinforced plastic composites. J Mater Process Technol 90:198–203
28. Yilbas BS, Akhtar SS (2012) Laser cutting of Kevlar laminates and thermal stress formed at cutting sections. Opt Lasers Eng 50(2):204–209
29. Yilbas BS, Karakas FC (2008) Laser hole cutting in Kevlar: modeling and quality assessment. Int J Adv Manuf Technol 38:1125–1136
30. Yilbas BS, Sahin AZ, Chatwin C, Ayar T (2011) Laser cutting of Kevlar laminates: first and second law analysis. J Mech Sci Technol 25(4):855–862
31. Gautam GD, Pandey AK (2017) Teaching learning algorithm based optimization of kerf deviations in pulsed Nd:YAG laser cutting of Kevlar-29 composite laminates. Infrared Phys Technol 89:203–217
32. Gautam GD, Mishra DR (2019) Evaluation of geometrical quality characteristics in pulsed Nd:YAG laser cutting of Kevlar-29/basalt fiber reinforced hybrid composite using grey relational analysis based on genetic algorithm. FME Trans 47(3):560–575

33. Gautam GD, Mishra DR (2019) Firefly algorithm based optimization of kerf quality characteristics in pulsed Nd:YAG laser cutting of basalt fiber reinforced composite. Compos Part B 176:107340
34. Tsai MJ, Li CH (2009) The use of grey relational analysis to determine laser cutting parameters for QFN packages with multiple performance characteristics. Opt Laser Technol 41:914–921
35. Pandey AK, Kumar A (2012) Simultaneous optimization of multiple quality characteristics in laser cutting of titanium alloy sheet. Opt Laser Technol 44(6):1858–1865
36. Pandey AK, Dubey AK (2013) Multiple quality optimization in laser cutting of difficult-to-laser-cut material using grey—fuzzy methodology. Int J Adv Manuf Technol 65:421–431

Improvement in Surface Finish and Geometrical Accuracy by Laser Micro-turning

Golam Kibria, B. Doloi and B. Bhattacharyya

Abstract Recently, laser micromachining and micro-fabrication processes have remarkable and diversified applications in the direction to manufacture highly precised and accurate dimensional parts or components which are used in bio as well as technological domains such as biomedical, dental and orthopaedic, aircraft engines, micro-electromechanical systems (MEMS), electronic devices, turbocharger rotor parts and nuclear reactors. The present chapter deals with experimental investigation into micro-turning process using pulsed Nd:YAG laser during machining of aluminium oxide ceramics. A number of experimental schemes were adopted to explore the parametric influences on process characteristics such as surface roughness and depth deviation. Experimental investigation was also carried out to improve the dimensional accuracy and surface characteristics of laser micro-turned components using laser defocusing technique.

Keywords Laser micro-turning · Laser defocusing · Aluminium oxide · Accuracy improvement · Overlap

1 Introduction

Due to some excellent and extraordinary properties of high-tech engineering ceramics such as high strength, corrosion and wear resistance, withstand ability at elevated temperature, high insulation capabilities, these ceramics have wide applications in the engineering fields like aerospace, electronics, electrical, textiles, mechanical, chemicals, food processing and in many others fields [1, 2]. Not only that, the demand of

G. Kibria (✉)
Mechanical Engineering Department, Aliah University, Kolkata 700156, India
e-mail: prince_me16@rediffmail.com

B. Doloi · B. Bhattacharyya
Production Engineering Department, Jadavpur University, Kolkata 700032, India
e-mail: bdoloionline@rediffmail.com

B. Bhattacharyya
e-mail: bb13@rediffmail.com

G. Kibria and B. Bhattacharyya (eds.), *Accuracy Enhancement Technologies for Micromachining Processes*, Lecture Notes in Mechanical Engineering,
https://doi.org/10.1007/978-981-15-2117-1_7

miniature products made of these high-tech advanced materials is rising gradually, and manufacturing of miniature products with complicated shape, required dimensional geometry and desired level of surface finish is a difficult task for the shop floor engineers. Therefore, to fulfil the demands of such, material scientists and manufacturing technocrats are always trying to develop new kind of micro-manufacturing and micro-fabrication techniques by utilizing which the macro- and micro-scale parts with desired tolerance and precision and ultraprecision surface features can be rendered [3]. Nowadays, laser micromachining and microforming techniques are playing a key role for manufacturing such precised components. This is possible due to some inherent features and capabilities of laser beam micromachining techniques. Some of these features are (i) no wastage of materials (ii) removal of material does not depend upon electrical conductivity of base material (iii) machine set-up and sub-components are highly flexible (iv) no tool wear and load bearing due to non-contact type machining (v) capability of generating sub-micron tolerances due to less size of laser beam diameter (vi) cost-effective processing due to faster machining, etc. [4, 5]. Laser-based micromachining processes like micro-cutting, micro-drilling, micro-chanelling, micro-scribing, micro-slotting, micro-milling, etc., have already been successfully implemented to micro-manufacture wide varieties of miniature components. However, due to overall shape and absence of jigs and fixtures, many of these processes cannot be employed for micro-features generation. Laser micro-turning is a recently developed micromachining technique which is applied to produce cylindrical-shaped products with required geometrical dimensions, tolerances and accurate geometry structures [6].

Basically, laser micro-turning process involves the elimination of slight portion of material from cylindrical-shaped material surface by irradiating the laser beam on top of the sample [7]. While rotating the cylindrical work sample about its axis, the workpiece has a feed movement along the direction of its axis, and very small amount of material is removed from top periphery surface. The length and depth of micro-turning depend on the amount of axial feed and number of layer scanning by high energy laser beam. Such type of micro-turned surface with specific surface geometry and features has important applications in electronics, electrical and mechanical engineering fields for the purpose of bearing rings, spikes and self-assemblies, power distribution components, etc. Moreover, to resharpen the ceramic grinding wheel from its blunted condition to grinding wheel condition, laser micro-turning process may be adopted to restore the cutting capability of micron-sized abrasives on the periphery of grinding wheel [8, 9].

2 Problems of Micro-turning of Ceramics

In micro-engineering and biomedical fields, there are a number of micro-components which have been benefited by advanced ceramics like silicon nitride (Si_3N_4), alumina (Al_2O_3), zirconia (ZrO_2), aluminium nitride (AlN), silicon carbide (SiC), etc., due to their diversified properties which include flow strength, wear resistance, fracture toughness, thermal and corrosion resistance, etc. [10, 11]. Due to these properties,

the lifespan of micro- and macro-products made of these engineering ceramics is high. However, manufacturing of miniaturized parts with greater accuracy, desired surface criteria and geometrical dimensions in conventional way is difficult and cost ineffective. Diamond turning is a possibility of conventional machining of high-tech ceramics to manufacture micro-parts of cylindrical shapes [12]. However, there are several drawbacks in this process like wear of high-cost tools, excessive cutting forces damages machine tool parts, cracks formation in machined surface, etc. [13, 14]. Another possibility of micro-turning of cylindrical material is wire electrical discharge turning (WEDT) for micro-manufacturing of micro-electrodes and micro-pins. However, this process needs the workpiece to be electrically conductive. Therefore, it is a difficult task to develop a reliable and efficient process which can be applied to manufacture micro-cylindrical parts made of high-tech ceramics.

It is already known that amongst various engineering ceramic materials, aluminium oxide (Al_2O_3) is widely accepted and employed advanced ceramics that have already been successfully used in wide range of applications from engineering micro-systems developments to biomedical fields. It is mainly due to numerous exceptional thermal and mechanical properties like wear and corrosion resistance, stiffness, high temperature withstand ability, excessive hardness, etc. [15]. Several research have already been reported in the literature for micromachining of aluminium oxide ceramics employing the processes like micro-cutting, micro-drilling, micro-grooving, etc. [16–18]. However, very few research have been reported in laser-based turning of aluminium oxide ceramics for fabricating desired geometrical parts with required level of surface features. It is already known that laser beam micromachining processes have several process factors like laser power, pulse frequency, pulse duration, laser scan speed, number of scans, duty factor, assist air pressure, etc., and these process parameters are dynamic or nonlinear in behaviour [19]. Thus, to micro-manufacture complex profile with desired level of accuracy and surface finish, at this stage, it is the duty of manufacturing technocrats to develop a reliable process, preferably in the category of non-traditional micromachining, which can deliver such micro-parts with desired geometries. As laser micro-turning process is recently developed non-traditional type micromachining process to process cylindrical micro-parts made of advanced engineering materials, several research activities may be carried out using high intense laser beam to micro-turn aluminium oxide ceramics.

3 Laser Micro-turning Process

Chryssolouris et al. proposed laser turning process utilizing two intersecting laser beams for removing ring-shaped material (in bulk form) from rotating cylindrical workpiece [20]. The schematic view of this process is shown in Fig. 1. However, to remove thin layer of material from cylindrical form workpiece outer surface (of desired length), this process cannot be applied. For this, it is preferable to employ single laser beam which can be focused onto the rotating workpiece surface for removing planer layer of material along desired length of sample. The scheme of laser

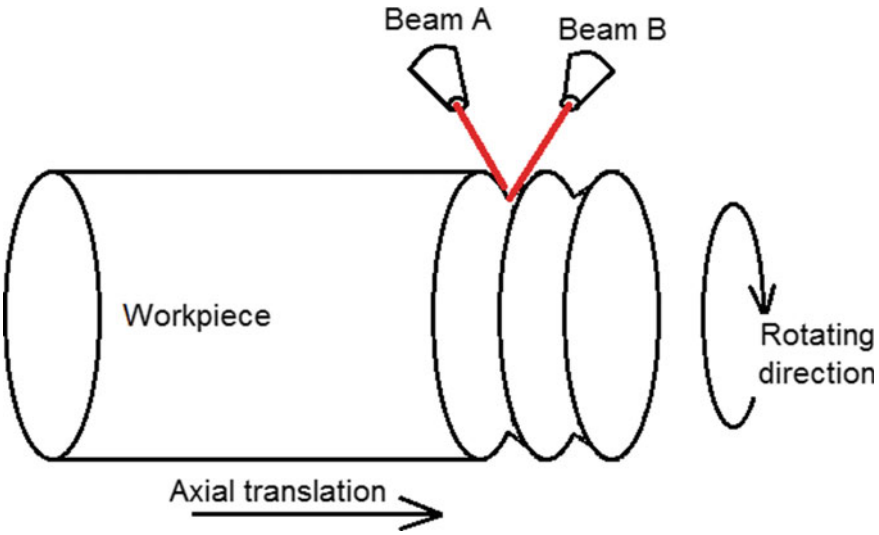

Fig. 1 View of utilizing two intersecting lasers for bulk material removal

micro-turning technology is shown in Fig. 2. At the time of rotating the workpiece, depending on the laser pulse repetition rate, there are very small overlap area between two consecutive laser spots.

Basically, the concept of laser micro-turning process revealed from two consecutive micro-grooves generated with overlap between them. This amount of overlap

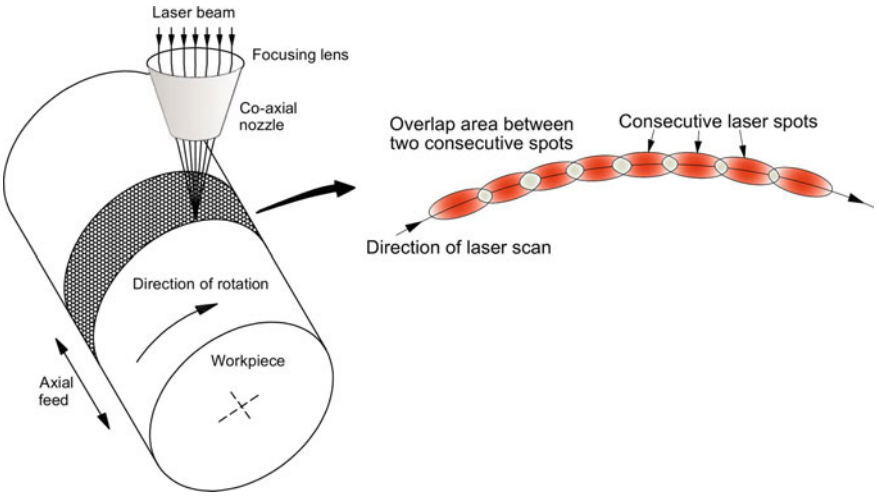

Fig. 2 View of mechanism of micro-turning using single laser beam with overlap area between two consecutive spots

controls the quality of laser micro-turned surface. For achieving desired micro-turned depth and surface features during the process, continuous to and fro scanning is carried out by controlling the axial feed rate of workpiece. Circumferential overlap is the amount of overlap between groove laser-scanned lines, whereas spot overlap is the overlap between two consecutive spots. For achieving desired quality surface in this process, it is recommended to keep these values more than 50% during laser micro-turning operation.

In Fig. 3, the schematic view of laser spot overlapping and circumferential overlapping is represented by utilizing consecutive laser spots and consecutive laser scan lines. In Fig. 4, the schematic view of overlap among two successive spots on the workpiece surface is shown. In this figure, the distance x_s represents the overlap distance (shown by hatched area) created among two consecutive spots (marked as 1 and 2). Due to Gaussian energy delivery on the job surface, the generated crater profiles have also some amount of overlap. As per the equation of laser spot overlap percentage shown in Eq. 1, the quantity of overlap region can be enlarged by two methods, (i) increasing pulse frequency or pulse repetition rate and (ii) increasing time taken by laser beam to scan the workpiece surface, i.e. reducing workpiece rotating speed [7]. If N is taken as workpiece rotating speed (unit is rpm), D_S is taken as sample diameter (unit is mm), F_P is taken as pulse frequency (in Hz), D is taken as focal spot diameter (unit is mm), and then, we can write

$$\text{Spot overlap } (SO_p) = \left(1 - \frac{\pi \times D_S \times N}{60 \times D \times F_P}\right) \times 100\% \tag{1}$$

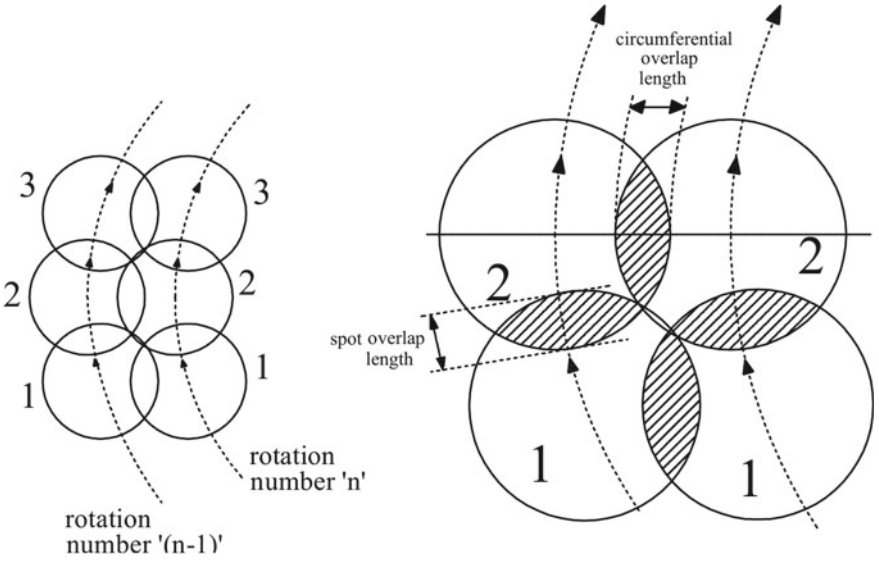

Fig. 3 Representation of circumferential and spot overlap in laser micro-turning

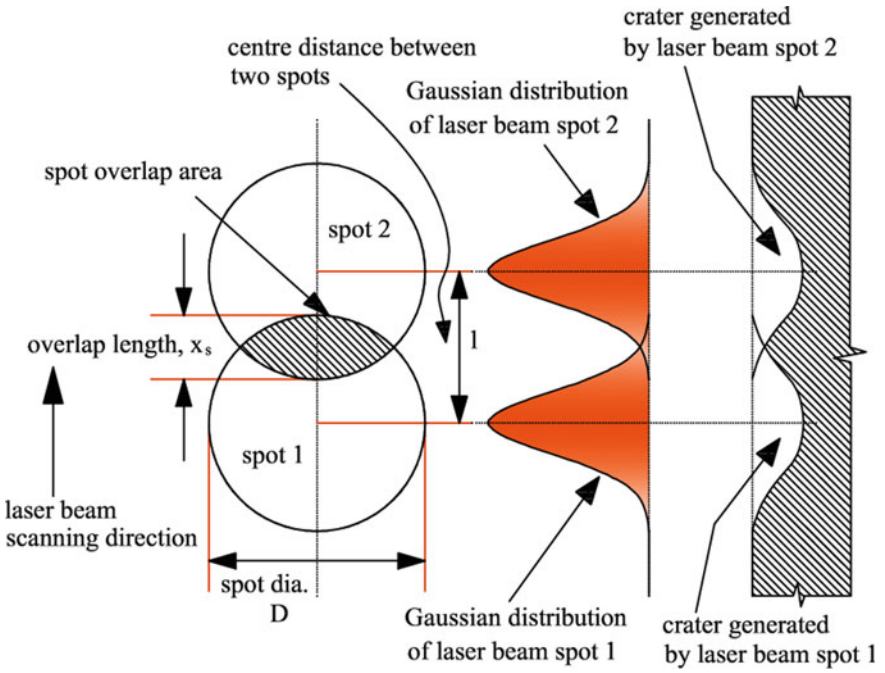

Fig. 4 Schematic of Gaussian energy distribution in spot overlap and possible crater depth generation [21]

Figure 5 represents the schematic illustration of circumferential overlap which is created among two laser spots generated alongside on the work surface for succeeding revolution of workpiece. Here, x_c is the circumferential overlap length. The Gaussian energy distributions of the laser spots are shown in the same figure also. It is seen from the overlap area and crater profiles that more amount of this overlap reveals quality machined surface. As depicted in Eq. (2), the value of circumferential overlap is altered by (i) changing the axial feed rate and (ii) changing the rotation speed of sample [7].

$$\text{Circumferential overlap } (CO_p) = \left(1 - \frac{60 \times f}{D \times N}\right) \times 100\% \tag{2}$$

In the above-mentioned equation, f represents the axial feed rate of work sample. Thus, it is summarized that by controlling the above-mentioned factors and precautions, desired level of surface finish and accuracy of laser micro-turning process can be carried out on high-tech engineering ceramics. Thus, in point of view of research and further developments for micromachining of engineering ceramic like aluminium oxide (Al_2O_3) and fulfilment the demand of miniaturized parts in several important fields, it is now urgently required to carry out extensive research work in

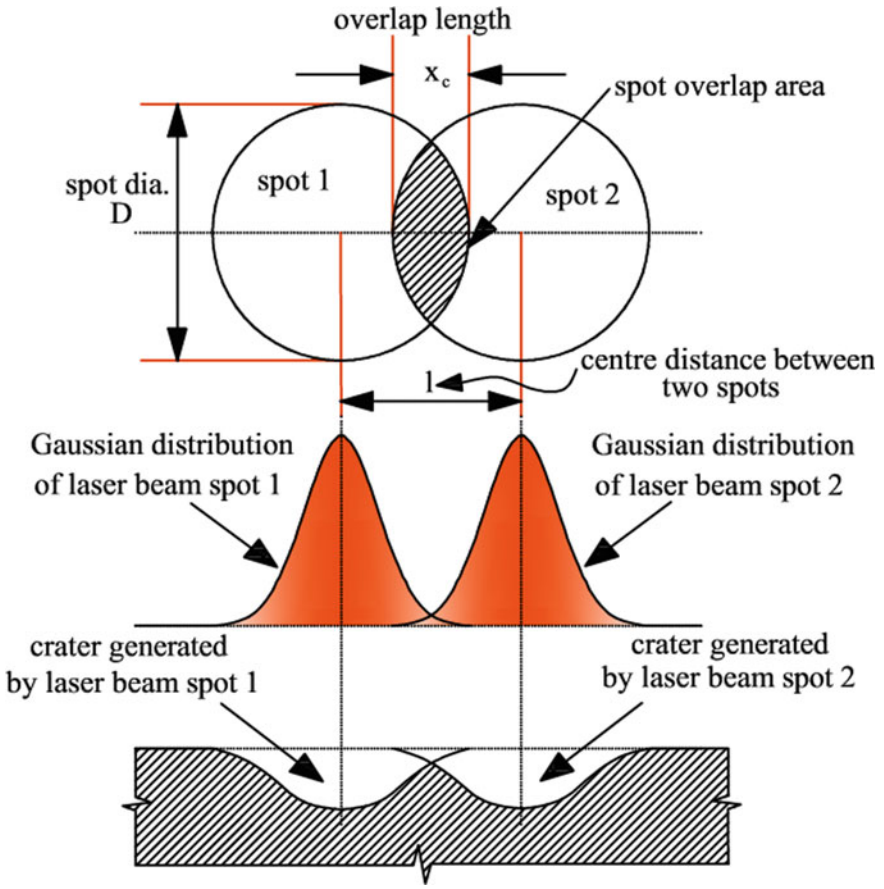

Fig. 5 Schematic of Gaussian energy distribution in circumferential overlap and possible crater depth generation [21]

this advanced micro-turning to manufacture micro-components with desired surface features and geometrical dimensions.

4 Materials, Machine, Method and Measurement Schemes

The experimentation is divided into two parts, (i) experimentation to investigate the parametric influence and overlap factors on the process performance of laser micro-turning of Al_2O_3 ceramic and (ii) experimentation to achieve desired surface quality and accurate shaped parts. The experiments were carried out in 99% pure aluminium oxide ceramics (99% pure) of cylindrical-shaped material. The overall dimensions of the materials were length of 40 mm and diameter of 10 mm. A high power (average

power is 50 W) pulsed Nd:YAG laser (wavelength 1064 nm) set-up was utilized to conduct experiments. The photographic view with all the sub-components of laser micromachining system is viewed in Fig. 6. The laser operates in TEM_{00} Gaussian mode. The laser set-up uses a focusing lens of 50 mm. To carry out laser micro-turning process, a workpiece rotating system was developed indigenously which is schematically shown in Fig. 7. The collet can accommodate cylindrical sample in the diameter ranging from 2 to 16 mm. However, rotational eccentricity of workpiece could not be completely minimized, and the value of it was found as 3 μm, which is acceptable. The servo motor with workpiece holding fixture was positioned on X–Y table of the machine. The rotating system has also the provision to rotate the work sample clockwise or counterclockwise directions. The choice of value of workpiece rotational speed can be provided by manual control knob or directly from servo motor controller. By focusing the high intense laser beam on workpiece surface, multi-pass laser micro-turning process can be carried out by providing laser scan of desired length of rotating workpiece with a feed movement along its axis. Thus, desired length of turn and depth can be achieved in this novel process. The target depth of micro-turning was 100 μm. After each laser scanning of desired length, the focusing lens was lowered at a value of 0.001 mm. Therefore, to achieve the desired depth, a total of 100 number of laser scanning was carried out. These values of depth and desired length of micro-turning were controlled by Multisawing software used by the set-up. Various experimental schemes were applied to study the process parameters on machined surface characteristics, study and analysis of surface features at laser defocusing conditions, etc.

A laser beam power measuring instrument was utilized for measuring laser beam average power at various parametric combinations. The depth deviation and surface roughness (Ra and Rt) were measured after experimentation. The target depth was

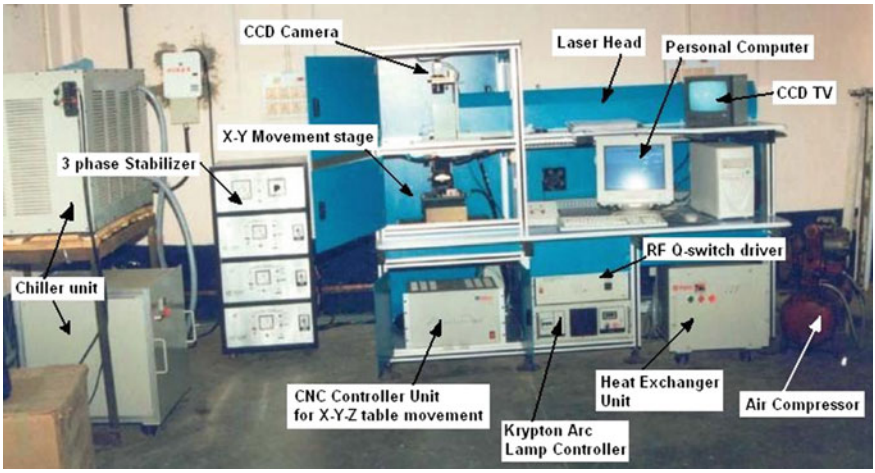

Fig. 6 Pulsed Nd:YAG laser micromachining set-up and sub-systems [7]

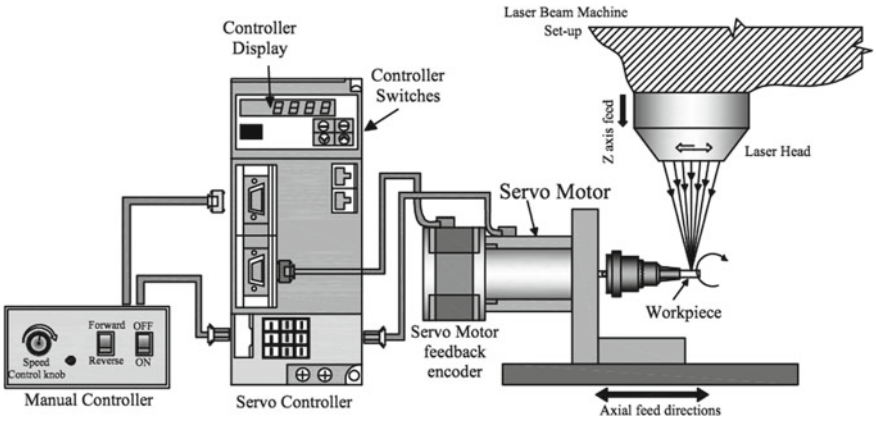

Fig. 7 Indigenously built up sample rotating unit [22]

100 μm. The depth deviation is the difference of target depth and actual depth. By differentiating the measurement of depth using 10× magnification lens at machined and unmachined surfaces, the values of micro-turning depth were obtained. The values of Ra and Rt were measured utilizing a roughness profilometer (supplied by Zeiss, Germany). For the purpose of elimination of form errors and taking the microirregularities into account, the length of measurement of surface roughness was selected as 2.5 mm. An average value of surface roughness was considered for further analysis after obtaining surface roughness values at different workpiece surface locations.

5 Results and Discussion

The experimental study of the present research is divided into two, (i) parametric study and analysis during laser micro-turning process and the effect of overlap criteria on machined surface characteristics and (ii) carry out experimentation according to RSM approach and find the optimal parametric combination to achieve simultaneously the minimum values of considered responses and then further improvement of surface finish by taking laser defocusing experimental scheme into consideration.

5.1 Investigation of Overlap Factors on Performance Criteria

For the purpose to study the effect of two overlap criteria on machining performance, in this section, detailed study and analysis have been carried out during laser micro-turning of alumina ceramic. It is already explained in Eq. (1) that spot overlap criterion

Table 1 Details of process parameters for experimentation

Parameters	Unit	Values
Pulse frequency	Hz	3000, 4000, 5000, 6000, 7000
Average power	W	7, 8
Y feed rate	mm/s	0.1, 0.2, 0.3, 0.4, 0.5
Workpiece rotating speed	rpm	200, 300, 400, 500, 600
Pulse width	% of duty cycle	3%
Air pressure	kgf/cm^2	1.3
Z feed rate	mm/s	0.01

mainly depends on rotational speed of workpiece, laser spot diameter at focal plane and laser pulse frequency. Moreover, as per Eq. (2), experimentation also carried out to study in-depth the effect of process parameters on circumferential overlap. Table 1 depicts the list of process factors with their values.

During selection of ranges and values of process parameters, lot of pilot experimentation was conducted, and the ranges of above-mentioned process parameters were selected so carefully that the effect of these overlap criteria can be studied in-depth. As shown in Fig. 8, the variation of spot overlap depends on laser pulse frequency and workpiece rotational speed. Moreover, the circumferential overlap depends on rotational speed and axial feed rate which is depicted in Fig. 9. From these two plots, it is confirmed that these dependent process parameters have huge influences on machined surface quality as well as features. Some data points have

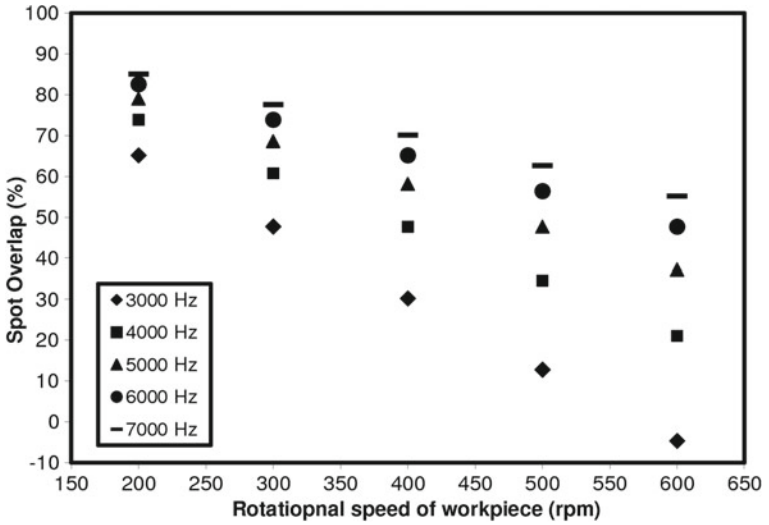

Fig. 8 Effect of process parameters on spot overlap values

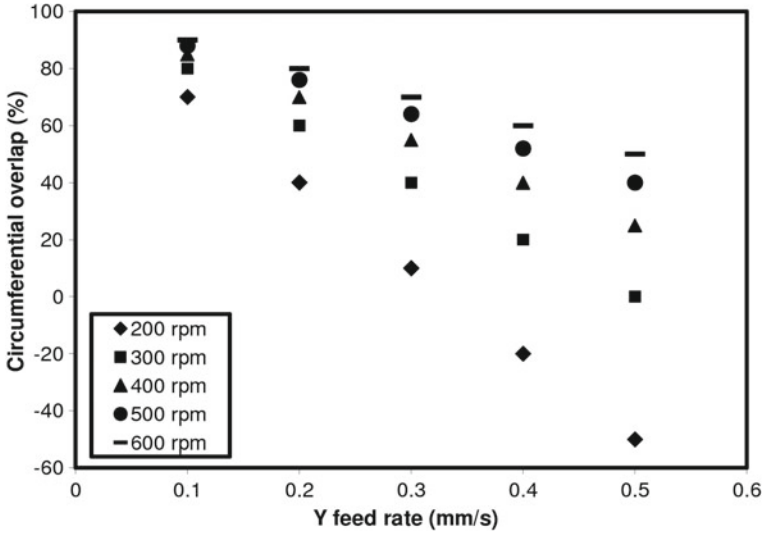

Fig. 9 Circumferential overlap values at different *Y* feed rate and rotational speed of workpiece

also been taken with negative overlap values to study and analyse the effect of no overlap.

The pictorial graph shown in Figs. 10 and 11 shows the surface roughness (Ra) values for different spot overlap values due to changing in workpiece rotational speed

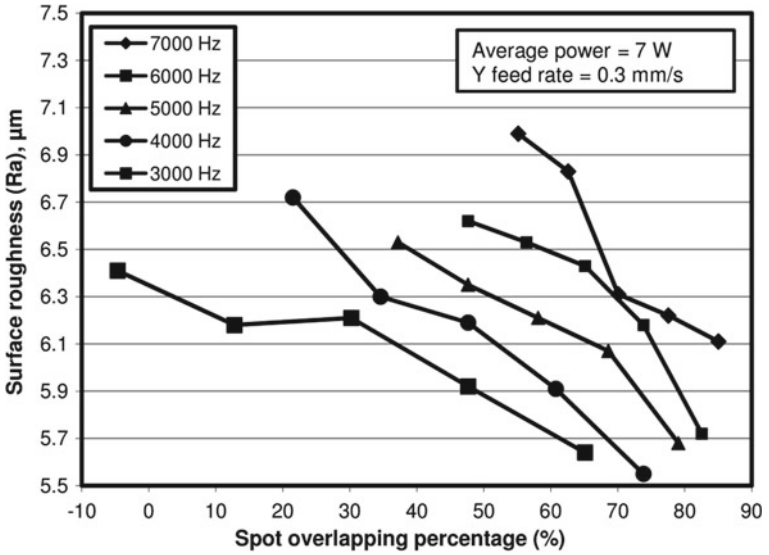

Fig. 10 Graphical plot of surface roughness (Ra) at various spot overlap and pulse frequency [23]

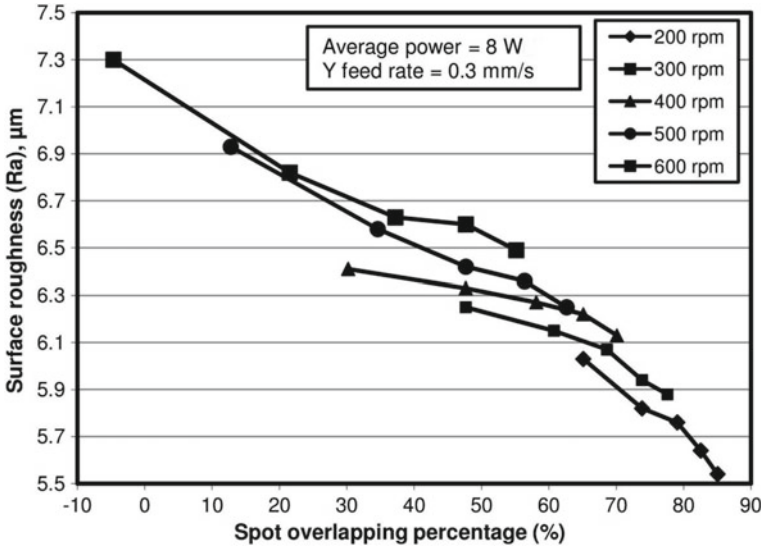

Fig. 11 Graphical plot of surface roughness (Ra) at various spot overlap and rotating speed of workpiece [23]

and laser pulse frequency, respectively. The plot shown in Fig. 10 clearly shows that increase in value of spot overlap causes reduce value of surface roughness at all pulse frequency settings considered. This is due to the fact that higher values of spot overlap percentage result in uniform machined surface with fewer micro-peak irregularities. The values of spot overlap directly increase with pulse frequency according to Eq. (1). However, the interval connecting two successive pulses is small at high pulse frequency setting. Thus, materials from beam radiated zone melt and evaporate immediately, and consequently, the total laser energy received by the top surface of material is high. Thus, higher value of crater depth is obtained, and it increases the values of surface roughness. Figure 11 shows decrease of surface roughness with spot overlap at different workpiece rotational speed. Due to removal of more material from top surface because of more spot overlap, quality surface is obtained. Furthermore, it is also obvious from the same plot that the roughness value obtained is high with increased values of rotational speed.

In Figs. 12 and 13, the plots show the surface roughness with circumferential overlap. Equation (2) shows that with rotational speed, the value of circumferential overlap percentage is increasing. Thus, surface roughness decreases. It is also seen that for higher value of *Y* feed rate, higher value of surface roughness (Ra) is obtained during machining. This is because there are many null region (unmachined) created on the work sample surface due to uneven laser scanning process, and ultimately, irregular machined surface is achieved.

Figure 13 shows graphical representation of surface roughness (Ra) with circumferential overlap while varying pulse frequency and workpiece rotating speed.

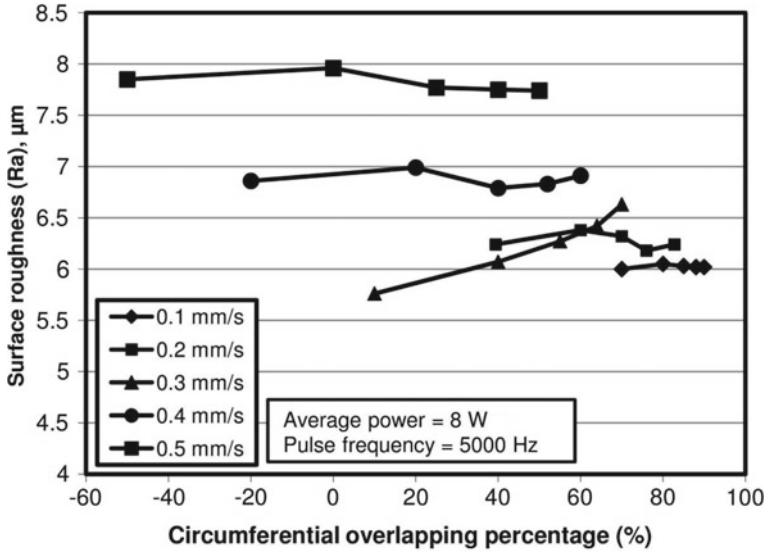

Fig. 12 Graphical plot of surface roughness (Ra) at various circumferential overlap and *Y* feed rate [23]

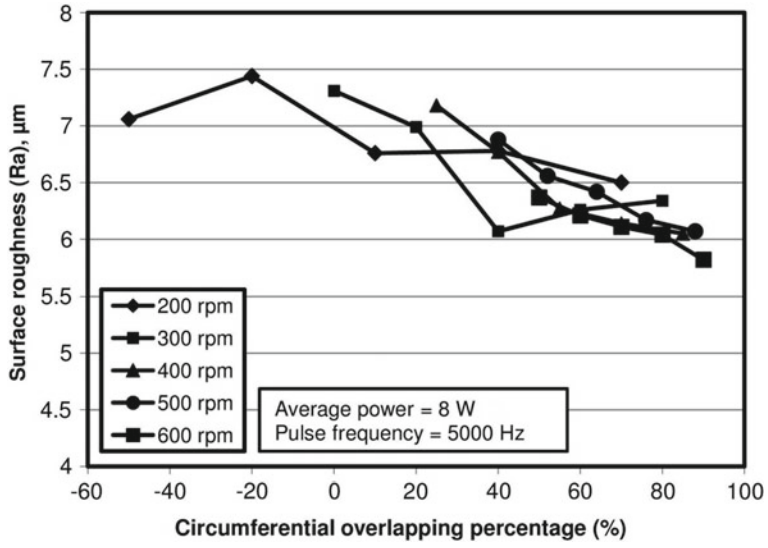

Fig. 13 Graphical plot of surface roughness (Ra) at various circumferential overlap and rotating speed of workpiece [23]

With increasing values of circumferential overlap, the machined surface roughness (Ra) values decrease, and this is mainly due to more circumferential overlap on the machined surface and uniform material removal phenomena. The same plot also shows that due to increase in rotating speed of workpiece, the circumferential overlap values increase, therefore reducing irregularities on micro-turning surface.

5.2 *Investigation of Laser Defocusing on Machining Performance*

Here, experimentation on laser micro-turning process has been performed utilizing RSM-based DoE, and then, multi-response optimization results were obtained to achieve optimal values of responses. Also, to obtain quality surface without hampering the dimension of machined part, experimentation utilizing laser defocusing condition was carried out on the already machine surface obtained from RSM optimal experimentation. In this set of experiments, another two additional process parameters were included, i.e. assist air pressure and number of laser scanning. The values of five process parameters and each having five levels are shown in Table 2. The total number of experiments conducted was 32. After conducting these experiments, response criteria were measured. To measure surface roughness values, the same surface profilometer was utilized (Model: SURFCOM 120A-TSK, Make: Zeiss, Germany). The depth deviation was calculated based on Eq. (3). Statistical software, MINITAB of version 13 was employed to analyse the results and to validate the empirical models developed. The developed mathematical models based on experimental output were developed for correlating the responses, and considered process variables are shown in Eqs. (4) and (5).

$$\text{Micro-turning depth deviation} = \text{Machined depth} - \text{Targeted depth} \tag{3}$$

$$Y_{\text{Ra}} = -3.3853 + 2.4496 \times X_1 + 0.0001 \times X_2 - 0.0008 \times X_3 + 0.5522 \times X_4 + 1.9032 \times X_5 - 0.0825 \times X_1^2 + 0.0000 \times X_2^2 + 0.0000 \times X_3^2$$

Table 2 List of process parameters and their values [22]

Parameters (unit) with symbol	Levels
Average power (W) X_1	6, 7, 8, 9, 10
Pulse frequency (Hz) X_2	3000, 4000, 5000, 6000, 7000
Rotational speed (rpm) X_3	200, 300, 400, 500, 600
Air pressure (kgf/cm^2) X_4	0.3, 0.8, 1.3, 1.8, 2.3
Y feed rate (mm/s) X_5	0.1, 0.2, 0.3, 0.4, 0.5
Coded values of process parameters	$-2, -1, 0, +1, +2$

$$-0.3400 \times X_4^2 + 23.0837 \times X_5^2 - 0.0000 \times X_1X_2 - 0.0009 \times X_1X_3 + 0.0975 \times X_1X_4 - 2.6381 \times X_1X_5 - 0.0000 \times X_2X_3 + 0.0000 \times X_2X_4 - 0.0001 \times X_2X_5 - 0.0007 \times X_3X_4 - 0.0016 \times X_3X_5 - 0.4104 \times X_4X_5 \quad (4)$$

$$\begin{aligned} Y_{\text{depth dev}} = {} & 0.053142 - 0.038222 \times X_1 + 0.000048 \times X_2 - 0.000191 \times X_3 \\ & + 0.094368 \times X_4 - 0.852803 \times X_5 + 0.003616 \times X_1^2 \\ & - 0.000000 \times X_2^2 + 0.000000 \times X_3^2 - 0.004544 \times X_4^2 \\ & + 0.926106 \times X_5^2 + 0.000004 \times X_1X_2 - 0.000071 \times X_1X_3 \\ & + 0.002107 \times X_1X_4 - 0.012561 \times X_1X_5 + 0.000000 \times X_2X_3 \\ & - 0.000016 \times X_2X_4 - 0.000015 \times X_2X_5 - 0.000070 \times X_3X_4 \\ & + 0.000423 \times X_3X_5 + 0.031346 \times X_4X_5 \end{aligned} \quad (5)$$

Equations 4 and 5 are valid in the process parametric ranges considered. To validate these developed models, analysis of variance was performed as shown in Table 3. From Table 6, it is seen that the calculated F-value for surface roughness (Ra) is 1.18. However, at 95% confidence level, this value is far less when compared to the standard F-value (4.06). Thus, mathematical model of surface roughness is valid. The table also shows that the calculated F-value for depth deviation is 3.11. However, this value is far lower compared to 4.06 value. Thus, empirical model of depth deviation is also valid. From Figs. 14 and 15, it is obvious that the empirical model can calculate the considered responses accurately and acceptably.

To obtain the surface profile and accurate geometrical shapes of micro-turning parts, multi-response optimization was achieved based on the RSM experiments. The illustrative view of multi-response optimization results is shown in Fig. 16. The parametric setting of multi-objective optimization is obtained as shown in Fig. 16.

Table 3 Analysis of variance test results

Source	Degree of freedom (DF)	For surface roughness (Ra)		For micro-turning depth deviation	
		F-value	p-value	F-value	p-value
Regression	20	11.28	0.000	11.44	0.000
Linear	5	1.31	0.328	2.94	0.063
Square	5	6.33	0.005	6.62	0.004
Interaction	10	1.64	0.215	2.15	0.112
Residual error	11				
Lack-of-fit	6	1.18	0.436	3.11	0.117
Pure error	5				
Total	31				

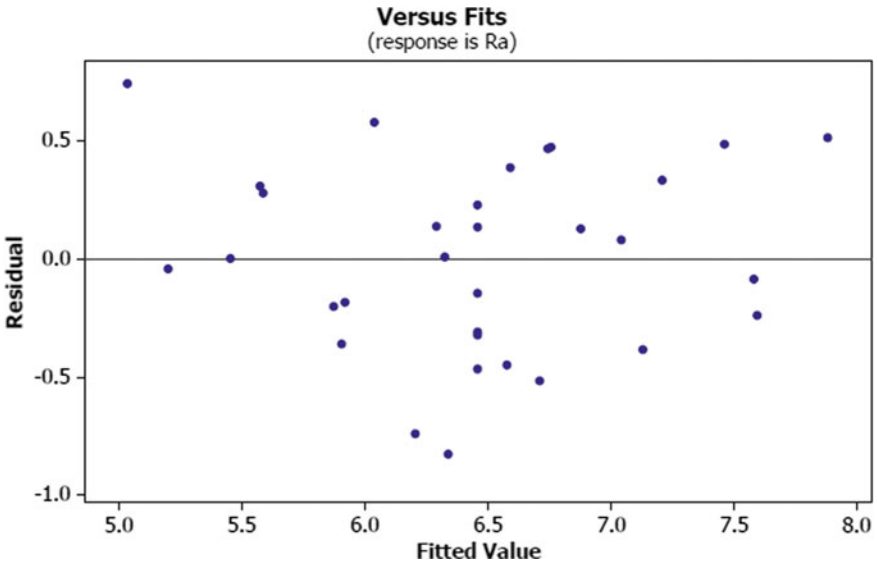

Fig. 14 Residuals versus fits plot for Ra [22]

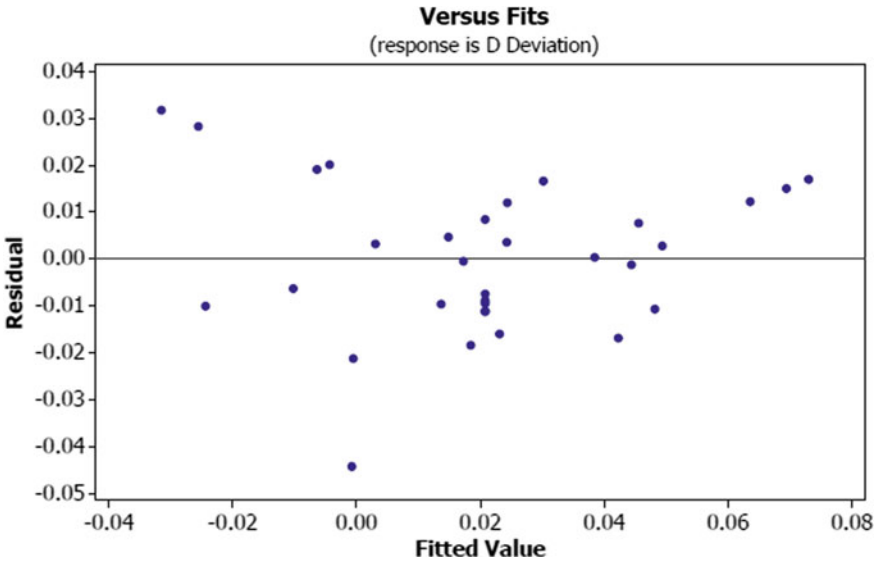

Fig. 15 Residuals versus fits plot for depth deviation [22]

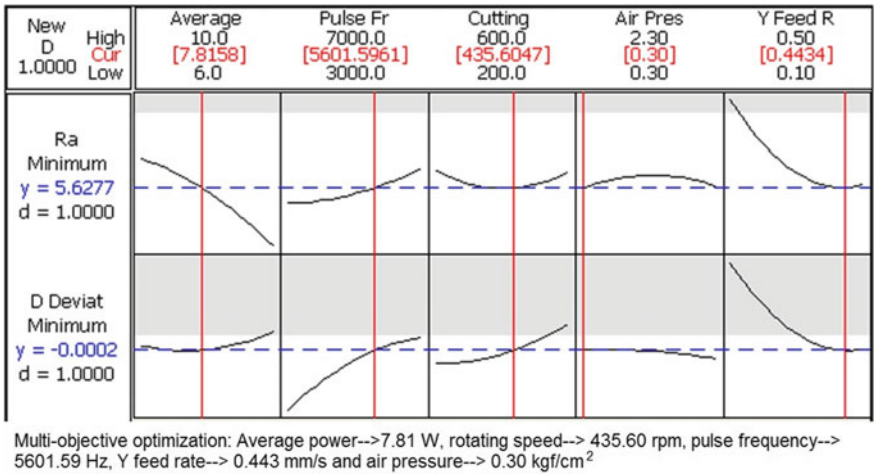

Fig. 16 Multi-objective optimization results [22]

Confirmation experiments show that the average prediction errors are within acceptable limit. For Ra, prediction error was 4.76%, and for depth deviation, prediction error was 4.78%.

The RSM-based optimization provides optimal parametric combination for minimum values of responses. However, for long life of products, it is always recommended to keep the surface quality at good condition. Mainly, Ra value is obtained high due to irregular micro-peaks on the machined surface. These types of peaks on the laser micro-turning surface may have generated due to variation in overlap factors or irregular solidification on machined surface. Thus, to achieve desired surface finish without hampering the geometrical dimensions of ceramic micro-parts, it urgently needs to apply novel technology to remove these micro-peaks for the sake of micro-manufacturing high-end products. Thus, laser micro-turning process is carried out at laser defocusing condition to remove such micro-peaks. At defocusing condition, due to enlarged spot size of laser, energy density of the beam lowered down, and correspondingly, the defocusing laser beam able to remove materials from top surface of work sample. At this stage, defocusing positions and number of laser scan passes were included as varying factor.

In Fig. 17, the schematic view shows the micro-peaks removal process from already laser micro-turning surface by laser scanning. To completely remove the micro-peaks and make the surface high-end quality, the laser scanning process at defocusing condition is an innovative strategy for the purpose. In Fig. 18, the schematic representation of various defocusing positions is shown. Laser defocusing condition is divided into two types (i) upward and (ii) downward. The defocusing condition called as upward is the position of laser focal point above the top surface of work sample. On the other hand, downward defocusing condition is the laser scanning when the laser focal point is underneath the top surface of work sample. In this

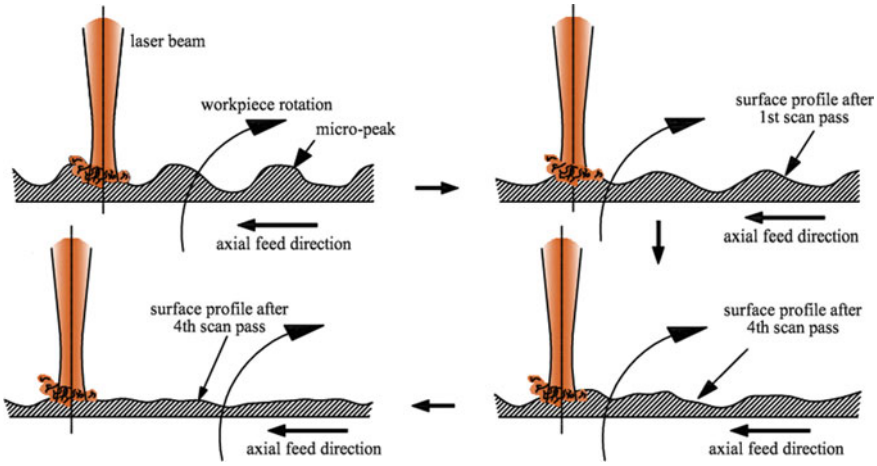

Fig. 17 Schematic representation of methodology micro-peaks removal by laser scanning [21]

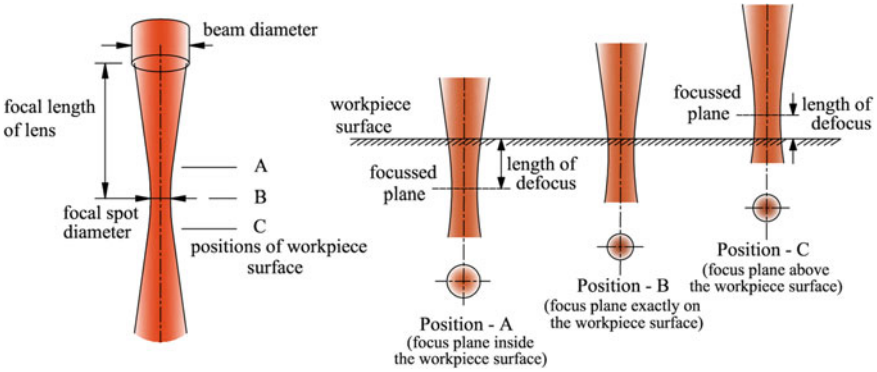

Fig. 18 View of upward and downward defocusing conditions of laser beam [24]

present experimentation, both Ra and Rt were measured as responses. The aim of the experiments and analysis is that to reduce surface roughness value of the already machined surface which is obtained by experiments conducted using RSM-based optimal parametric combination. For this, a total of eight numbers of samples were manufactured by parametric combination of RSM-based multi-objective optimization. The initial values of surface roughness of these eight samples are enlisted in Table 4. Table 5 shows the list of process parameters for the present experimentation of laser defocusing. Here, laser scanning passes is considered as ten as so that complete removal of micro-peaks is ensured. For the purpose of roughness measurements, the same profilometer set-up was utilized, and the obtained values of Ra and Rt were graphically plotted and analysed.

Table 4 Values of surface roughness of work samples obtained from RSM-based multi-objective optimal parametric combination

Optimization setting	Ra and Rt values (in μm)	
	Ra	Rt
Pulse frequency = 5600 Hz Average power = 7.81 W Air pressure = 0.30 kgf/cm^2 Rotating speed = 436 rpm *Y* feed rate = 0.443 mm/s	5.94	45.38
	5.87	46.21
	5.84	46.02
	5.89	45.68
	5.98	45.69
	6.00	45.88
	5.88	46.39
	5.81	46.01

Table 5 Factors and their corresponding values for further experiments [24]

Varying factors	Values
Defocus position (in mm)	±0.2, ±0.4, ±0.6, ±0.8
Laser beam passes	1–10 at increment of 1

Figure 19 shows the graphical plot of Ra with passes at different positions of laser defocusing (upward). This plot shows surface roughness decrease. With defocusing condition of laser beam, as the passes increases, the elevation of micro-peaks on the surface decreases caused by melting and evaporation. Therefore, the overall quality of surface finish increases. From the same figure, it is also revealed that with constant value of laser scan passes, with increasing value of upward defocusing value, the value

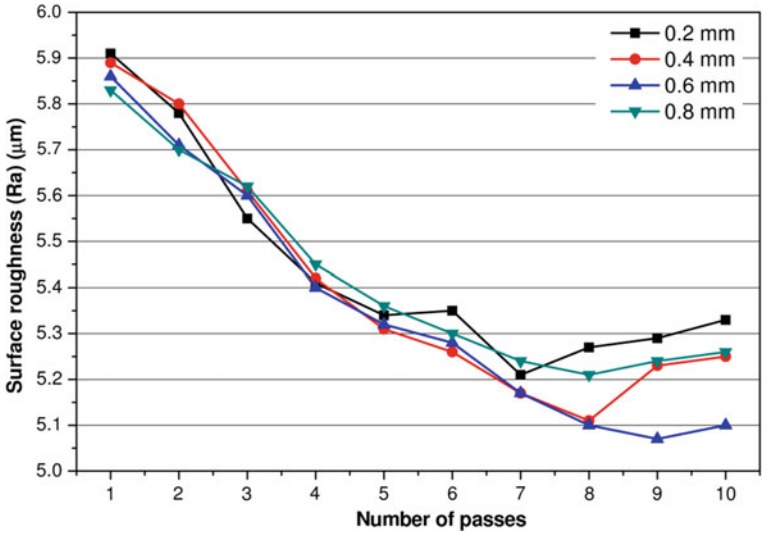

Fig. 19 Plot of Ra with laser scan passes (upward defocus) [24]

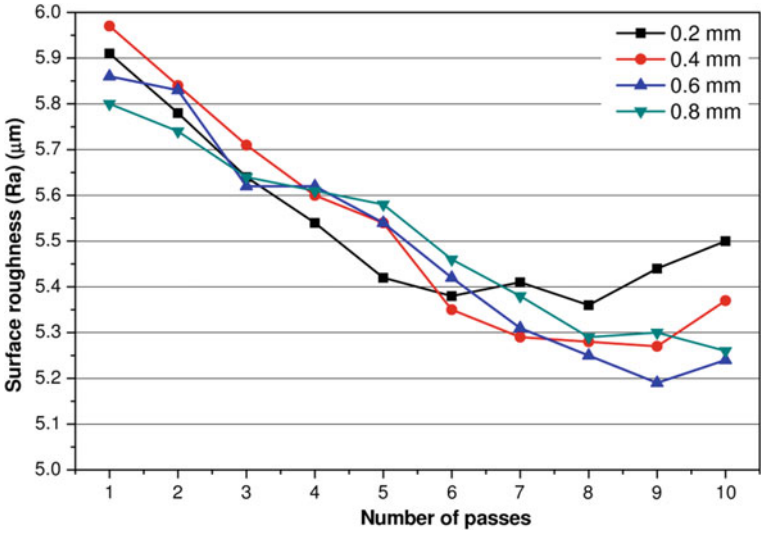

Fig. 20 Plot of Ra with laser scan passes (downward defocus) [24]

of surface roughness (Ra) decreases due to irradiation of adequate laser beam energy falling onto the workpiece surface. This adequate energy is able to melt and remove the peaks from the surface. However, at too much defocusing Ra value increases. At higher defocusing, the irradiated laser intensity is so much low that it is incapable to remove the surface irregularities.

In Fig. 20, it is obvious from the plot that surface roughness value decreases at all defocusing positions with increasing number of laser passes. It is because of irradiation of desired laser beam energy which efficiently removes surface irregularities. After certain number of laser passes, the value of surface roughness increases to some extent. The material removal phenomena are not uniform after some particular value of laser passes, and micro-peaks again melt and resolidify onto the workpiece surface. At 0.8 mm defocus, the beam energy density is lower, and therefore, the laser beam ultimately unable to eliminate the peaks.

In Fig. 21, the plot of Rt with scan passes is depicted. It is obvious that with number of laser scan passes, Rt values decrease. This is because micro-peaks melt and removed by several number of laser scan. The graphical plot also revealed that with a definite value of laser scan, Rt value is high at less defocusing. At different defocusing conditions, due to variation in laser energy density, therefore, variation in roughness achieved is accounted. Moreover, 0.8 mm defocusing position, due to much lower value of energy density, value of surface roughness is high in contrast to other defocusing settings.

In Fig. 22, the graphical plot shows that up to definite value of laser scan passes, the values of surface roughness (Rt) reduce at all values of defocusing positions. It is so because of diminish of overall heights of micro-peaks on the machined surface. However, after seventh laser scan number, the variation of surface roughness is not

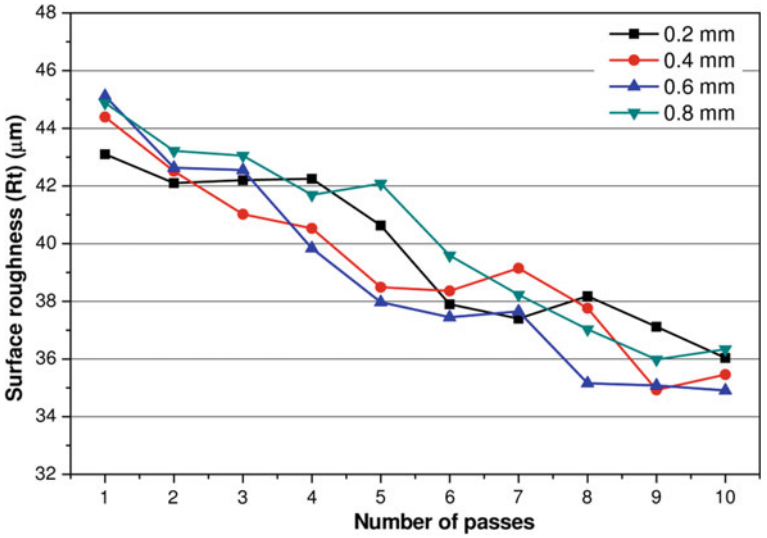

Fig. 21 Plot of Rt with laser scan passes (upward defocus) [24]

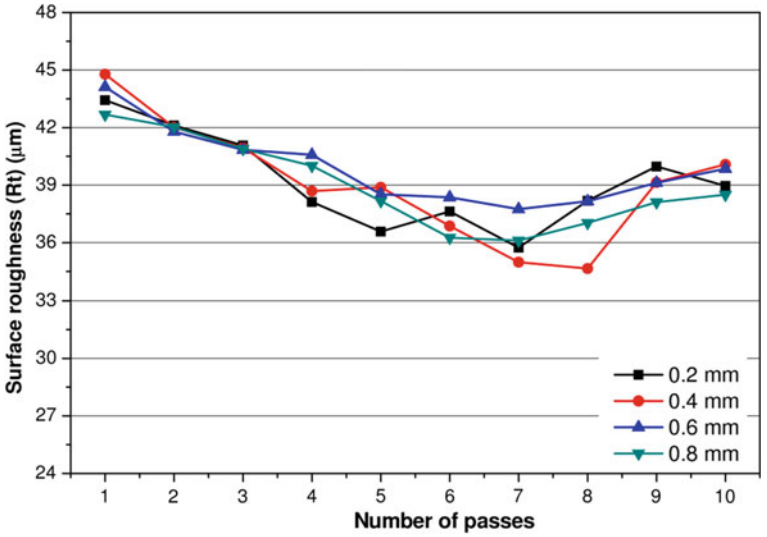

Fig. 22 Plot of Ra with laser scan passes (downward defocus) [24]

significant, and it may be due to material again resolidifies after melting due to irradiation of low energy density of laser beam. The line plot of different values of defocusing positions is very random.

It is concluded by considering above-mentioned experimentation and discussion that the novel micromachining strategy of laser defocusing has great influence on

Table 6 Parametric combinations and corresponding minimum values of surface roughness obtained in laser defocusing experiments

Roughness criteria	Optimal parametric combination of RSM experiments	Newly added parameters		Surface roughness (in μm)	
		Number of laser scan passes	Defocus value with position	Ra	Rt
Ra	7.81 W/5600 Hz/436 rpm/0.30 kgf/cm^2/0.443 mm/s	9	0.6 mm and upward	5.07	35.08
Rt		8	0.4 mm and downward	5.28	34.65

achieving desired surface finish in this process. The parametric combinations for obtaining minimum values of surface roughness were identified, and these parametric combinations are enlisted in Table 6.

6 Assessments of Machined Images Taken in Precision Microscope

For in-depth study and analysis as well as qualitative assessments of the process, scanning electron micrograph (SEM) was observed for the machined surface. Figure 23a–f depicts the surface morphology of the surfaces at two magnifications (27× and 200×) for the parametric settings in RSM experimentation. The parametric settings for these images are shown in figure itself. By comparing qualitatively these micrographs and values of surface roughness, it is concluded that higher value of *Y* feed rate and lower value of air pressure result in good surface finish during laser micro-turning. Furthermore, micrograph shown in Fig. 23b has more number of micro-peaks and valleys compared to micrographs shown in Fig. 23d. However, at RSM-based optimal parametric setting, the machined surface topography (Fig. 23e, f) obtained is having less number of such micro-peaks and valleys.

In Fig. 24a–d, the topography of machined surfaces obtained from SEM image analysis machined at different parametric combinations is shown. Comparing Ra values obtained in Fig. 24a, b, it is obvious that reduced from 6.72 to 6.18 μm when rising pulse frequency value as of 4000–6000 Hz, dropping rotational speed of workpiece as of 600–300 rpm. The spot overlap percentage was increased to 73.81 from 21.43%. Again, comparing Fig. 24c, d, it is obvious that Ra is dropped from 7.77 to 6.02 μm when rotational speed of workpiece is increased from 400 to 600 rpm and reducing the *Y* feed rate from 0.5 to 0.1 mm/s. Also, the circumferential overlap is increased from 25 to 90%.

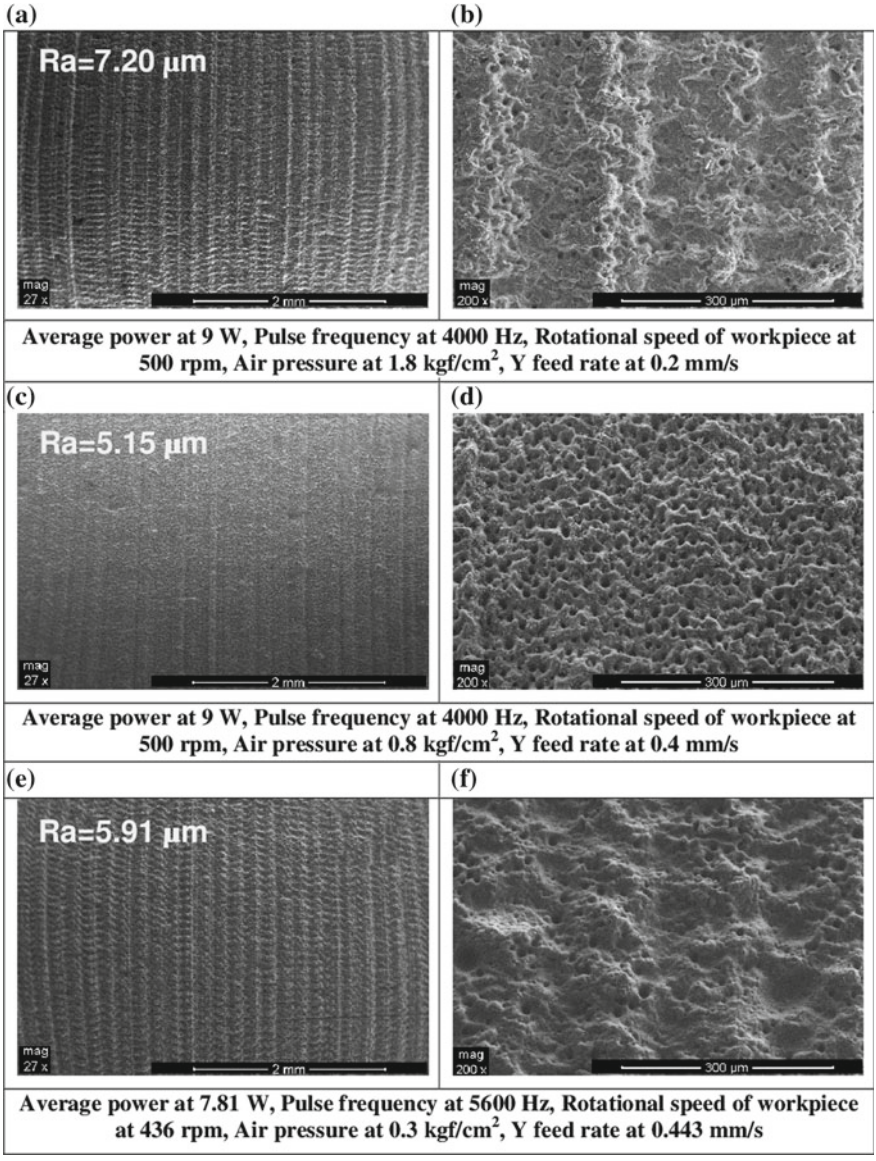

Fig. 23 Micrographs of surfaces machined at different parametric combinations [22]

Figure 25a–f shows SEM images of the machined surface at various parametric settings as shown. It is concluded that quality surface has been obtained parameters combination of defocusing of 0.6 mm (upward) and at tenth number of passes in respect of other surfaces shown in Fig. 25d–f. From high magnified SEM images shown in Fig. 25b, d, e, it is observed that the number of micro-peaks and valleys is

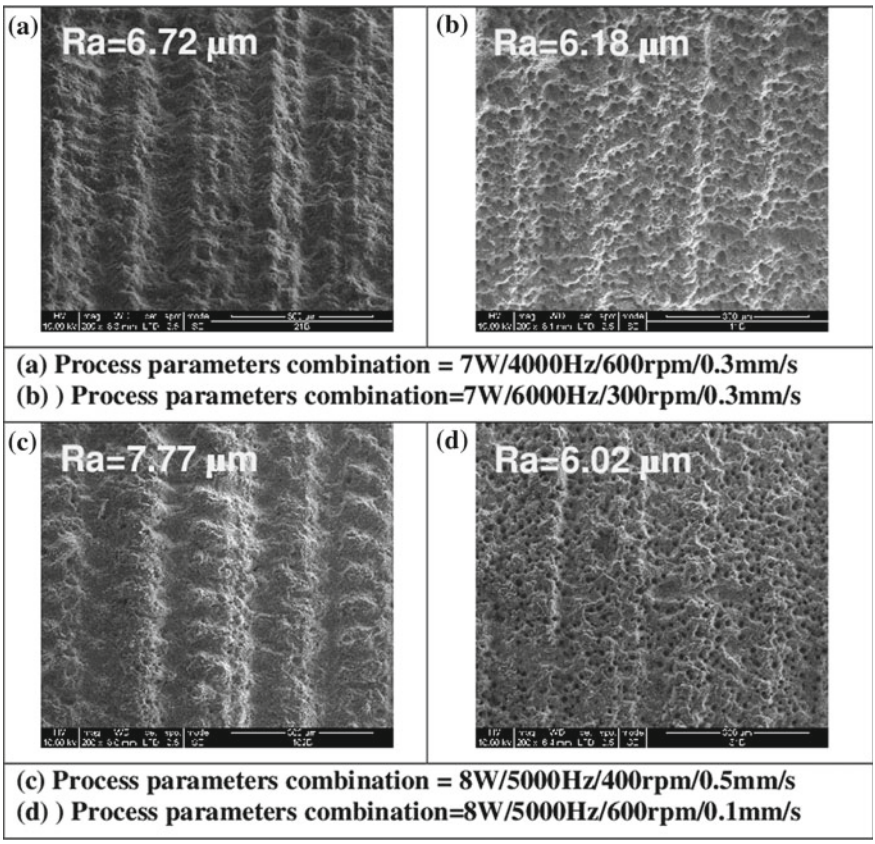

Fig. 24 SEM micrographs of micro-turning surface obtained at different parametric combinations for overlap study experimentation [23]

less after carrying out laser defocusing experimentation compared to SEM images shown in Fig. 23 for RSM-based experiments.

7 Summary

In this chapter, laser micro-turning is applied to micro-turn aluminium oxide (Al_2O_3) ceramic of 99% purity for achieving desired micro-turning depth and surface features in terms of surface roughness (Ra and Rt). Employing a variety of experimental designs like effect of spot and circumferential overlap, experiments by laser defocusing method, etc., it is concluded that high intense laser beam has great impetus

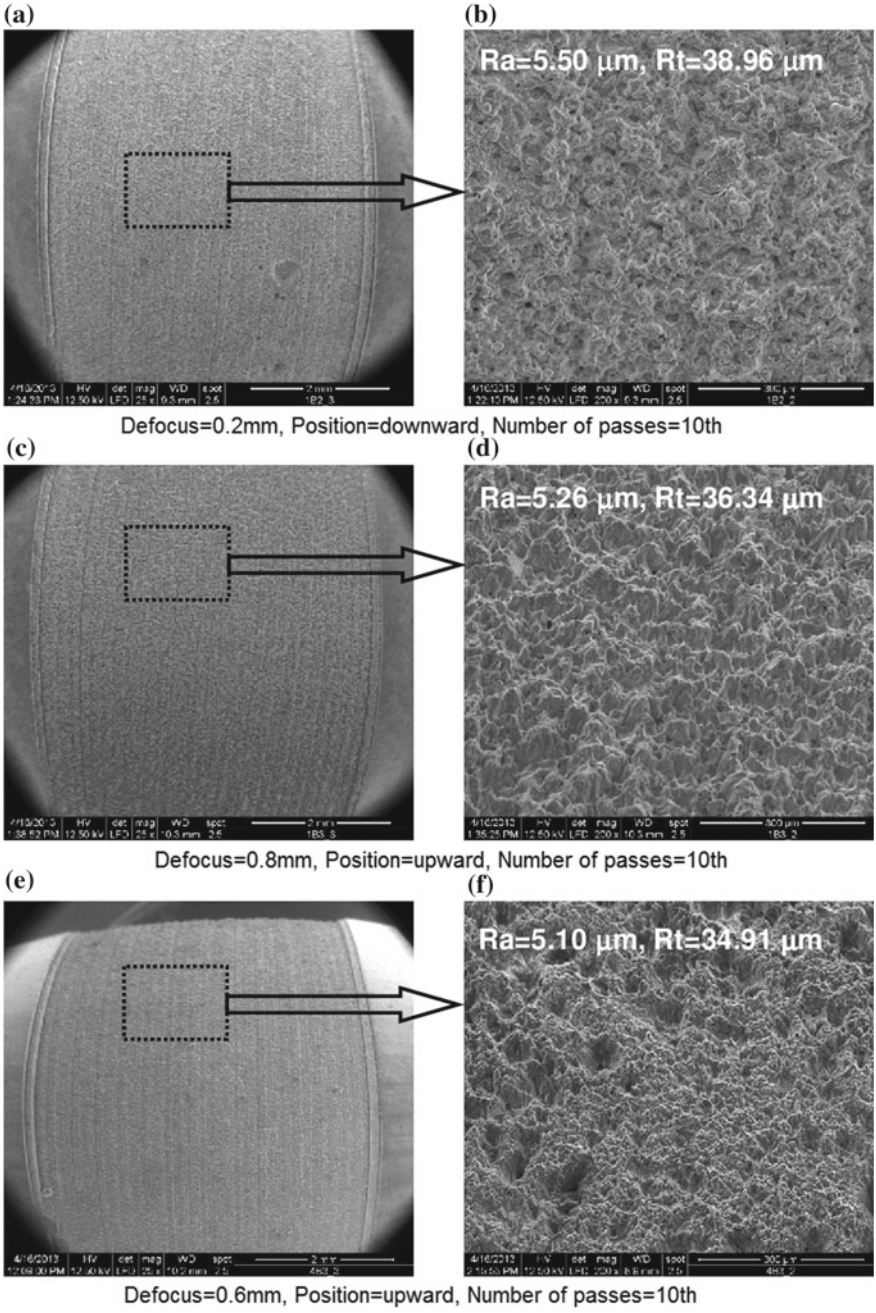

Fig. 25 Microscopic surfaces machined at different defocus conditions and laser scan passes

to achieve desired process performances and has potential to manufacture micro-components of cylindrical shapes made from various engineering ceramics. Moreover, with proper control of various process parameters and also by considering novel strategy of micromachining such as defocusing of laser beam, desired dimensional accuracy and surface featured can be successfully achieved. The present research and outcomes will be utilized to predict the parametric combination for achieving desired goal of laser micro-turning process performances. Furthermore, experimental schemes and results obtained in the experimentation will provide the precision manufacturing technocrats as technological guidelines for successful implementation of this novel micromachining process in precision engineering domains.

References

1. Kingery WD, Browen HK, Uhlmann DR (1976) Introduction to ceramics. Wiley & Sons, Inc., New York
2. König W, Verlemann E (1991) Machining advanced ceramics—a challenge in production technology. In: Davidge RW, Van de Voorde MH (eds) Designing with structural ceramics. Springer, Dordrecht
3. Jha S, Jain VK (2006) Nanofinishing techniques. In: Micromanufacturing and nanotechnology. Springer, Berlin, Heidelberg
4. Miller PR, Aggarwal R, Doraiswamy A, Lin YJ, Lee YS, Narayan RJ (2009) Laser micromachining for biomedical applications. JOM 61(9):35–40
5. Kibria G, Doloi B, Bhattacharyya B (2010) Experimental analysis on Nd:YAG laser micro-turning of alumina ceramic. Int J Adv Manuf Technol 50(5–8):643–650
6. Kibria G, Sharma B, Doloi B, Bhattacharyya B (2011) Experimental Investigation into pulsed Nd:YAG Laser Micro-turning of engineering ceramics. Adv Mater Res 264–265:1318–1323
7. Kibria G, Doloi B, Bhattacharyya B (2012) Optimisation of Nd:YAG laser micro-turning process using response surface methodology. Int J Precis Technol 3(1):14–36
8. Yung KC, Chen GY, Li LJ (2003) The laser dressing of resin-bonded CBN wheels by a Q-switched Nd: YAG laser. Int J Adv Manuf Technol 22(7):541–546
9. Khangar A, Dahotre NB, Jackson MJ, Robinson GM (2006) Laser dressing of alumina grinding wheels. J Mater Eng Perform 15(2):178–181
10. Samant AN, Dahotre NB (2009) Differences in physical phenomena governing laser machining of structural ceramics. Ceram Int 35(5):2093–2097
11. Islam MU, Campbell G (1993) Laser machining of ceramics: a review. J Mater Manuf Process 8(6):611–630
12. Zhong ZW, Lin G (2005) Diamond turning of a metal matrix composite with ultrasonic vibrations. Mater Manuf Processes 20(4):727–735
13. Shih AJ (2000) An experimental investigation of rotary diamond truing and dressing of vitreous bond wheels for ceramic grinding. Int J Mach Tools Manuf 40:1755–1774
14. Zhang Z, Yan J, Kuriyagawa T (2011) Study on tool wear characteristics in diamond turning of reaction-bonded silicon carbide. Int J Adv Manuf Technol 57(1–4):117–125
15. Doremus RH (2008) Alumina. In: Shackelford JF, Doremus RH (eds) Ceramic and glass materials. Springer, Boston, MA
16. Dahotre NB, Harimkar SP (2008) Laser fabrication and machining of materials. Springer, New York, NY, USA
17. Samant AN, Dahotre NB (2009) Laser machining of structural ceramics—a review. J Eur Ceram Soc 29(6):969–993

18. Wang XC, Zheng HY, Chu PL, Tan JL, The KM, Liu T, Ang BC, Tay GH (2010) Femtosecond laser drilling of alumina ceramic substrates. Appl Phys A Mater Sci Process 101(2):271–278
19. Dhupal D, Doloi B, Bhattacharyya B (2008) Pulsed Nd:YAG laser turning of micro-groove on aluminum oxide ceramic (Al_2O_3). Int J Mach Tools Manuf 48(2):236–248
20. Chryssolouris G (1991) Laser machining theory and practice. Springer, New York
21. Kibria G, Doloi B, Bhattacharyya B (2017) Laser micro-turning process of aluminium oxide ceramic using pulsed Nd:YAG laser. In: Kibria G, Bhattacharyya B, Davim J (eds) Non-traditional micromachining processes. Materials forming, machining and tribology. Springer, Cham
22. Kibria G, Doloi B, Bhattacharyya B (2013) Predictive model and process parameters optimization of Nd:YAG laser micro-turning of ceramics. Int J Adv Manuf Technol 65(1–4):213–229
23. Kibria G, Doloi B, Bhattacharyya B (2014) Investigation into the effect of overlap factors and process parameters on surface roughness and machined depth during micro-turning process with Nd:YAG laser. J Opt Laser Technol 60:90–98
24. Kibria G, Doloi B, Bhattacharyya B (2015) Investigation and analysis on pulsed Nd:YAG laser micro-turning process of aluminium oxide (Al_2O_3) ceramic at various laser defocusing conditions. Int J Adv Manuf Technol 76(1–4):17–27

Accuracy Improvement Techniques in Electrochemical Micromachining (EMM)

V. Rathod, B. Doloi and B. Bhattacharyya

Abstract Electrochemical micromachining (EMM) has several advantages over its competitive micromachining techniques, and hence, it is one of the best micromachining techniques applied in various fields. However, further investigations are required to augment the machining accuracy for overcuts, taper formation, profile accuracy, and surface excellence, to discover the utility of EMM for various applications. Generally, microstructures like microholes, microslots, microgrooves, and 3D microfeatures are machined on various metallic components by EMM. Geometrical profile, dimension, and tribology of machined microfeatures mainly affect the performance as well as life of these components. Therefore, machining of such microfeatures of few tens to hundreds of microns with correct shape profile and better quality is ever demanding area for exploration. Availability of electrolyte at inter-electrode gap, removal of slush and hydrogen gas bubbles from machining zone, stray-current control, and microtool feed rate control to maintain uniform inter-electrode gap are the major challenges for the researchers to increase the machining accuracy. Machining accuracy can also be upgraded by selecting proper shape and size of the microtool, by insulating the sidewalls of the microtool, and also by utilizing the innovative machining strategies. In addition to these techniques, controlling and optimizing influencing process parameters of EMM and hybrid electrochemical micromachining are some of the areas by which machining accuracy can be enhanced in EMM.

Keywords EMM · Accuracy · Taper · Overcut · Surface finish · Microtool · Sidewall insulation · Machining strategy · Hybrid EMM

V. Rathod (✉)
Mechanical Engineering Department, Government Polytechnic Mumbai, Mumbai, Maharashtra 400051, India
e-mail: vurathodju@gmail.com

B. Doloi · B. Bhattacharyya
Production Engineering Department, Jadavpur University, Kolkata 700032, India
e-mail: bdoloionline@rediffmail.com

B. Bhattacharyya
e-mail: bb13@rediffmail.com

G. Kibria and B. Bhattacharyya (eds.), *Accuracy Enhancement Technologies for Micromachining Processes*, Lecture Notes in Mechanical Engineering,
https://doi.org/10.1007/978-981-15-2117-1_8

1 Introduction

EMM has an ability to produce the microfeatures on metallic surfaces for different applications. Machining uniqueness such as re-utilization of tool, machining surfaces without any stresses, and ability to machine any metallic surfaces makes the EMM as the best micromachining technique. Generally, microfeatures like microholes, microslots, and three-dimensional microfeatures need to be fabricated on different metallic surfaces of microcomponents or macrocomponents. While machining such microfeatures on microproducts by EMM, overcuts, taper formation, microsparks, stray-current effects, surface quality, etc., are the main issues to be considered. Therefore, to explore the complete potential of EMM for machining accurate microfeatures, further study is still required to boost the machining accuracy in the form of overcut, taper formation, surface quality, and path or profile of microfeature by regulating various process parameters. Geometrical profile, its dimensions, and tribological properties of the microfeatures directly influence the efficiency and product lifespan of the microparts. Therefore, machining of such accurate microfeatures on metallic surfaces of few tens of microns is significant areas of exploration. Stray-current monitoring and control is one of the key issues for improving the machining accuracy. Supply of fresh electrolyte at very small machining zone by removing sludge, precipitates, and hydrogen gas bubbles is one more challenge in EMM. Improper flushing of machining zone and deficient microtool movement may result into microsparks between microtool and workpiece surface, which may affect the surface quality of the machined microfeatures or it may damage the microtool also. EMM accuracy can also be enriched by innovative machining approaches and controlling and optimizing different influencing EMM process parameters. Combination of one or more principles of micromachining with EMM, i.e., hybrid micromachining, may also improve the machining accuracy of machined microfeatures.

In EMM, metallic workpiece material is dissolved by anodic dissolution, in which the material is liberated atom by atom from anodic surface. Material dissolution mainly depends upon the important EMM process parameters, namely applied potential, machining current, pulse frequency, electrolyte type and its concentration, interelectrode gap (IEG), etc. The process parameter greatly influences the machining criteria such as material dissolution rate, surface quality, and machining accuracy. To accomplish precise machining in sub-microns range on difficult to cut metallic surfaces, the EMM process variables are to be controlled at optimum level [1–3].

Machining accuracy in EMM can also be amended by regulating:

(i) Geometry, geometrical dimensions, and surface finish of microtool, along with its sidewall insulation,
(ii) Nature of electrolyte, circulation of electrolyte, and electrolyte concentration,
(iii) Process monitoring and control of some of the factors like flushing of narrow IEG, vibration of microtool, control of microspark phenomena, selection of microtool movement strategy, and
(iv) Combining one or more principles of micromachining with EMM, i.e., hybrid micromachining.

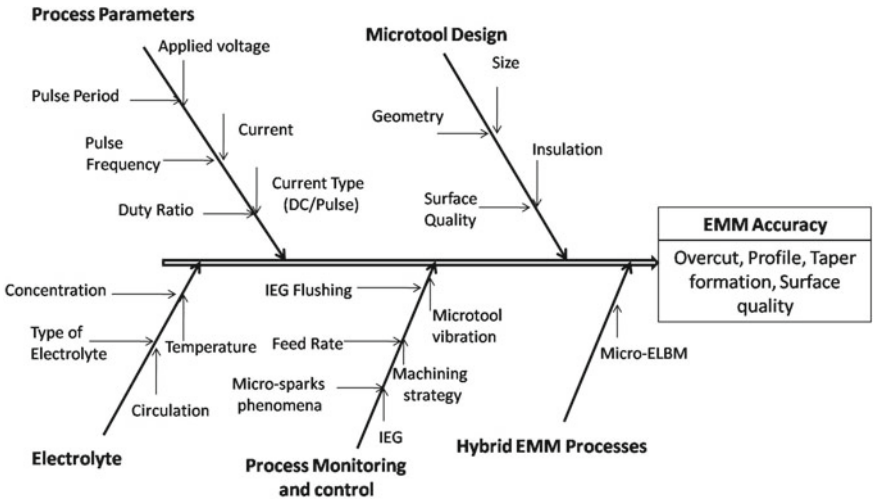

Fig. 1 Root cause diagram of EMM for machining accuracy improvement

Figure 1 shows fish bone diagram considering all these parameters for machining accuracy improvement.

Some of the important parameters which mainly influence the machining accuracy in EMM are discussed in detail to know the inside facts about enhancing the machining accuracy in the form of overcut, profile accuracy, taper formation, and surface quality.

2 Design of Microtools

Geometrical dimensions and surface quality of microtool play the significant role in electrochemical dissolution of material at atomic level to achieve desired microfeatures. Microfeatures such as cylindrical microhole, complex microgrooves, and 3D microstructures of higher aspect ratios are to be fabricated on metallic surfaces of microproducts or macroproducts in various applications. Sidewall of the structures tapers during fabrication of microfeatures of higher depths. This is because of the dissolution time difference between upper and lower faces of the microfeature as shown in Fig. 2a. Therefore, machining of taper-free microfeatures of higher aspect ratio is very essential in EMM. Difference between the dissolution time at top and bottom faces can be reduced by insulating the lateral surface of the microtool. Insulation prevents the material dissolution along lateral surface of microtool and limits the material dissolution from the front portion of the microtool only. This minimizes the development of inclined walls along the edge of as shown in Fig. 2b.

Macrosized tools can be easily insulated by various available insulating materials and techniques, whereas very few techniques have been reported for insulating the

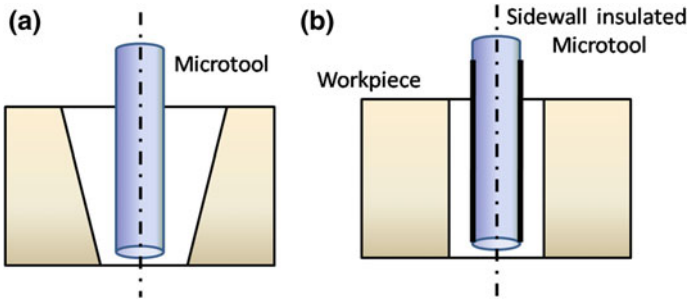

Fig. 2 Machining with **a** cylindrical microtool and **b** sidewall-insulated cylindrical microtool

sidewalls of the microtools. In EMM, IEG is in the range of few microns; hence, thickness of insulating film has to be lower than this gap for continuation of the EMM process smoothly. Smaller machining gap restricts the insulating film thickness to be of few microns, i.e., 3–5 μm only. Insulating material utilized for insulation must form uniform insulating film of few microns. Insulating film should not liquefy in electrolyte, it should not react with electrolyte, and it should not corrode the microtool surface also. It should stick to microtool, sturdy, and mainly simple to apply and to remove from the microtool [4]. There are various techniques for insulating the lateral surfaces of the microtool. Spin coating demands specific fixture for microtool holding. Selection of insulating material is main criteria in PVD and CVD processes. Need of costly equipments to maintain vacuum with specific microtool holding fixture is some of the main aspects. Regulating the insulation thickness of few microns in dip and drop coating is also difficult task [5]. For opening the front end of the microtool, insulation process may be followed by end-rubbing process, which includes the threat of microtool or microtool tip damage. For reutilizing the same microtool in EMM, worn-out insulating film has to be detached wholly and new insulating film is applied. Hence, to deal with these challenges, further development is required in developing simple methods for insulating the lateral surfaces, i.e., sidewalls of the microtool, with very thin insulating film. Workpiece material dissolution can be restricted to the lateral surface of the microtool by modifying the geometry of the microtool. Geometrical shape of the microtool and its tip shape play significant role in machining accurate microfeatures in EMM [6]. Figure 3 shows the types of microtools according to tip shape, i.e., end shape, of the microtool that has been designed, developed, and utilized by various researchers for generating microfeatures on metallic surfaces by EMM [7].

Flat-faced cylindrical microtools can be used in the fabrication of various microfeatures by regulating the microtool movement. Straight cylindrical microholes of high aspect ratio can be machined with less efforts using cut edge microtool with rotary motion during machining. The cut portion of microtool boosts the amount of electrolyte at confined machining gap and enhances the profile accuracy. Conical microtools can be used for machining tapered microholes for micronozzles.

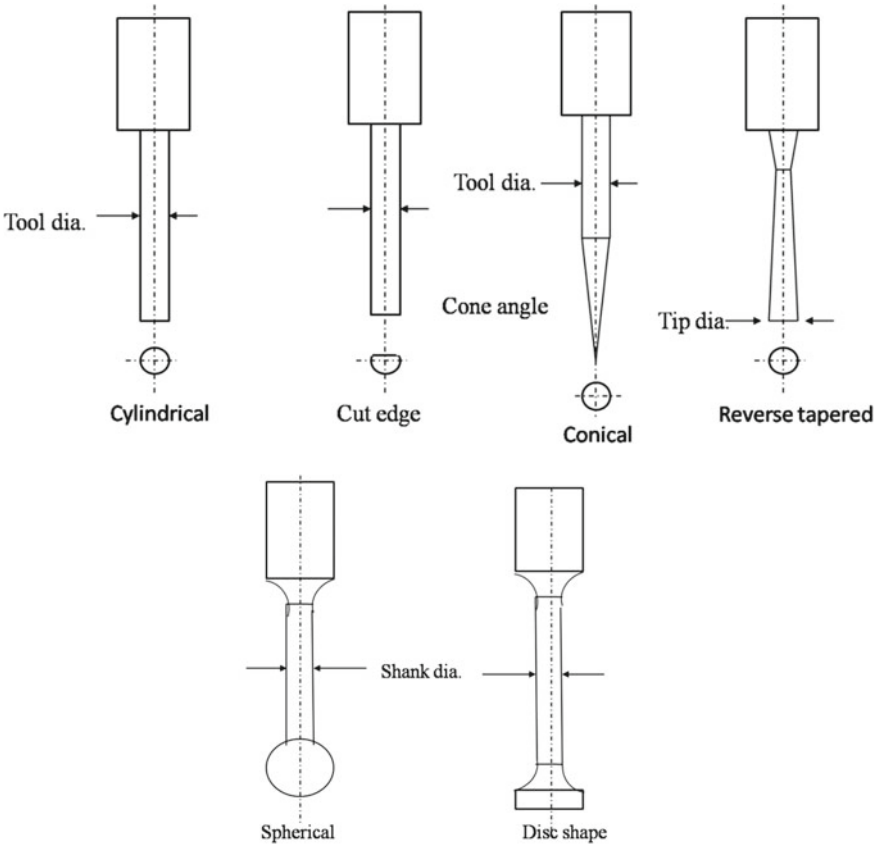

Fig. 3 Microtools of different end shapes

Reverse-tapered microtools are suitable for minimizing taper in microfeatures. Disc-shaped and spherical-based microtools are suitable for machining straight-walled microfeatures by EMM.

Tip geometry of the microtool plays significant role in electrochemical dissolution of material in EMM. While machining the microfeatures with flat-end straight cylindrical microtool, width at the top face of the microfeature is higher than that at the bottom face. This is because of the difference in dissolution time at top and bottom surfaces of the microfeature. This difference in machining width at top and bottom faces causes the taper in the sidewalls of the machined microfeature as shown in Fig. 4a. Application of disc-shaped microtool restricts the material dissolution at disc region only. Disc shape microtool confines the continuous dissolution of work-piece material by the lateral surface of the microtool and avoids the formation of taper along the wall of microfeature as shown in Fig. 4b [8]. Spherical base microtools can also be used to machine the taper-free microfeatures as shown in Fig. 4c. Use of spherical electrode results microfeatures without taper due to lesser current density

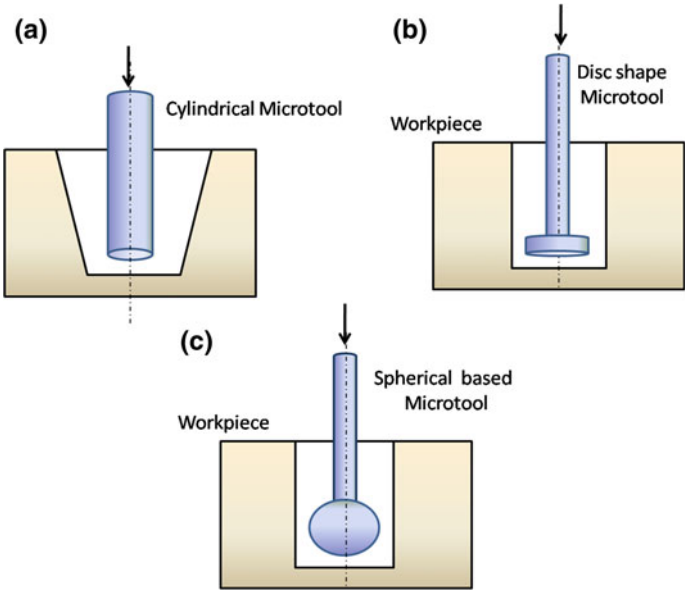

Fig. 4 Effect of microtool tip shape on wall profile of microfeature

along the cylindrical surface of microtool that limits the continuous dissolution of the workpiece material [9].

Figure 5a, b depicts the SEM micrographs of the vertical microcolumn machined in vertical-walled square cavity and vertical microwall of 10 μm width using disc-shaped microtool on SS304 by EMM, respectively [8]. However, Fig. 5c shows the SEM micrograph of the straight-walled microhole fabricated using spherical-based microtool [9].

Effective lengths, i.e., dipping length, and diameter of microtool also have an important role during fabrication of microfeatures by EMM. For the long length microtool, electrolyte path resistance is longer than the path resistance of shorter length tool; therefore, the charging time constant of the shorter path is relatively small as compared to charging time constant for long path. The amount of faradaic current decreases with the increase in effective tool length, in turn decreases the material removal rate, and consequently increases the machining time. Current flows through the lesser electrolyte resistance route that restricts the machinable area to adjacent region of the tool only. For a longer tool, the dissolution of material takes place over from the larger space from anodic workpiece surface, resulting non-precise machining as shown in Fig. 6a, b. Hence, for accurate machining of the microfeatures by EMM, shorter effective length of the microtool is desired.

Diameter of microtool has significant role in electrochemical machining of micro-features. Increase in microtool diameter increases the effective machining area,

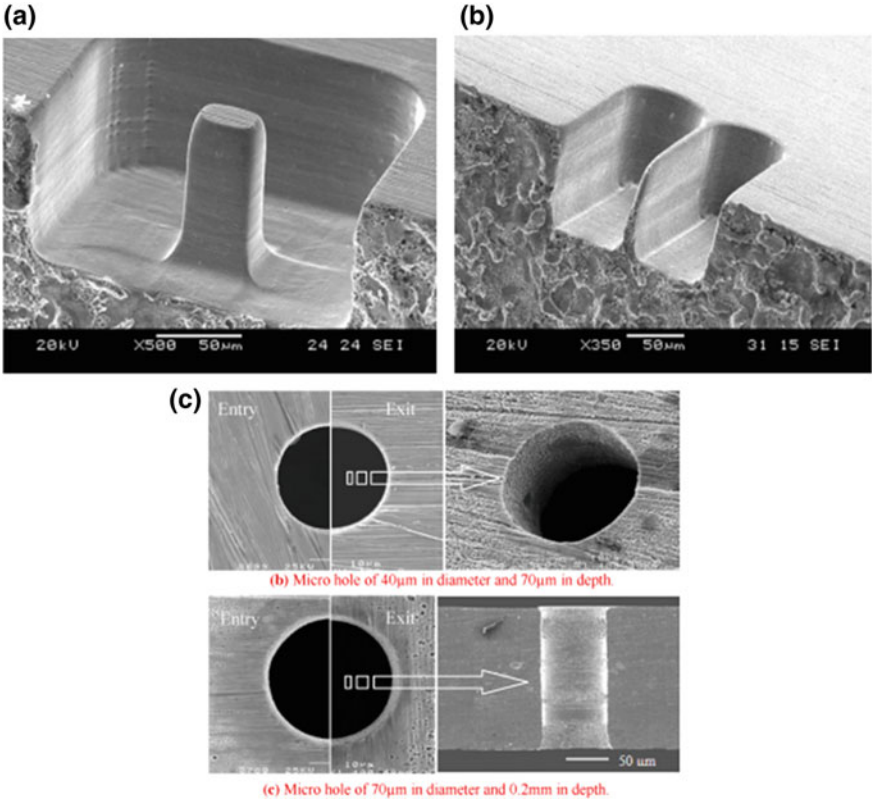

Fig. 5 Microfeatures machined by disc-shaped microtool [8, 9]

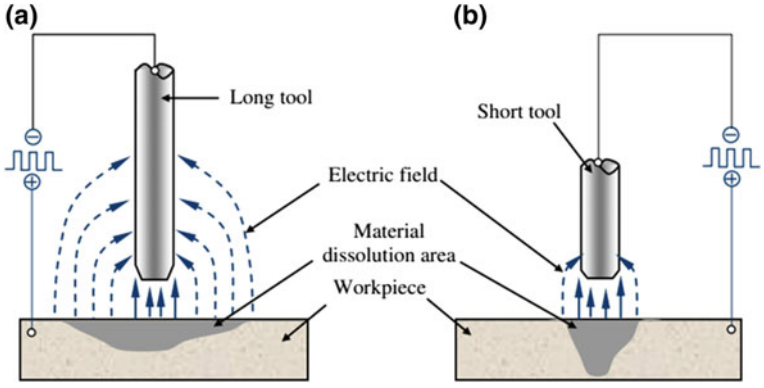

Fig. 6 Schematics for machining region in EMM for **a** long and **b** short microtool [10]

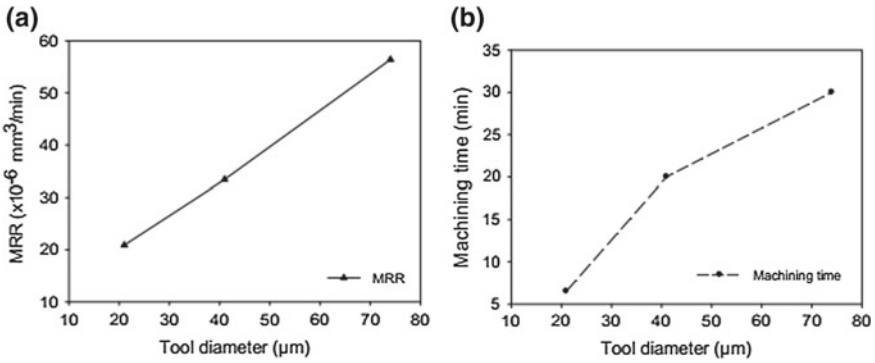

Fig. 7 Influence of tool diameter on **a** material dissolution and **b** machining time [12]

decreases the electrolyte resistance which decreases the cell impedance and ultimately increases the double-layer capacitance. Increased inductance rises the charging time of double-layer potential, as a result machining rate decreases with increase in microtool diameter. Hence, microtool electrodes of higher diameter need longer pulse on-time for effective and accurate fabrication of microfeatures by EMM [11].

Mithu et al. [12] performed experimentation for investigating the effect of tool geometry on performance during electrochemical microdrilling. Figure 7a, b plots the influence of microtool diameter on material dissolution and machining time. From the figure, it can be observed that metallic dissolution and machining time increase with increase in tool diameter. This is because of the rise in electrical double-layer capacitance and decreases in electrolyte resistance at higher microtool diameter. Reduced path resistance enhances the current density into the electrolyte. This increase in machining current results increased material dissolution. Hence, the microtool feed rate has to be adjusted in such a way to control the material dissolution, which eventually increases the machining time.

3 Electrolyte Circulation

Continuous supply of electrolyte at very small machining region is necessary for effective and accurate electrochemical machining of microfeatures. Machining gap is precisely small, and maintaining continuous supply of fresh electrolyte through this opening is a challenging job. Stagnant electrolyte is generally preferred to avoid the delicate microtool vibration which may damage it also. For continuation of EMM process, it is essential to take out the slush and gas bubbles from machining area. Various methods have been developed to enhance electrolyte circulation in narrow machining zone.

Electrolyte supply at narrow machining zone can be enhanced by incorporating low-frequency longitudinal vibrations to the microtool [13]. Piezoelectric transducer

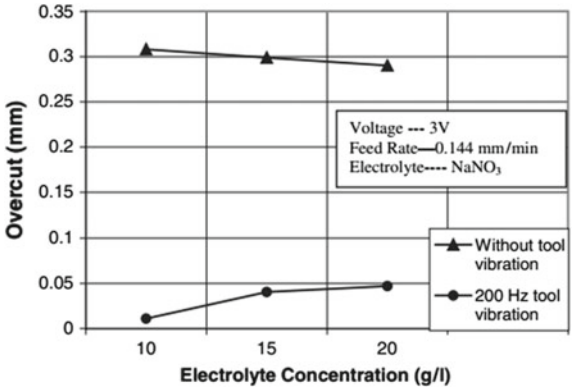

Fig. 8 Effect of electrolyte concentration and tool vibration on overcut [15]

(PZT) can be used for providing vibrations to the microtools in EMM [14]. Microtool vibration has hydrodynamic effects on the bubbles that can be applied for the removal of process by-products and the replacement of electrolyte at narrow IEG. Figure 8 graphically presents the effect of microtool vibration over machining accuracy. From the figure, it can be observed that accuracy improves with microtool vibration [15]. Electrolyte circulation at narrow IEG can also be boosted by applying rotational movement to the microtool during its movement in predetermined path.

4 Microtool Insulation

Microfeatures of higher depths are favoured in various applications. Cylindrical microtools are utilized for the fabrication of high aspect ratio microfeatures on metallic surfaces by EMM. Un-insulated cylindrical microtools are generally used in the fabrication of microfeatures by EMM, due to challenges in microtool handling and sidewall insulation. While machining deep microstructures by EMM, the vertical walls taper along the depth. This is because of the dissolution of the workpiece material from lateral surface as well as front face of the microtool, which dissolves more material from lateral surface as compared to bottom surface of the microtool. Hence, for effective material removal of deep microfeatures, the cylindrical surface of the microtool is to be appropriately insulated. Figure 9a schematically illustrates the machining width at top and bottom surfaces while machining deep microhole utilizing un-insulated microtool. Machining width at the top surface is higher and decreases gradually towards the bottom surface, because of the continuous dissolution of workpiece by cylindrical surface of microtool. This can be constrained using insulated microtool during machining deep microfeatures. Microtool insulation constrains the metallic dissolution alongside the walls of the deep microfeatures. Electric field can be confined to the front face of the microtool to give uniform machining rate and uniform machining gap regardless of machining depth. Following these techniques, straight-walled deep microfeatures can be machined as shown in Fig. 9b.

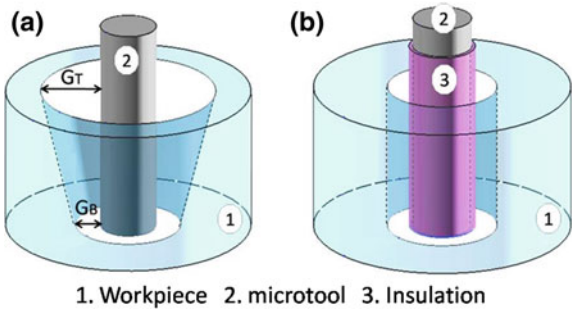

Fig. 9 Microfeatures fabricated using **a** un-insulated and **b** insulated microtool

Figure 10a, b depicts the microscopic images of the microgrooves machined on SS sheet with applied voltage of 3V, pulse frequency 8 MHz, and 35% duty ratio, utilizing un-insulated and sidewall-insulated microtools, by layer-by-layer microtool movement strategy. While machining microgroove with un-insulated microtool, very high width overcut can be observed due to continuous metallic dissolution along the length of microtool. Also, the stray current at top face results in rough surface around the microgroove with curved edges of microgroove. Lateral surface insulation of microtool confines width overcut, as well as stray-current effect, and generates more accurate microgroove with improved surface quality of microgroove.

For minimizing unwanted material dissolution by lateral surface of microtool, the material dissolution should take place from front face of the microtool only. In ECM, tools are of macrosize and are easy to insulate using different insulating resources, but

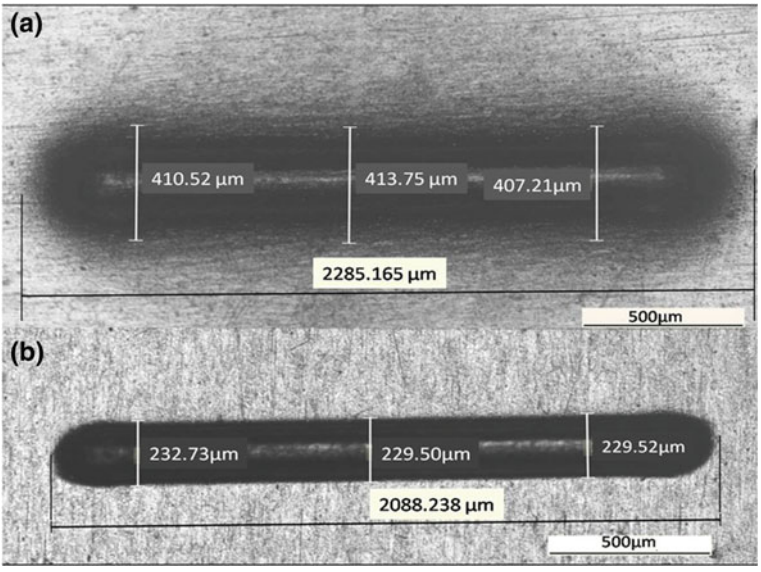

Fig. 10 Microgrooves using **a** un-insulated microtool and **b** insulated microtool [4]

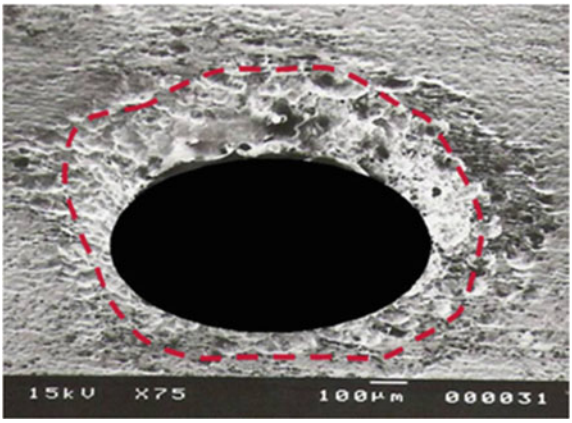

Fig. 11 Microspark and stray-current affected zone microfeature [16]

in EMM insulating the microtool by very thin insulating film is challenging because of micron-sized tools.

5 Microsparks Phenomena in EMM

Various reasons that may lead to the microspark at narrow IEG are (i) variation in inter-electrode gap resistance due to hydrogen gas bubbles generated, (ii) accumulation of sludge particles at narrow machining zone, (iii) inadequate movement of tool, (iv) increased temperature at machining zone, (v) poor electrolyte quality, etc. Microsparks reduces accuracy, as well as deprives surface finish. Machining accuracy deteriorates due to the presence of microsparks in narrow machining zone; however, in EMM, microsparks cannot be eliminated completely [16].

Figure 11 depicts the surface condition of microhole machined by EMM, with microspark and stray-current affected zone. To obtain the better machining accuracy and surface finish, microtool feed rate should be as low as possible. Influence of stray current increases with higher applied voltage and reduces with higher pulse frequency. Some of the significant features that influence the occurrence of microsparks are microtool feed rate, electrolyte flow, and machining gap regulation [17]. Microtool movement should be synchronous with machining rate for smooth machining. Higher microtool feed rate may continuously reduce the machining gap and increases the chances of occurrence of microsparks that may lead to the short circuit.

6 IEG Control Strategy

Rigid, reliable, economic, and easy to operate machine setup is desired to apply EMM process for production of microfeatures on different industrial products. Considering

the complexity, mechatronics involved in the setup, online process monitoring, and its control plays very important role. In EMM, machining gap regulates the machining precision. At higher microtool feed rate, IEG reduces progressively which may lead to the short circuit. This may destroy the microtool or work surface. Lower tool feed rate lags the metallic dissolution, resulting gradual increase in machining gap affecting the machining accuracy. Hence, to maintain uniform IEG, the microtool feed rate must harmonize with the material dissolution. While machining microfeatures by EMM, the material dissolution rate varies, and various machining gap monitoring and regulating techniques have been developed by researchers [18, 19]. Still some works are required in EMM setup to develop reliable online measurement system during machining for further improvement in machining accuracy.

7 Machining Strategy

Microtool movement policy greatly influences machining accuracy in EMM. Proper tool movement strategy minimizes uncontrolled machining by enhancing the electrolyte flushing and localization effect. Researchers have developed various types of microtool movement policies in EMM. Straight-walled three-dimensional microfeatures can be machined by (i) layer-by-layer machining and (ii) sinking and milling method. Microtool moves along the *X*-, *Y*-, and *Z*-axis adopting suitable movement approach for microfeature generation as shown in Fig. 12.

Figure 13 shows the schematics for machining the microgrooves by sinking and milling method. During this microtool movement strategy, microtool is first moved downward into the workpiece surface for the required depth, and then, it is moved in a horizontal plane along the required path.

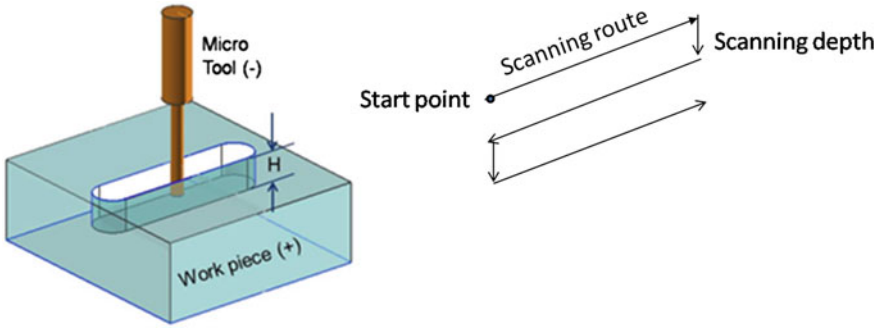

Fig. 12 Scanning-type microtool movement strategy for 3D EMM

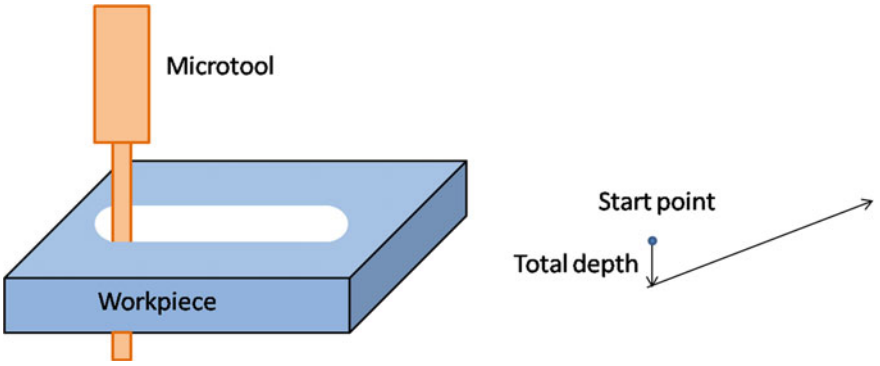

Fig. 13 Sinking and milling microtool movement strategy for 3D EMM

8 Selection of Combined Process Parameters

Effective application of EMM for precise manufacturing demands the appropriate combinations of process parameters. Various methods have been reported by researchers to find and optimize the machining parameters for better machining performance. Taguchi-based methodology, response surface methodology, etc., can be applied to obtain these machining parameters.

9 Hybrid EMM Processes

Hybrid processes are used to exploit the combined effect of individual processes. Each individual process may either directly involve in the material removal or assist for better machining conditions. Figure 14 shows the commonly used hybrid micromachining processes. Anodic dissolution in EMM process has some integral process limitations such as poor and unrestrained machining localization, deficient flushing of narrow machining region, formation of oxide layer on work surface, and more machining duration. To overcome these difficulties and to make process more precise, EMM is combined with other metal removal processes [20–27].

10 Summary

For machining microfeatures on advance engineering metallic surfaces, EMM is one of the best techniques. As compared to the other micromachining techniques, EMM has important benefits such as machining complex microfeatures without any heat-affected zone, best surface finish, and mainly capability to machine all metallic surfaces irrespective of their mechanical properties. Hence, EMM is widely accepted

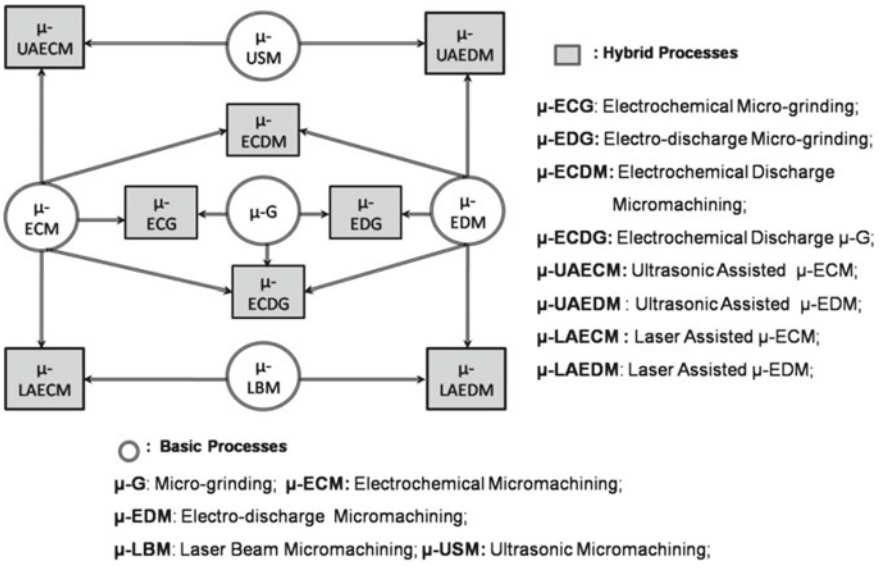

Fig. 14 Different hybrid micromachining processes

for precise machining applications, namely MEMS, electronic and aerospace applications, and biomedical applications to machine high aspect ratio microholes, microgrooves, 3D microstructures, micropins, etc. Continuous developments and extensive research efforts are essential for effectual use of this process. This comprises the improvement in machining setup, design of microtool, monitoring and governing of machining gap, controlled metallic dissolution, precise power source, eradication of short circuits, and with proper electrolyte choice. For better control over the process, shape of microtool, lining of cathode surface, availability of electrolyte, and disregarding short circuits during process are the essential parameters to be considered. Selection and combination of process parameters are an important aspect for precise and accurate machining of microfeatures. EMM has many opportunities that can be explored further. EMM process can be combined with other micromachining techniques resulting in hybrid micromachining process. All of these aspects enable the EMM as a promising micromachining technique to fabricate the complex microstructure on advanced metallic materials. For enhancing the machining accuracy to atomic level, further research is still open. EMM will be more successful and lead an important part in microfabrication and nanofabrication seeing various benefits of it such as excellence, mobility, efficiency, and finally economy.

References

1. Kozak J, Rajurkar KP, Makkar Y (2004) Selected problems of micro-electrochemical machining. Int J Mater Process Technol 149:426–431
2. Munda J, Bhattacharyya B (2008) Investigation into electrochemical micromachining (EMM) through response surface methodology based approach. Int J Adv Manuf Technol 35:821–832
3. Bhattacharyya B (2015) Electrochemical micromachining for nanofabrication, MEMS and nanotechnology, 1st edn. Elsevier, Oxford, USA
4. Rathod V, Doloi B, Bhattacharyya B (2014) Sidewall insulation of microtool for electrochemical micromachining to enhance the machining accuracy. Mater Manuf Processes 29(3):305–313
5. Bunshah RF (1994) Handbook of deposition technologies for films and coatings, science, technology and applications, 2nd edn. Noyes, Park Ridge, NJ
6. Park BJ, Kim BH, Chu CN (2006) The effects of tool electrode size on characteristics of micro electrochemical machining. CIRP Ann 55(1):197–200
7. Kibria G, Bhattacharyya B, Davim JP (eds) (2017) Non-traditional micromachining processes fundamentals and applications. Springer International Publishing, Switzerland
8. Kim BH, Ryu SH, Choi DK, Chu CN (2005) Micro electrochemical milling. Micromech Microeng 15:124–129
9. Liu Y, Cai H, Li H (2015) Fabrication of micro spherical electrode by one pulse EDM and their application in electrochemical micromachining. J Manuf Process 17:162–170
10. Mithu MAH, Fantoni G, Ciampi J (2014) How microtool dimension influences electrochemical micromachining. Int J Adv Manuf Technol 70:1303–1312
11. Park BJ, Kim BH, Chu CN (2006) The effects of tool electrode size on characteristics of micro electrochemical machining. Ann CIRP 55(1):1–6
12. Mithu MAH, Fantoni G, Ciampi J, Santochi M (2012) On how tool geometry, applied frequency and machining parameters influence electrochemical microdrilling. CIRP J Manufact Sci Technol 5:202–213
13. Ghoshal B, Bhattacharyya B (2014) Shape control in micro borehole generation by EMM with the assistance of vibration of tool. Precis Eng 38:127–137
14. Chikamori K (1998) Possibilities of electrochemical micromachining. Int J Jpn Soc Precis Eng 32(1):37–38
15. Bhattacharyya B, Malapati M, Munda J, Sarkar A (2007) Influence of tool vibration on machining performance in electrochemical micro-machining of copper. Int J Mach Tools Manuf 47:335–342
16. Munda J, Malapati M, Bhattacharyya B (2007) Control of micro-spark and stray-current effect during EMM process. Int J Mater Process Technol 194:151–158
17. Yong L, Yunfei Z, Guang Y, Liangqiang P (2003) Localized electrochemical micro machining with gap control. Sens Actuators A Phys A 108:144–148
18. Kuritaa T, Chikamori K, Kubota S, Hattori M (2006) A study of three-dimensional shape machining with an ECmM system. Int J Mach Tools Manuf 46:1311–1318
19. Mithu MAH, Fantoni G, Ciampi J (2011) A step towards the in process monitoring for electrochemical microdrilling. Int J Adv Manuf Technol 57:969–982
20. Rajurkar KP, Zhu D, McGeough JA, Kozak J, Silva De (1999) New developments in electrochemical machining. CIRP Ann 48(2):567–579
21. Pa PS (2009) Super finishing with ultrasonic and magnetic assistance in electrochemical micromachining. Electrochim Acta 54:6022–6027
22. Zhu D, Zeng YB, Xu ZY, Zhang XY (2011) Precision machining of small holes by the hybrid process of electrochemical removal and grinding. CIRP Ann Manuf Technol 60:247–250
23. Masuzawa T, Sakai S (1987) Quick finishing of WEDM products by ECM using a mate-electrode. Ann CIRP 36:123–126
24. Nguyenn MD, Rahman M, Wong YS (2012) Simultaneous micro-EDM and micro-ECM in low-resistivity deionized water. Int J Mach Tools Manuf 54–55:55–65

25. Davydov AD (1994) Laser electrochemical machining of metals. Russ J Electrochem 30(8):871–881
26. Yang I, Park MS, Chu CN (2009) Micro ECM with ultrasonic vibrations using a semicylindrical tool. Int J Precis Eng Manuf 10(2):5–10
27. Skoczypiec S (2011) Research on ultrasonically assisted electrochemical machining process. Int J Adv Manuf Technol 52(5):565–574

Surface Micromachining—Advances and Advanced Characterization Techniques

Arjyajyoti Goswami

Abstract Surface being the outermost layer of a body is the first point of contact between a body and the environment in which it is intended to work. By modifying the surface properties, the characteristics exhibited by a material can be controlled. With the need for reducing the structure sizes for different applications, the conventional machining has been scaled down to micromachining in which micro tool is used and micron-sized structures are created. Among the different types of micromachining techniques, surface micromachining stands out as a process which is intended only for the surface of a workpiece. In contrast to other micromachining techniques which target the bulk of the workpiece, surface micromachining aims at creating patterns, structures or features on the surface of the workpiece thus inducing unique and controllable properties. This chapter discusses different micromachining techniques and methods of characterization. The first section will include brief introduction to well-known processes like photolithography, reactive ion etching, deep reactive ion etching; some advanced processes capable of micron as well as nanometric scale fabrication like focused ion beam fabrication, electron beam lithography. Almost all these techniques are physical in nature, as in they do not involve use of chemical etching for creating the surface structures. Thus, they enable one to achieve high level of accuracy in the process and to actively control the features of the structure. As the fabrication methods have evolved with time, so did their characterization methods. Conventional measurement techniques are not suitable for evaluating the structures fabricated by the advanced surface micromachining methods. The second section of the chapter discusses three measurement and characterization methods. First of which is stereo zoom microscope which is used mostly at macro scale, followed by scanning electron microscopy which is capable of operating at micron and nanometric scale. The last of the characterization methods is scanning tunneling microscopy which is capable of imaging and characterization at atomic scale.

A. Goswami (✉)
Department of Mechanical Engineering, National Institute of Technology Durgapur, Durgapur, West Bengal 713209, India
e-mail: arjyajyoti.goswami@me.nitdgp.ac.in

G. Kibria and B. Bhattacharyya (eds.), *Accuracy Enhancement Technologies for Micromachining Processes*, Lecture Notes in Mechanical Engineering,
https://doi.org/10.1007/978-981-15-2117-1_9

Keywords Surface engineering · Photolithography · Reactive ion etching · Focused ion beam fabrication · Electron beam lithography · Scanning tunneling microscopy

1 Introduction

Civilization is defined as complex society, designed in a manner such that it creates agricultural surpluses, specialization in labor, hierarchy in social order and establishment of cities [1]. One of the fundamental driving forces in the growth of civilization is human beings' inherent nature to explore the unknown and to better their own condition from the present status. In this continuous endeavor, tools have played an imperative role. The earliest documented tool ever used by a species of early human being was the stone. Apart from being a source of lighting up fire by rubbing, they were an important asset while hunting. It is found that the production of stone tools by our ancestors was not random, rather they were methodical and meticulous in their approach. The *tool–makers* of the tribe were experts in determining whether a particular stone under consideration was suitable for producing a sharp edge or not. The *tool-makers* knew how top chip off each flake so that a new surface can be obtained which can later be used for producing another flake [2].

With progress of civilization, the needs and desires of a person became increasingly varied and complicated. What started from use of stones, over the centuries, moved on to bronze, copper, iron to present day's use of steels, reinforced composites, diamonds, high strength alloys, etc. Also it was noted that different materials are suited for different types of uses; hence, softer materials were used for low load applications whereas stronger and tougher materials were used for withstanding heavy loads during its operation. This led to invention of different types of materials which expanded the type of processing needed for converting them into a finished product.

Not only materials, the design of the product and the quality requirement from the finalized product also became increasingly stringent. The size of the product has been reduced consistently over the past few decades and even if the size is kept same, the output from the product is increased so that ultimately the performance of the product has been increasing consistently. A large amount of impetus have been given to miniaturization wherein the size of the product is being consistently and continuously reduced. A very well-known example of miniaturization is the general purpose computer, which has reduced in its size from gigantic machines to handheld devices. It is also interesting that not only the size of computer has been reduced but its processing capabilities have also been increased many folds. This is made possible by substituting mechanical elements in the computer with electrical circuits and integrated chips. The next step in this direction is using optical circuits for computing which will increase the processing capabilities of the machines by 100 folds compared to present day status. To realize such advanced functionality, the conventional routes of fabrication are no longer be sufficient.

Hence, the material processing methods have advanced side by side with the human needs. From the brute force method of manufacturing which involved use of manual power like rubbing against a stone or breaking into smaller parts using force, we have shifted to using high precision machines which have advanced features like aerostatic bearings, vibration isolation platform, etc. [3, 4]. With the evolution of materials to be processed, the functional and dimensional requirements of final products and the processing methods have also evolved. For advanced applications, we have shifted from bulk machining to micromachining mostly to cope up with the demands of smaller components required for more specialized applications.

Even the field of micromachining has been further classified into bulk and surface micromachining. Where bulk micromachining deals with creating 3D products whose bulk has to be utilized as the functional part, using a scaled down version of their macro scale counterparts like—micro milling, micro drilling, micro EDM, etc., surface micromachining deals exclusively with the surface of the product and aims at creating different applications from it.

Surface can be defined as the uppermost layer or extent of an object or body which is generally used for describing its form or extent [5]. It is an important feature of an object since it is the first layer of contact between the body and its surroundings, and in most cases, it governs the interaction of the body with its environment. Various important properties exhibited by a body like tribological properties [6], optical properties [7, 8], energy transport, chemical reactivity [9], hardness [10, 11], etc., are dependent on its surface and can be actively controlled or modified by changing the surface and its features.

Surface processing is a little different than the bulk processing which is more conventional and has evolved over centuries. Surface processing involves materials and feature sizes that are not possible through conventional processing routes. Surface micromachining is one of the many surface processing techniques, in which movable structures are fabricated on different thin films deposited on a bulk substrate. One of the major differences between surface micromachining and bulk-micromachining is that in bulk machining, the substrate itself is used as the functional layer on which the required device is fabricated using etching, but in case of surface micromachining, first one or several layers of thin films are deposited on the substrate surface and then the etching is performed on the deposited layer [12].

This chapter is divided in two broad sections. In the first section, various surface micromachining processes like photolithography, reactive ion etching (RIE), deep reactive ion etching (DRIE) and processes suited for both micro and nanometric scale surface machining such as focused ion beam fabrication and electron beam lithography will be discussed. The major sources of errors, errors which are unique and characteristic to a particular process and methods to prevent the errors will also be discussed. In the second section of the chapter, different characterization tools for the micro machined surfaces will be discussed. Characterization tools starting from microscopic scale (stereo microscopes) to nanometric scale (scanning electron microscopy) and up to atomic scale (scanning tunneling microscopy) will be discussed. By discussing the characterization tools at different scales of operation, the difference in the design of the tools and their operating principles can be compared.

2 Photolithography

Lithography is a combination of two Greek words, *lithos* meaning stone and *graphy* which means to write. So lithography basically refers to a technique of writing (or printing) using stones. The process of lithography was invented by Johann Aloys Senefelder in Germany in the year 1796, where he used stones to transfer a carved image onto a paper. Prior to carving, the stones were treated with chemicals which made selective areas on the stone as oil receptive and other areas as oil repellant. When the stone was inked, selective regions on the stone attracted the paint which was then transferred to a paper or a cloth [13].

Since then the process of selectively altering regions of a substrate has evolved and different methods have been used for transferring a pattern onto a substrate. The most widely used form of lithography is photolithography which makes use of a source of light to transfer a given pattern onto a substrate through a light sensitive polymer known as the photoresist. The general flow of processes in photolithography is shown in Fig. 1. As can be seen from Fig. 1, photolithography is a combination of various processes which starts with coating the substrate with a photoresist. Photoresists are polymers which change their properties upon exposure to light.

Photoresists are coated onto the substrate through spin coating. Spin coating setup is a small instrument which is basically an isolated chamber with a rotating disc. A drop of the polymer to be coated (photoresist) is put onto the rotating disc which holds the substrate through a vacuum chuck. Depending upon the speed of the rotating disc, the viscosity of the polymer drop and the duration of rotation, different thicknesses of photoresist on the substrate can be obtained. Generally speaking, for obtaining the same thickness of the deposited coating, a highly viscous polymer should be coated at higher speeds for longer duration as compared to a polymer having low viscosity. The spin coating setup is pre calibrated in terms of the duration and speed of rotation while the viscosity of the photoresist drop is known in advance; thus the thickness of the deposited photoresist on the substrate can be closely controlled as per requirement [14]. Modern variants of spin coating setup have a vacuum chamber for a highly clean deposition process, provision for heating which facilitates the curing of the deposited photoresist on the substrate.

The photoresist can basically be of two types depending upon their behavior when exposed to light. If the binding link of the polymer undergoes scission when exposed to light, they are called as positive photoresist. Due to scission of the polymer chains, in the next stage when the substrate is chemically cleaned, the region exposed to light gets cleansed away. On the other hand, if upon exposure to light the links of the polymer forms cross-links between them, it is called as negative photoresist. Due to cross-linking, the areas which have been exposed to light becomes stronger as compared to other regions, and during the chemical cleaning stage the exposed area remains on the substrate while the rest of the deposited photoresist gets cleaned away. Post exposure chemical treatment of the wafer is done to selectively remove the exposed areas on the photoresist; this step is called as developing. After developing

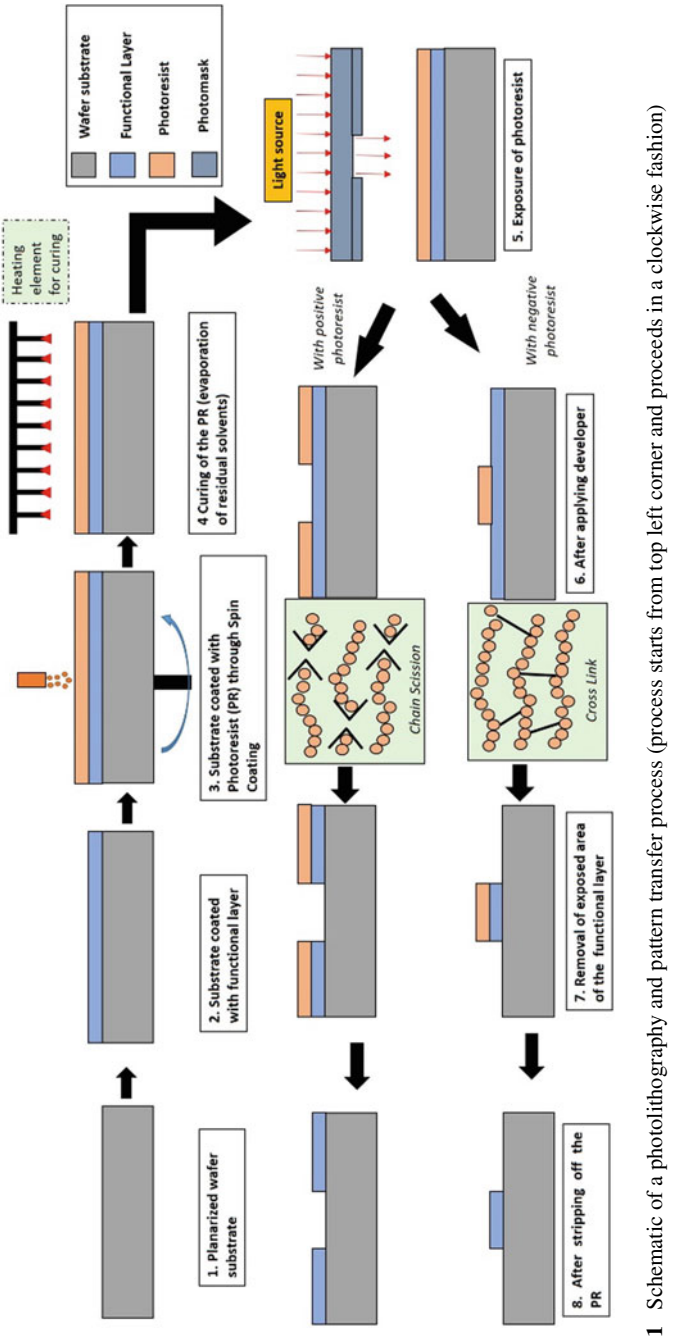

Fig. 1 Schematic of a photolithography and pattern transfer process (process starts from top left corner and proceeds in a clockwise fashion)

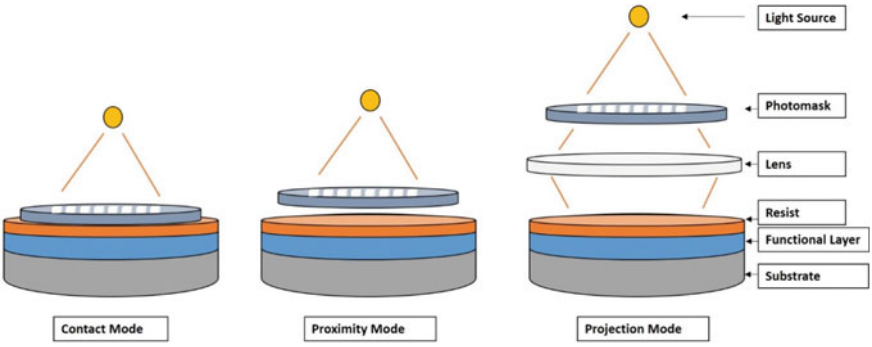

Fig. 2 Alignment of photomask relative to resist (from left to right): contact mode, proximity mode and projection mode

the exposed regions, the residual resist from the rest of the regions is also stripped off, and the end product is selectively patterned functional layer on the substrate.

One of the major important components of the photolithography process is the photomask. Photomask ensures that the exposure of the photoresist to the light is selective. The pattern which has to be made on the photoresist has to be first made on the photomask (the pattern on the photomask can be exact or reverse, depending upon the positive or the negative type of the polymer). Typically, the photomasks are made of optically flat glass, quartz plate or an absorber pattern metal (like thin films of chromium). Patterns on the photomask are generated through electron beam lithography. The mask can be aligned with respect to the photoresist coated wafer through three methods: contact aligner, proximity aligner, projection aligner. The schematic of the three processes is shown in Fig. 2.

In contact aligner, the mask is kept in direct contact with the substrate. Through this method, the transfer of patterns on to the photoresist is highly accurate but with repeated use the photomask can get damaged. Hence, the life of the photomask in this type of printing is quite less. To counter this, the masks can be lifted slightly above the photoresist by a distance of 10–20 μm. Although this method ensured the longevity of the photomasks, the replication of pattern in this case was not accurate and mostly some dimensional variations were observed.

The third method for mask alignment is the one in which optical elements are put between the photomask and the photoresist coated substrate. Through this, there is no direct contact between the photomask and the substrate, also there is an added flexibility of magnifying or de-magnifying the dimensions of the pattern during its transfer from the photomask to the photoresist. Projection mode of mask alignment is mostly used.

2.1 Accuracy Enhancement in Photolithography

In general terms, accuracy refers to the extent of match between the desired dimensions and the actual (or measured) dimensions. Ideally, the desired dimension and the actual dimension should be exactly equal and if it happens, the process is called 100% accurate.

Accuracy in context of photolithography refers to the degree of closeness between the dimensions of patterns on the photomask and the dimensions of pattern transferred on to the substrate. Accuracy is also needed in terms of alignment of the mask with respect to the substrate in case of projection printing, especially so, if more than one type of pattern is being fabricated on a large scale on the same substrate so that the relative location of the patterns on the wafer is accurate.

As discussed in the previous section, photolithography is a multi-step process so the accuracy in photolithography is affected by a number of factors like alignment of the mask with respect to the substrate, the process of stripping off of the residual photoresist, photoresist losing its fidelity in the subsequent steps after its deposition and curing, etc.

Few of the factors which affects the accuracy can be avoided simply by choosing the right type of chemical and following the correct procedure in the correct sequence. For example, if after spin coating the photoresist is allowed to cure for the required interval of time it will retain its dimension and shape throughout the process of photolithography [15]. This in turn will ensure that the dimensions of the pattern do not vary much from the desired values.

Mask alignment is the major factor which results in loss of accuracy when the process of photolithography is used for fabricating more than one type of pattern on the substrate or different types of patterns are to be made on different layers and the patterns are required to be made over a larger area. Errors in mask alignment can render a device incapable of operating, hence it is a critical issue in the photolithography process. For proper alignment of the masks with respect to the wafer, indicator marks are made on the wafer called as *Fiducial Marks*. The high resolution image of the photomask reticle is focused onto the substrate with reference to the fiducial marks by the projection lens. Applications requiring different types of patterns on different layers have fiducial marks with the mask number, which acts a guide while selecting the correct mask for the process and aligning it properly. The mask which is being used for the exposure acts as an indicator to of the extent till which the process has completed. Another feature which can help in improving the accuracy of the mask alignment is use of optical vernier patterns created on different layers of the deposited material and on the photomask which is to be aligned. It allows very precise alignment of the mask which exceeds the limit of dimension of the feature being fabricated. Different possible mask alignment errors in projection printing are shown schematically in Fig. 3.

Alignment issues become even more critical in the fabrication process of **3D micro electromechanical systems (MEMS)**. MEMS involves structures which have high aspect ratio as well as low degree of freedom and often times one is required to

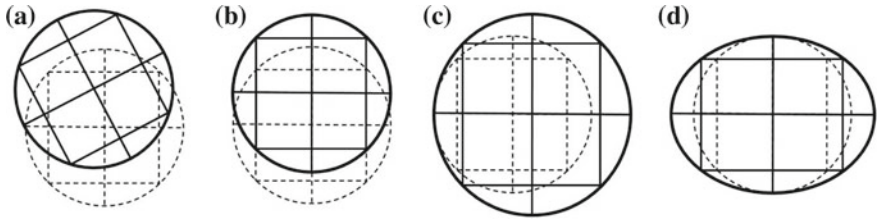

Fig. 3 Errors in projection printing **a** Rotation, **b** Translation, **c** Magnification, **d** Ovality

align 3D features on both sides of the wafer. One approach for proper alignment in 3D fabrication is using cross hair marks both on the wafer as well as on the mask. For the alignment, first the cross hair mark on the photomask is observed through a microscope and stored electronically. Then the wafer is loaded in its place and observed through the microscope and its position adjusted till the cross hair mark on the wafer coincides with the electronically stored cross hair mark of the mask. Another comparatively simple and relatively cheap way of ensuring proper alignment is by developing a three-pin jig on which the substrate can be placed; this will ensure proper positioning of at least two of its sides as shown in Fig. 4. By providing cross hair on the substrate and on the photomask, the accuracy of the alignment can further be enhanced. This is useful if only a single and similar type of pattering is being done on the substrate.

Planarization is another important consideration in photolithography process. If the deposited resist layer in not planar in its topography, the extent of exposure that the resist gets will be different. Thicker regions will be over exposed while the thinner regions will be under exposed. It is an important requirement to have plane surfaces after deposition of each layer, and not only deposited layers but the base substrate must also be planar in its topography to ensure accurate pattern transfer. A non-planar layer will also result in partially blurred projection of the photomask image onto the surface, leading to dimensional distortion and loss of accuracy in the final product as shown in Fig. 5. The problem increases while processing thicker deposited layers.

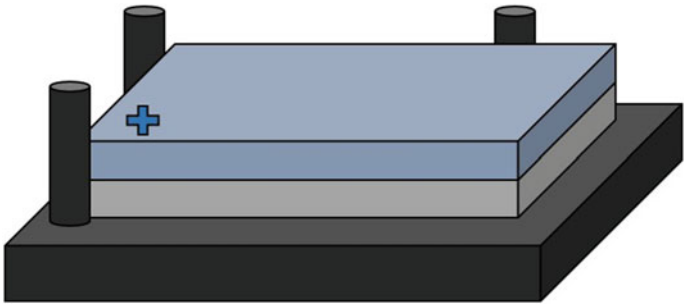

Fig. 4 Alignment jig for proper and quick alignment of substrate and mask

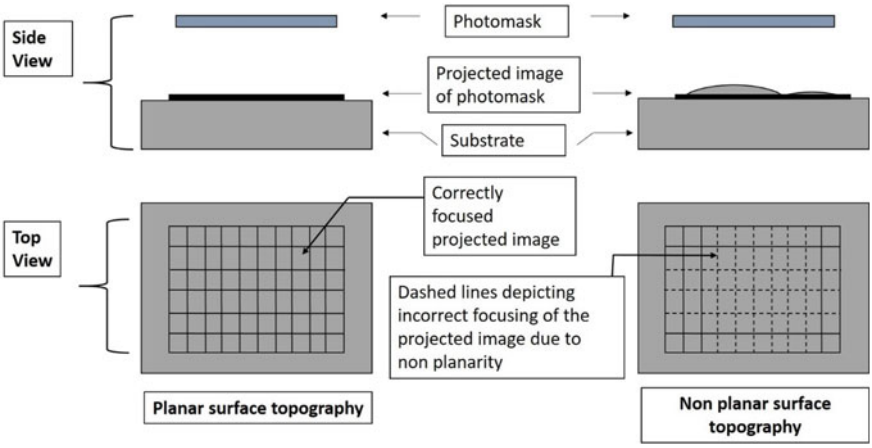

Fig. 5 Effect of non-planarity of the substrate one the focusing of the projected image

The **stability of the resist** during the development stage is an important consideration. As seen in Fig. 1, development is done by application of chemicals after the exposure stage. During development the regions exposed to light get chemically attacked and are removed from the surface of the substrate (in case of positive photoresist and reverse is true for negative photoresist). This is followed by selective removal of the functional layer through some other process. During the development stage, if the resist loses its stability it will result in erosion of some portion of the unexposed resist as well. During the removal of the functional layer, it may lead to inaccurate pattern dimensions. The resist may lose its stability due to swelling, resistance to chemical etching, etc. This can be overcome by choosing a resist with the proper chemical composition.

To obtain good dimensional control during the exposure stage, the image of the photomask being projected on the resist layer must remain in focus throughout the depth of the resist layer. This becomes an issue in case of thick resist layer. An out of focus exposure will result in inaccurate dissolution of resist in the developmental stage and will ultimately result in loss of accuracy in the process. This can be overcome by ensuring proper planarization of the substrate surface and the deposited layers. Also by using an exposure apparatus with high depth of focus the projection can be ensured throughout the depth. As can be seen from Fig. 6, in case of a resist layer with planar topography the focusing of the projected image from the photomask is consistent throughout the thickness of the layer, but in case of resist layer with non-planar topography the focusing is inconsistent as depicted through dashed lines.

Another factor which needs to be accounted for in photolithography is the **interference effect**. Thin film effects arises due to coherent interference between the incident light and the reflected light from the substrate surface. This results in a periodic intensity distribution throughout the thickness of the resist and causes intensity variations in a direction perpendicular to the resist film. This variation in intensity

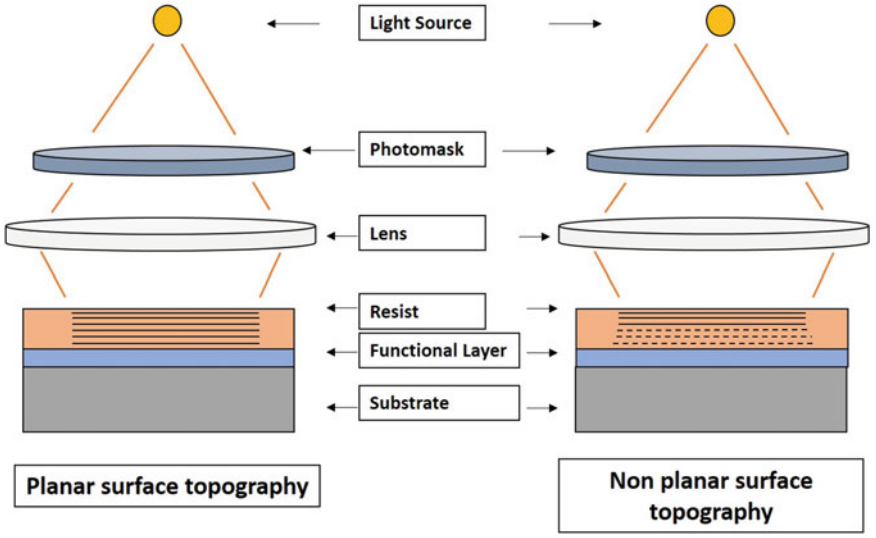

Fig. 6 Effect of non-focusing of the patterns through the thickness of resist layer during exposure

of the light during exposure stage results in periodic variation of the resist composition throughout the thickness and consequently the resist removal is not uniform in the development stage. As can be seen from Fig. 7, the interference effects result in formation of crests and troughs on the resist. The crests are the regions which are overexposed, whereas the troughs are the regions of underexposure of resist. All this manifests itself in the form of loss of accuracy during the stage when functional layer is to be removed. Thin film effects are observed when exposure is done through a monochromatic light; hence, it can be countered by using a broadband source of light.

Another feature that is used for accuracy improvement in photolithography is **optical proximity correction (OPC)**. It is a technique used for compensating the image

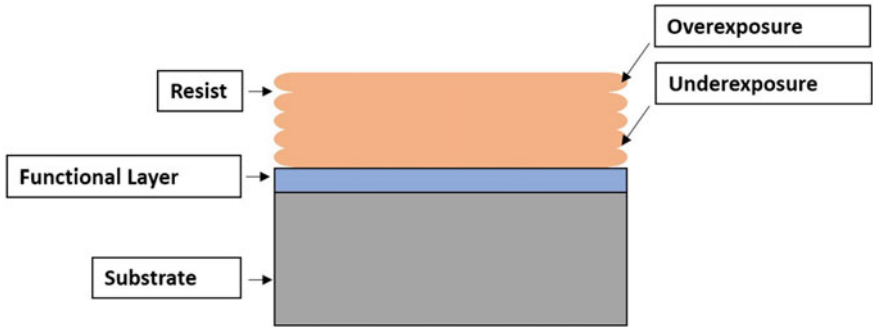

Fig. 7 Interference effect on the resist layer leading to overexposure and underexposure

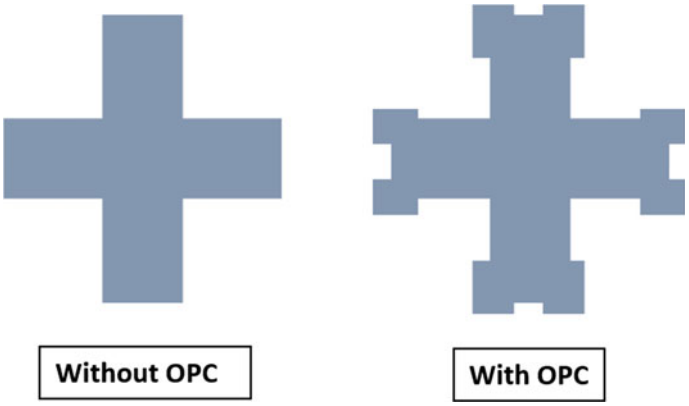

Fig. 8 Photomask with and without OPC

distortions that occurs during sub-wavelength photolithography. Sub-wavelength lithography is special class of photolithography in which the dimensions of the structures being printed are less than that of the wavelength of the light source being used. Presence of other features nearby to an existing feature will affect the optical behavior. As a result of which sharp features are blurred since higher spatial frequencies are lost due to diffraction. OPC helps in compensating for errors such as corner rounding, line-end shortening and changes in line width, etc. As can be seen from Fig. 8, OPC makes it possible to use sharp features on the photomask, while without OPC the features are relatively simple since complex and sharp features may not get transferred properly onto the resist.

2.2 Applications of Photolithography

Photolithography is extensively used in the fabrication of microscopic patterns on different types of substrate surface. It is commonly used for fabricating arrays of holes, projections, gratings, etc. Other than that it can also be used for fabricating specific structures like micro rotors, torsional ratcheting actuators, gear chains, etc. Such components are useful in miniaturized devices.

3 Reactive Ion Etching

Through photolithography, we can create a pattern of our choice on the photoresist layer through the series of steps as discussed in the previous section. Once the patterns have been created on the photoresist layer, the next step is to remove the exposed functional layer. Reactive ion etching is one such process through which

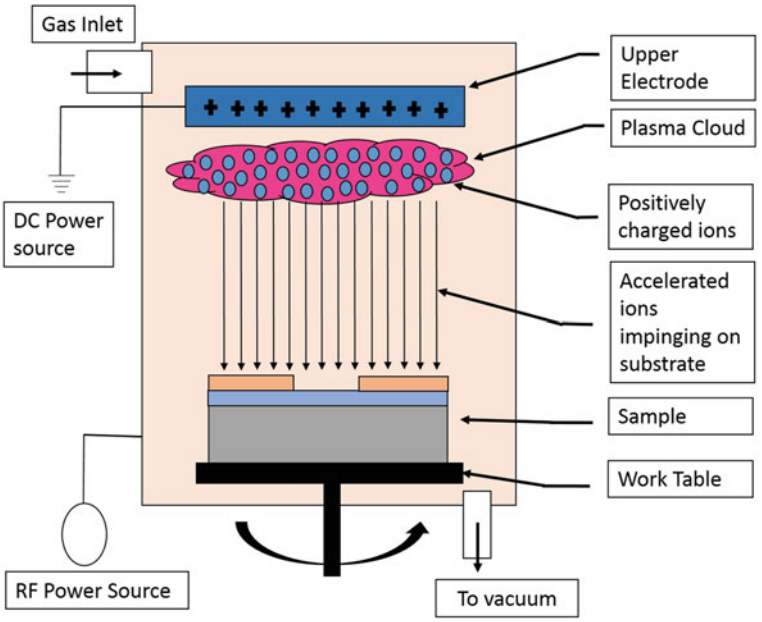

Fig. 9 Schematic of reactive ion etching

the functional layer can be removed from the top of the surface and thus a functional pattern of choice can be created on the substrate [16]. Reactive ion etching (RIE) is a dry etching process which removes the material from the substrate. The process of reactive ion etching (RIE) is driven by a plasma contained in a small chamber. The schematic for RIE is shown in Fig. 9. Initially a gas is fed into the chamber depending upon the type of material being etched. Different chemistry of gases for etching different types of materials is available in literature [17].

Initiation of etching gas into plasma is done by applying a strong RF electromagnetic field, in the order of 13.56 MHz [18]. The oscillating electric field causes ionization of gas molecules and removes electrons from them, creating a plasma. The free electrons travels vertically through the chamber in each cycle of the applied field, while the heavier, positively charged ions are unaffected by the electric field. Some electrons get absorbed in the wafer and results in build-up of a negative charge on its surface. This creates a voltage difference between the plasma and the wafer as a result of which the positively charged ions get attracted toward the negatively charged wafer, where they collide with the functional layer. The photoresist layer (modified with monomers from a CHF_3 additive [16]) or sometimes a thin layer of oxide acts as a sufficient mask against the incoming ions [19]. The ions can react chemically with the functional layer causing its removal and can also cause physical removal of the functional layer through sputtering (a momentum transfer process). Reactive ion etching allows more control over the structure that is being fabricated. In contrast to chemical etching, which is more isotropic in nature, RIE results in

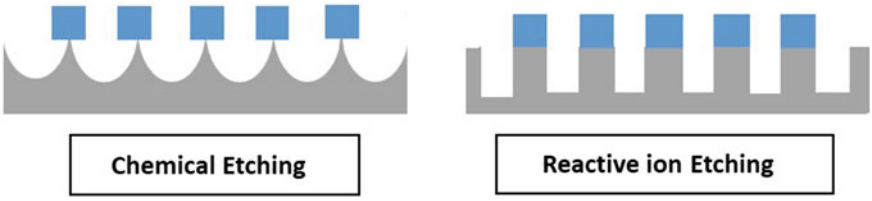

Fig. 10 Difference between chemical etching and RIE of a wafer

greater accuracy, control and directionality of the structures being fabricated as can be seen from Fig. 10.

3.1 Accuracy Enhancement in Reactive Ion Etching

Reactive ion etching is quite sensitive to a lot of factors which can result in errors or inaccuracies in the process. Several such factors are pressure inside the plasma chamber, power used, temperature of the plasma reactor, target materials, cleanliness, etc.

Doping of the target material influences the final etch profile. It is seen that N-type silicon etches faster and with more directionality as compared to p-type Si. The lateral etch rates of differently doped Si is different, hence through doping the profile shape can be controlled in trench etching of Si.

Temperature is an important factor in RIE. The temperature at the substrate surface may increase due to conversion of kinetic energy of the incoming ions into heat energy during ion bombardment or due to exothermic reactions at the substrate surface. This can be negated by providing surface cooling by circulating water around the target platen. Alternatively, cooling from backside can be done though helium. Uncontrolled temperature can alter the dimensions of the structure on a microscopic scale.

Dimensions of the trench being etched influences the etching time, which if not controlled properly will lead to incomplete or inaccurate etching. It is observed by different researchers that trenches with small openings etch at slower rates as compared to trenches with wider openings. This effect is also called **aspect ratio dependent etching** or ARDE. Effect of ARDE is seen as decreasing etch rates for longer etch times [20].

Another important factor in RIE is the **sidewall etching**. The main difference between RIE and other chemical etching processes is the directionality. Sidewall etching results in loss of directionality and the profile dimensions. It can be controlled by providing coating with a sidewall inhibitor.

When RIE is used for fabricating deep trenches the impingement of ions onto the substrate is no longer governed only by electrostatic forces, rather **diffusive forces**

also comes into picture to some extent. As a result of which the process no longer remains directional and the structure being fabricated is longer accurate.

Other factors which can influence the accuracy of the RIE process are applied voltage between the two electrodes which influences the depth of the trenches being milled, close monitoring of the plasma conditions which ultimately affects the process, etc.

One of the important requirements of the RIE process is repeatability of the output when the input is kept same. It means the same gas chemistry, pressure inside chamber, temperature of processing, applied electrode bias must result in the same output whenever it is used for the same substrate. This is ensured by a robust design of the equipment and close monitoring as well as control of the process parameters. As a rule, more robust the machine, the tighter is the process control window. Using higher gas flow, higher gas pressure, higher RF power and better gas utilization can improve the productivity of the overall process as well as its accuracy.

3.2 Applications of Reactive Ion Etching

The major use of RIE has been in the fabrication of high aspect ratio structures. RIE has been used extensively for fabrication of micro-electro-mechanical systems. By modifying the gas used in RIE, different profiles of sidewall can be created. Cl_2 results in wider top than bottom (positive slope) while SF_6/CCl_2F_2 results in negative slope [21].

Diamond waveguides were fabricated by reactive ion etching using oxygen plasma and the mask is removed through a hydrofluoric acid [22]. RIE has also been used for fabricating large area multi crystalline silicon solar cell. SF_6/O_2 RIE has been used for the texturing process. Performance of such textured solar cells is found to be better in comparison with chemically etched silicon wafers [23].

4 Deep Reactive Ion Etching Process

As discussed in the previous section, reactive ion etching suffers from several limitations when it is applied for fabricating deep trenches. A variant of the process called deep reactive ion etching (DRIE) has been developed which is capable of fabricating very deep tranches and high aspect ratio structures. The process of DRIE can be divided into cryogenic DRIE and the BOSCH process.

Cryogenic DRIE:

It aims at slowing down the chemical reaction at the substrate surface by artificial cooling using either liquid N_2 or Helium cooling. The wafer is cooled down to a temperature of ~110 °C. While the chemical reaction is slowed down, the incoming ions continue to bombard the substrate surface and the etching it away. Since the

chemical reactions have been arrested by the cold temperature the chances of sidewall erosion is very less in this process, as a result of which very high aspect ratio surfaces are produced.

The major issue with the cryogenic DRIE, which can ultimately affect its accuracy, is the stability of the masks (photoresists) on the surface. Some masks have a tendency to crack under the very low temperature of the process. Also due to the low temperature the etch by-products have a tendency to get deposited on the nearest cold substrate that is available to them. Mostly, the etch by-products get deposited on the substrate or the electrode and the dimensions of the final pattern get altered.

BOSCH process:

BOSCH process is named after the German company Robert Bosch GmbH which patented the process. It works by alternating between two modes during the operation:

a. A standard etching through ions. This is similar to the process of reactive ion etching.
b. Depositing a chemically inert passivation layer onto the substrate.

Each of the two modes of operations lasts for few seconds each. The chemically inert layer is deposited throughout the substrate, but during the etching phase the incoming directional ions attack only the bottom of the trench and not the sidewalls. Thus, the etch profile is vertical and highly isotropic. This feature makes this process suitable for fabricating high aspect ratio structures [24].

The major difference between RIE and DRIE is the etch depth. While in case of RIE general etch depth is of the order of 10 μm at an etch rate of 1 μm/min, in case of DRIE the etch depth can be up to 600 μm or even more (based on conditions) with etch rate up to 200 μm/min. Aspect ratio as high as 30 or more can be obtained in DRIE of silicon, a feat that is not possible through RIE [25].

4.1 Accuracy Enhancement of DRIE

The basic operating parameters and conditions for DRIE are same as that of RIE. And both the processes suffer from almost similar problems and limitations, which have been discussed in previous section. But DRIE has a very specific and unique problem owing to the process route. It is the presence of **scallop-like structure** on the sidewalls as seen in Fig. 11.

This occurs due to the alternation between etching and passivation modes. After the first cycle of etching, when passivation of the surface is done, the chemically inert layer covers the entire surface of the substrate. In the next etching cycle, the incoming ion attacks the base of the substrate and predominantly etches away the material from the center but not from the sides. So a micro scale projection remains at sides. This entire sequence is repeated throughout the process.

It is periodic in nature and accounts for sidewall roughness. In critical applications like submicron-sized resonators, such scallops are not acceptable and if present they tend to deteriorate device performance. Increasing the cycle time results in increased

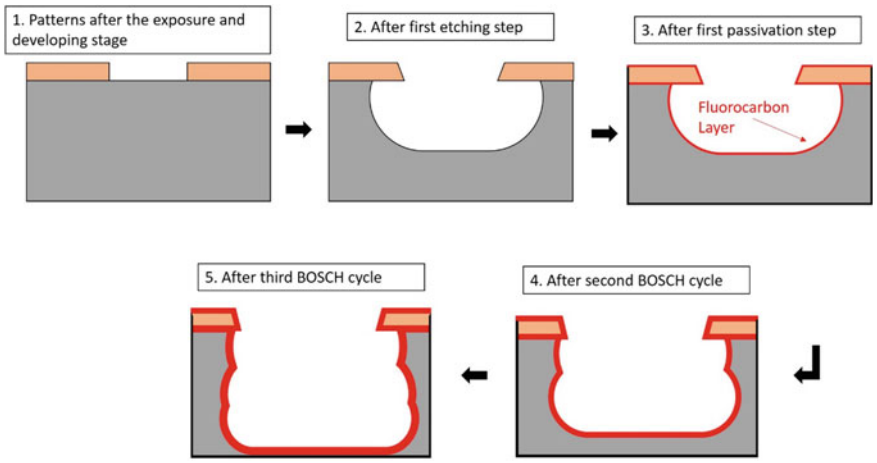

Fig. 11 Schematic of scalloping in DRIE [26]

etch rate but it also pronounces the scalloping effect. Using ultrafast passivation gas pulses of ~100 ms duration and etching cycles of 1–2 s can produce structures with almost no scalloping. But due to this, the overall process becomes highly sensitive toward micro masking by all kinds of surface contaminants which can increase the surface roughness at the bottom of the trench [27]. Another characteristic feature from DRIE is the **notching effect**. It is observed during the DRIE of Si on a silicon oxide surface. When the plasma etching reaches the insulator surface charging of the interface leads to ion deflection and ion-enhanced sideways etching, resulting in structures as shown in Fig. 12 [28].

The incoming electrons get trapped by the sidewalls of the structure while the positive ions, being highly directional, impinges at the bottom of the trench. A part of the incoming ions gets stuck and accumulates at the trench floor. This leads to formation of an electric field between the positively charged trench floor and the negatively charged silicon sidewalls. This electric field redirects the incoming ions

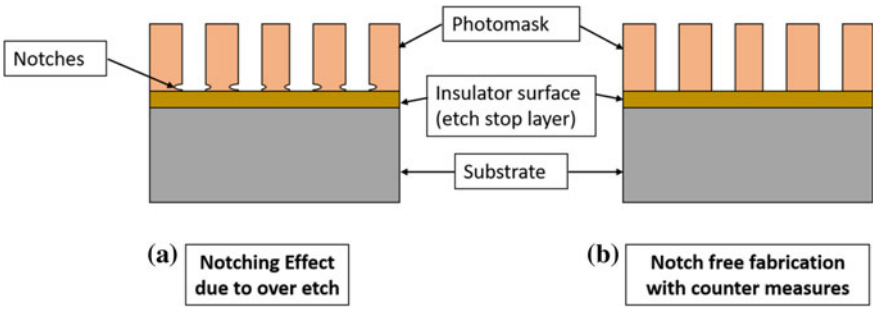

Fig. 12 Notching effect as compared to notch free fabrication

to the sidewalls at the interface between silicon and the dielectric and results in formation of notches as shown in Fig. 12a [29]. Formation of notches results in inaccurate fabrication and makes the fabricated structures unsuitable for any kind of application, since the structures with notch at their bottom are mechanically very weak.

Since formation of notches is due to charging of the substrate, the solutions for this effect aim at reducing the charge separation in high aspect ratio structures. One way of addressing the problem is through **pulsing the bias on the substrate** which gives the accumulated charges a chance to neutralize and prevent the build-up of an electric field. More efficient solution is **pulsing the plasma source power**. Switching off the plasma periodically allows the electrons to reach the bottom of the trench and effectively neutralize the accumulated positive charges [30]. The notch free structures are shown in Fig. 12b. Few other variants of the DRIE system which improves the performance have also been developed. These variations make possible the fine tuning of different aspects of the DRIE process. Some modern variants of DRIE systems have an **optical emissions spectroscopy (OES)** as one of its functional elements. OES can be used to detect and analyze the light emitted from a plasma source which is then used for deducting the information regarding the physical and chemical state of the plasma. This is helpful in determining the plasma process termination time and prevents any possibility of over etching. Conventional DRIE system exhibits a sudden change in pressure when switching between passivation and etching step. This sudden change of pressure is also termed as "pressure burst." Modern DRIE systems are equipped with a closed-loop-based **hold and release pressure control** which eliminates the sudden change in pressure and ensures very reproducible and stable process.

4.2 Applications of Deep Reactive Ion Etching

DRIE has been used for fabricating Bragg reflectors. Since such structures are used in optical applications, a very smooth surface and sidewall finish is required to be produced. The process have been optimized for a slower etch rate but with minimum scalloping effect [27]. By changing the DRIE gas chemistry, it is possible to obtain sloped sidewall angles [31]. Positively sloped sidewalls are useful in casting and imprinting applications where the master has to be detached from the molded piece. A negatively sloped sidewall can be connected to fluidic devices [32]. DRIE has also been used in the fabrication of low loss fiber optic switches [33] and silicon couplers for microfluidic applications [34].

5 Focused Ion Beam Fabrication

Focused ion beam (FIB) fabrication makes use of a stream of highly focused ions, which are derived from an ion source (mostly a liquid metal ion source is used like Ga) and are accelerated by a strong electric field. The ions are focused using a series of electrostatic lenses. This accelerated and focused stream of ions are made to impinge on the substrate to be processed. When the incoming stream of ions collides with the substrate surface it transfers its momentum to the atoms of the substrate surface and displaces the atoms from their lattice sites. Thus, the process of material removal is caused through momentum transfer. This phenomenon is also known as sputtering. It is schematically shown in Fig. 13. The main advantage of FIB over other processes is that it is a maskless, direct-writing process which can be used for fabricating structures of any given geometry both at micro as well as nano scale.

5.1 Accuracy Enhancement in FIB

FIB is an inherently very high accuracy process. It can fabricate structures in the order of few nanometers with very high degree of repeatability. Also the entire process of material removal is through physical means, so the complete process can be closely controlled and very high degree of accuracy can be maintained.

The major reason of the very high accuracy and repeatability of the process is the equipment used for FIB. The FIB machine has three main parts: the ion source (which is also called liquid metal ion source of LMIS), ion optics column and stage control. LMIS is a metallic cup filled with Ga through which a W needle is passing. The source material, i.e., Ga in this case is heated through electrical heaters provided in the cup. Ga melts at ~30 °C. The molten Ga moves to the edge of the W needle through capillary action. An **extraction electrode** is provided right at the tip of W

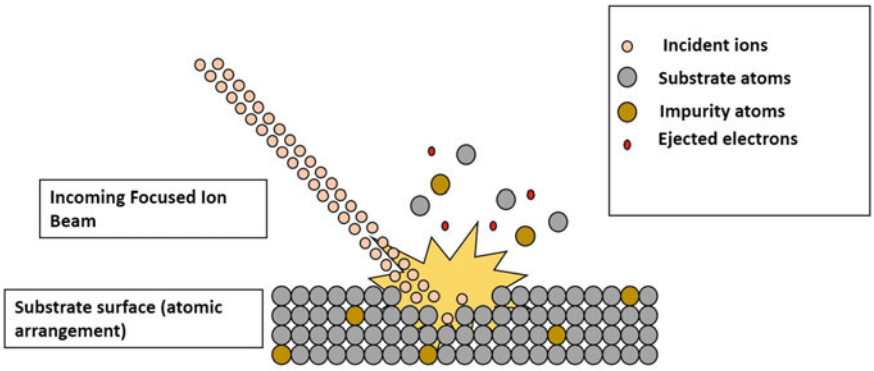

Fig. 13 Schematic of sputtering process

needle which applies a strong electrostatic field at the tip. The molten drop of Ga tends to form a conical shape under the influence of the electrostatic field due to the high force density. The cone of the molten Ga is called as Taylor cone [35]. Typically, a very high extraction voltage of ~7000 V is applied at the tip of the electrode which results in extraction of Ga ions from the tip of the cone. A **suppressor** is provided between the W needle tip and the extractor electrode. By controlling the ratio of extraction voltage and the voltage on the suppressor, the flux of extracted Ga ions from the W needle tip can be controlled.

The Ga ion stream, thus extracted, is made to pass through series of apertures and focusing elements, so that by the time it actually impinges on the substrate surface its diameter has been reduced by several orders of magnitude. **Electrostatic lens** does the first focusing which basically reduces the diameter of the Ga ion stream. Below the electrostatic lens is a long and thin tube called as **drift tube**. This eliminates the ions that are not directed vertically. This helps in ensuring that the fabrication process is highly exact and the desired dimensions are closely controlled. It is followed by a stigmator. **Stigmator** maintains the circularity of the ion stream and helps in proper focusing at the substrate. If the stigmator is not working properly, then the ion beam will not be focused and the structures which are being fabricated on the substrate will also be inaccurate. After stigmator, the ion stream is made to pass through aperture. **Aperture** controls the size of the beam based on the beam current that is used in machining process. For FIB machining with higher beam current the beam diameter is high, since aperture of bigger diameter is engaged while for FIB machining at lower beam current the beam diameter is less, since lower aperture size is engaged. It is well known from several experiments that FIB processing at higher beam current (higher aperture size) results in higher material removal rate (MRR) but the accuracy of the patterns is low and the reverse is also true. So in order to obtain highly accurate structures it is recommended to operate the FIB at lower aperture sizes. After the beam size has been controlled by the aperture, the Ga ion stream passes through octopole. **Octopole** is basically a set of eight lenses which have been arranged in an octagon. Its function is similar to that of stigmator. In some variants of FIB, octopole is also called as **lower stigmator**. The terms octopole and stigmator are also used interchangeably across various literatures. After octopole, the Ga ion beam goes through deflector and deflector aperture. The **deflector** controls the movement of the beam within the field of vision. For fabricating structures using FIB, first a drawing of the structure is created using basic CAD tools provided as part of the operating system of the FIB, within the field of vision (as seen from a SEM which is generally a part of the FIB system). As per the drawing made, the ion beam will be deflected by the deflector to carry out the material removal. If the structures are to be repeated outside the field of vision, the ion beam has to be stopped and the stage has to be moved to the next location to position itself at the next starting position.

For example, if a series of micro holes are to be fabricated on a Si substrate, the stage with the Si wafer will position itself at the starting position. The Ga ions will be deflected by the deflector to fabricate the structure as per the CAD drawing in the field of vision. Once it is done, the ion beam has to be stopped and the stage has to be moved to position itself at the next location where the structures will be fabricated

as controlled by the deflector. The last element in the FIB column is the **second electrostatic** lens which reduces the spot size of the beam and helps in improving the focus of the beam. The stream of ions which have been focused and accelerated through the series of elements is finally made to impinge upon the substrate on which material removal has to be done. The substrate is mounted on a **high precision stage** which can move in three directions X, Y and Z, can rotate 360° and can be tilted from −15° to 60°. The uncertainty in rotation repetition is of the order of 0.09° while the uncertainty in tilting repetition is around 0.03° [36]. Schematic of the FIB machine is shown in Fig. 14.

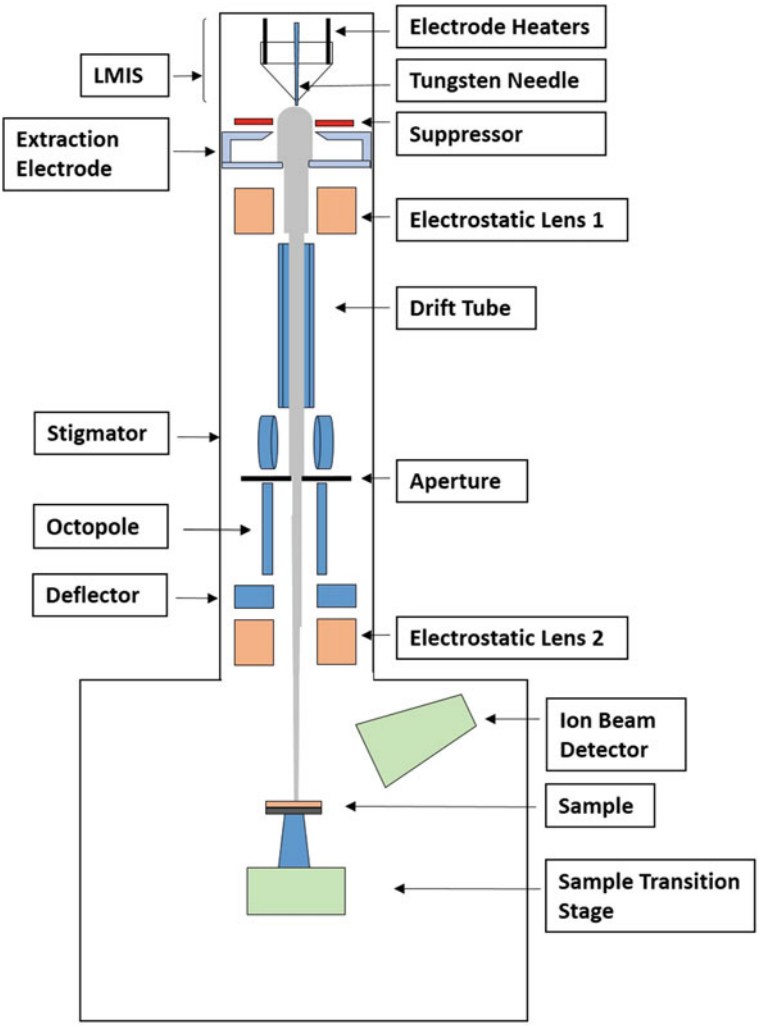

Fig. 14 Schematic of FIB set up

As can be seen from the discussion above, the FIB machine is constituted of number of high precision elements, and if operated as per guidelines, there is very little scope of any inaccuracy in the FIB fabrication of micro or nano scale structures [37].

The chief process parameters which affect the quality of machining and structure fabrication in FIB are beam current, beam voltage, percent overlap and dwell time. The beam diameter is smaller at higher values of beam voltage, so for fabricating very small structures it is recommended to use high beam voltage and lower beam current. Using such setting will nevertheless increase the overall machining time but the structures fabricated will be highly accurate. Controlling the input parameters become more critical while fabricating nanoscale structures where minute variations in input parameters can change the dimensions.

One important process feature in FIB which can affect the final dimensions is **redeposition**. Redeposition is the phenomenon in which the atoms sputtered from its lattice locations get deposited at the bottom of the cavity being machined. In some cases, the sputtered atoms are deposited at the edges of the cavity or trench getting milled, as a result of redeposition the depth of the trench being milled is less than what it should be (as per the beam current and beam voltage) and bottom surface roughness is high. Also the edges of the cavity being milled is rounded and not accurate as per requirement. The difference between FIB machining of a cavity with and without redeposition is schematically shown in Fig. 15.

Redeposition can be avoided by increasing the number of passes of the ion beam over the trench or cavity being milled [38].

Few general things which must be kept in mind while operating FIB are:

- The samples should be clean and free from any dirt/dust. Since FIB operates in a vacuum environment, presence of any kind of dust or dirt will result in the contaminants entering the ion column (owing to the vacuum) and damaging it.
- For accurate fabrication of structures using FIB, the sample/substrate surface should be plane; otherwise, the fabricated structures will be slanted in a direction and will not be as per requirement.

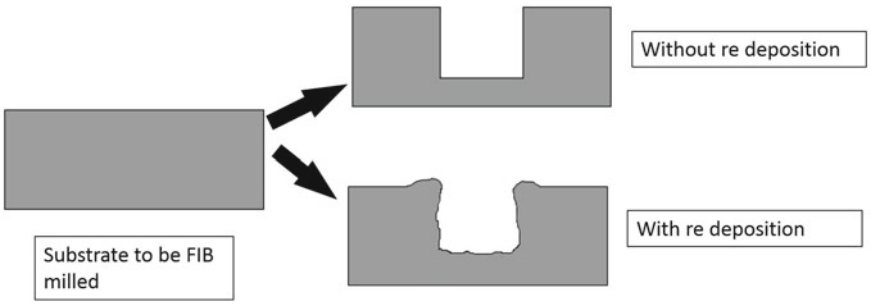

Fig. 15 FIB milling of a cavity with and without redeposition effect

- FIB can result in some degree of ion implantation within the substrate as well. So if after FIB fabrication, the sample needs to be processed thermally or chemically; suitability of FIB must be checked before using it. For example, FIB machining of Si at lower angles of incidence results in implantation of Ga ions inside its surface. If such Si wafers are thermally processed at a later stage, the Ga tends to move out of its implanted location and results in damage to the structures which have been already fabricated.
- The stigmator in the ion column should be calibrated periodically. Improper calibration of stigmator results in the beam losing its circularity and ultimately its accuracy in the fabrication of structures.

5.2 Applications of FIB

Major application of FIB is in fabrication of nanometric scale structures but it has been utilized in fabrication of micron scale structures as well. FIB milling has been used for creating microstructures on diamond tools which were then used in micro lathes for performing operations like micro cutting, etc. Different types of geometries have been machined on tool materials such as tungsten carbide, high speed tool steel and crystalline diamond, etc. [39].

FIB has been used for creating micro end mill cutter which is then used for micro end milling operations for applications such as creating channels and grooves on a planar substrate. Although fabrication of micro end mill cutters has been attempted through mechanical grinding but the cutting diameter through this approach is in the range of 45–100 μm [40]. Through FIB fabrication, cutting edge diameters below 25 μm can be obtained. Also the number of cutting edges can be directly controlled through this process [41]. FIB has also been used for producing micro cavities which are later used for micro replication, a process which is a combination of FIB and LIGA termed as FIB LIGA process [42]. The capabilities of FIB make it a suitable candidate for machining at nanometric scale [43]. FIB has been used for fabricating nanometric cavities which were then used for nanoreplication [44], patterning metallic nanostructures for ion-beam induced dewetting [45], nanohole arrays, etc.

6 Electron Beam Lithography

Electron beam lithography (EBL) is a maskless fabrication technology used for fabricating nanometric scale structures on substrates. Process of EBL is almost similar to that of photolithography, with only difference being the exposure stage. Similar to photolithography, EBL also starts with coating a layer of polymer on the surface of the substrate. Typically, a layer of poly methyl meth acrylate (PMMA) is coated

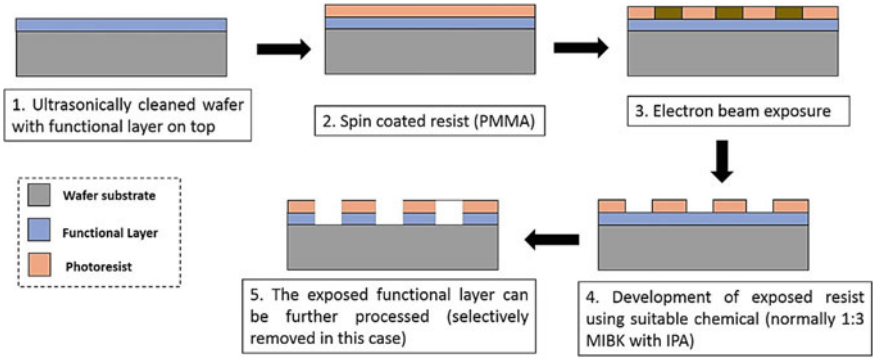

Fig. 16 Schematic of the EBL process

onto the substrate. The layer can be few hundreds of nanometers thick which is cured through two-stage baking, in an oven. This is followed by exposure of the photoresist.

While in photolithography, exposure of the resist-coated substrate is done through a photomask, in EBL the electron beam directly impinge onto the substrate as per a pre-defined pattern. The pattern in which the beam of electrons impinge onto the substrate is to be fed into the controller prior to the start of the operation. The pattern to be generated on the resist is prepared initially using commercially available CAD software, which is then converted into a format that is usable by the e-beam writer. The e-beam is then scanned onto the resist surface. Practically any kind of pattern can be transferred onto the resist. Similar to photolithography during the exposure stage, the portion through which the electron beam passes is altered, and depending upon the tone of the resist (positive or negative tone), the exposed or the unexposed portion is removed. After exposure, the EBL patterned sample is developed. If the resist layer is PMMA, an 1:3 mixture of methyl isobutyl ketone with isopropyl alcohol is used as a developer. After developing stage, through holes are formed in the resist layer which expose the functional layer underneath for further processing. The schematic of the process is shown in Fig. 16.

Once the functional layer is exposed through a pattern on the resist layer, further processing can be done which can be removing the functional layer or adding some other layer in a selective fashion. The major benefit of the EBL process is the maskless exposure step. Rather than using a mask for selective exposure of the deposited layer, the electron beam is made to impinge directly onto the resist as per a set pattern. This makes the EBL process much more versatile as compared to photolithography process. Since the photomask is not required, the steps required for the fabrication and alignment of the photomask along with the related possible errors are eliminated. Also any changes in the required pattern can be effected by simply changing the input design to the EBL controller. The minimum size of the pattern that can be transferred onto the substrate is much smaller in case of EBL as compared to photolithography since electron beam can be focused more tightly as compared to light.

6.1 Accuracy Enhancement in EBL

The EBL system comprises several subsystems like electron column, digital electronics to store and transmit the pattern data, high vacuum system, high precision XY stage and an extensive software system to control all the subsystems and to make them work in synchronization. Like FIB, the EBL process is inherently highly accurate with very little scope of error. But still some error can creep into the process. Error in the EBL process, if any, manifests itself in the form of inaccurate dimensions of the fabricated patterns.

There can be several factors which results in inaccuracy in the EBL process, few of which are listed below:

(i) The electron beam is deflected over the sample surface for carrying out the targeted exposure. The deflection coils and the deflection plates may have an inherent error in their set up, which is called as **average deflection distortion**. Due to the distortion, the focusing of the electron beam may not be proper which will ultimately result in fabrication with a loss of accuracy.

(ii) The resist layer on top of the sample is generally a polymer, which is not very conductive. During the exposure stage, the incoming stream of electrons may get accumulated on the surface of the polymer sample and repel the further incoming of the electrons. This is called as **charging effect** and because of it the exposure may not be proper.

(iii) As the stream of electrons impinge on the substrate and penetrate inside the resist, it may experience forward scattering (low angle scattering). Because of this the diameter of the beam increases once it enters the resist layer. If the patterns are very tightly located, it will result in variation in the dose that each pattern will receive, owing to the location of similar patterns nearby. This variation in the dose arising from the nearness of other patterns is called as **proximity effect**. It results in non-uniform exposure of the resist.

(iv) **Backscattering** of the electrons may cause an additional exposure of the resist a significant distance away from the point of desired exposure. Depending upon the type of substrate and the energy of the incident beam the electrons are backscattered through different distances.

(v) As the beam of incident electrons pass through the resist layer, their energy is dissipated in the form of **secondary electrons**. They are responsible for the actual bulk of the resist exposure process. Effect of the secondary electrons can be seen as increase in the size of the patterns after developing, as compared to the size in which they were written.

(vi) **Fluctuations in the dose** of the electron beam during the exposure stage. Dose is defined as charge incident per unit area of the resist. If the dose during exposure is not uniform, it will result in non-uniform reaction in the resist which in turn will lead to variations in the resist profile within the exposed section. This will ultimately manifest itself by improper removal of resist during the development stage.

(vii) **Electromagnetic noise** resulting from improper shielding of the EBL setup may cause beam wandering. It may result into random errors in the pattern placement.

(viii) EBL being a highly sensitive process must have mechanical vibration isolation as well. **Shocks or vibrations** from the operator movement during the exposure process can also result in random errors.

Some errors are predictable and repeatable in nature which can be avoided simply by making few changes in the design or the process parameters. The average deflection distortion can be minimized by using **double magnetic deflection** with a pair of matched coils. Such a system, although slower than the electrostatic system of deflection, will be less prone to inaccuracy. The charging effect can be avoided by coating a thin (~10 nm) layer of gold or silver on top of the resist before putting it in for exposure. The proximity effects and the effects of backscattering can be avoided by choosing a suitable design of patterns (with distance between the patterns as much as possible) and using a resist of suitable chemical composition and thickness. Some of the errors are, however, unpredictable and non-repeatable like fluctuations in the dose, mechanical jitters and electromagnetic noise, etc. But such errors can be corrected with automated measurement, computation and correction. To minimize such errors and iterative process of measurement, deduction and reduction has to be followed.

6.2 Applications of EBL

The stream of electrons is also the smallest known pencil that can be used in fabrication. EBL has been used mostly for fabricating nanometric scale structures [46]. EBL has been used to fabricate precisely controlled nanostructured substrates used for the studies in surface enhanced Raman spectroscopy (SERS) [47]. For the fabrication purpose, PMMA was used as the resist and the electron beam energy was 50 keV with a beam current of 50pA. A 7:3 volume of isopropyl alcohol and deionized water was used as developer after the exposure. EBL has been used for fabrication of Fresnel zone plates for hard X-ray applications. Structure widths as low as 50 nm and a width of 600 μm were fabricated using this process [48]. The complete set of experiments were conducted at 50 keV.

7 Advanced Characterization Methods

As seen from the preceding discussions, the surface micromachining technologies have been constantly pushing the minimum feature sizes to lower and lower dimensions. Thus, it is but natural that alongside fabrication processes the characterization methods must also evolve so that the fabricated structures can be inspected properly

prior to putting it into operation and even during its use. In Sect. 3, characterization methods have been discussed which are capable of characterizing structures at different scales of fabrication.

7.1 Stereo Zoom Microscope

It is basically an optical microscope which is used for observation of samples in low magnification. The major difference between conventional microscope and stereo microscopes is that the former used transmitted light through the sample while stereo microscopes make use of light reflected from the sample surface [49].

The schematic of the stereo microscope is shown in Fig. 17.

Contrary to conventional optical microscopes, stereo microscopes provide two separate optical paths for the left and right eyes thus providing two slightly different viewing angles. This arrangement produces a 3D visualization of the sample being examined, as opposed to the 2D images produced by conventional optical microscopes. The stereo microscopes have larger working distance and depth of field as compared to conventional microscopes which make it useful for examining relatively large solid objects. The zoom feature on the stereo microscope provides a range of viewing possibilities. It allows quick shift from low to high zoom. The sample can be viewed in the entire field of view and then a particular area of interest can be selected and zoomed for closer inspection.

Stereo microscope magnification is calculated by taking into account several variables: eyepiece magnification, built-in objective lens magnification and auxiliary lens

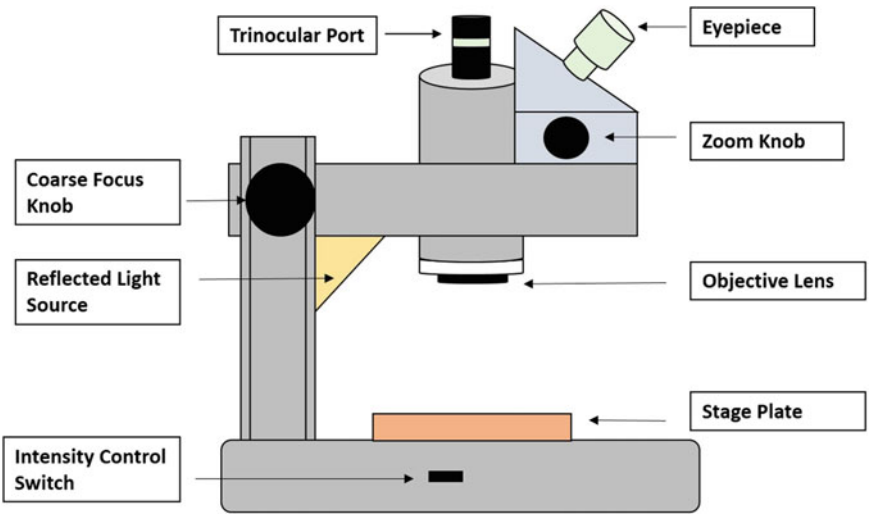

Fig. 17 Schematic of stereozoom microscope

magnification. To calculate the overall magnification, the magnification of all these lenses has to be multiplied and the resultant product will be the overall magnification of the microscope. For making measurements using stereozoom microscope, an eyepiece reticle is used [50]. When the image is viewed through such an eyepiece, the reticle is superimposed on the image under observation. Using the reticle, measurements can be made directly on the sample image under consideration. Some modern variations of stereo microscopes come with an image-processing module. The images taken through the stereo microscopes can be observed directly in a computer screen and measurements can be made on the screen using the toolbox which is provided with the microscope. One of the benefits of this approach is that one can take the images of the sample earlier and make the measurements later. Also a digital copy of the image can be obtained for later use.

7.2 Scanning Electron Microscopy

Scanning electron microscopy or SEM is the most common tool which is used for observing and characterizing micro machined surfaces. It comprises an electron column which has an electron emission source followed by a series of focusing apertures and beam manipulating elements. Commonly, tungsten and carbon filaments are used as electron emitters. In some variants of SEM, LaB_6 is used as the electron emitter to increase the life of the electron emission gun. Older versions of SEM operate on the principle of thermal emission in which the electron emitting filaments are heated to a high temperature which results in emission of electrons from the tip [51].

Most modern SEM nowadays are designated as **field emission scanning electron microscopes (FESEMs**). FESEMs operate by expelling electrons from the tip of the emitter by applying a very strong electric field which are then focused by the elements in the electron column. FESEMs typically use a zirconium oxide emitter. The electron column has elements like focusing lens also called as condensers, variable aperture to control the beam current, stigmator for maintaining the circularity of the beam, deflection coils for scanning the electron beam over the area to be characterized, secondary electron detector and backscattered electron detectors. The general schematic of the SEM system is shown in Fig. 18.

The elements in the electron column focus the emitted electrons into a stream and make it to impinge upon the substrate. The stream of primary electrons impinges upon the substrate in a set pattern, and through the exchange of energy between the incident electrons and the atoms of the substrate different signals are generated such as backscattered electrons, Auger electrons, secondary electrons, X–rays, etc. These signals are collected by a detector and a morphological image of the substrate under consideration is formed and displayed on the digital screen which is a part of the SEM system. Mostly an Everhart-Thornley detector is used for collecting the secondary electrons and the backscattered electrons. Spatial resolution in a SEM depends upon beam spot size and the volume of material with which the electrons interact.

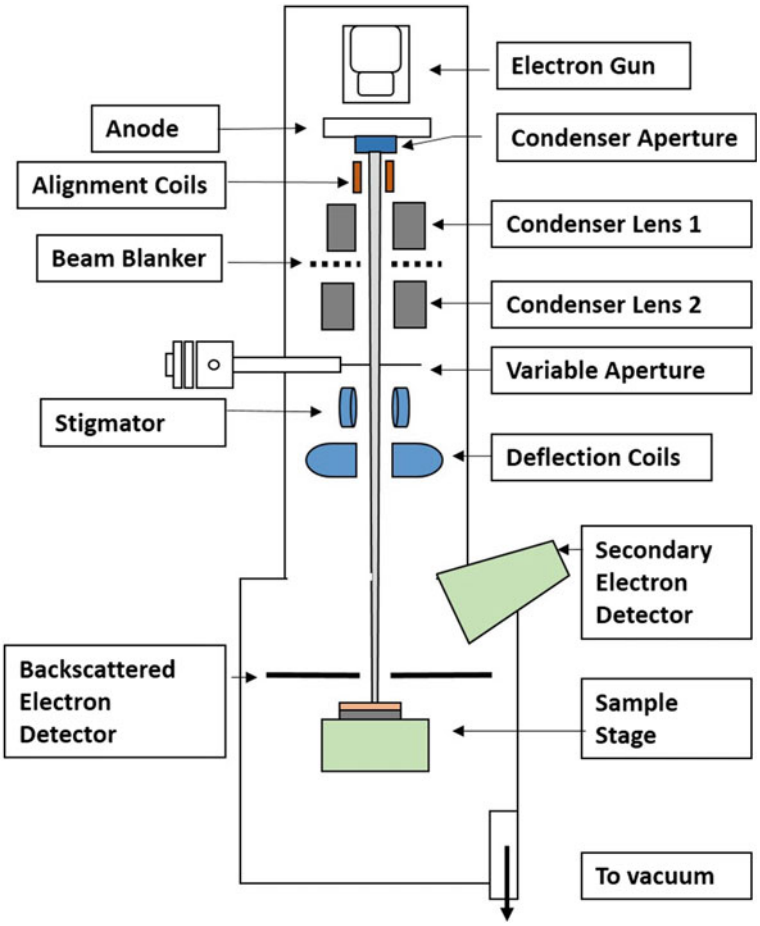

Fig. 18 Schematic of scanning electron microscope

When used with proper input parameters such as high accelerating voltage, properly aligned apertures, no stigmatism, small and highly focused spot size and no sample charging, resolutions as low as ~3 m can be achieved using a SEM. One limitation of SEM is that it is applicable only for conducting samples. If a non-conducting sample is attempt to be imaged using SEM, it will result in accumulation of electrons on its surface. The accumulated electrons will prevent further electron from impinging on the substrate and generating any signal which can be processed. This is called as **charging effect**. In order to prevent charging effect, the non-conducting samples must be coated with a thin layer of highly conducting metal prior to imaging [52].

The image obtained through a SEM has an associated scale bar at the bottom. The scale bar is a function of the magnification at which the image has been obtained. The SEM image can be opened in any image-processing software for making the

measurements. The scale bar can be used as a reference for setting the scale in the image. It basically provides a relation between the number of pixels in the image and the corresponding distance in the image. Some SEMs are provided with basic measurement facility and basic dimensions such as length and distance can be found directly from the image. Some advancements made in SEM are discussed below.

Environmental SEM (ESEM) is a variant of SEM which can be used for observing living biological samples. ESEM was developed because conventional SEMS requires the sample to be put into a vacuum, so the samples which can produce vapor are not fit to be examined using SEM. Samples like wet biological samples, oil-bearing rocks, etc. must be cryogenically frozen prior to observation. In ESEM, the chamber is evacuated of air but the vapor is maintained at its saturation pressure and the residual pressure is relatively higher. This was possible when a secondary electron detector was developed which was capable of operating in presence of water vapor and pressure-limiting apertures with differential pumping to separate the vacuum region from the sample chamber [53].

The images generated through SEMs are normally in gray scale. They do not produce any color. This creates a problem while imaging complex systems where a distinction is necessary to be made [54]. For example, in biological systems with drugs, for this purpose, a system is developed which is known as **density dependent color SEM (DDC-SEM)**. This is made possible by using multiple detectors to gather more information per pixel. As a common example, secondary electron and backscattered electron detectors are superimposed and a color is assigned to each of the images captured. The topographical information of a DDC-SEM image is obtained by the secondary electrons while the information about density is obtained from the backscattered electrons. The end result is a combined color image where colors are dependent on the density of the components.

7.3 Scanning Tunneling Microscopy

Scanning tunneling microscopy (STM) makes use of a metallic tip (usually tungsten, gold, carbon nano tube or an alloy of Platinum-Iridium is used as the tip) which is scanned over the substrate to be characterized. The tip is few atoms in thickness, and when it is brought sufficiently close to the surface being characterized there comes a position when there is an equilibrium between tip attraction and repulsion (typically in the range of 4–7 Å). At this position, the bias between the substrate to be characterized and the tip results in flow of electrons between the two. This flow of electrons between the tip and the substrate through the air barrier between them is called as **tunneling effect** [55].

The current flowing between the tip and the substrate is a function of distance between the tip and the substrate, material of the tip and the substrate (their work function), bias applied, tip material, etc. The process makes use of the tunneling effect while scanning the probe over the surface to create a minuscule image, hence this is called as scanning tunneling microscopy. The process is schematically shown

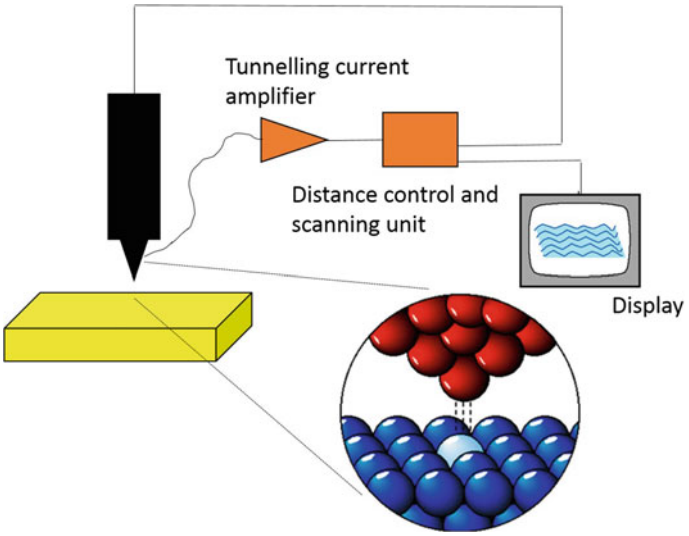

Fig. 19 Schematic of scanning tunneling microscopy

in Fig. 19. STM can be operated in two modes: constant height mode and constant current mode. The schematic of two modes of operations is shown schematically in Fig. 20.

In **constant height mode,** the tip is held at a constant height as it is scanned over the area. Based upon the topology of the substrate, the distance between the tip and substrate keeps on varying from pixel to pixel, which results in variation in the tunneling current at different pixel points. The tunneling current is inversely proportional to the distance between the tip and the substrate. The difference in the tunneling current at different pixel points is taken as the basis for creating the image of the substrate under consideration. For example, if a grating array is to be characterized using STM in constant height mode, when the probe scans over the top land the tunneling current will be more, but when the probe enters the groove of the grating the tunneling current decreases (since the distance between the tip and the substrate, which is now the bottom land, increases). The decrease in the tunneling current is proportional to the depth of the groove.

Constant height mode of operation is faster of the two but it becomes problematic if the sample has random projections on it. Since the height is constant throughout the scanning cycle, if any such projection is encountered by the tip it will result in a collision between the two which can damage the tip. Preparation and setting up the STM tip is a time consuming and tedious task.

The second mode of operation in STM is the **constant current mode**. In this mode, the operating current is fixed throughout the scan. Based on the topology if the distance between the tip and the substrate changes, the tip moves up or down (as per requirement) so that the tunneling current is always at a constant value. The distance moved by the tip at each pixel is taken as the basis for creating the image. For

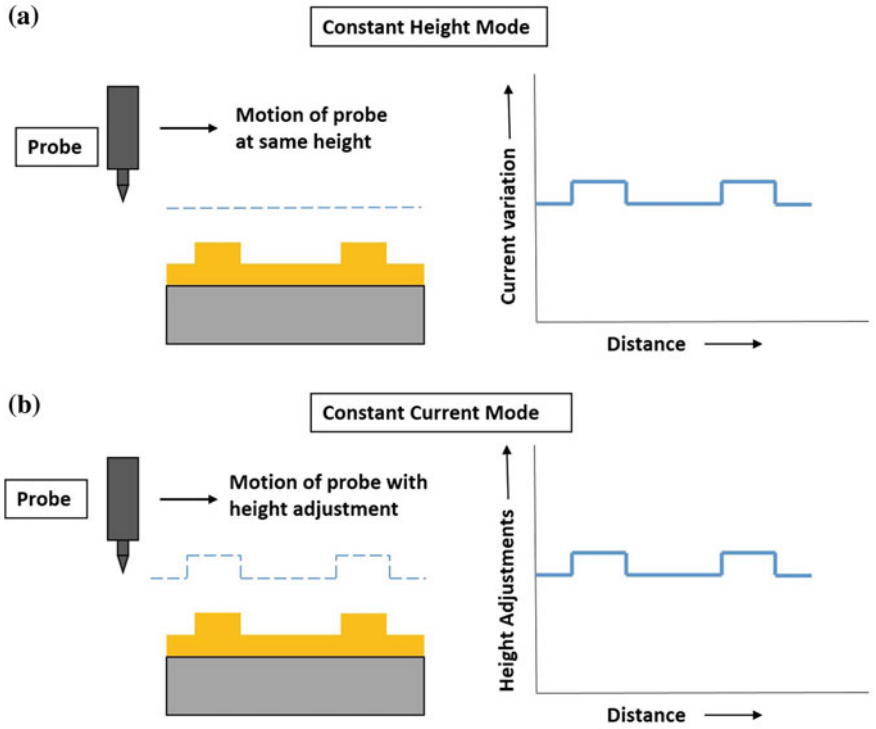

Fig. 20 Modes of operating STM **a** Constant height mode, **b** Constant current mode

example, suppose STM is operated at constant current mode for imaging a grating array. First, the operating tunneling current will be fixed. The current will be constant when the tip moves over the top land. When the probe tip enters the groove of the grating, the tunneling current will decrease since the distance between the tip and the substrate will increase. To maintain a constant current level, the tip will move down till the current is at the operating level and the scan will then proceed to the next pixel. The distance moved by the tip is proportional to the groove depth.

The STM is used for imaging conducting or semi conducting materials surfaces [56]. The movement of the tip is achieved through piezoelectric actuators. For the accurate operation of STM, the setup must be mounted on a vibration isolation platform and acoustically shielded. A properly constructed STM can achieve up to 0.1 nm lateral resolution and 0.01 nm depth resolution.

8 Summary

The structure sizes of the required patterns are moving from lower to lower scales. Surface micromachining has already evolved into nano-machining to a large extent. Researchers all over the world are also trying to combine more than one type of process to come up with different ways which can take the best of all processes and counter the limitations of each of the processes. The techniques discussed in this section form the basis on which the later modifications can be made. Processes like photolithography, RIE, DRIE, FIB, EBL are being continuously upgraded and combined with a wide variety of processes to achieve dimensions which were earlier unthinkable. Tools like STM and SEM are being extensively used by the researchers. The next big challenge in this direction is the scalability. Presently, structures of very small dimensions (few nanometers) can be fabricated over a very small area (few square microns) or if one wants to increase area coverage (in centimeter squares) the dimensions have to be high (few hundred nanometers at least, but generally micron sized). Another thing which needs to be controlled is the cost and the robustness of the fabricated devices.

References

1. Christian D (2011) Maps of time: an introduction to big history. University of California Press, California
2. Roche H, Delagnes A, Brugal JP, Feibel C, Kibunjia M, Mourre V, Texier PJ (1999) Early hominid stone tool production and technical skill 2.34 Myr ago in West Turkana, Kenya. Nature 399:57–60
3. Dongsheng Q et al (2019) Manufacturing method of precision machine tool bearing with high precision stability. United States Patent, Patent Number US 10,228,022B2
4. Xiao H, Li W, Zhou Z, Huang X, Ren Y (2018) Performance analysis of aerostatic journal micro-bearing and its application to high-speed precision micro-spindles. Tribol Int 120:476–490
5. Evans CJ, Bryan JB (1999) "Structured", "textured" or "engineered" surfaces. CIRP Ann 48:541–556
6. Hutchings I, Shipway P (2017) Tribology: friction and wear of engineering materials. Butterworth-Heinemann, Oxford
7. Goswami A, Aravindan S, Rao PV (2016) Optimization of nanohole array parameters for improving the ultimate efficiency of nanohole structured c-Si solar cells. Proc Inst Mech Eng Part N J Nanoeng Nanosyst 230:367–385
8. Goswami A, Aravindan S, Rao PV (2016) Fabrication of substrate supported bimetallic nanoparticles and their optical characterization through reflection spectra. Superlattices Microstruct 91:252–258
9. Schmid G, Simon U (2005) Gold nanoparticles: assembly and electrical properties in 1–3 dimensions. Chem Commun 6:697–710
10. Yang FL, Song D, Ma AB, Jiang JH, Cheng ZJ (2019) Recent studies of surface self-nanocrystallization (SSNC) of metallic materials. Mater Sci Forum 956:160–168
11. He X, Song M, Du Y, Shi Y, Johnson BA, Ehmann KF, Chung YW, Wang QJ (2020) Surface hardening of metals at room temperature by nanoparticle-laden cavitating water jets. J Mater Process Technol 275, 116316. (online first at https://doi.org/10.1016/j.jmatprotec.2019.116316)

12. Leinenbach CH, Kattelus H, Knechtel R (2010) Surface micromachining. In: Handbook of silicon based MEMS materials and technologies. William Andrew Publishing, Boston
13. Moreau WM (2012) Semiconductor lithography: principles, practices, and materials. Plenum Press, New York, Springer Science & Business Media
14. https://www.ossila.com/pages/spin-coating. Retrieved on 7 Sept 2019 at 0900 hours
15. Akcalt E, Nemoto K, Uzsoy R (2001) Cycle-time improvements for photolithography process in semiconductor manufacturing. IEEE Trans Semicond Manuf 14:48–56
16. Jansen H, Gardeniers HM, Elwenspoek M, Fluitman J (1996) A survey on the reactive ion etching of silicon in microtechnology. J Micromech Microeng 6:14–28
17. Sze SM (2008) Semiconductor devices: physics and technology. Wiley & Sons, New York
18. http://www.plasmatherm.com/etch.html. Retrieved on 7 Sept 2019 at 0900 hours
19. Marrian CRK, Snow ES (1996) Proximal probe lithography and surface modification. Microelectron Eng 32:173–189
20. Gottscho RA, Jurgensen CW, Vitkavage DJ (1992) Microscopic uniformity in plasma etching. J Vac Sci Technol B Microelectron Nanometer Struct Process Meas Phenom 10:2133–2147
21. Rangelow IW, Löschner H (1995) Reactive ion etching for microelectrical mechanical system fabrication. J Vac Sci Technol B Microelectron Nanometer Struct Process Meas Phenom 13:2394–2399
22. Hiscocks MP, Ganesan K, Gibson BC, Huntington ST, Ladouceur F, Prawer S (2008) Diamond waveguides fabricated by reactive ion etching. Opt Express 16:19512–19519
23. Yoo J, Yu G, Yi J (2011) Large-area multicrystalline silicon solar cell fabrication using reactive ion etching (RIE). Sol Energy Mater Sol Cells 95:2–6
24. Laermer F, Schilp A (1996) Method of anisotropically etching silicon. U.S. Patent No. 5,501,893, U.S. Patent and Trademark Office, Washington
25. Yeom J, Wu Y, Selby JC, Shannon MA (2005) Maximum achievable aspect ratio in deep reactive ion etching of silicon due to aspect ratio dependent transport and the microloading effect. J Vac Sci Technol B Microelectron Nanometer Struct Process Meas Phenom 23:2319–2329
26. Chang B, Leussink P, Jensen F, Hübner J, Jansen H (2018) DREM: Infinite etch selectivity and optimized scallop size distribution with conventional photoresists in an adapted multiplexed Bosch DRIE process. Microelectron Eng 191:77–83
27. Marty F, Rousseau L, Saadany B, Mercier B, Français O, Mita Y, Bourouina T (2005) Advanced etching of silicon based on deep reactive ion etching for silicon high aspect ratio microstructures and three-dimensional micro-and nanostructures. Microelectron J 36:673–677
28. Arnold JC, Sawin HH (1991) Charging of pattern features during plasma etching. J Appl Phys 70:5314–5317
29. Hwang GS, Giapis KP (1997) On the origin of the notching effect during etching in uniform high density plasmas. J Vac Sci Technol B Microelectron Nanometer Struct Process Meas Phenom 15:70–87
30. Laermer F (2008) Method for etching structures in an etching body by means of a plasma. U.S. Patent No. 7,361,287, U.S. Patent and Trademark Office, Washington
31. Yun SS, You SK, Lee JH (2006) Fabrication of vertical optical plane using DRIE and KOH crystalline etching of (1 1 0) silicon wafer. Sens Actuators, A 128:387–394
32. Rossi C, Briand D, Dumonteuil M, Camps T, Pham PQ, De Rooij NF (2006) Matrix of 10 × 10 addressed solid propellant microthrusters: review of the technologies. Sens Actuators, A 126:241–252
33. Mita Y, Sugiyama M, Kubota M, Marty F, Bourouina T, Shibata T (2006) Aspect ratio dependent scalloping attenuation in DRIE and an application to low-loss fiber-optical switches. In: 19th IEEE international conference on micro electro mechanical systems, Istanbul, Turkey, pp 114–117
34. Meng E, Wu S, Tai YC (2001) Silicon couplers for microfluidic applications. Fresenius' J Anal Chem 371:270–275
35. Suvorov VG, Zubarev NM (2003) Formation of the Taylor cone on the surface of liquid metal in the presence of an electric field. J Phys D Appl Phys 37:289–297

36. Ritter M, Hemmleb M, Lich B, Faber P, Hohenberg H (2006) SEM/FIB stage calibration with photogrammetric methods. In: ISPRS Commission V Symposium 2006 (Int. archives of photogrammetry, remote sensing and spatial information sciences), vol 36, pp 1–6
37. Morio M, Katakura T (2003) Focused ion beam equipment and focused ion beam processing method using same. U.S. Patent No. 6,639,226. U.S. Patent and Trademark Office, Washington
38. Bhavsar SN, Aravindan S, Rao PV (2010) Effect of redeposition—an important consideration in existing mathematical model of sputtering process in focused ion beam milling. In: 10th IEEE international conference on nanotechnology, Seoul, South Korea, pp 768–770
39. Picard YN, Adams DP, Vasile MJ, Ritchey MB (2003) Focused ion beam-shaped microtools for ultra-precision machining of cylindrical components. Precis Eng 27:59–69
40. Schaller T, Bohn L, Mayer J, Schubert K (1999) Microstructure grooves with a width of less than 50 μm cut with ground hard metal micro end mills. Precis Eng 23:229–235
41. Adams DP, Vasile MJ, Benavides G, Campbell AN (2001) Micromilling of metal alloys with focused ion beam–fabricated tools. Precis Eng 25:107–113
42. Ali MY (2002) Ion beam micromachining of crystalline solids. Ph.D. Thesis, School of Mechanical and Production Engineering, Nanyang Technological University
43. https://www.azom.com/article.aspx?ArticleID=14895. Retrieved on 7 Sept 2019 at 0900 hours
44. Goswami A, Singh K, Aravindan S, Rao PV (2017) Optimizing FIB milling process parameters for silicon and its use in nanoreplication. Mater Manuf Processes 32:1052–1058
45. Lian J, Wang L, Sun X, Yu Q, Ewing RC (2006) Patterning metallic nanostructures by ion-beam-induced dewetting and Rayleigh instability. Nano Lett 6:1047–1052
46. Meena K, Kumar H, Goswami A, Aravindan S, Rao PV (2016) Fabrication of large-area ordered array of gold nanoparticles on c-Si substrate and its characterisation through reflectance spectra. Micro Nano Lett 11:819–821
47. Yue W, Wang Z, Yang Y, Chen L, Syed A, Wong K, Wang X (2012) Electron-beam lithography of gold nanostructures for surface-enhanced Raman scattering. J Micromech Microeng 22:1–9
48. Tennant D, Spector S, Stein A, Jacobsen C (2000) Electron beam lithography of Fresnel zone plates using a rectilinear machine and trilayer resists. In: AIP conference proceedings, pp 601–606
49. https://www.microscopeworld.com/t-stereo_zoom_microscopes.aspx. Retrieved on 7 Sept 2019 at 0900 hours
50. https://www.microscopyu.com/techniques/stereomicroscopy/introduction-to-stereomicroscopy. Retrieved on 7 Sept 2019 at 0900 hours
51. Goldstein JI, Newbury DE, Michael JR, Ritchie NW, Scott JHJ, Joy DC (2017) Scanning electron microscopy and X-ray microanalysis. Springer, New York
52. Reimer L (2013) Scanning electron microscopy: physics of image formation and microanalysis, Springer, p 45
53. Danilatos GD (1993) Introduction to the ESEM instrument. Microsc Res Tech 25:354–361
54. Antonovsky A (1984) The application of colour to SEM imaging for increased definition. Micron Microscopicaacta 15:77–84
55. Tersoff J, Hamann DR (1985) Theory of the scanning tunneling microscope. Phys Rev B 31:805–813
56. Wong D, Velasco J Jr, Ju L, Lee J, Kahn S, Tsai HZ, Germany C, Taniguchi T, Watanabe K, Zettl A, Wang F, Crommie MF (2015) Characterization and manipulation of individual defects in insulating hexagonal boron nitride using scanning tunnelling microscopy. Nat Nanotechnol 10:949–953

Generation of Nano-Level Surface Finish by Advanced Nano-Finishing Processes

A. Barman and M. Das

Abstract Nowadays, nano-level surface finish is a necessary requirement in different industries. To enhance the performance of a component, nano-level surface roughness is an essential quality. The main drawback of the traditional finishing processes is a longtime requirement for finishing and its dependency on manual labor. The surface morphology requirement of the present era is also very difficult to achieve using conventional finishing processes. Different advanced finishing processes like abrasive flow finishing, elastic emission finishing and magnetic field-assisted finishing processes are developed for achieving nano-level finish. Magnetic field can be used to control finishing forces precisely in magnetic field-assisted finishing processes. Magnetic abrasive finishing and magnetorheological finishing processes belong to this group. Different types of magnetorheological finishing processes are developed to finish a vast selection of components using magnetorheological fluid as the polishing medium. Magnetorheological abrasive flow finishing, rotational magnetorheological abrasive flow finishing, ball end magnetorheological finishing and magnetic field-assisted finishing using novel polishing tool are some of the processes which generate nanometer level surface finishing on flat and free-form surfaces using MR polishing medium. Semiconductor industries use chemical mechanical polishing process due to its planarization capability. Also, CMP process is able to provide nanometer level surface finish in metals and non-metals alike. The required surface characteristics and surface finish in automotive, aerospace, medical and other industries are dependent on the application of the component. These required surfaces can be generated using advanced nano-finishing processes.

Keywords Surface roughness · Nano-finishing · Abrasive flow finishing · Elastic emission finishing · Magnetic abrasive finishing · Magnetorheological finishing · Chemical mechanical polishing

A. Barman · M. Das (✉)
Department of Mechanical Engineering, IIT Guwahati, Guwahati, Assam 781039, India
e-mail: manasdas@iitg.ac.in

A. Barman
e-mail: anwesa02@gmail.com

G. Kibria and B. Bhattacharyya (eds.), *Accuracy Enhancement Technologies for Micromachining Processes*, Lecture Notes in Mechanical Engineering,
https://doi.org/10.1007/978-981-15-2117-1_10

1 Introduction

Surface roughness of a component is a very important criterion for its application, performance and longevity. Surface roughness requirement of any component depends upon its particular application. To accomplish longer component life and also to increase the quality of the component performance, highly precise manufacturing process is required. In the present-day scenario, different industries like automotive, aerospace, medical, etc., require nano-finished products for different purposes. The nano-finished surface requirements are very hard to achieve using finishing processes which are traditional in nature. Many advanced finishing processes are proposed by researchers capable of generating nano-level surface finish. Abrasive particles are primarily used as finishing medium in most advanced finishing processes. Generating surface finish at nanometer level on free-form surfaces is difficult than the flat surface. However, the loose abrasive particles in advanced nano-finishing processes can reach over different faces of free-form surfaces and provide nanometer level surface roughness.

A brief description of different advanced finishing processes and generated surfaces is discussed in the present study. Also, two main types of advanced nano-finishing processes are considered in the present discussion. First one is the general advanced nano-finishing process, i.e., abrasive flow finishing (AFF) and elastic emission finishing (EEF). The second one is magnetic field-assisted nano-finishing processes, i.e., magnetic abrasive finishing (MAF) and magnetorheological finishing (MRF). Different versions of MRF processes like magnetorheological abrasive flow finishing (MRAFF), rotational magnetorheological abrasive flow finishing (R-MRAFF), ball end magnetorheological finishing (BEMRF) and magnetic field-assisted finishing (MFAF) are also discussed. Also, the chemical mechanical polishing (CMP) process is discussed here due to its ability to provide nano-level surface finish for both metals and non-metals. All this processes are defined as nano-finishing process due to their ability to generate nano-level surface finish on flat and free-form surfaces.

2 Abrasive Flow Finishing (AFF)

AFM is mentioned here as AFF process due to its finishing capability. AFF is a nano-finishing process used for finishing internal and external surfaces of complex free-form components. This process is repeatable in nature giving it a widespread importance in industrial applications. Extrude Hone Corporation, USA, first industrialized AFM in 1960. In AFF process, a viscoelastic polishing medium mixed with abrasive particles is used to finish workpiece surface precisely [1]. The workpiece in its respective place during finishing is held by workpiece tooling. Two vertically opposed cylinders which are used to hold the polishing mediums are kept on both

sides of the tooling. Hydraulic unit is used to provide necessary pressure to the polishing medium to go backward and forward between two vertically opposed cylinders over the workpiece during AFF [2]. The main process parameters in AFM process are cycle number, extrusion pressure, media flow rate, viscosity of the media, abrasive particle concentration and size, rheology of the media and workpiece surface roughness [3]. AFM process produces uniform finishing in the nanometer level on different types of complex geometries [4–6]. The process parameters are changed according to finishing requirement. The polishing medium in this process is viscoelastic in nature which is made of polymer, abrasive particles, plasticizers and additives. Figure 1 shows the schematic diagram of AFF process along with finishing forces. In this process, radial force (F_r) helps abrasive particles to indent on workpiece to remove surface unevenness by shearing. Applied extrusion pressure on the elastic constituent of polishing medium generates radial force. Application of extrusion pressure on the viscous constituent of the polishing medium creates axial force (F_a) which helps in removing indented material. AFF process is used in aerospace, biomedical, etc., industries to nano-finish different types of surfaces. Kavithaa and Balashanmugam [4] used AFF process for polishing knee joint femoral component. Some components finished with AFF process are shown in Fig. 2 [7]. Different types of AFF setup is proposed over time to countermeasure the shortcomings of AFF process and to finish various types of surfaces.

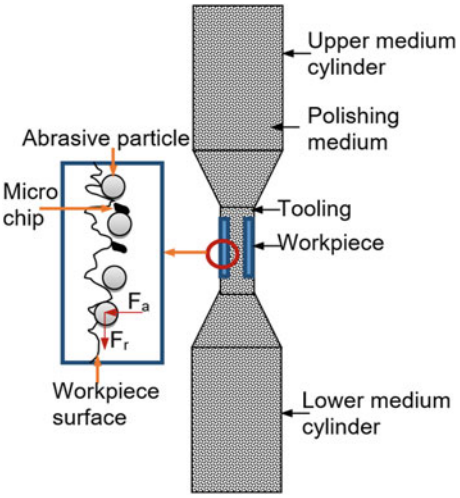

Fig. 1 Schematic diagram of AFF process along with finishing forces which acts on active abrasives while finishing

Fig. 2 Component finished with AFF [7]

3 Elastic Emission Finishing (EEF)

Elastic emission machining is mentioned as EEF due to its ability to produce surface finish in the nanometer range. Figure 3 shows the schematic diagram of material removal mechanism during EEF process. This process removes material at atomic level. In this process, ultra-fine abrasive powder mixed with ultra-pure water is accelerated and transported to the workpiece surface by rotating a polyurethane sphere. A small load is applied to the sphere so that hydrodynamic conditions amidst abrasive particles and workpiece are met. Abrasive particles remove the material atom by atom by creating a bond between the atoms on workpiece surface and abrasive particles [8]. EEF process performance mostly rests on abrasive particle properties and workpiece type. The material removal rate (MRR) in EEF happens at a very slow rate generating crystallographically and geometrically perfect surface [9]. The probable step-by-step atomistic removal mechanism during EEF process is shown in Fig. 4 [10]. Materials are slowly removed from workpiece surface by this step-by-step atomistic removal which constitutes a cycle. Abrasive particles going through the lubrication film between rotating polyurethane sphere and workpiece experiences different forces are shown in Fig. 5. The abrasive particle's behavior can be traced from the equation of motion involving the forces. The main forces which act on the abrasive particles during EEF process and affect the material removal from the workpiece surface are F_L, i.e., the lift force created inside fluid flow with velocity

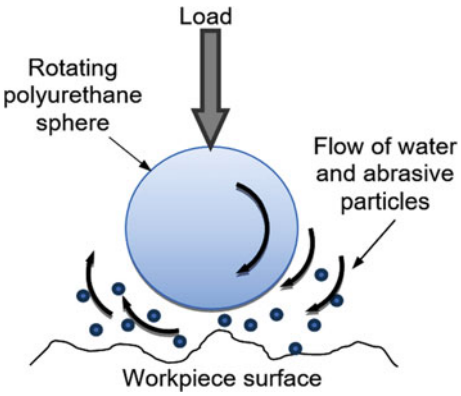

Fig. 3 Schematic diagram of polishing mechanism in EEF process

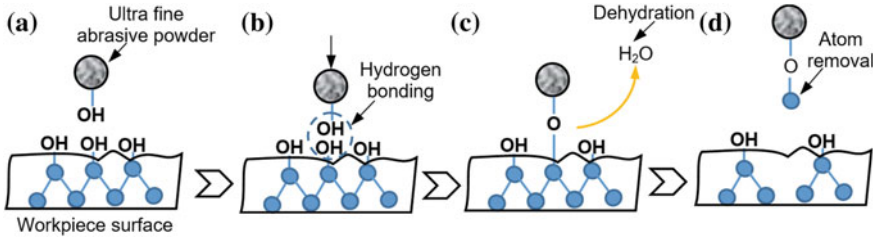

Fig. 4 Interaction among ultra-fine powder surfaces and workpiece surfaces, **a** structure of surfaces before contact, **b** surfaces making hydrogen bonding, **c** interfacial structure formation after dehydration and **d** after exclusion of work atom parting of absorbed powder

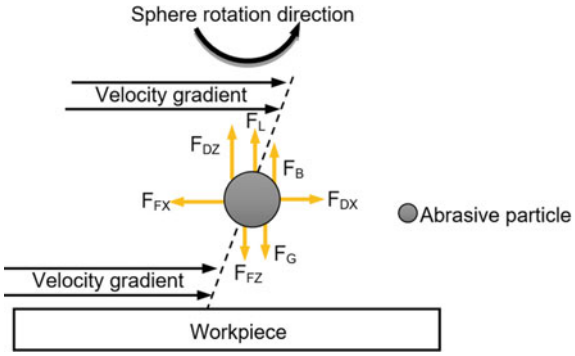

Fig. 5 Graphical description of forces applied on ultra-fine abrasive particle which go through rotating polyurethane sphere and workpiece (F_{Dx}—Stokes drag force in x direction, F_{Dz}—Stokes drag forces in the z direction, F_G—gravity force, F_B—buoyant force, F_L—lift force created due to velocity gradient in flowing fluid, and F_{Fx} and F_{Fz} are the forces created due to common contact of particles in x and z direction)

gradient and F_F, i.e., force generated by a mutual interaction of particles (Fig. 5) [11]. Generally, optical components are finished using EEF process [12].

4 Magnetic Abrasive Finishing (MAF)

MAF produces high-quality nanometric surface using external magnetic field. Electromagnet or permanent magnets are used to deliver required magnetic field during finishing. Permanent magnet or electromagnet is used depending on the process requirement. A permanent magnet is used when simple MAF process setup is required. For precise and efficient control of the MAF process, electromagnet is required. In this process, polishing medium is prepared by mixing iron particles with abrasive particles which is known as magnetic abrasive particles (MAPs). MAPs are

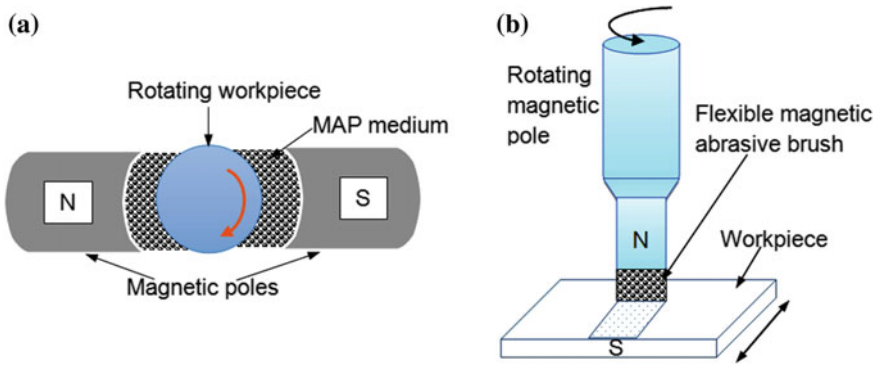

Fig. 6 Schematic representation of MAF experimental setup while finishing **a** cylindrical and **b** flat workpiece

kept amidst magnet and workpiece. MAPs align itself as a chain which follows magnetic flux lines creating a pliable magnetic abrasive brush (MAB). MAB performs like a cutting tool under the presence of external magnetic field [13]. Abrasive particles make very small indentation in this process resulting in low material removal rate. MAF process can be used for finishing both external as well as internal surfaces. The schematic representation of MAF process for cylindrical and flat surfaces is shown in Fig. 6. The indentation by the abrasive particles on workpiece surface occurs due to magnetic force or normal force. Rotation of pliable MAB generates tangential force which helps in shearing of the indented material [14, 15]. The important process parameters in MAF process are magnetic field intensity, finishing gap within magnetic pole face and the work piece surface, workpiece (material, size and shape), pole size and shape and composition of magnetic abrasive brush. Verma et al. [15] finished internal surface of a steel pipe using MAF. The deep scratch marks in initial surface of SS304 pipes are removed by MAF process. Both metal and non-metal can be finished using this process.

5 Magnetorheological Finishing (MRF)

MRF process provides nanometer level surface roughness without subsurface damage on the workpiece surface. Polishing medium in MRF process is magnetorheological (MR) fluid which is a combination of magnetic carbonyl iron particles (CIPs), non-magnetic abrasive particles dispersed in the base medium. This process is primarily used to finish optical materials with different profiles like flat, spherical, convex and concave. The development of the process is started at Center for Optics Manufacturing (COM) in Rochester, New York [16]. A schematic representation of MRF process is shown in Fig. 7. MRF process is fully commercialized by QED technologies in 1999. As presented in Fig. 7, MR fluid is continuously supplied on a rotating carrier

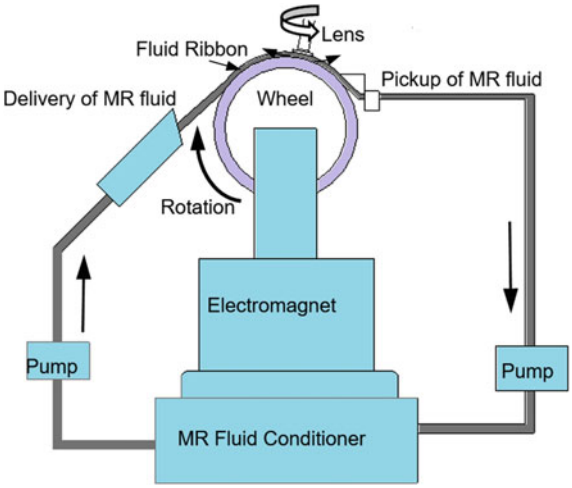

Fig. 7 Graphical representation of MRF process

wheel using a MRF delivery system in MRF process. Electromagnet is kept under the carrier wheel. While applying and changing magnetic field, the rheological properties like viscosity and yield stress of MR fluid change. A chain structure is formed by the CIPs along the magnetic flux lines making the fluid stiff. During polishing, the magnetic CIPs in MR fluid go near the magnet pole, and non-magnetic abrasive particles are dispersed near workpiece surface. This described phenomenon in MR fluid is known as the magnetic levitation force.

Pressure is distributed in the finishing zone of stiffened MR fluid ribbon (Fig. 8). A moving boundary which is quasi-solid by nature is created near workpiece surface

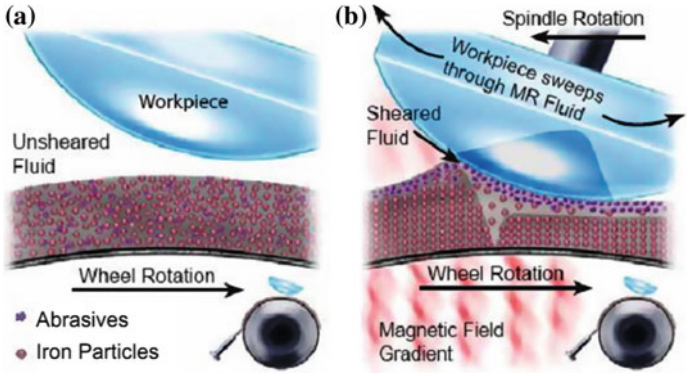

Fig. 8 MR fluid model in the zone of finishing **a** the random arrangements of abrasives and iron particles without magnetic field and **b** polishing spot produced by plunging an optic into the stiffened MR fluid in MRF process [18]

which leads to the generation of large shear stress in the contact zone. The material removal from a particular area of workpiece surface occurs due to large shear stress. That area where the polishing took place at a particular time is defined as polishing spot. The drag force is generated due to the flowing MR fluid ribbon shear stress. The drag force helps in material removal [16, 17].

Figure 9a shows the main components of MRF experimental setup. The polishing wheel (Fig. 9b) encloses permanent ring magnet. Normal force (indentation force) is a combination of forces applied by the surrounding CIPs (i.e., magnetic force), force due to MR fluid squeezing at the finishing zone and gravitational force. Tangential force (indented material removal force) is generated due to rotating carrier wheel [19]. Figure 9c represents finishing forces in MRF process. Important process parameters in MRF are magnetic flux density, CIP concentration, abrasive particle concentration, carrier wheel speed and workpiece parameters [20]. Several researchers have developed different types of wheels and also used permanent magnets instead of electromagnets. Figure 10 shows the optical mold before and after finishing with MRF.

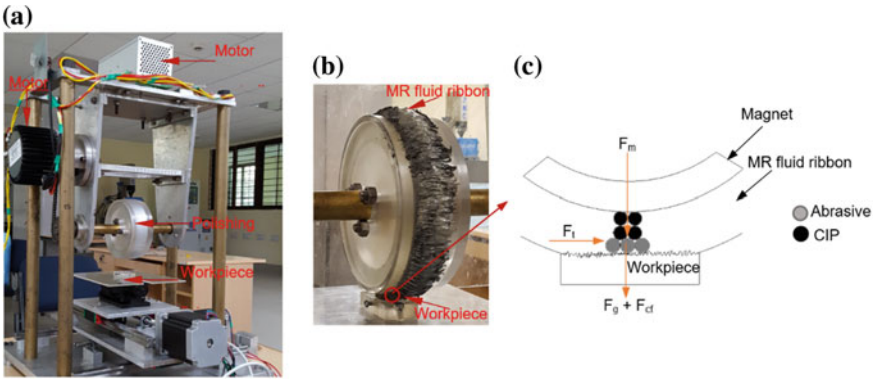

Fig. 9 **a** MRF experimental setup (micromachining laboratory, IITG), **b** polishing wheel (enclosing permanent magnet) with MR fluid ribbon under magnetic field and **c** finishing forces acting on active abrasive particles

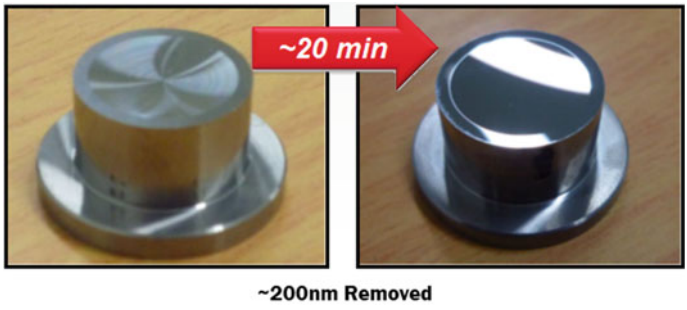

Fig. 10 Improving surface roughness, smoothing and correction of optical mold using MRF [21]

Some magnetic field-assisted finishing processes are developed which generally use MR fluid along with abrasive particles as a medium for polishing. MR fluid composition is varied depending upon workpiece material composition. Also, the properties of MR polishing medium vary due to the change in composition. MRAFF, ball end MRF and magnetic field-assisted finishing with novel polishing tool, etc., are some of the processes which use MR polishing medium. These processes provide nanometer level surface finish on different types of surfaces (flat and free-form) precisely and efficiently. A brief discussion about these processes is discussed below.

5.1 Magnetorheological Abrasive Flow Finishing (MRAFF)

MRAFF is a hybrid process combining both AFF and MRF processes. MRAFF provides advantages of both the processes like the flexibility of AFM process and deterministic in-process controllability of MRF polishing medium [22]. In MRAFF process, MR polishing fluid is used in a same way as the polishing medium in AFF process. The medium goes to and fro between two upright cylinders opposing each other and the channel created by workpiece fixture and workpiece. Application of magnetic field near workpiece makes MR polishing medium stiff. The finishing operation is carried out by stiffened MR polishing medium. Hence, finishing does not occur in other areas. The main limitations of MRAFF process include its small finishing rate and non-uniform finishing across the workpiece surface. To countermeasure this problem, a swirling motion of the polishing medium is introduced by using a revolving magnetic field (Fig. 11). After incorporating the rotational motion, it is referred as rotational-MRAFF or R-MRAFF process. Here, uniform magnetic field is provided in the finishing zone using four permanent magnets which are placed 90° apart from each other [23]. Hence, uniform finishing occurs across workpiece surface. Figure 12 represents the experimental setup of R-MRAFF process.

Two opposite pistons are driven in the medium cylinders periodically to thrust MR polishing medium through the fixture-cum-workpiece surface in R-MRAFF process. A belt drive is attached between the magnet fixture and a motor to impart rotational motion to the magnet fixture (Fig. 12). The polishing medium rotates around the cylinder axis due to this rotational motion. A relatively high velocity of the polishing medium is attained by superimposing these two motions which leads to a smooth mirror-like finished surface. From AFM images of ground workpiece (stainless steel) surface before finishing, it is found that the surface exhibits very high peaks and deep valleys. MRAFF could not entirely be able to remove the deep grinding marks [24, 25]. The workpiece surface becomes smoother, and number of valleys also reduced after finishing the surface using R-MRAFF process at 20 rpm [24, 25]. The surface smoothness increases resulting in a flattened surface after increasing magnet fixture rotating speed from 20 to 67 rpm. Its Ra value is decreased from 140 to 110 nm.

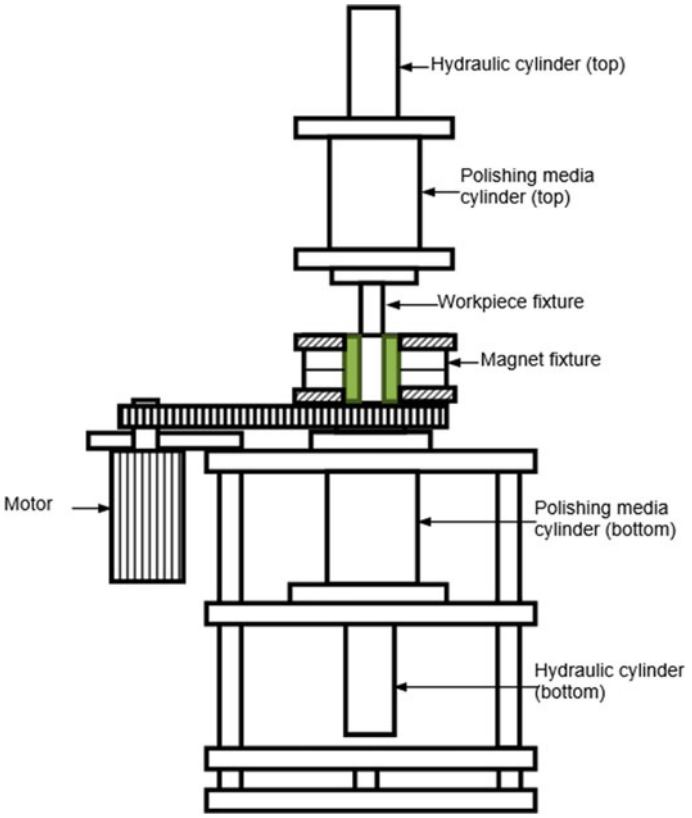

Fig. 11 Graphical representation of R-MRAFF experimental setup

5.2 Ball End MR Finishing (MRF) Process

Ball end MRF [26] is developed to finish 3D complex shapes as represented in Fig. 13. In this process, MR polishing fluid is pressurized to go into the central rotating core from the top end. MR fluid stiffens once it reaches at surface of the tool tip owing to applied magnetic field. A semisolid structure in the shape of a ball at the end of rotating core tip is formed. The electromagnet central core/tool is rotated like in conventional ball end milling process, and the feed is provided to the workpiece which is attached to an X-Y table. This process generates nanometer level surface finish in metals and also non-metals [27, 28]. The workpiece surface before and after finishing is observed using SEM as represented in Fig. 14a, b, respectively. The final surface has less deep valleys than the initial surface.

Fig. 12 Photograph of R-MRAFF experimental setup (micromachining laboratory, IITG)

5.3 Magnetic Field-Assisted Finishing (MFAF) Process

To finish free-form surfaces precisely in MFAF process, a polishing tool is designed and fabricated [30]. The required magnetic field during finishing is supplied by a permanent magnet. High permeable material, mu-metal, is considered for enclosing the permanent magnet. It will allow the magnetic field to flow through the mu-metal fixture instead of going outside which reduces magnetic field loss. The developed experimental configuration is represented in Fig. 15a. Expanded view of the MFAF tool is displayed in Fig. 15b. The MFAF tool is clamped in the tool holder of CNC milling machine while finishing. A free-form surface of femoral component of knee implant is finished using MFAF tool. Before and after finishing 3D surface topography of the femoral knee implant is shown in Fig. 16. As represented in Fig. 16a, the deep valleys and high peaks are visible in initial workpiece surface. Nevertheless, it is not visible on final surface as given in Fig. 16b. Hence, MFAF polishing tool can generate surface finish in the nanometer level on free-form surfaces.

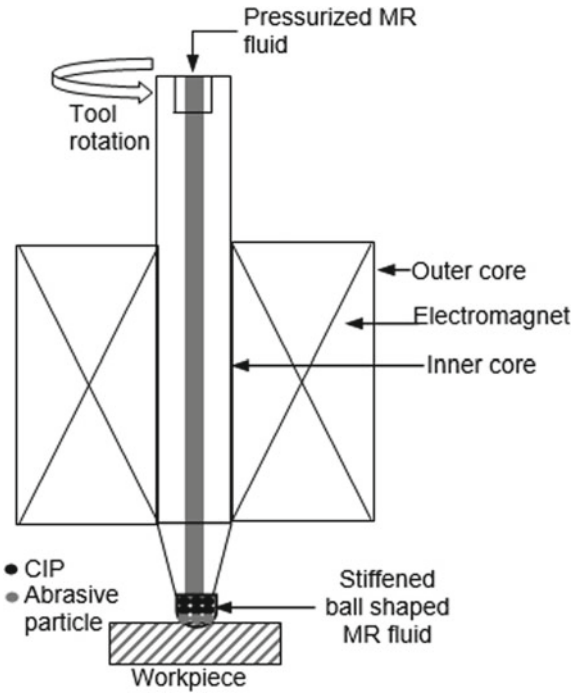

Fig. 13 Graphical representation of ball end MRF showing development of ball-shaped stiffened MR polishing medium at tool tip

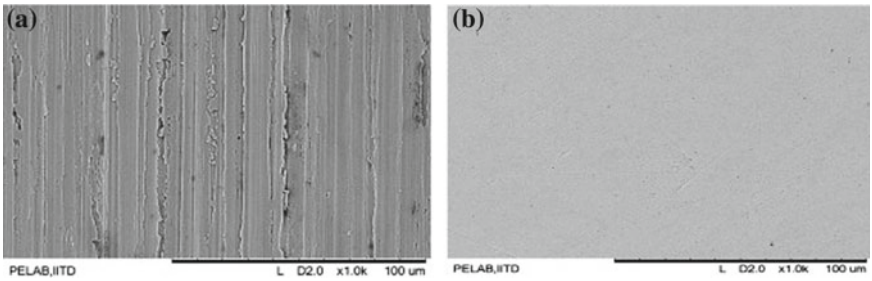

Fig. 14 SEM micrographs of **a** initial (grounded) and **b** finished surface (finishing time—120 min). With permission from [29]. Copyright (2012) Elsevier, License No. 4676551388210

6 Chemical Mechanical Polishing (CMP) Process

IBM first developed CMP in the mid-1980 to planarize inter level dielectric (ILD) layers. The main industrial application of CMP is to polish silicon wafers. Later, CMP is also applied to finish metals along with semiconductors [31, 32]. The graphic presentation of the CMP process is given in Fig. 17. Wafer carrier is used to hold

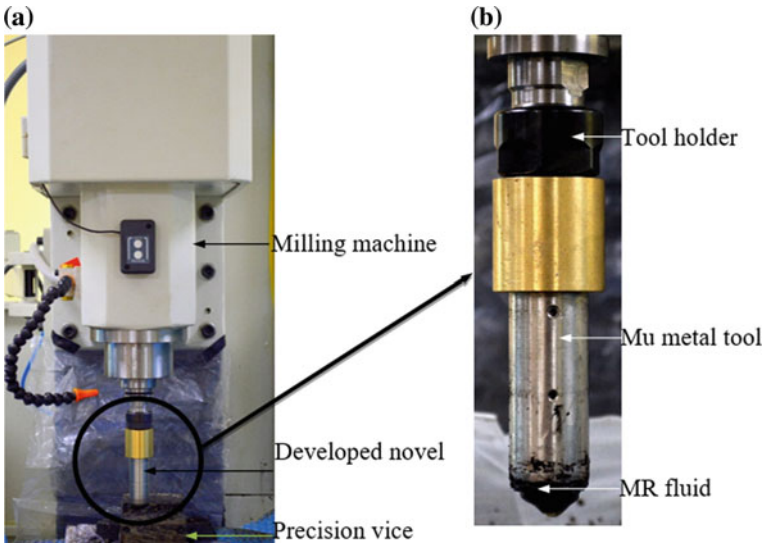

Fig. 15 **a** Magnetic field-assisted finishing experimental setup and **b** novel tool. With permission from [30]. Copyright (2017) Elsevier, License No. 4677080572961

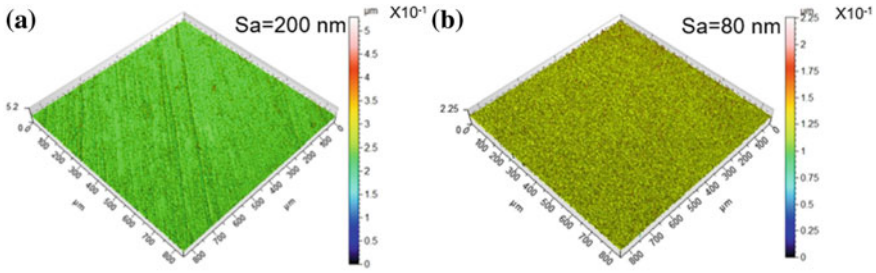

Fig. 16 Femoral knee joint 3D surface topography **a** before and **b** after finishing

the wafer, and it presses down the wafer on the rotating polishing pad. A rotational motion is provided to the wafer carrier along with a downward force. The polishing pad is covered with abrasive slurry. Abrasive slurry delivery system is used to supply the abrasive slurry onto the polishing pad. The platen supports the polishing pad.

In this process, abrasive particles remove material from the workpiece surface by two mechanisms, i.e., two body and three body abrasion. The two body abrasion mechanism takes place when the abrasive particles are attached with the polishing pad permanently. If the abrasive particles freely rotate between polishing pad and the workpiece surface, then three body abrasion occurs. Also, chemical reaction between the slurry and workpiece helps in material removal from the workpiece surface [33]. CMP provides nano-finished surface along with smooth and damage-free surface [34].

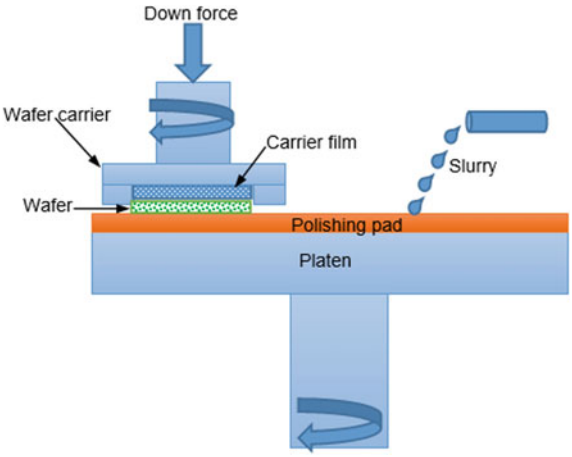

Fig. 17 Graphical presentation of CMP process showing three main elements: workpiece (semiconductor wafer), polishing pad and polishing slurry

7 Summary

The need of advanced nano-finishing processes in different industries is a necessity. For widespread use of these processes in commercial fields, it is required to have a clear idea of the process mechanism so that the processes can be used more efficiently. To employ these processes to generate nano-finished surfaces according to the requirement, study of these processes is very important. The present discussion explains the capability of these advanced nano-finishing processes.

References

1. Rhoades L (1991) Abrasive flow machining: a case study. J Mater Process Technol 28:107–116
2. Jain RK, Jain VK, Dixit PM (1999) Modeling of material removal and surface roughness in abrasive flow machining process. Int J Mach Tools Manuf 39:1903–1923
3. Mali HS, Manna A (2009) Current status and application of abrasive flow finishing processes: a review. Proc Inst Mech Eng Part B J Eng Manuf 223:809–820
4. Kavithaa TS, Balashanmugam N (2016) Nanometric surface finishing of typical industrial components by abrasive flow finishing. Int J Adv Manuf Technol 85:2189–2196
5. Sankar MR, Jain VK, Ramkumar J (2016) Nano-finishing of cylindrical hard steel tubes using rotational abrasive flow finishing (R-AFF) process. Int J Adv Manuf Technol 85:2179–2187
6. Ravi Sankar M, Jain VK, Ramkumar J, Joshi YM (2011) Rheological characterization of styrene-butadiene based medium and its finishing performance using rotational abrasive flow finishing process. Int J Mach Tools Manuf 51:947–957
7. Abrasive flow machining (AFM)—Extrude hone. https://extrudehone.com/products/abrasive-flow-machining-afm
8. Yamauchi K, Hirose K, Goto H et al (1999) First-principles simulations of removal process in EEM (Elastic Emission Machining). Comput Mater Sci 14:232–235
9. Mori Y, Yamauchi K, Endo K (1988) Mechanism of atomic removal in elastic emission machining. Precis Eng 10:24–28

10. Inagaki K, Yamauchi K, Mimura H et al (2001) First-principles evaluations of machinability dependency on powder material in elastic emission machining. Mater Trans 42:2290–2294
11. Kanaoka M, Takino H, Nomura K, Mimura H, Yamauchi K, Mori Y (2008) Factors affecting changes in removal rate of elastic emission machining. In: Proceedings of ASPE 2008 annual meeting and the twelfth ICPE, pp 615–618
12. Kubota A, Shinbayashi Y, Mimura H et al (2007) Investigation of the surface removal process of silicon carbide in elastic emission machining. J Electron Mater 36:92–97
13. Jain VK (2012) Advanced machining processes. Allied Publisher Private Limited
14. Pashmforoush F, Rahimi A (2015) Nano-finishing of BK7 optical glass using magnetic abrasive finishing process. Appl Opt 54:2199
15. Verma GC, Kala P, Pandey PM (2017) Experimental investigations into internal magnetic abrasive finishing of pipes. Int J Adv Manuf Technol 88:1657–1668
16. Golini D, Kordonski WI, Dumas P, Hogan SJ (1999) Magnetorheological finishing (MRF) in commercial precision optics manufacturing. In: Stahl HP (ed) Proc. SPIE 3782, Optical manufacturing and testing III, pp 80–91
17. Shorey AB, Jacobs SD, Kordonski WI, Gans RF (2001) Experiments and observations regarding the mechanisms of glass removal in magnetorheological finishing. Appl Opt 40:20–33
18. MRF: How it works. https://qedmrf.com/en/mrfpolishing/mrf-technology/how-it-works
19. Sidpara A, Jain VK (2012) Theoretical analysis of forces in magnetorheological fluid based finishing process. Int J Mech Sci 56:50–59
20. Sidpara A, Jain VK (2014) Rheological properties and their correlation with surface finish quality in MR fluid-based finishing process. Mach Sci Technol 18:367–385
21. Improve Roughness (Optical Molds). https://qedmrf.com/en/mrfpolishing/mrf-applications/improve-roughness-optical-molds
22. Jha S, Jain VK (2004) Design and development of the magnetorheological abrasive flow finishing (MRAFF) process. Int J Mach Tools Manuf 44:1019–1029
23. Das M, Jain VK, Ghoshdastidar PS (2010) Nano-finishing of stainless-steel tubes using rotational magnetorheological abrasive flow finishing process. Mach Sci Technol 14:365–389
24. Das M, Jain VK, Ghoshdastidar PS (2011) The out-of-roundness of the internal surfaces of stainless steel tubes finished by the rotational–magnetorheological abrasive flow finishing process. Mater Manuf Process 26:1073–1084
25. Das M, Jain VK, Ghoshdastidar PS (2012) Nanofinishing of flat workpieces using rotational–magnetorheological abrasive flow finishing (R-MRAFF) process. Int J Adv Manuf Technol 62:405–420
26. Singh AK, Jha S, Pandey PM (2011) Design and development of nanofinishing process for 3D surfaces using ball end MR finishing tool. Int J Mach Tools Manuf 51:142–151
27. Tamaki Y, Miyazaki T, Suzuki E, Miyaji T (1989) Polishing of titanium prosthetics (Part 6). The chemical polishing baths containing hydrofluoric acid and nitric acid. Shika Zair Kikai 8:103–109
28. Saraswathamma K, Jha S, Rao PV (2015) Rheological characterization of MR polishing fluid used for silicon polishing in BEMRF process. Mater Manuf Process 30:661–668
29. Singh AK, Jha S, Pandey PM (2012) Nanofinishing of a typical 3D ferromagnetic workpiece using ball end magnetorheological finishing process. Int J Mach Tools Manuf 63:21–31
30. Barman A, Das M (2017) Design and fabrication of a novel polishing tool for finishing freeform surfaces in magnetic field assisted finishing (MFAF) process. Precis Eng 49:61–68
31. Ozdemir Z, Ozdemir A, Basim GB (2016) Application of chemical mechanical polishing process on titanium based implants. Mater Sci Eng, C 68:383–396
32. Chang Chun-Yen, Lin Hsiao-Yi, Lei Tan Fu et al (1996) Fabrication of thin film transistors by chemical mechanical polished polycrystalline silicon films. IEEE Electron Device Lett 17:100–102
33. Nanz G, Camilletti LE (1995) Modeling of chemical-mechanical polishing: a review. IEEE Trans Semicond Manuf 8:382–389

34. Komanduri R, Lucca DA, Tani Y (1997) Technological advances in fine abrasive processes. CIRP Ann Technol 46:545–596
35. Wei X, Yang X, Xie X, Hu W (2016) A material removal rate model-based chemical action of ultra-thin SUS304 substrate in chemical mechanical polishing. Int J Adv Manuf Technol 85:287–290